Operation of biofilters : a numerical approach to some couplings between hydrodynamic and biofilm growth Modeling

Hoang Lam Pham

Communauté
UNIVERSITÉ Grenoble Alpes

THÈSE

Pour obtenir le grade de

DOCTEUR DE LA COMMUNAUTÉ UNIVERSITÉ GRENOBLE ALPES

Spécialité : MEP : Mécanique des fluides Energétique, Procédés

Arrêté ministériel : 25 mai 2016

Présentée par

Hoang Lam PHAM

Thèse dirigée par **Philippe SECHET**, Maitre de Conférence, Grenoble INP
et codirigée par **Zhujun HUANG**, Maître de Conférences, Grenoble INP

préparée au sein du **Laboratoire Laboratoire des Ecoulements Géophysiques et Industriels**
dans **l'École Doctorale I-MEP2 - Ingénierie - Matériaux, Mécanique, Environnement, Energétique, Procédés, Production**

Fonctionnement des biofiltres : approche numérique de certains couplages hydrodynamique/bioflms et modélisation

Operation of biofilters: a numerical approach to some couplings between hydrodynamic and biofilm growth Modeling

Thèse soutenue publiquement le **18 octobre 2018**,
devant le jury composé de :

Monsieur PHILIPPE SECHET
MAITRE DE CONFERENCES, GRENOBLE INP, Directeur de thèse
Monsieur ARNAUD COCKX
PROFESSEUR, INSA TOULOUSE, Rapporteur
Monsieur JEAN-MARC CHOUBERT
INGENIEUR DE RECHERCHE, IRSTEA CENTRE DE LYON-VILLEURBANNE, Rapporteur
Madame ZHUJUN HUANG
MAITRE DE CONFERENCES, GRENOBLE INP, Co-directeur de thèse
Monsieur YVES ANDRES
PROFESSEUR, ENS DES MINES DE NANTES, Examinateur
Monsieur LAURENT OXARANGO
PROFESSEUR, UNIVERSITE GRENOBLE ALPES, Président

Abstract. Solute transport coupled with biofilm growth in porous media is encountered in many engineered applications, for instance biofiltration of wastewater and air pollutant treatment. In terms of modelling, the interaction between biology, hydrodynamic and chemistry are still difficult to understand at the fine scale: that led to a wide dissemination of macroscopic model, simpler to handle. However, one issue consists in providing a macroscopic model complex enough to take into account the relevant processes accounting for the coupling between the biomass development and system functioning, but simple enough for operational use. This thesis focused on few selected processes that influence the macroscopic behavior of such system. First, we investigated the permeability reduction modeling accounting for biofilm development. A model including two features that result in permeability reduction (pore radius reduction and pore plugging) was developed. This model was assessed in a wide range of experimental data. Another part of the thesis focused on the initial biomass attachment that is an important feature to characterize the system initial state. Following the concept that bacterial cell can be treated as soft colloids, a new correlation equation was developed to estimate the bacteria attachment efficiency. This correlation is based on the regression analysis of a wide range of experimental data of colloid deposition in various electrolyte conditions, flowrates and geometries of porous media. New dimensionless parameters have been introduced to represent the coupled effects of Derjaguin-Landau-Verwey-Overbeek (DLVO) forces, hydrodynamic forces and to account for geometry of porous media. These features were introduced in a 1D dimensional model that have been developed for the numerical simulation of solute transport coupled with biofilm growth. An important issue in this model was to properly represent biofilm detachment. Another distinctive feature of our model is an attempt to account for the "sloughing" process in modeling biofilm detachment. Sloughing is a different process than erosion which corresponds to a discrete removal of large fraction of biofilm. In this study, biofilm sloughing has been separately accounted in the numerical modeling porous media bioclogging. Biofilm sloughing was considered as a stochastic process and quantified by random generator. So this discrete events could be incorporated into other continuous processes to determine the biomass transfer from biofilm to the liquid phase. Numerical simulations have been performed using OpenFoam to implement the model. Simulation with and without the sloughing term were performed and discussed in the frame of available literature data.

Résumé. Le transport de soluté en présence de biofilms en milieux poreux est un problème rencontré dans de nombreuses applications industrielles (biofiltration des eaux usées et traitement de polluants atmosphériques notamment). En termes de modélisation, l'interaction entre biologie, hydrodynamique et chimie reste difficile à comprendre aux échelles les plus fines: cela a conduit à une large utilisation de modèles macroscopiques, plus simple à manipuler. Cependant, la question consiste à écrire des modèles macroscopiques suffisamment complexes pour prendre en compte les processus pertinents représentant le couplage entre développement de la biomasse et fonctionnement du système, mais suffisamment simple pour une utilisation opérationnelle. Cette thèse s'est focalisée sur certains processus qui régissent le comportement macroscopique de tels systèmes. Nous avons étudié la modélisation de la réduction de la perméabilité induite par le développement du biofilm. Un modèle incorporant deux processus caractéristiques du colmatage (réduction de la taille pores et formation de « plugs ») a été développé. Ce modèle a été évalué pour une large gamme de données expérimentales. Une autre partie porte sur les processus d'adhésion initiale de la biomasse, processus important pour caractériser l'état initial du système. Sous l'hypothèse que les cellules bactériennes peuvent être traitées comme des colloïdes non rigides, une nouvelle corrélation a été développée pour estimer l'efficacité d'attachement des bactéries. Cette corrélation est basée sur l'analyse d'un large éventail de données expérimentales pour des conditions variées en termes d'électrolyte, débit et géométrie des milieux poreux, et introduit de nouveaux paramètres adimensionnels pour représenter les effets couplés des forces de Derjaguin-Landau-Verwey-Overbeek (DLVO), des forces hydrodynamiques et prendre en compte la géométrie des milieux poreux. Ces processus ont été introduits dans un modèle 1D développé pour la simulation numérique du transport de soluté en présence de biofilm dans un milieu poreux. Une autre question importante dans ce modèle était de représenter correctement le processus détachement de biofilm. Un autre trait distinctif de notre modèle est une tentative de rendre compte du processus de «sloughing» dans la modélisation du détachement de biofilm. Le « sloughing » est un processus différent de l'érosion, phénomène continu, et qui correspond à une élimination discrète d'une grande fraction de biofilm.Dans cette étude, le phénomène de « sloughing » a été incorporé séparément etodélisé comme un processus stochastique. Des simulations numériques ont été effectuées en utilisant OpenFoam pour implémenter le modèle. Des simulations avec et sans le terme de « sloughing » ont été effectuées et discutées dans le cadre des données de la littérature disponibles.

.

Contents

List of Figures

List of Table

Abbreviation

BAP: Biomass-associated products

CFT: Classical filtration theory

CLSM: Confocal laser scanning microscopy

D: dimension

DLVO-theory: Derjaguin, Landau, Verwey, Overbeek-theory

EPS: Extracellular polymeric substances

EDL: Electrical double layer

IbM: Individual based Model

NOMs: natural organic matters

OpenFoam: Open Source Field Operation and Manipulation

REVs: Representative Elementary Volumes

UAP: Utilization-associated products

VDW: Van der Waals

Chapter 1
Context

1.1 Biofilm and its application in porous media

In natural and engineering processes, microbes are ubiquitous that exit in both planktonic and biofilm phenotypes. Microbial biofilm starts with the initial adhesion of planktonic microbial cells to a surface and then, attached cells grow, reproduce, embed themselves in extracellular polymeric substances (EPS) and develop a biofilm (Flemming and Wingender, 2010). Compared to the planktonic phenotype, biofilm is more resistant to harmful environmental conditions because of the function of EPS which is to stabilize biofilm structures, facilitate cell adhesion to surface and protect biofilm from external stress such as biocide, shear forces, antibiotics (Sutherland, 2001; Hall-Stoodley et al., 2004; Anderson and O'Toole, 2008; Flemming and Wingender, 2010). On one side, biofilm may be troublesome to humankind as microbial contaminants impose problems to many processes such as cleaning medical devices, drinking water distribution, membrane fouling, food processing (Pedersen, 1990; Chmielewski and Frank, 2003; Mack et al., 2006; Inaba et al., 2016) that a great effort is required to prevent and remove biofilm. In the other side, developing biofilm in porous media is widely applied in environmental treatment and protection to handle toxic substances. In situ bioremediation of groundwater, biofilm creates the effective permeable reactive barrier for the treatment of contaminated plume (Langwaldt and Puhakka, 2000; Kao et al., 2001; Cunningham et al., 2003; Folch et al., 2013). The same principle is applied to enhance biomass accumulation in soil pores for soil decontamination (Wilson and Brown, 1989; Claxton et al., 1991; Komlos et al.,2004). In biofiltration, thickness biofilm is conditioned to growth in packed column for wastewater and air pollutant treatment (Shareefdeen et al., 1993; Canler and Perret, 1994; Mauclaire et al., 2006; Dumont et al., 2008; Ramirez et al., 2008). Bioclogging is desirable to form an impermeable barrier to prevent leachate

leakage from landfill to ground water (VanGulck and Rowe, 2004; Ivanov and Chu, 2008). Low permeability resulting from biofilm proliferation is the important objectives to construct a good site for carbon storage in geological carbon sequestration (Bachu, 2000; Orr, 2004; Mitchell et al., 2008, 2009).

In some applications, the performance of the system is highly dependent on the transient state. For example, in drinking water or wastewater treatment, biofilters are widely used to remove to dissolved and suspended matters. The excess accumulation of biomass or abiotic particles can influence the headloss of biofilter or the quality of treated water. To maintain the biofilter's performance, proper backwashing is applied at the end of each cycle of the biofilter to remove the excess mass. Therefore, the steady-state is never reached in the operating biofilter. Instead, the performance of biofilter is evaluated under the transient-state. However, simulating transient-state of the biofilter is one of the most challenging tasks that many attempts have been carried out but the satisfaction is not obtained (Taylor and Jaffe, 1990; Ham et al., 2007; Brovelli et al., 2009). The difficulty underlies the complex evolution of biological and physiochemical processes.

1.2 Coupling biofilm growth with solute transport in porous media.

Biofilm development in porous media is a process that couples fluid flow, solute transport and biological reactions. On one hand, biomass growth, decay and biomass attachment/detachment modify local pore space. So as porous media structure is changed, fluid flow pattern is changed also. On the other hand, fluid flow governs the transport of different solutes that are needed for biofilm growth, as well as the shear stress applying on biofilm. In the feedback, fluid flow influences biofilm structure, morphology, and its distribution inside porous media.

The interdependency of biofilm and fluid flow establishes the two main characteristics of solute transport in porous media: the involvement of multi-scale processes and the heterogeneity of systems. The multi-scale processes herein mainly refer to multi-spatial scales which biofilm activity at pore scale of few micro meters interacts to global

hydraulics at porous media scale of few meters or larger **(Figure 1.1).** Moreover, the interaction is very complex due to the heterogeneous structure of biofilm. It is well known that biofilm is highly stratified and contains a network of voids and spaces (Zhang and Bishop, 1994; Lewandowski, 2000). The main part of biofilm-EPS which determines the function of biofilm is highly variable. It depends not only on biofilm age but also nutrient and aquatic conditions (Leriche et al., 2000). Besides that, biofilm formation is associated with uncontrolled processes. For example, the diversity or initial seeding of biofilm were reported to be related to stochastic processes (Baty et al., 2000; Bohn et al., 2007) so that the same biofilm structures were not secured in the experiments under identical conditions.

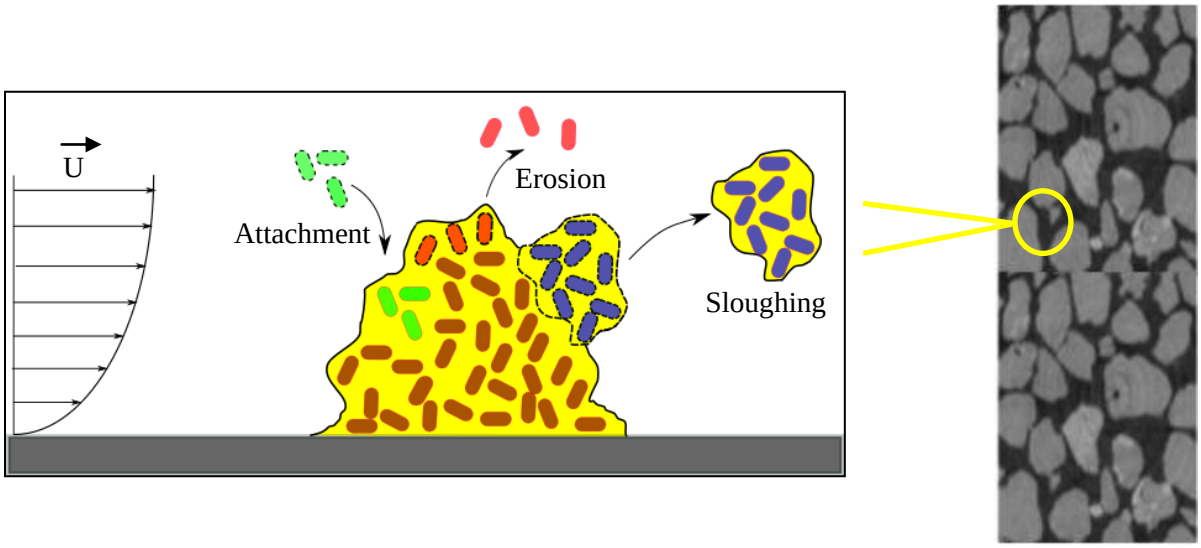

Figure 1.1: Schematic illustration of biofilm growth at pore-scale in porous media

1.3 Problematic statement in studying processes in porous media

1.3.1 Experimental system

In order to better understand the complicated processes occuring in porous media, experiments have been performed either at macro-scale or biofilm scale. In the experiments at porous media scale (Taylor et al., 1990; Karrabi et al., 2011; Rubol et al., 2014; Proto et al., 2016), the solute concentration, biofilm volumetric fraction and global

permeability usually are the indicators to evaluate hydraulic conditions in porous media. However, macro-scale experiment may not be enough to elucidate the underlying mechanisms of the coupling in porous media. One of the limits of macro-scale experiment is that information at pore scale is hardly accessible. The experimental data from macro-scale experiments usually are the result rather than the root of the interactions of solute transport, biofilm growth and hydrodynamic conditions.

Micro-scale experiments are designed to overcome this limit. Studying biofilm in the microfluidics device permits to obtain biofilm information at cell-scale (Davit et al., 2011; Lecuyer et al., 2011). Although micro-scale experiments may unveil the main source for the interaction of biofilm and hydrodynamic condition at cell-scale, the translation this data to the operational application has not been well addressed (Golfier et al., 2009; Orgogozo et al., 2010).

1.3.2 Numerical model

Concerning the limits of the experimental system, numerical models are considered as an alternative solution that can be used independently or with the accompanying of experimental data. The flexibility of numerical model in producing scenarios by changing a set of input parameters provides a convenience in studying multi-processes in porous media (Taylor and Jaffe, 1991; Kildsgaard and Engesgaard, 2001; Brovelli et al., 2009). Theoretically, the multi-scale problem can be solved by direct numerical simulation. At pore scale, Navier-Stokes equation can be used to describe the physic state of fluid flow and mass of solutes is obtained by solving diffusion-advection-reactions equations. However, this approach requires an extremely high computer cost that is not feasible for field-scale applications.

Macroscopic model is proposed in the demand of working with operational scale with the current computer capacity. This type of model should not only be complex enough to capture the prevailing processes that govern the global change of hydrodynamic condition but also simple for field scale application. For example, conventional

macroscopic model considers biofilm as impermeable, and biofilm growth rate is taken as the average value of bacteria growth rate and EPS growth rate. Biomass attachment follows the framework of classical filtration theory which is applied to colloid motion although this theory may not suitable for living organisms. In biomass detachment, sloughing is usually neglected or merged to erosion process to characterize biofilm detachment.

Recent studies have attempted to describe processes involved in porous media closer to their physical nature to increase the capacity of the predicting of macroscopic model. Ebigbo et al. (2010) accounted biofilm porosity for the secondary pathway of solute transport that contribute to global hydraulic change. Bohn et al. (2007) regarded biomass sloughing as an important mechanism to detach biofilm. Torkzaban et al. (2007) developed a framework to combine thermodynamics and hydrodynamics to estimate bacteria attachment. Stewart and Kim (2004) accounted bacteria and EPS activities in biofilm development. However, as mentioned above, solute transport in porous media involves in many poorly understood processes that their mathematical expressions contain lots of empirical parameters or relate to unavailable data, which can influence the performance of the model, especially for the plausibly temporal and spatial prediction.

1.4 Outline of thesis

The thesis is organized in 07 chapters to address the issue of macroscopic numerical modeling of solute transport coupling with biofilm growth in porous media. At the beginning of the manuscripts, chapter 1 presents the context of our work with the general introduction of (i) the important application of solute transport coupling with biofilm growth in porous media. (ii) the issue of experimental study and (iii) the role and issue of numerical study.

Chapter 2 is dedicated to a literature survey about biofilm in porous media with the focus on experimental evidence and modeling issues. This chapter discusses the challenge about the mathematical formalism required to describe the prevailing processes: permeability reduction, biomass attachment, biofilm detachment. The choice of these

processes comes with the analysis of different modeling approach and the recent advances gathered about coupling biofilm in porous media. Then, we present the issue in the macroscopic model and from the above reviews, the objectives of the thesis are given at the end of chapter 2.

Chapter 3 presents our effort to develop a model to estimate bioclogging in porous media. The introduction of permeability reduction and the issue of the existing models is provided at the beginning of the chapter. Then, the model is mathematical derived and validated by a wide range of documented experimental data.

Chapter 4 is assigned for initial biomass attachment. The chapter starts with an overview of the application of classical filtration theory (CFT) in estimating initial biomass attachment in both analytical and semi-empirical solutions. New correlation equation with new dimensionless parameters is then introduced.

Chapter 5 is dedicated to the one dimensional macroscopic modeling of solute transport coupled with biofilm growth in porous media. The improvements made in chapter 3 and chapter 4 are incorporated in the model. The model performances are tested on data gathered from experimental results available in literature.

Chapter 6 presents the attempt to account for biofilm sloughing in a macroscopic model. The new approach that applies a stochastic, discrete process to describe biofilm sloughing is given in this chapter. Then a documented experimental data is applied to valid the numerical work.

At the end of the manuscripts, the conclusion and perspectives of the study are given in chapter 7.

Chapter 2

Biofilm in porous media, experimental evidences and modeling issues

Considering the important application in nature and engineering systems, solute transport in porous media coupled with biofilm development has been rigorously investigated.Those studies cover a wide range of laboratory experiments and numerical models, at both microscale and macroscale.

A porous media colonization by a biofilm follow different steps which can be summarized as follow. The first stage results in the primary adhesion of planktonic bacteria transported with the flow. The second stage results from the growth of these adhered microorganisms (using nutrient brought by the flow and transferred to the microorganisms) giving rise to micro-colonies on the surface then to more complex structures ranging from a more or less continuous biofilm on the surface to plugs which can make bridge between grains or obstruct pore throats. The biofilm development and its interaction with the modified local flow leads to detachment of fragments or individual cells that can colonize other parts of the system. The system is strongly coupled as there is a retroaction between the biofilm development and the modified flow structures (that affects mass transfer, local shear)

For the field-scale application, macroscopic models are considered as a flexible tool to study the interaction of solute transport, biofilm growth and flow rate in porous media. However, it is questionable that whether a macroscopic model is sophisticated enough to capture the complicated processes that occur in porous media given their strongly coupled characteristics, but also simple enough to be applied in a field-scale system?

This chapter aims to briefly present the main feature of the coupling between biofilm growth and hydrodynamic conditions in porous media and the ensuing issues in terms of modeling through a macroscopic approach perspective. More detailed litterature will be developed later in each dedicated chapter concerning specific points addressed in this thesis.

The first part of this chapter is then first devoted to experimental evidence obtained about those coupling. As it will be seen various processes are in play, at various scales, and a question arises about their relative importance on the behavior of the system at the macroscale.

In a second part, we present the main strategies and issues for modeling those systems, (still remaining in the frame of this macroscale approach) and how the various couplings highlighted from the experiment have been more or less successfully taken into account in the models.

List of symbol

Symbol	Unit	Definition
Basic notation		
B	-	Number of bacterial cells in the medium
B	s^{-1}	Mortality rate
C_{BAP}	kgm^{-3}	BAP concentration
C_{ea}	kgm^{-3}	Electron acceptor concentration
Cm	kgm^{-3}	Suspended biomass concentration
Cs	kgm^{-3}	Solute concentration
C_{si}	kgm^{-3}	concentration of substrate *i* in the culture medium
C_{UAP}	kgm^{-3}	UAP concentration
C_b	kgm^{-3}	Active biomass concentration
D_{disp}^{eff}	m^2s^{-1}	Effective longitudinal dispersion coefficient
D_{disp}	m^2s^{-1}	Longitudinal dispersion coefficient
dg	m	Grain diameter
dp	m	Bacterial cell diameter
h	m	Hydraulic load
k	m	Longitudal dispersivity
K	m^2	Permeability of porous media
K_{ij}	m^2	Hydraulic conductivity tensor

K_s	kgm^{-3}	Saturation constant for the substrate
K_{ea}	kgm^{-3}	Saturation constant for electron acceptor
K_{si}	kgm^{-3}	Saturation constant for the substrate *i*
katt	-	Attachment coefficient
k_{det}	-	Detachment coefficient
k_{dec}	s^{-1}	Decay rate of biomass
k_{EPS}	-	EPS formation efficient
k_{UAP}	-	UAP formation efficient
L	m	Length of porous media
L_f	m	Biofilm thickness
L_x	m	Biofilm thickness in pore
l_{ij}	m	Tube length
q_i	m^3s^{-1}	i_{th} component of the specific flow vector
q_{ij}	m^3s^{-1}	Flow in a capillary between two nodes i and j
r_0	m	Initial pore radius
Ra	$kgm^{-3}s^{-1}$	Biomass attachment rate
r_{BAP}	s^{-1}	Specific BAP utilization rate
r_{det}	s^{-1}	Specific detachment rate
r_{ij}	m	Corresponding radius
r_{UAP}	s^{-1}	Specific UAP utilization rate
r_s	s^{-1}	Specific substrate utilization rate
r_x	s^{-1}	Specific biomass growth rate
t	s	Time
U	ms^{-1}	Approaching velocity
u	ms^{-1}	Pore velocity
X_a	kgm^{-3}	Concentration of suspended biomass
X_s	-	Volumetric fraction of biofilm
ΔP	Pa	Pressure loss
ΔP_{ij}	Pa	Pressure loss between the node i and j
Greek letters		
α_{att}	-	Attachment probability
$\emptyset$	-	Porosity
$\emptyset_0$	-	Clean-bed porosity
$\emptyset_a$	-	Porosity of continuum a
$\emptyset_b$	-	Porosity of continuum b
$\in$	-	Biofilm porosity
μ_b	$kgm^{-3}s^{-1}$	Viscosity of fluid in biofilm
μ_l	$kgm^{-3}s^{-1}$	Fluid dynamic viscosity
μ	s^{-1}	Bacterial growth rate

μ_{max}	s^{-1}	Maximum growth rate
η	-	Limiting growth function
η_0	-	Contacting probability
ρ_b	kgm^{-3}	Biomass density
ρ_{bulk}	kgm^{-3}	Bulk density
τ	Pa	Shear stress

2.1 Laboratory experiments

2.1.1 Macroscale experiments

To study solute transport in porous media and its coupling with biofilm growth, macro-scale experiments are widely used to resemble industrial processes as closely as possible. The experimented setup can be packed column for 1D systems (Taylor et Jaffe, 1990a; Cuningham et al., 1991; Vandevivere and Baveye, 1992; Bielefeldt et al., 2002; Seifert and Engesgaard, 2007; Hand et al., 2008; Karrabi et al., 2011; Rolland du Roscoat et al., 2014; Proto et al., 2016) or packed box for 2D systems (Kildsgaard and Engesgaard, 2002; Thullner et al., 2004, Sharp et al., 2005; Seki et al., 2006; Rubol et al., 2014) to investigate the interactions of solution concentration, biofilm growth and hydrodynamics (**Figure 2.1**). One of the advantages of macro-scale experiments is the possibility to observe the global behaviors of porous media and associated quantities, i.e. solute concentration, hydraulic conductivity of porous media as well as dispersivity. However, the information on biofilm (thickness density, composition...), the key factors for the processes in porous media is not easily accessible in macro-scale experiments. Many attempts have been carried out to obtain biofilm information, such as biofilm thickness (Taylor and Jaffe, 1990; Cunningham et al., 1991; Wanner et al., 1995), biofilm mass (Bielefeldt et al., 2001; Karrabi et al., 2011; Rolland du Roscoat et al., 2014); extracellular polymeric substances (Rubol et al., 2014), biofilm morphology (Hand et al., 2008). Nevertheless, such information on biofilm may not be enough to interpret the underlying mechanisms of the behavioral modification of porous media.

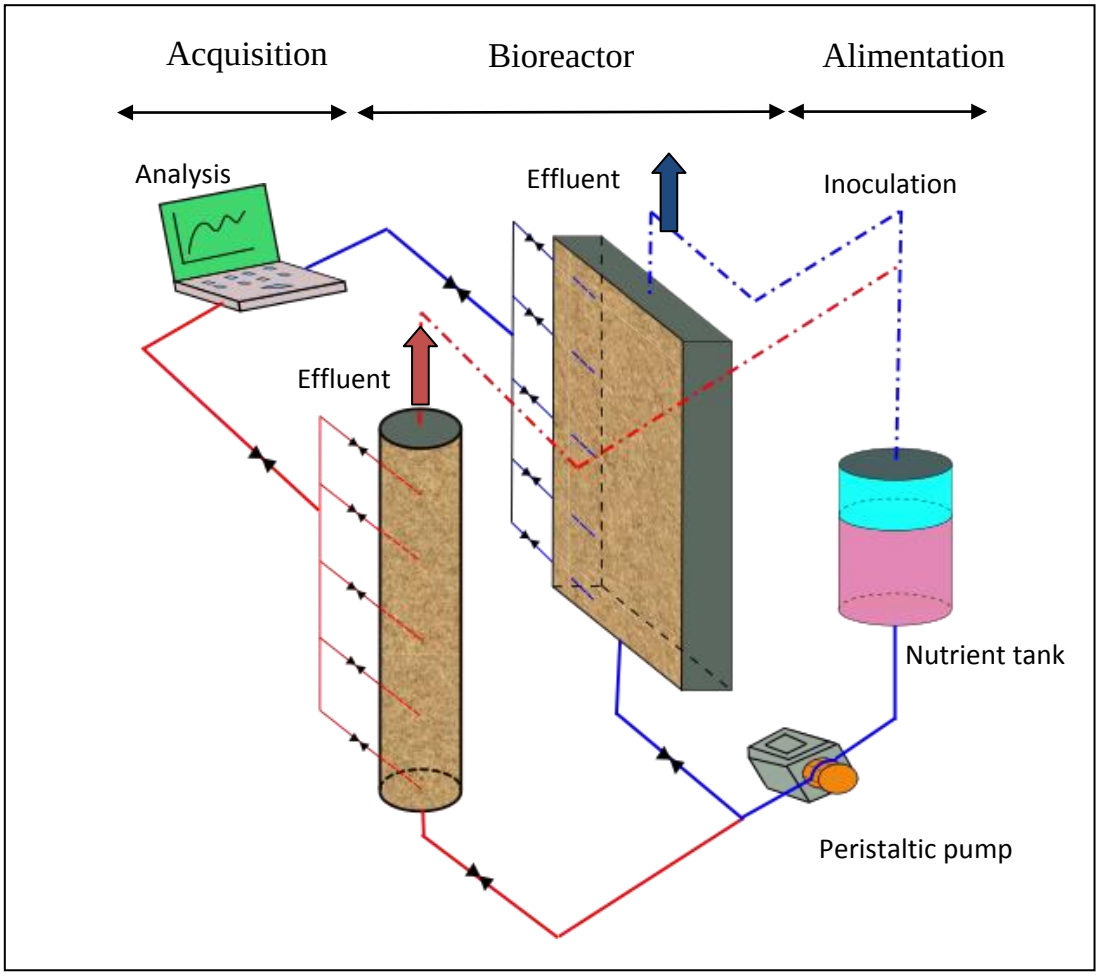

Figure 2.1: Schematic of experiment set up for 1 D or 2D investigation of bioclogging in porous media. Alimentation component suplied nutrients in seeding process and for biofilm growth in bioreactor. Bioreactor, the main component of experiment system, is the place where all the interactions occur. Bioreactor can be packed column or box for 1D or 2D study. Experimental data is obtained in acquisition component. The red line and blue line present fluid flow for column or plate-box experiment, respectively. The dash lines (---) present inoculation process at seeding stage.

Among all the parameters affecting the flow in the porous media, permeability (or hydraulic conductivity) was the most studied parameter as it is one of the main macroscopic parameters which highlights the effect of biofilm growth on the system behavior. It is also a parameter which can be relatively simple to measure. Results of (Shaw et al., 1985) using the volumetric fraction of dead and live bacteria in pore clearly indicate that the effect of living bacteria on the porous media permeability is quite

different as the effect observed for dead bacteria **(Figure 2.2).** The pore volume in **Figure 2.2** is another way to represents time using the multiples of the pore volume which flowed through the column

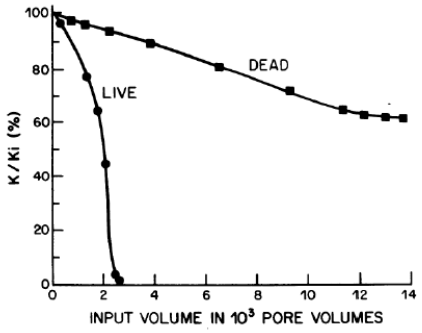

Figure 2.2: The effect of dead cells and live cells on permeability reduction in porous media (Shaw et al.1985)

The mechanisms of bioclogging seem to be different from those promoted by inert colloïds. Sand column experiments performed by Taylor and Jaffe (1990a) used methanol-utilized bacterias. Two operating conditions were tested in term of substrate concentration S_0 and flowrate Q, namely S_0=7,20 mg/l and Q=13.3 cm^3/min for column 1 and S_0=5,59 mg/l and Q=4,43 cm^3/min for column 2. Their results showed that the biofilm thickness decreased along the column and the steady-state of biofilm thickness was reached after 85 days. However, the permeability pattern of columns appeared different with time in the long-term experiment of 284 days for column 1 and 356 days for column 2 (**Figure 2.3a**). When plotted against the biofilm content (expressed in term of bacterial organic carbon), the permeability seems to be a function of the pore occupation with a maximum saturation value reaching 1/1000 of the initial permeability **(Figure 2.3b).** Karrabi et al. (2011), obtained the same behavior when correlating the relative porosity and the relative permeability (for a different bacterial strain, flow rate and a fixed, high carbon source concentration) with an ultimate permeability reduction by a factor of 10000.

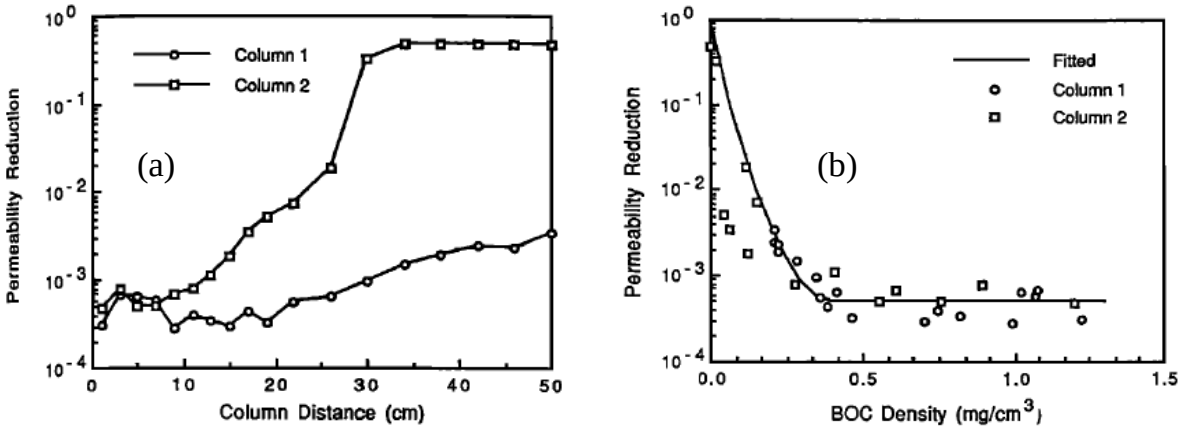

Figure 2.3: (a) permeability reduction at steady-state of column 1 and column 2 and (b) permeability reduction as a function of biomass density (bacterial organic carbon) in the experiments by Taylor and Jaffe, (1990a)

Others experimental results seem, however, to suggest that the biomass content is not the only factor required to explain the permeability reduction as argued by Brovelli et al. (2009). This remark is, for instance, consistent with the report from Bielefeldt et al. (2002) for experiments performed in a sand column with propylene glycol as an electron donor and bacteria were enriched from soil. Although biomass content under low flow rate (8ml/min) was higher than that under high flow rate (12ml/min) in all column heights, permeability reductions at these two flow rate were similar. In these experiments small flow rate of 1.5 ml/min and 3.5 ml/min produced furthermore more severe permeability reduction than the high flow rate of 8ml/min and 12ml/min. The results were contrary to those obtained by Karrabi et al. (2011), in which permeability declined faster under higher flow rate.

The effect of grain sizes on permeability reduction was reported by Cunningham et al. (1991). The pattern of hydraulic conductivity of porous media inoculated by *Pseudomonas aeruginosa* highly depended on grain sizes. Biofilm developed faster in the fine grain size than in the large grain size. The maximum biofilm thickness was 60 µm on 1 mm -glass beads, while the maximum values were 40 µm for 5 mm glass beads and and 10µm for 12 mm-glass beads.

The involvement of biofilm component, such as EPS, was attempted to elucidate the underlying mechanisms of changing the hydraulic conductivity of porous media. Proto et al. (2016) reported that permeability could remain unchanged after two months of starvation condition. It was suggested that EPS was the primary mechanism for permeability reduction and may induce permeability reduction even though substrate was not supplied for existing biofilm.

Although the effect of grain sizes were confirmed by Hand et al. (2008), permeability reduction appeared to correlate better with EPS concentration. Permeability reductions were similar if EPS concentrations produced from columns packed by various grain sizes were not different. Environmental conditions seems also at play : in the aerobic environment, Hand et al. (2008) report that bacteria produced higher EPS amount, driving permeability to decline more drastically than in anaerobic environment **(Figure 2.4).** However, this point may not be agreed by Rubol et al. (2014) : in their experiments, performed on soils, the presence of EPS seemed not to be governed by the presence of either oxic and hypoxic conditions

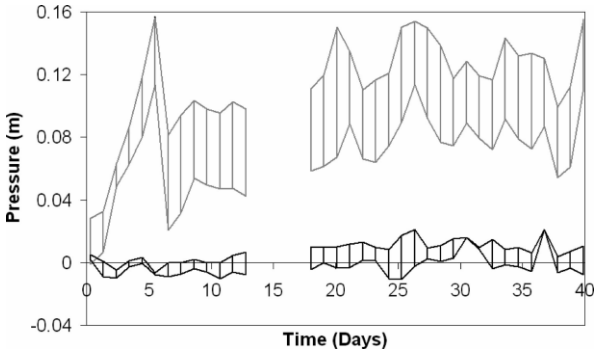

Figure 2.4: The effect of environment on pressure change in porous media. Grey areas indicate the columns of two grain size of 250–355 and 500–710 μm under aerobic conditions. Black areas present the columns of grain size of 500–710 μm under anaerobic conditions (Hand et al., 2008).

The prevalence of the role of EPS is anyway still unclear. For instance, Baveye et Vandevivere (1992) performed permeability reduction measurement on sand columns with four different bacteria strains. Among the four bacterial strains tested, one formed a capsule, one produced slime layers, and two did not produce any detectable exopolymers. The last two strains were nonmucoid variants of the first two. Those authors observed

that only one strain (namely, the slime producer) had a large impact on the column permeability. The production of exopolymers had no effect on either cell multiplication within the sand columns or cell movement through the sand columns. Therefore, the hydraulic conductivity reduction observed with the slime producer was tentatively attributed to the obstruction of flow channels with slime.

The same difficulties to define clear trends between experiments have also been encountered on other global parameters such as the dispersion. Experiments were indeed conducted on the effect of the biofilm growth on the longitudinal dispersion coefficient D_{disp} or dispersivity $k=D_{disp}/u$, where u is the pore velocity.

For instance, Bielefeldt et al. (2002), performed experiments with two differents substrates (decane and naphthalene). With decane, they observed that the dispersivity increased whereas the hydraulic conductivity decreased. However, they found an opposite behavior for naphthalene. In both cases, the changes were of one order of magnitude. Bielefeldt at al. (2002) stated that these different behaviors were due to the different biofilm structures obtained with decane or naphthalene, and were also dependent on the biofilm "age". With naphthalene, the biofilm was postulated to be discontinuous. The biomass accumulation at the pore throats led to preferential path creation at the beginning of the experiment and the permeability decrease came along an increase of the dispersivity. When the biofilm is "older", the biomass distribution becomes more homogeneous in the column and, according to their results, the dispersivity begins to decrease. So their curves ’dispersivity versus permeability’ depend on the period when the sampling was performed.

Harleman et al. (1963) found that the dispersivity increases with permeability following a power law. Bear (1972) showed instead that dispersivity could vary inversely with the square of permeability. The first result then shows that dispersivity decreases with biofilm accumulation whereas the second result shows that the dispersivity increases with the biofilm accumulation.

Taylor and Jaffé (1990a) have made experiments in a column (diameter=5.08 cm, length=52 cm) filled with 0.07 cm sand particles. They have measured dispersivity value in the presence of biofilms which is 100 to 1000 times the value encountered in the clean column. From theoretical consideration on a simple porous media geometry, they developed a model which correlate the dispersivity and the ratio between the biofilm thickness and pore radius. The results show that the dispersivity increases with the biofilm thickness. Kone et al. (2014) performed DTS measurement in a 2D-flow cell packed with a homogeneous media made of silica sand **(Figure 2.5a)**. Both the dispersivity and the biofilm volume fraction was estimated through tracer experiments with the Blue Dextran molecule. Their results gave a relatively good agreement with Taylor and Jaffe theory **(Figure 2.5b).**

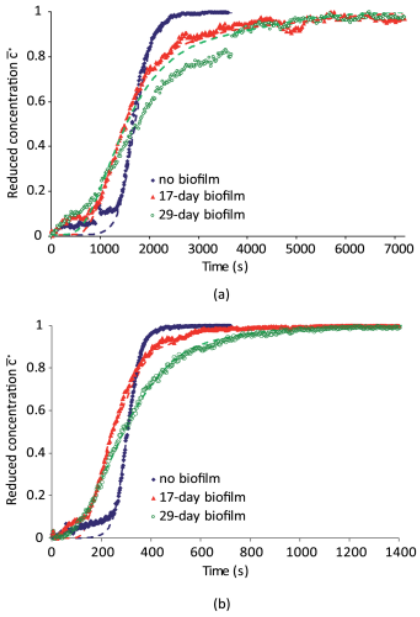

Figure 2.5a Breakthrough curve at different stage of biofilm development (from Kone et al. 2014)

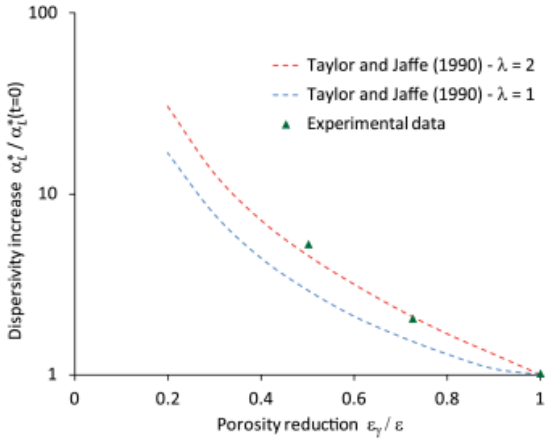

Figure 2.5b: The comparison of the measured dispersivity increase with Taylor and Jaffe theory (from Kone et al. 2014)

Sharp et al. (1999) also reported that dispersivity increases with biofilm growth in a system containing glass beds. This increase was lower compared to the results given by Taylor and Jaffe (1990a). These authors measured an increase of the dispersity "only" in the range of 35 to 300 %.

The initial heterogeneity of the clean porous media is also at play according to Yen (1990). Indeed, areas with high permeability would also correspond to hydraulic preferential paths formation. They constitute selectively clogged area compared to the zone of lower permeability. Therefore, an initial heterogeneous porous media can experience, over time a permeability homogenization in a cross section (with the disappearance of the preferential paths) and a decrease of the dispersivity.

As a conclusion, there is no commonly acknowledged experimental behavior (and consequently theoretical formulations) both for the permeability and dispersivity in a porous media with the presence of biofilms.

Finally, macroscale experiments may not be enough to understand underlying mechanisms of interactions in porous media. The experimental results gathered from the studies about biofilm growth in porous media have been mixed and sometimes reveal contradictions on the behavior of macroscale effective properties such as permeability and dispersivity. It can be explained by the limits of macro-scale experiments. The observations obtained from such experiments are the results rather than the origin of the interactions. Biofilm growth in porous media involves multi-scale processes, in which the reactions at pore-scale and biofilm microstructuration under local flow conditions are the main source of the global behavior of porous media. It is especially true with a biofilm, which is a living system, and as such, is submitted to strongly coupled phenomena involving not only purely mechanical effects due to the local flow (mass transfer, shear rate...) but also the response of a given bacteria strain to external conditions (polymer productions, structures created at the local scale,…) as suggested by the previous results on macroscale experiments. To reach such information, experiments at the biofilm scale are necessary.

2.1.2 Microscale experiments

Microscale experiments are designed to study the behavior of biofilm at cell-scale **(Figure 2.6)**. In microfluidics with device size ranging from 1µm to 1mm (Tabeling,

2003), interactions of biofilm and hydrodynamics conditions at cell-scale can be well studied (**Figure 2.6**).

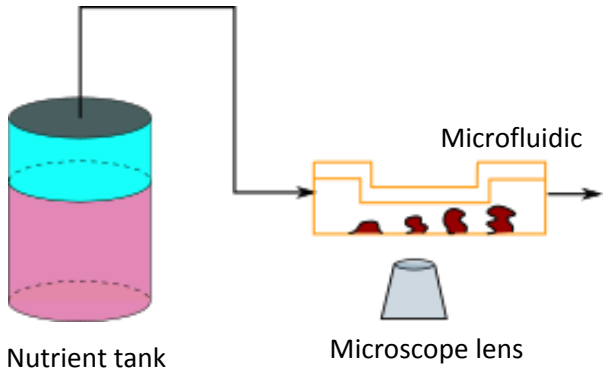

Figure 2. 6: Schematic present of micro-scale experiment to study biofilm at pore-scale

The micro-scale studies have been conducted in wide range of objectives: EPS production (Qi et al., 2008), biofilm composition in terms of number of bacterial cells (Tsai, 2005), or in terms of volumeric fraction of live cells and dead cells (Medeiros, 2016), mass transfer (Vieira et al.,1993, Lopez et al., 2003), morphology (Lemos et al., 2015; Vrouwenvelder et al., 2010), detachment (Stoodley et al., 1999; Walter et al., 2013) bacterial initial attachment (Mbaye, 2011) and biofilm strength (Lemos et al.,2015; Stoodley et al., 2002).

The behavior of the biofilm morphology as a function of the external conditions are a good way to introduce the complexity of interacting processes that microscale experiments highlighted when a biofilm develops. Usually, the hydrodynamic conditions especially, the shear stress was used as the parameter which characterizes the flow near the biofilm interface.

Many authors observed indeed that shear stress had a clear influence on the biofilm morphology (Liu and Tay, 2002; Pereira et al.,2002; Stoodley et al., 1999; Vieira et al., 1993). According to these authors, biofilms are more compact and dense at high shear rate and their structure is less heterogeneous compared to biofilms grown under laminar flow (which develops ‘mushroom”-like structures: **Figures 2.7** and **2.8**). Those

differences were primarily attributed to the detachment process (sloughing and erosion) dependence with the flow conditions. This process affects locally the biofilm interface but also contributes to the cells redistribution on neighboring surfaces after detachment.

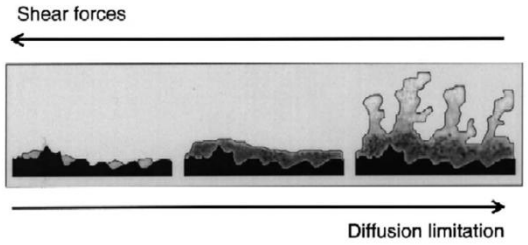

Figure 2.7 : Shematic representation of the interaction between growth and detachment on the biofilm structure (from Van Loodsrecht et al., 2002)

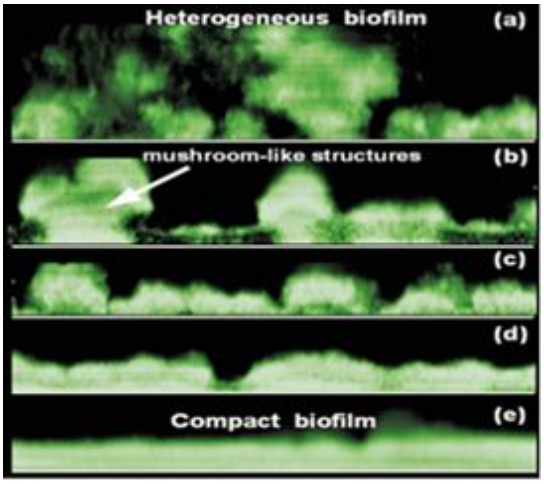

Figure 2.8: Visualization of biofilm morphology for different shear stress conditions τ_w (Picioreanu et van Loosdrecht, Delft University, Pays-Bas. Shear increase from the top image to the bottom.

Another biofilm morphology characteristic, that microscale experiments pointed out, is the existence of filamentous structures called streamer (Drescher et al., 2013;Kim et al., 2010; Rusconi et al., 2010). One extremity of the streamer is generally attached to the surface while the rest of the structure moves freely in the bulk fluid. Those streamers have been mostly observed in turbulent flow conditions (Stoodley et al., 1998;Stoodley et al., 2002a,), although several recent reports have demonstrated streamer formation in low Reynolds number conditions **(**Re <1). **(**Rusconi et al., 2010; Valiei et al., 2012; Yazdi et Ardkani, 2012**)**. Their formation is the result of fluid-structure interaction. At a given stage of the biofilm formation, the difference of pressure between the upstream and downstream front of micro-colonies initiates the formation of a wake. The high shear stresses value due to the turbulent flow causes a streamlined growth as cells divide and multiply. Preferential accumulation occurs and growth of biomass takes place in the downstream section (i.e., in the wake region). Because of the drag force due to the

streamwise pressure drop and the large shear stress, this biomass starts to elongate and forms a streamer. Those structures disrupt the flow and cause dissipation.

These streamers could be involved in the early stage of pressure loss in a porous media colonized by a biofilm. Streamers can create bridges between particles and can catch cells, nutrients, and debris that pass by, leading to clogging and termination of local flow (Drescher et al., 2013). An example of streamer structure produced by bacteria is given in **Figure 2.9**

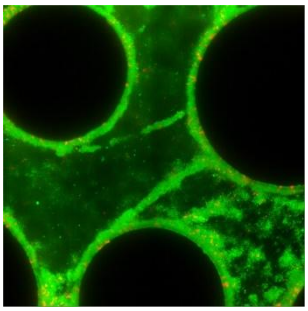

Figure 2.9: Streamers structures produced by wild-type P. aeruginosa PA14 (green) in microflow cell including obstacles (Nadell et al., 2017)

The mechanisms presented above are a first example of the coupling between flow and biofilm structure. As detachment process is involved to explain some features of the biofilm morphology, it raises also the issue about the biofilm resistance or "strength" in regards of its structure and composition, as the EPS matrix gives specific rheological properties to the biofilm.

Many microscale experiments relate the viscoelastic nature of biofilms (Towler et al., 2003; Shaw et al., 2004; Stoodley et al., 1999), although others behavior such as rheofluidification were sometimes reported (Houari et al., 2008). A very wide range of elasticity and viscosity values has been previously observed for various samples of biofilms, either artificial biofilms or biofilms coming from natural aquatic environments (Towler et al., 2003; Vinogradov et al., 2004; Witchurch et al., 2002). Many researches focused on experiments to explain this variability.

For instance, Stoodley et al. (2002) studied biofilms of various *Pseudomonas aeruginosa* strains under laminar and turbulent flows. Their study suggested that biofilms grown under high shear are more strongly adhered and have a stronger EPS matrix than those grown under low shear. Qi et al. (2008) have suggested that the EPS secretion was a physiological response which acts as a protection against the external forces exerted by the fluid. In their experiment, a sudden shear increase on the biofilm leads to a significant EPS production after a period of acclimation. However, as soon as the biofilm reached a new equilibrium state, the EPS secretion decreased to a relatively constant volume. Simoes et al. (2007) reported that their biofilms grown under a turbulent flow generated less EPS than a biofilm grown under laminar conditions. Fish et al. (2017) showed that the temporal hydraulic pattern had an influence on the biofilm structure and composition. In their experiments, great flow variation during growth was associated with increased cell quantity but was inversely related to EPS-to-cell volume ratios and bacterial diversity. Ultimately, biofilms developed under low-varied flow conditions had lowest amounts of biomass and the greatest EPS volumes per cell. Some authors like Lemos et al. (2015) observed that biofilm grown under high shear stress were more resistant to mechanical or a combination of mechanical/chemical impact, but contrary to Qi et al. (2008) they did not notice a direct relationship between the increase of the shear stress and the EPS production.

Those observations led to the wide acceptation that biofilms in differing environments exposed to different hydrodynamic conditions will encounter changes in the structure, composition and then physical properties of their EPS matrix. The relationship between the biofilm mechanical properties and the EPS quantitative content is not straightforward. Classical results coming from polymer studies (an increase in the concentration of a polymer in a gel will increase the gel viscoelasticity, a physical effect that does not depend on polymer chemistry) may be not relevant in the case of biofilms (Gordon et al. 2017).

In a modern view of the biofilm, the stability of the biofilm matrix is indeed dominated by entanglement of EPS and weak physicochemical interactions between different types

of molecules. These interactions give rise to various binding forces such as electrostatic attractive forces, repulsive forces (preventing collapsing), hydrogen bonds, van der Waals interactions and ionic attractive forces (Lembre et al. 2012-**Figure 2.10)**. Active processes such as the involvement of microbial enzymes are also considered, those enzymes allowing the destruction of the exopolymeric matrix and the release of cells that are able to colonize new surfaces. Because of this complexity and variability of the EPS matrix, mechanisms, such as a physical arrangement of polymers as well as regulation processes in response to the external environment (either through the increase of EPS production, which changes in the length of the polymeric chains or through EPS chemical composition, due to the modification of metabolic pathways in response to shear…) were considered to explain biofilm resistance to external stresses, and consequently the different morphologies that were observed.

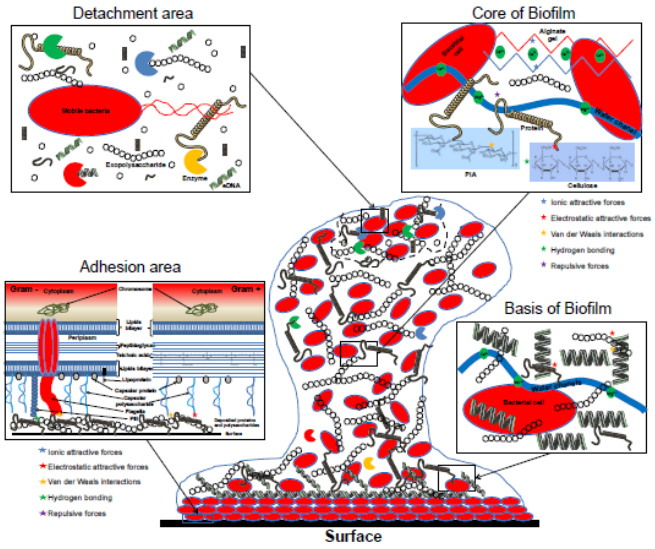

Figure 2.10 Schematic drawing of a mature biofilm (taken from Lembre et al., 2012). The internal cohesion depends on various forces between molecules. The surface adhesion relies on the bacteria strains and its strategy to colonize the surface (secretion of surfactant/EPS...)

Stoodley et al. (2002) suggested that their results on the biofilm properties could be related to the physical arrangement of individual polymer strands in the biofilm EPS matrix. At higher shear, a possible process would be a stretching of the polymer strands which become physically aligned and pulled closer. That would allow a greater chance

for electrostatic interactions and hydrogen bonding (the author made the comparison with a rope whose strength is increased by the spinning together of weak individual fibers).

Studies on *P aeruginosa* biofilm give an example about the influence of the chemical composition of the EPS matrix on biofilm properties: *P.aeruginosa* biofilms feature three known polysaccharides: Psl, Pel, and alginate (Gordon et al. 2017). Kovach et al. (2017) have shown that increasing Pel and alginate production in a *P Aeruginosa* biofilm does not increase the biofilm elasticity whereas increasing Psl production does stiffen biofilms, so that specific matrix components may give rise to specific biofilm mechanics. This means that molecular mechanisms are indeed involved in the mechanical behavior of the biofilm.

So far, we focused on the biofilm structure at the local scale and its relation to biofilm behavior in term of morphology. If we look at the dynamic evolution of the biofilm, the interaction between mechanical, biological and biochemical processes at the microscale is also highlighted by many researchers from the early stage of adhesion till the production of a mature biofilm.

At the early stage of biofilm formation, Mbaye (2011) has pointed out that the increase in initial contact and ionic strength promotes cell adhesion. He also observed the discrete character of the detachment: the detachment takes place when a threshold of constraint is reached. This threshold is characterized by a sharp increase in the amount of cells released (Fig.**2.11**). Concerning the adhesion rate, Lecuyer et al. (2011) observed that an increase in the shear stress results in an increase in the efficiency of the transport of bacteria to the surface accompanied by a decrease in the probability of adhesion to the surface: the number of adherent bacteria is growing exponentially with the shear rate.

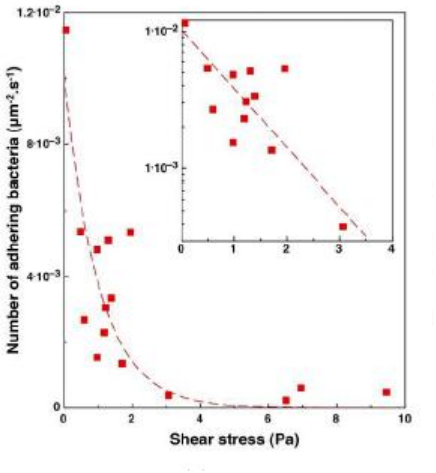

Figure 2.11: Influence of the shear stress on the adhesion of wild-type PA14 on glass surface (Lecuyer et al., 2011)

They also observed that the characteristic residence time of bacteria on the surface before being released, increases approximately linearly with shearing as long as it is below a critical value of about 3 Pa (**Figure 2.11).** Beyond this value, the probability of detachment increases (decrease of the characteristic time). This is related to the threshold effect found by Mbaye (2011). These phenomena can be partially explained by mechanical effect (for instance the increase in the transport efficiency due to the increase of the velocity gradient near the wall and its relation to mechanical forces on the bacteria as in suspensions). However, at this stage, biological phenomena exist: in particular, the adhesion of planktonic (suspended) bacteria to a surface comes along a change of bacteria phenotype and genotype (Liu and Tay, 2001) as well as different strategies to colonize the surface : in the area of contact between bacteria and surface, the microbial cells can interact with the surface via several protein and polysaccharide appendages (pili, flagella, LPS, capsular polysaccharides) depending on the type of bacteria as well as their phenotype (**Figure 2.10**)

The biofilm development itself involves the reproduction of bacteria, which depends among other processes, on nutrient availability. Mbaye et al. (2013) conducted experiments on the growth of adhered cell on a surface in flow chamber using P. Putida as bacteria strain, in condition where nutrient is not a limiting factor. He observed the

dependency of the maximum growth kinetic parameter on the hydrodynamic condition, with the characteristic bacteria division time decreasing with the increase of flow shear stress **(Figure 2.12**). The measured kinetic parameter was also different of the corresponding value for the planktonic strain, raising the issue of using growth kinetics measured in batch experiment to characterize the intrinsic growth of adhered bacteria cells.

For more mature biofilm, the characteristic time governing the bacteria multiplication depends also on different factors. On the mechanical point of view, the biofilm morphology changes presented above were correlated with mass transfer processes modification by some authors. Vieira et al. (1993) as well as Lopez et al. (2003) noted that, in turbulent condition, the shear increase led to a decrease of the internal diffusion within the biofilm, that influence the nutrients transport toward the bacterial cell. This seems consistent with the morphology changes discussed previously (namely thicker and denser biofilm with a stronger internal cohesion of the biofilm component as the shear stress increase) and diffusivity was often correlated with biofilm dry density (Melo, 2005). No clear trends were observable for biofilm grown in laminar conditions however (Melo, 2005). That author proposed tortuosity as a more relevant concept to describe mass transfer inside biofilm matrices in relation to its internal structure, and also includes the effect of dry biomass density.

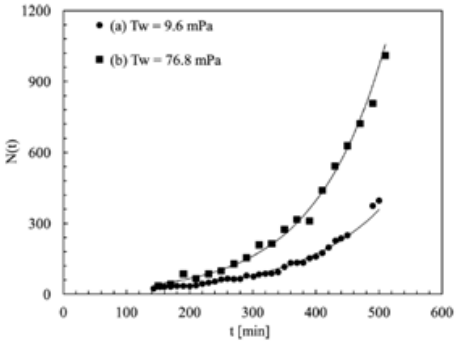

Figure 2.12: Growth kinetics of P.putida on glass surface under different flow shear stress (Mbaye et al., 2013)

The discovery of “stealth swimmers”, a subpopulation of microorganisms inside the biofilm which maintain the motility phenotype, highlighted some biological mechanisms leading to this internal structure, change of tortuosity and its link with nutrient transport and biofilm diffusive properties. Indeed, although they constitute only 0.1–1% of the cells, these kinds of bacteria impact the nutrient diffusion by tunneling into the biofilm structure (Karimi et al., 2015).

On a more general point of view, it is now acknowledged that the dynamic behavior of bacterial community within biofilm is related to biochemical regulation processes. For instance, by performing respirometric measurements, Simoes et al. (2007) note that the decrease of EPS production observed in turbulent conditions comes along a diminution of the cell metabolic activity. However, despite this lower microbial activity, the biofilm global activity was greater in turbulent conditions as the cellular density (number of cell/cm^2) and the mass of cells per unit surface was greater.

These regulation processes would be promoted by specific molecules (autoinducers) which trigger some functions. This regulation may come from either a sensing of the local population density or a sensing of the local environmental properties (i.e the regulation process is sensitive to the local diffusion rate through the local accumulation of the autoinducer around the bacteria cell).

For the former point of view, the autoinducer molecule allows inter-cellular communication *(quorum sensing)*. Quorum sensing is based on the production of a signal molecule (synthase), a signal receptor in the bacteria as well as a gene regulatory circuit which controls the production of the signal and receptor. An example of such signal molecule is acylhomerosine lactone (AHL) which is common to many gram negative bacteria (such as *Pseudomonas putida*). These molecules can diffuse through the bacteria membrane to reach the specific receptor. Each cell produces a basal level of AHL. When the population is high enough (thus the name “quorum” sensing), AHL concentrations within the cell reaches a threshold that activates target genes. The new expression of some genes leads then to the activation of different functions.

Whether the regulation comes from a diffusion limited process or a real inter-cellular communication was questioned (Redfield et al., 2002), but most studies at the biofilm scale rely on quorum sensing.

For instance according to Liu and Tay (2000, 2001), one important process regulated by cell to cell communication is the secretion of EPS. However quorum sensing is involved in a wide range of mechanisms such as the regulation of surfactant secretion. The controlled secretion of surfactants directs the formation of mature biofilm structures as well as biofilm detachment. In the case of *P.aeruginosa* for instance, quorum sensing would control secretion of a molecule which is associated with the formation of channel structures that facilitate nutrient exchange within the biofilm (Diggle et al., 2003) but also mediate biofilm detachment. Using different *P. aeruginosa* strain, Drescher et al. (2013) showed how quorum sensing would determine cell phenotypes and would induce the formation of streamers.

Whatever the mechanism (diffusion-limited or quorum sensing), the regulation process involves transport of molecular signals between cells or in the local environment of a cell. The regulation dynamics is thus coupled with the local hydrodynamics conditions but also with the micro-environment properties (Karimi et al., 2015). This could explain the variability of biofilm observed not only under different flow conditions, but also different nature or concentration of nutrients.

2.1.3 Partial conclusions

There were a lot of experiments on biofilms, both at macroscale and microscale. These experiments highlight the strong coupling between various processes occurring at local scale and affecting the macroscale behaviors of the systems. For instance, in the field of porous media, some processes (such as biomass attachment and detachment, EPS production, biomass activity and replication) are crucial to understand how the overall biomass distribution evolves within the system and how it affects related phenomena such as clogging and preferential path creation. These processes come directly from complex coupling at the biofilm and bacteria cell scale.

The fact is that a lot of progress is still required on the knowledge of biofilm behavior at the local scale to fully understand how the biofilm distribution develops at the porous media scale. Indeed, at first sight a biofilm appears as a gel-like material with a strong coupling with the hydrodynamic that affects its local structure and composition. Some of this coupling can be investigated through classical mechanics approaches (for instance the biofilm morphology, which relies on biofilm resistance to external hydrodynamic forces due to its rheological properties). Some change in the physical properties can be also related to purely mechanical effects (such as polymers strand reorganization under physical stress). But, biofilms are also living material, they are able to grow and modify their internal structure in order to adapt to the operating conditions. That may explain contradictory results between experiments either at the micro or macroscale. The question is how to translate these data into the operational application.

2.2 Numerical investigation

The above paragraphs show that modeling the development of a biofilm in a porous media required to address mechanisms that can be difficult to translate simply in terms of relation between averaged macroscale parameters. It is especially true for mechanisms that somewhat are the expression of a biological and biochemical response of the biofilm to an external mechanical and/or environmental stress. One example is the biofilm "growth kinetics" which involved many interacting processes (division of the bacteria themselves, but also secretion of a more or less resistant polymer matrix).

Finding unified generalized constitutive law that can account for biofilm properties and their evolution with time, that are based on few representative parameters, is a great challenge. This is nevertheless a key issue in producing operational models for engineering purpose. Various attempted have been made to take up this challenge through numerical simulation.

2.2.1 Constitutive laws

Whatever the strategy adopted to write models accounting for biofilm development in porous media, it is required to write equations describing the biofilm development, and

that must account for some biofilm-specific features. These features include kinetic terms (namely the kinetic of “growth” and "decay" of bacteria within the biofilm) as well as other processes such as bacteria/biofilm attachment or detachment under the effect of the flow. Section 2.1 showed that those terms could be difficult to express simply as they are the expression of a biological and biochemical response of the biofilm to an external mechanical and/or environmental stress.

The objective of this paragraph consists in presenting briefly classical formulations of these terms encountered in many models. A discussion of these model will be made and hint for possible improvement presented in paragraph 2.3 and 2.4.

2.2.1.1 Permeability reduction

Permeability reduction is an important parameter to determine the capacity of conveying fluid flow media, and is mathematically expressed following Darcy‘s law

$$U = -\frac{K}{\mu}\frac{\Delta P}{L} \qquad (2.1)$$

Where U is the approaching velocity (ms^{-1}), K is the permeability of porous media (m^2), ΔP is the pressure loss (Pa), μ is the dynamic viscosity ($kgm^{-1}s^{-1}$) and L is the length of porous media (m).

It is observed that biomass buildup in porous media drives the decrease of porosity, reducing permeability. Hence, the relationship between porosity and permeability have been the objective of many attempts to develop permeability models. The detail presentation can be found in chapter 3, where existing permeability models are analyzed and a new model are mathematically derived with the validation of documented experimental data.

2.2.1.2 Biomass growth rate

Biomass growth occurs in both solid or liquid medium. The growth kinetics is classically divided into several distinct phases: lag phase, exponential phase, stationary phase, decline phase and the dynamics of bacterial growth is frequently modeled as:

$$\frac{dC_b}{dt} = (\mu - b)C_b \qquad (2.2)$$

C_b is the biomass concentration or the number of bacterial cells in the medium, μ [s^{-1}] is the growth rate, b the mortality rate [s^{-1}], and t is the time [s].

In this equation, the mortality rate b is often described by a constant and we will focus on growth that depends on external conditions. In the general case, the growth rate (μ) is not constant and depends on the physicochemical conditions, in particular, different substrates which limit or inhibit the growth. One of the most used formulations is the Monod law that writes:

$$\mu = \mu_{max} \prod \frac{C_{Si}}{K_{Si}+C_{Si}} \qquad (2.3)$$

Where C_{Si} is the concentration of substrate i in the culture medium, K_{Si}, the saturation constant for the substrate i , μ_{max} the maximum growth rate. The expression is simplified if for any element i, the C_{Si} concentration is much greater than K_{Si} , then μ tends toward 1. In that case, C_{Si} does not intervene in the growth rate. Otherwise, growth is slowed down if C_{Si} is less than or of the same order of magnitude as K_{Si}. The substrate i is then said to be limiting.

It is noted that Monod equation was formulated to characterize the growth rate of bacterial cells in batch conditions. The use of this equation to model biofilm growth in conventional models may not be enough to describe the development of different components in the biofilm such as EPS (S_{BAP} + X_{EPS}).

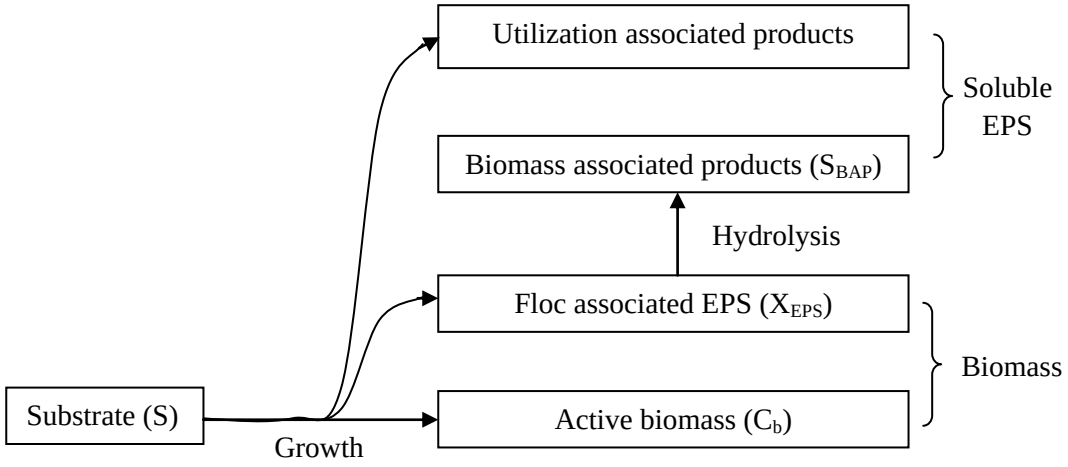

Figure 2.13 Schematic presentation of the formation of biomass (active biomass and floc associated EPS) (Menniti et al., 2009)

In the recent studies about biofilm modeling, active biomass has been modeled separately from EPS and inert substances (Nielsen et al., 1997; Laspidou and Ritmann, 2002, 2004; Alpkvist et al., 2006). The formation of active biomass is related to the synthesis of substrate, utilization-associated products (UAP), biomass-associated products (BAP) (Menniti et al., 2009-**Figure 2.13**)

$$r_x C_b = r_S(1 - k_{UAP} - k_{EPS})C_S + r_{UAP}C_{UAP} + r_{BAP}C_{BAP} \quad (2.4)$$

where C_b is the active biomass concentration (kg/m^3). r_x is the specific biomass growth rate (s^{-1}). r_S , r_{BAP} , r_{UAP} is the specific substrate utilization rate (s^{-1}), specific UAP utilization rate (s^{-1}) and specific BAP utilization rate (s^{-1}), respectively. k_{UAP} is UAP formation coefficient (-) and k_{EPS} is EPS formation coefficient (-).

The first term of the right-hand side of equation expresses the division of electron donor source. The substrate is used not only for the synthesis of active biomass but also for the synthesis of UAP and EPS. This description of biofilm seems close to its nature but, in macro scale systems, the application of the equation is still not common. The most challenging issue is to address the availability of data required for the computation of the conversion from substrate to BAP and EPS, or from UAP, BAP to active biomass. Furthermore, EPS is mainly composed of protein, polysaccharides, humic acid and DNA.

The distribution of these components in EPS is dependent on many factors such as C/N ratio, shear stress... (Flemming and Wingender, 2010). Hence, using average values for the coefficients in Eq (2.4) may not be enough for EPS descriptions.

2.2.1.3 Biomass attachment

Biomass attachment, which is a reverse process of detachment, is defined as a mass transfer process of biomass from the liquid phase to solid biofilm phase. Together with detachment, biomass attachment is very important for biofilm accumulation and removal of suspended biomass. However, biomass attachment is still poorly understood. Currently, the process of suspended biomass captured on solid biofilm is modeled as in filtration theory for colloids deposition on a solid surface.

The attachment rate in the transport equation is modeled as a function of the first order of suspended biomass concentration:

$$R_a = k_{att} \emptyset C_m \qquad (2.5)$$

where C_m is suspended biomass concentration ($kg.m^{-3}$), k_{att} is attachment coefficient which is often assumed to be constant (Taylor and Jaffe, 1990b)

In the case of biofilm developed in porous media, the attachment coefficient is based on more physical consideration by applying deep filtration theory in most of the studies (Clement et al., 1996; Kildsgaard and Engesgaard, 2002; Thullner et al., 2004; Tufenkji, 2007). The attachment rate is linearly proportional to pore velocity, contact probability and attachment probability (Harvey and Garabedian, 1991; Anders and Chrysikopoulos, 2005; Scheibe et al., 2007)

$$k_{att} = \frac{3(1-\emptyset)u}{2d_g\emptyset}\eta_0\alpha_{att} \qquad (2.6)$$

where η_0 is the contacting probability and α_{att} is the attachment probability. u is the pore velocity (ms^{-1}) defined as: $u = \frac{U}{\emptyset}$ (2.7)

Contact probability:

Contact probability is defined as the ratio of the number of colloids contacting the collector to the total number of colloids approaching the collector. Generally, there are three modes that drive colloids to contact to the collector: interception, sediment and diffusion. A schematic presentation of particle contact to collector surface is presented in **Figure 2.14.** There are many studies that have been carried out for the calculation of contact probability. The equation proposed by (Tufenkji and Elimelech, 2004) that is the most widely used. This equation resulted from the numerical simulation of convective−diffusive equation following Eulerian approach and collector was treated by the application of Happel's model (the detail of Happel's model is given in chapter 4).

Attachment probability

Attachment probability is defined as the ratio of a number of successfully attached colloids to a total number of colloids contacting to the collector. The estimation of attachment probability in both analytical solution and empirical equations is based on the classical DLVO theory of colloidal stability, which considers two interaction forces: (i) van der Waals attraction and (ii) electrical double layer forces. Many attempts have been conducted to study attachment probability to seek either an analytical solution or correlation equation but concerning the complicated interaction between particle and collector, the satisfaction is still not reached when comparing computed data and experimental results. The detailed presentation of models or correlations aiming to estimate contacting and attachment probability is given in Chapter 4.

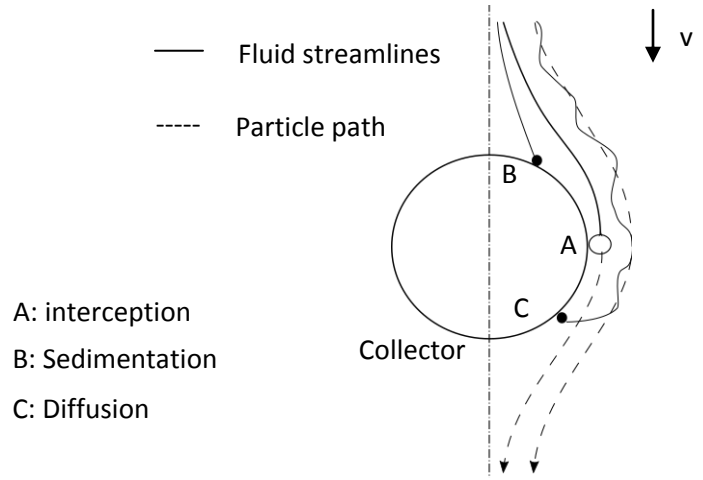

Figure 2. 14: Schematic presentation of particle contact to the collector surface

2.2.1.4 Biofilm detachment

Detachment can be defined as the release of mass from the attached biofilm to fluid phase. Five categories of biofilm detachment have been classified by Bryers (1988): erosion, sloughing, human intervention, grazing and abrasion. While the three last categories are driven by external forces, erosion and sloughing are the consequences of the interaction of internal biofilm processes with shear and normal forces acting on biofilm surface (Stewart, 1993). Erosion is the continuous process that small particles in the range of 10 μm are transferred to the liquid phase. In contrast, sloughing is considered as discontinuous and involves the removal of large particles up to several mm (Horn and Lacker, 2014). The sloughing thus promotes the heterogeneity of biofilms morphology whereas erosion reduces their roughness and makes it smoother and thicker. Erosion and sloughing are considered as the main mechanisms of detachment.

Detachment occurs when the local shear exceeds a certain threshold corresponding to the internal cohesion of the biofilm. Many factors have been reported to be responsible for biofilm detachment but they can generally be divided into two main groups:

(i) Increase of local shear: fluid shear stress (Picioreanu et al., 2001), microbially generated gas bubbles (Ohashi and Harada, 1994);

(ii) Decrease of internal cohesion of biofilm: matrix-degrading enzymes and lytic bacteriophages (Fischetti, 2005; Orgaz et al., 2006), nutrient supply (Stewart, 1993), availability of multivalent cross-linking cations (Chen and Stewart, 2002), and quorum sensing signals (Yarwood et al., 2004).

a) Modeling approach at the biofilm scale

Concerning numerical modeling of biofilm structure and morphology, great efforts have been carried to study biofilm detachment. In modeling work, several approaches have been used to model the detachment.

Hermanowicz (2001) used a stochastic method for the removal of biomass at the biofilm–liquid interface. Detachment occurred with a given probability, defined as a function of overall shear stress and a parameter quantifying biofilm strength.

Picioreanu et al. (2001) assumed the biofilm structure to be an elastic material; detachment occurred when stresses exceeded the local strength of the biofilm according to the von Mises yield criterion. A modeling framework, which was based on individual based modelling (IbM) was proposed by Xavier et al. (2005). This framework considered biofilm detachment as a function of a detachment rate coefficient, the distance to the flat solid substratum, and local biofilm density. Furthermore, discrete detachment event can be integrated into the framework to model biofilm sloughing.

In the continuum fluid biofilm model proposed by Alpkvist and Klapper (2007a), a biofilm is considered as a system of viscoelastic, breakable springs embedded in a fluid flow. Detachment occurs due to spring breakage, which is assumed to happen when a spring between two connected particles extends beyond a given length, hence reaches a critical strain **(Figure 2.15).**

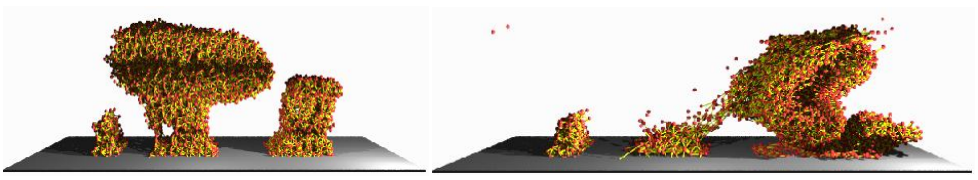

Figure 2.15: Biofilm deformed and detached under the fluid flow (Alpkvist and Klapper, 2007a)

Chambless and Stewart (2007) combined detachment dependent on the height above a flat substratum, nutrient concentration, and an erosive process in which individual cells are lost from the surface of a biofilm cell cluster with a detachment probability which is inversely proportional to the number of neighboring cells. The height-dependent mechanism produced flat, steady-state biofilms that did not produce sloughing events. Detachment based on nutrient limitation produced significant sloughing events. The erosion mechanism did not produce a non-zero steady state or sloughing events. A mechanism combining all three detachment mechanisms produced mushroom-like structures (**Figure 2.16**).

Figure 2.16: A mushroom structure of biofilm was generated by the combined detachment: height dependent, substrate limitation, erosion mechanisms (Chambless and Stewart, 2007)

b) Existing formulation in the frame of continuous models: As mentioned above, biofilm detachment is the interaction of biological, chemical-physical processes and each process is involved in many factors. In general, detachment rate can be interpreted as a function of multi-parameters, such as biofilm thickness (L_f), biofilm growth rate (μ), biofilm density (ρ), shear rate (τ), biomass concentration (X)

$$r_{det} = f(L_{f,}\mu, \rho, \tau, X \ldots .) \qquad (2.8)$$

Table 2. 1: Existing detachment models

No	Model	Reference
1	$r_{det} = k_{det} L_f$	Peyton and Characklis (1992)
2	$r_{det} = k_{det} X L_f$	Bakke et.al (1984); Melo and Bott (1997)
3	$r_{det} = k_{det} X L_f^2$	Wanner and Gujer (1986)
4	$r_{det} = k_{det} L_f^2$	Stewart et.al (1996)
5	$r_{det} = k_{det} X^2$	Bryers (1987) ; Trulear and Characklis (1982)
6	$r_{det} = k_{det} \mu L_f$	Speitel and DiGiano (1987)
7	$r_{det} = k_{det} \mu X L_f$	Peyton and Characklis (1993)
8	$r_{det} = k_{det} \mu X L_f^2$	Stewart (1993)
9	$r_{det} = k_{det1} \mu X L_f^2 + k_{det2} \mu X L_f^2$	Stewart (1993)
10	$r_{det} = k_{det1} \mu L_f + k_{det2} L_f$	Speitel and DiGiano (1987)
11	$r_{det} = k_{det} X \tau$	Bakke et.al (1990)
12	$r_{det} = k_{det} X \tau^{0.58}$	Rittmann (1982)

The complexity of its nature and the lack of a single mechanism of biomass detachment result in various proposal for detachment models as it can be seen in **Table 2.1**. However, these models include empirical parameters and are capable of predicting detachment in only for specific conditions. In the effort to clarify biomass detachment, Roald Kommedal and Rune Bakke (2003) conducted experiments for the investigation of detachment of *Pseudomonas aeruginosa* and tested existing detachment models (**Table 2.1**). A quite general model which includes specific growth rate, biofilm thickness and shear stress was proposed for its simplicity and best fit to experimental data

$$r_{det} = k_{det1} (\mu L_f)^{k_{det2}} \tau^{kdet3} \qquad (2.9)$$

Where k_{det1}, k_{det2}, k_{det3} are detachment coefficients

2.2.2 Numerical modelling of biofilm growth in porous media

Earlier models were basically based on two main approaches. A first class sees the porous media as a network of interconnected capillaries. The network models still provide a detailed description of the important processes while keeping a fairly simple model structure (Thullner et al., 2002; Kildsgaard and Engesgaard, 2002; Stewart and Kim, 2004). The second class of models sees the porous media as a continuum where the biofilm develops.

2.2.2.1 Network model

In the first approach, the porous medium is represented by a network of capillaries of various diameters and lengths (**Figure 2.17a**). The flow in each capillary tube is then described by the equation of Hagen- Poiseuille:

$$q_{ij} = \frac{\pi}{8}\frac{r_{ij}^4}{\mu l_{ij}}\Delta P_{ij} \qquad (2.10)$$

with q_{ij} the flow in a capillary between two nodes i and j, r_{ij} the corresponding radius , l_{ij} the tube length, μ the dynamic viscosity of the fluid and ΔP_{ij} the pressure loss between the node i and j . The conservation of mass in node i is then:

$$\sum_{j=1}^{n} q_{ij} = 0 \qquad (2.11)$$

The flow field is calculated explicitly (often assuming a Poiseuille flow) and the effect of the biofilm on the porous media requires to modify the capillary geometry according to the biomass content. This is usually done by solving a set of convection-diffusion-reaction equation accounting for the biomass and nutrient concentration.

The reaction terms include all the processes presented in paragraph 2.2.1 (kinetic of growth and decay, detachment rate etc...) Knowing the mass concentration of the biomass in each pore, given certain assumptions on the distribution of biomass in the pore as well as the biofilm structure, the volume occupied by the biofilm and its thickness can be calculated and the capillary geometry updated (**Fig. 2.17b**).

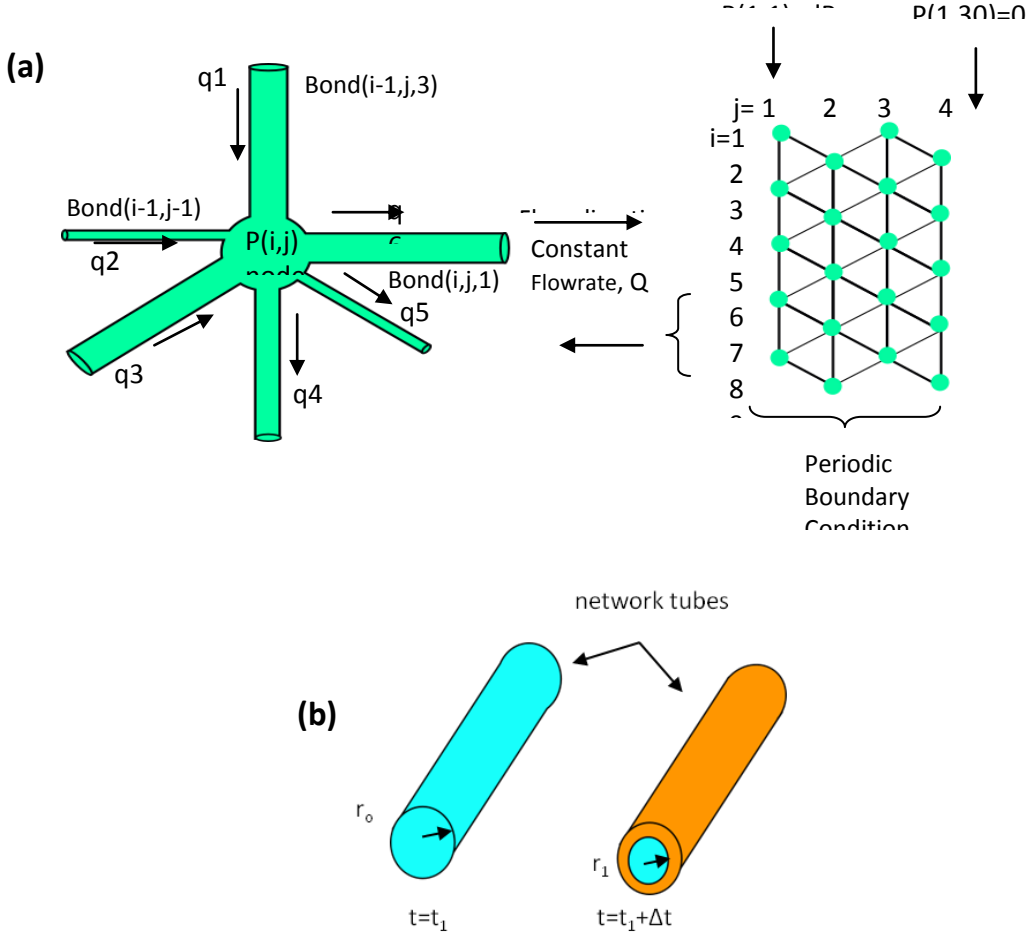

Figure 2.17 (a) Schematic of network presentation of porous media and (b) biofilm occupation in pore space (Stewart and Kim, 2004)

Solving the problem on the whole capillary networks allows then to calculate some global properties of the porous media modified by the biomass growth (for instance the permeability knowing the pressure field) and ensure the coupling between biomass growth and the flow field.

Model of Thullner (2002) giving the relation between the permeability of the medium and the amount of biofilm within the pores are based on simulations from this type of representation. The model of Shafahi and Vafai (2008) falls into this category, but here the network is constituted from a sphere arrangement.

2.2.2.2 Continuous model at the Darcy scale

In the second approach, to perform the coupling between the flow field and the biofilm development, apart from the various kinetics terms required to describe the biofilm development, some effective properties accounting for the porous media properties must be implemented in the model (effective permeability, effective dispersivity etc). These effective properties are either set directly in the model through phenomenological and semi-empirical consideration (model written directly the Darcy scale) or computed using an upscaling method (model based on volume averaging of local properties, homogenization).

Model written directly at the Darcy scale

Those models have been widely developed in order to reproduce experimental data at large scale (Taylor and Jaffe, 1990b; Kildsgaard and Engesgaard, 2001; Ham et al., 2007; Brovelli et al., 2009; Ebigbo et al., 2010) In general, the biofilms components are represented by different fields representing the volume fraction (or mass concentration) of each component in a point of the porous medium. These constituents may be the active biomass, the inactive biomass, the EPS... In some cases, suspended biomass is also taken into account. The flow in the porous medium is represented by Darcy's law. The transport of chemical species and various fields representing the biofilm are governed by convection-diffusion-reaction or diffusion-reaction equations. The bacteria growth is modeled by a formulation similar to the Monod law. The decrease in the availability of the different substrates as the biofilm grows is taken into account using a limiting function (initially proposed by Zysset et al., 1994). This function decreases the growth rate with the volume fraction of the biofilm in the pore. This function aims to simulate the damping of the growth kinetic as the biofilm thickness increases and the different substrates availability decrease.

As previously presented, the effect of the biomass growth on the flow field requires the definition of effective properties for the permeability and dispersivity. Often, these effective properties are written as $K/K_0=f(\emptyset/\emptyset_0)$ (which is used in momentum

conservation, Eq 2.14) and $D/D_0 = g(\emptyset/\emptyset_0)$ (which is used in mass conservation, Eq 2.15 and Eq 2.17). K, D and $\emptyset$ are the actual permeability, dispersivity and porosity, K_0, D_0 and $\emptyset_0$ correspond to the clean porous media. In the literature, numerous studies exist trying to set the exact form of the function f and g: some of these models will be detailed in chapter 3

It should be noted that, usually, the quantity of biofilm is described by a concentration field for the biomass. An additional constitutive law is then required for transforming the biomass concentration into biofilm volume fraction. These constitutive laws are often based on experimental results using a fixed value of the biofilm density and other properties such as its porosity. This semi-empirical approach may be not satisfactory. It is well known that biofilm structure is complex and these parameters can not be defined simply by generalized values. However, this drawback can be overcome by using upscaling techniques.

Such model were derived for instance by Kildsgaard and Engesgaard (2001) and Brovelli et al. (2009). The equations won't be detailed here as it will be the main subject of chapter 5. However, the mass conservation and momentum conservation equations used in these studies can be inferred from **Table 2.2** (in **section 2.2.2.3).** It is noted that **Table 2.2** consists of equations used for two-continuum model, which treats biofilm as a porous media and his thus more general. Some considerations must be taken into account to use the equations in **Table 2.2** for conventional continuous model:

- Eq (2.13) is used for unsaturated system. Therefore, this equation is neglected for saturated system.

- Velocity field (Eq 2.14) is only applied for water phase.

- Eq (2.15) for mobile biomass and Eq (2.16) for fixed biomass are kept in the conventional continuous models. It is noted that biofilm porosity (ε) is equal to 1 since biofilm is considered impermeable in this approach

- The exchange term ($e_{w,k}^{s}$) in Eq (2.17) is neglected for the conservation law of substrate

Model based on an upscaling procedure

Another method to derive macroscopic model is based on upscaling procedures (Golfier et al., 2009; Orgogozo et al.,2010). Upscaling methods rely on the choice of a Representative Elementary Volume (REV), not only large enough compared to the heterogeneities at the microscale, but also small enough to account for large-scale heterogeneities **(Figure 2.18)**. This REV must represent accurately the media geometry and the different components which constitute the studied media (with their physical properties and associate physical variable such are pressure, velocity, volume fractions, kinetics …). The equation that governs these variables and their relations are written at the microscopic scale. Resolution of such micro-problems at the microscale, coupled with an averaging process on the REV, leads to the definition of effective properties representative of the microstructure in the REV. It allows then a continuous formulation of the equations at the higher scale for the averaged variables.

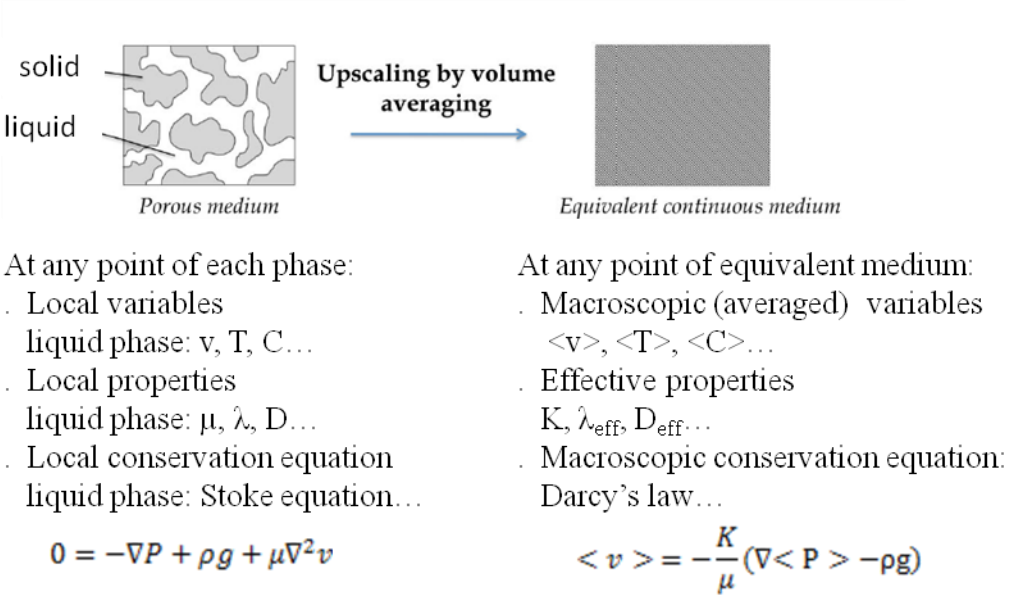

Figure 2.18: Example of upscaling from volume averaging (taken from Habibi, 2014)

For example, in Golfier et al. (2009), the upscaling of a system describing mass transport in a biofilm-affected porous medium. However, biofilm geometry and thickness is

assumed to be stationary (provides the averaged estimation of the effective dispersion tensor).

The micro-scale description does not necessarilly requires a steady system and the various processes for the biofilm mentioned in the first part of this literature survey could be in theory accounted for. For instance, van Noorden et al. (2010) derived an effective model for biofilm growth in a porous medium and its coupling with fluid flow. They assumed a simple local geometry for the pore, which is represented as a thin strip. From asymptotic expansions and volume averaging on this simple geometry, they could explicitly calculate the porous media effective properties. The model accounted for the deposition or detachment of biomass along the pore walls, leading to biofilm layers of variable (in time and space) thickness. The main mechanisms affecting the biofilm thickness was assumed to be the biomass growth and decay, attachment of biomass from the fluid phase, and detachment due to shear stress. Pore clogging was not taken into account.

Upscaling methods lead to macroscopic models that can be similar in terms of the equation to those written directly at the pore scale. The interest of the method is to give directly the parameters and functional relationships which appear in the effective properties that are required in the macro-scale equations (for example the effective permeability as a function of the averaged biofilm fraction)

2.2.2.3 Model with two porosities

In the models above, either based on a network approach, or based on a continuous approach, the biofilm is considered impermeable and advection-diffusion-reaction processes inside biofilm are negligible. (Baveye and Valocchi, 1989; Brovelli et al., 2009) However, the biofilm structure is highly heterogeneous and contains lots of voids and spaces (Lewandowski, 2000; Zhang and Bishop, 1994). Its characteristics can make biofilm as a second porous media that convey flow and contribute to the global transport in porous media.

Thullner and Baveye (2008) included flow through permeable biofilms in their pore network model, assuming that water has a different viscosity in the biofilm than in the open space. More precisely, to describe flow in biofilm region, an artificial viscosity was introduced:

$$\mu_b = \mu X \qquad (2.12)$$

Where μ_b and μ are the viscosity of the fluid in biofilm and bulk phase. X is a coefficient to define flow in the biofilm. The value of X is empirically obtained (Thullner and Baveye, 2008) by model calibration. When X is ∞, biofilm is impermeable and when X is equal to 1, biofilm does not insert resistance to fluid flow. Thullner and Baveye (2008) used values of $X=10^9$ (tagged as impermeable biofilm) and 10^3 (permeable biofilm) in their simulation studies.

The local equation for a Stokes flow in an individual capillary was integrated, taking into account the correct viscosity depending on the position in the capillary :

$$v_{ij} = \frac{\Delta p_{ij}}{4\mu l_{ij}} \begin{cases} r_{ijb}^2 - r_{ij}^2 + \frac{1}{X}\left(R_{ij}^2 - r_{ijb}^2\right) & for\ r_{ij} < r_{ijb} \\ \frac{1}{X}\left(R_{ij}^2 - r_{ijb}^2\right) & for\ r_{ijb} < r_{ij} < R_{ij} \end{cases}$$

where index ij refers to quantities between node i and j. R_{ij} is the external radius of the capillary and r_{ijb} the biofilm radius in the capillary between node i and j.

This equation is then integrated over the pore cross-section to calculate the water flux in the open section of the pore

$$q_{ijw} = \frac{\pi \Delta p_{ij}}{8\mu l_{ij}} r_{ijb}^4 \left[1 + \frac{2}{X}\left(\frac{R_{ij}^2}{r_{ijb}^2} - 1\right)\right]$$

as well as in the biofilm

$$q_{ijb} = \frac{\pi \Delta p_{ij}}{8\mu l_{ij}}$$

The total flux is then given by the sum of the two flux

$$q_{ij} = \frac{\pi \Delta p_{ij}}{8 \mu l_{ij}} \left[r_{ijb}^4 + \frac{\left(R_{ij}^4 - r_{ijb}^4\right)}{X} \right]$$

A set of linear equation for each capillary is then obtained and can be solved to get the pressure loss Δp_{ij} between to nodes boundary conditions at the inlet and outlet. The geometry is then updated at each time step solving a dispersion-reaction for the biomass as in the original network model (paragraphe 2.2.2.1).

Using this approach Thullner and Baveye (2008) were able to simulate comparatively larger reductions of the overall hydraulic conductivity of the pore networks, similar to those obtained in laboratory experiments and observed in field situations **(Figure 2.19)**

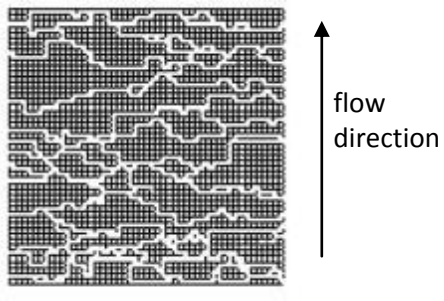

Figure 2.19: The change of pore radius, resulting from biofilm growth in 2 D simulation (Thullner and Baveye, 2008). Biofilm is considered permeable with $X = 10^3$. Biofilm growth was indicated by grey color, and ranging from black color (no biofilm growth $r_{ib}=R_i$) to white color (all pore spaces were filled by the biofilm, $r_{ib}=0$)

In a macroscopic approach, Delay et al. (2013) treated biofilm and the bulk as a separated continuum, for a case where a steady biofilm is considered (so no equation where written for the biofilm growth, attachment and detachment). Only the solute transport in each continuum where considered and where described by a set of coupled advection-diffusion-reaction. At the boundary surface of the two continua, a nonlocal equilibrium or local equilibrium boundary condition is set up to define mass transfer between biofilm and bulk phases. In this work, the flowrate in each continua was imposed so that the flowrate in the biofilm continuum was smaller than the flowrate of bulk continuum. The ratio between the two flowrates was fitted from a sensitivity analysis.

The most completed dual continuum model was developed by Ebigbo et al. (2010) (**Figure 2.20).** The porous media is represented by two continua: a continuum *a* that account for the bulk flow in the open pore, and a continuum *b* that account for the flow within the biofilm embedded in the porous medium. The model was written directly at the macro-scale so no upscaling techniques were applied to define some effective properties of each continuum.

Fluid flow and solute transport are characterized by setting up equations of momentum conservation and mass conservation in each continuum and interaction between these continuums is presented in term of mass transfer.

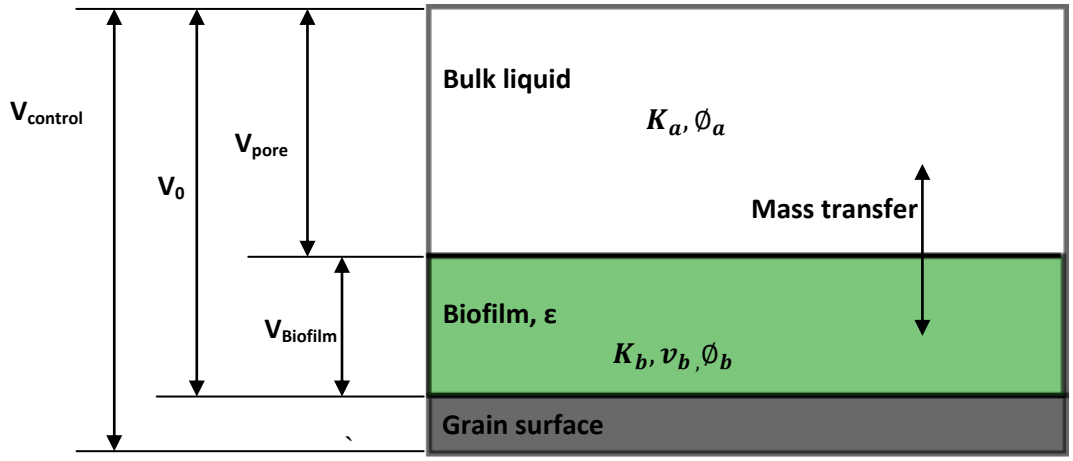

Figure 2.20: Schematic presentation of dual continuum model that account for biofilm permeability

More precisely, volume fraction characteristics of each continuum are first defined as :

- Initial porosity of porous medium: $\emptyset_0 = \frac{V_0}{V_{control}}$ where v_0 is the pore volume of the porous medium unaffected by biofilm
- Porosity of continuum *a*: $\emptyset_a = \frac{V_{pore}}{V_{control}}$ where v_{pore} is the pore volume of the porous medium excluding biofilm pore volume
- Porosity of continuum *b*: $\emptyset_b = \frac{V_b}{V_{control}}$ where v_b is the pore volume within the biofilm (continuum b)

From those quantity, the biofilm porosity can be defined as :

- Biofilm porosity $\in = \frac{volume\ of\ void\ in\ the\ biofilm}{V_{biofilm}} = \frac{v_b}{v_0 - v_{pore}} = \frac{\emptyset_b}{\emptyset_0 - \emptyset_a}$

It is noted that if the biofilm is considered impermeable v_b=0 or $\epsilon = 0$.

The model of Ebigbo considers a porous media which can be unsaturated, i.e. the pore space contain water (*w*) + a gas phase (*n*). The volumetric fraction above being defined, mass conservation of each phase α (α=*w* or *n*) , in continuum *k* (*k*=*a* or *b)* can be written according to the **Table 2.2**

Table 2. 2: Equations used in two continuum models

Mass conservation for phase α in continuum *k*	$\frac{\partial(\emptyset_k S_{\alpha,k}\rho_{\alpha,k})}{\partial t} + \nabla.\left(\rho_{\alpha,k}V_{\alpha,k}\right) = q_{\alpha,k} + e_{\alpha,k}$ (2.13)
Velocity field for each phase in continuum *k*	$V_{\propto,k} = -\frac{kr_{\alpha,k}}{\mu_{\alpha,k}} K_k\left(\nabla P_{\alpha,k} - \rho_{\alpha,k} g\right)$ (2.14)
Mobile biomass conservation law in continuum a (open pore)	$\frac{\partial(\emptyset_a C_w^{bio} S_{w,a})}{\partial t} + \nabla.\left(C_w^{bio} V_{w,a}\right) = q_a^{bio} + e_a^{bio} + \nabla.(D_a^{bio}\nabla C_w^{bio})$ (2.15)
Fixed biomass conservation law in continuum *b* (biofilm)	$\frac{\partial([\emptyset_0 - \emptyset_a]\rho_{bio})}{\partial t} = \frac{\rho_{bio}}{\varepsilon}\frac{\partial \emptyset_b}{\partial t} = q_b^{bio} + e_b^{bio}$ (2.16)
Growth-limiting substrate conservation law	$\frac{\partial(\emptyset_k S_{w,k} C_{w,k}^S)}{\partial t} + \nabla.\left(C_{w,k}^S V_{w,k}\right) = q_{w,k}^S + e_{w,k}^S + \nabla.\left(D_k^S \nabla C_{w,k}^S\right)$ (2.17)

In its more general formulation, $S_{\alpha,k}$ is the saturation of each phase α in continuum k so that $S_{w,k}+S_{n,k}=1$

$\rho_{\alpha,k}$ and $\mu_{\alpha,k}$ are the fluid properties for each fluid phase and each continua. In its general formulation, the model takes into account that these properties maybe different in each continuum and dependent on the pressure.

$V_{\alpha,k}$ and $P_{\alpha,k}$ are the velocity field and the pressure of phase α in continuum k

C_w^{bio} is the suspended biomass concentration in continuum *a*

Finally, $C^s_{w,k}$ is the substrate concentration in the water phase for each continuum

The model includes sources/sink terms q that account (except for Eq 2.13) for the kinetics of biomass growth and decay (q_a^{bio}, q_b^{bio}) or substrate consumption ($q_{w,k}^s$). These terms are modeled using classical Monod formulation as in previous models.

The coupling between the two continua is performed through the exchange terms noted e in the equations:

- In Eq (2.13), $e_{\alpha,k}$ account for fluid exchange between two continua and is pressure driven ;

$$e_\alpha = -e_{\alpha,a} = e_{\alpha,b} = a_\alpha\left(P_{\alpha,a} - P_{\alpha,b}\right)$$

a_α is a parameter which describes the rate at which the exchange takes place.

- In Eq (2.15) and (2.16), $e^{bio} = e_b^{bio} = -e_a^{bio}$ describe the biomass transfer between suspended biomass in continuum *a* and fixed biomass in continuum *b*. Those terms are similar to the terms of biomass attachment and biomass detachment presented in paragraphes 2.2.1.3 and 2.2.1.4

- Finally, in Eq (2.17), $e_{w,k}^s$ account for the solute mass transfer between continuum a and b.

$$e_w^s = -e_{w,a}^s = e_{w,b}^s = K_{la}\left(C_{w,a}^s - C_{w,b}^s\right)$$

K_{la} is a mass transfer coefficient depending on porous medium specific surface of the porous media, the pore radius and the effective diffusivity of the solute in the biofilm.

The model requires also to define some properties of each continuum :

- ρ^{bio} the dry biomass density in the biofilm (continuum *b*)

- The effective diffusions coefficient D^s_k for the substrate in each continuum. This diffusion depends on the porosity $\emptyset_k$ of each continuum k and on the water saturation $S_{w,k}$
- The relative permeability of each phase in each continua : $kr_{\alpha,k}$ which depends on water saturation in each continua $S_{w,k}$
- The intrinsic permeability of each continuum K_k .

As usual, the coupling between the flow field and biofilm development occurs through the modeling of the permeability in Eq (2.14). Ebigbo solved the set of the general equations presented above assuming that the pressure $P_{\alpha,k}$ was the same in continuum a and b. In that configuration it can be shown that the intrinsic permeability K of the overall porous media is equal to the some of the intrinsic permeability K_k (k=a or b) of each continua. So $K=K_a + K_b$.

In that case, K must fulfill several constraints:

- When there is no biofilm ($\emptyset_a=\emptyset_0$), $K=K_0$. In that case, $K_a=K_0$ and $K_b=0$
- When the porous media is completely clogged ($\emptyset_a < \emptyset_{a,critical}$), $K=K_{min}$. In that case, $K_a=0$ and $K_b=K_{min}$.

Given these constraints, the relative permeability K_a/K_0 is modeled according to formulation similar to those detailed in Chapter 4. In particular the ratio K/K_0 decreases with the value of $\emptyset_a$ until it reaches 0 when $\emptyset_a = \emptyset_{a,critical}$.

K_b is modeled with a simple linear function where K_b evolves from 0 to K_{min} as the porosity $\emptyset_a$ decrease from $\emptyset_0$ to a critical value $\emptyset_{a,critical}$. This choice is rather arbitrary and aims to take into account the biofilm structure evolution with its “age” and thickness….

This model was tested in different configuration. One of this test corresponds to a monophasic case aiming to simulate the experiments of Taylor and Jaffé (**Figure 2.21**). However only results concerning the steady state at the end of each experiment are

presented and it is not possible to say if the model fits well the data during the transient stage.

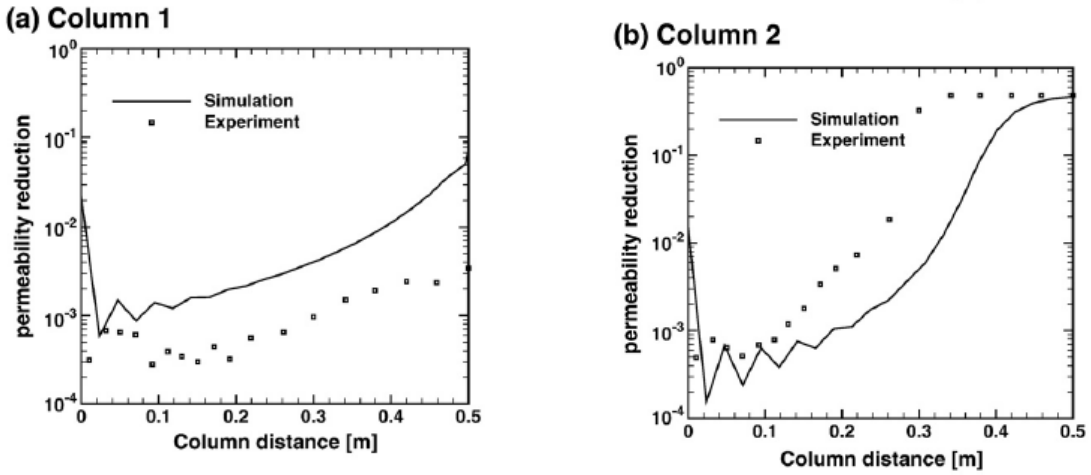

Figure 2. 21: Comparison of the simulation of permeability reduction with the model of Ebigbo et al., (2010) with the experimental results of Taylor and Jaffe, 1990a.

2.2.2.4 Multi-scale model

The models above are still based on a very simplified representation of the biofilm geometrical structure. Recently more complete models have been derived where the processes at different scales are explicitly simulated in order to get a representative description of the biofilm distribution in the porous media (for instance Kapellos, 2007). In the pore space, the bulk fluid and biofilm are seen as two different media separated by an interface. This kind of models follows a general algorithm which is made of several steps.

1- The equations managing the different transformations and growth of the biomass are solved.

2- The biomass is propagated which allows to update the biofilm geometry as well as its distribution in the pore space

3- For a given biomass distribution and structure, the flow field is simulated in the pore space as well as in the biofilm.

4- In a final step, knowledge of the velocity field allows then to solve the problem of nutrient transport toward the biofilm and within the biofilm.

5- Step 1 is then reiterate for the next time step.

In step 1 and 2, various techniques can be used to perform a detailed simulation of biofilm structure evolution over the time. Among these techniques, we can cite the cellular automata (Picioreanu et al., 2001) or techniques related to discrete elements (Jayathilake et al., 2013) as shown in **Figure 2.22**. These techniques allow the detailed description of different components of the biofilm as well as their interaction according to specific rules.

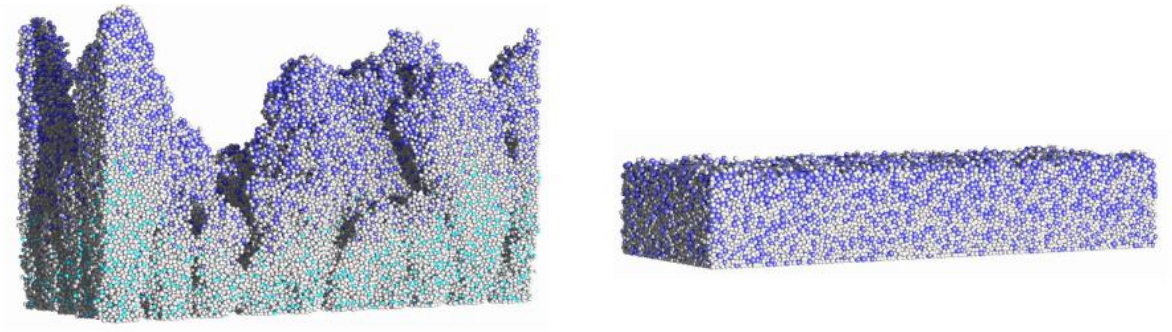

(a) (b)

Figure 2.22: Biofilm morphology obtained from a discrete element model (a) low nutrient supply and growth substrate limited (b) growth not substrate limited an high nutrient supply (from Jayathilake et al., 2013).

These interactions among other processes include biological mechanisms (cell divisions and EPS secretion) as well as physical interactions (EPS mediated adhesion and detachment, sloughing,...). At this stage, some researchers tried to include some specific behavior due to the bacteria reaction to environmental conditions. For instance, in his multi-scale model, Kapellos tried to include local effects such as the modulation of the intrinsic maximum growth rate of bacteria under the effect of mechanical stress or the concentration of chemical "signal" molecules (“quorum sensing”).

When the biofilm structure and its interface is updated, knowing the local biofilm composition, the effective parameters accounting for the biofilm local properties can be

then calculated. For instance, in Kapellos model, this calculation is performed by replacing the local inhomogeneous biofilm structure by a simplified equivalent representation. A unit cell is defined as a sphere made of different layers: the center contains a rigid spherical core surrounded by a concentric spherical porous shell and represents a single bacterial cell surrounded by hydrated fibrous EPS matrix. This composite sphere is itself surrounded by a concentric spherical fluid envelope which is embedded in an external effective porous medium. The fluid envelope represents the volume between neighboring bacterial cells, which is occupied by water. The external effective porous medium represents the neighboring bacterial cells and the EPS in which they are enmeshed. Kapellos solved analytically the creeping flow and passive diffusion problems over this unit cell configuration, and derived closed-form expression for the calculation of the hydraulic permeability as well as diffusion coefficient of each substrate at any point.

The flow field is then calculated (step 3) coupling the Navier-Stokes equation in the pore space and the flow in the biofilm (using the Brikman equation for instance). The boundary conditions at the biofilm interface allow then to solve the mass transfer problem and the profile concentration of each substrate are updated outside and within the biofilm (step 4).

An example of simulation results is given in **Figure 2.23**, Biofilm plugs can be seen that, in return, disrupt the flow field.

.

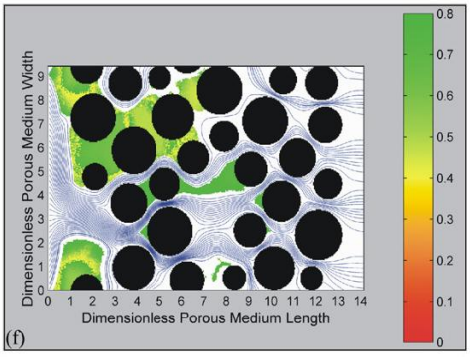

Figure 2.23: Simulation of biofilm development and flow paths in porous media (from Kapellos, 2007)

2.3 Choice of the model and the appropriate scale

The multi-scale models (Kapellos, 2007, Pintelon et al., 2012) try to model at the finest phenomena at the level of biofilm. As mentioned above, modeling biofilm at cell scale can capture more accurately some biological phenomena (quorum sensing, EPS production…). However, the gains gathered from the refinement of these models can be lost on the parametrization of certain phenomena which are hard to measure. Furthermore, the problem of expensive computer cost of the multi-scale models limit them in modeling biofilm at pore scale at current computer technology.

Using a macroscopic model, based on a set of continuous convection-dispersion-reaction equations, appears more suitable for the industrial application. The option of writing directly the model at the Darcy scale or deriving the model through an upscaling technique can be discussed.

Even if the interest of upscaling method is to give directly the parameters and practical relationships which appear in the effective properties, it is important to notice that these effective parameters obtained through upscaling depend on the assumed micro-scale geometry of the systems and the way some processes accounting for the biofilm development are written at the local scale. As for multi-scale models, there still issues on the modeling of some processes at that scale accounting for the biofilm structure evolution.

Given these uncertainties, in the case of an operational model for industries, it can be better to use the model directly written at the Darcy scale. In this thesis, we have then made the choice to write a 1-D continuous model directly at the Darcy scale

2.4 Feature to improve in the model at the Darcy scale and the objectives of the thesis

This study will focus on a limited number of mechanical processes that can have a high importance on the global behavior of the porous media rather than biological processes that governed by bacteria themselves. Indeed, as seen in the literature survey in paragraphe 2.12, biological processes occuring at the bacteria/biofilm scale are not well

understood, even if their importance in the biofilm structuration and behaviour are aknowledged by the scientific community. Approaches using discrete modelling of biofilm coupled with the knowledge gathered from biofilm scale experiments are expected to help solving these issues. But we are far from having closure law « usable » in higher scale models.

The classical approach of using a Monod-like formulation for the growth or production of different components of the biofilms gave reasonnable results in most models written at the Darcy scale even if it is not completly satisfactory in regards of the complexity of the processes at play. In particular, at least for biofilms, the parameters of the Monod formulation (in particular the maximum growth rate) can be seen as fitting parameters which hides some of this complexity (Mbaye 2011). In the following, we will then assume that those kind of formulation can be used and we will focus more on some mechanical coupling that can be still improved in order to get more relevant models for field scale models.

A) Permeability : This is the main macro-scale parameter which couple the flow and biofilm through the pressure. As it will be seen chapter 3, many models have been developed but the formulations for this effective parameter are commonly based on simple assumptions. As a result, the satisfaction of the existing permeability models are usually obtained in certain specific experimental conditions. *The development of a new permeability model for a wide range of experimental data is one the objectives of this study.*

B) Simulation of bacterial attachment efficiency in porous media

In the industrial application such as biofiltration, the system is never working at steady-state. At the end of operation time, biofilm is backwashed for a new cycle of biofiltration. After each backwashing, even if some biomass remains still attached to the surface, modeling properly the process of bacterial attachment at this stage of the process, is important for the long-term behavior of the systems.

Besides that, when a model is validated with the numerous experiment performed on pilot scale system (Taylor and Jaffe, 1990a ; Karrabi et al., 2013), the initial conditions are not accessible precisely on these experiments. So it is crucial to simulate properly the stage of the pilot inoculation in order to get more meaningful comparison between models results and experiments especially during the unsteady phase.

Biomass attachment is a complicated process involving physicochemical characteristics of bacteria and porous media. This process is still poorly understood and not agreed in the modeling approach. Although many studies adopt colloid filtration theory, its validity for properly predicting biomass attachment should be considered. Tuefenkji, (2007) reported that this theory might not be applicable for bacteria motion, which can result in overestimation of attachment rate. However the alternation for modeling biomass attachment is still unclear and most studies continue to use colloid filtration theory. It is noted that if this theory is accepted, one must cope with the complicated task to determine the attachment efficiency. As mention previously, there are various closed forms containing many empirical parameters which these closed-forms may show its limit in certain conditions. *Second objective of this thesis will be to improve those formulation to better represent the attachment process.*

C) Development of a macroscopic model for the numerical simulation of biofilm growth in porous media

Modeling solute transport coupling with biofilm growth in porous media is a complex task because of the strong coupling existing between the multi-physics and multi-scales processes. One of the difficulties is to apply the appropriate constitutive laws to describe the important processes that govern the behavior of porous media. Many 1-D models have been developed to numerical simulate solute transport in porous media at field scale. However, current models still have not secured satisfaction in temporally and spatially predicting the behavior of porous media (Taylor and Jaffe, 1990b; Ham et al., 2007; Brovelli et al., 2009; Ebigbo et al., 2010). *With the new improvements of the first two*

objectives, this study aims to develop a new 1-D macroscopic model to improve the description of the spatial and temporal behavior of a porous media colonized by a biofilm

D) Modeling of the biofilm detachment.

Detachment models based on formulation such as those found in **Table 2.1** are more suitable for continuous erosion. Models accounting for sloughing still requires to be implemented and tested although, models of sloughing at the biofilm scale begins to appear in the literature. The models of sloughing can be categorized into two groups.

Mechanistic one based on a characterization of the biofilm cohesion (microscale model of Picioreanu et al., 2001; Xavier et al., 2005, Duddu et al., 2008) or three dimensions (Xavier et al.,2005; Alpkvist and Klapper, 2007a). At macro-scale, Stewart and Kim (2004) tried to include sloughing term in biofilm detachment. Biofilm sloughing was specifically set to occur at the bottom of biofilm. If the fluid shear is greater than biofilm cohesion, which was a constant in the simulation, all the biofilm was removed from the surface.

One issue is how to define this cohesion in a general way. The EPS matrix resistance in a given biofilm can evolve depending on mechanistic but also chemical and biological effect. So the cohesion may be not defined simply by a set of a constant parameter.

The problem of the definition of constant cohesion for the biofilm led to another concept of biomass sloughing which was proposed by Bohn et al. (2007). It was assumed that sloughing could be considered as a stochastic process (Lewandowski et al., 2004). Biofilm detachment was modeled as the combination of the deterministic process (erosion) and the stochastic process (sloughing) that occur at different time scales. This modeling approach can neglect the difficulty of biofilm strength but can result in adjustable parameter to fit experiment result (Bohn et al., 2007), which reduce the freedom of numerical simulation. Moreover, the setup of the new concept was based on a very simple mathematical framework that only indicates the potential of modeling biomass sloughing (Bohn et al., 2007). *So the fouth objective of this thesis is to implant this concept on macro-scale model.*

Chapter 3

A modified model for the prediction of bioclogging in saturated porous media.

A new mathematical model has been developed in this chapter to predict the permeability reduction due to bioclogging in saturated porous media. Derived from the Hagen–Poiseuille equation that characterizes the laminar flow rate in a capillary tube and Darcy's law that defines fluid flow in porous media at macroscopic scale, the macroscopic model takes into account two mechanisms that result in permeability reduction: pore radius reduction and pore plugging. Then, the derived model is compared with a wide range of experimental data in term of permeability of clean-bed and bioclogging in porous media.

List of symbol

Symbol	Unit	Definition
Basic notation		
a_{T1}, a_{T2}	-	Thullner 's constants in equation 3.6
A	m^2	Cross section area of capillary tube
C_K	-	Kozeny constant in equation 3.2
d_G	m	Grain diameter
$d_{G,0}$	m	Initial grain diameter
$F(\emptyset_B)$	-	Biomass distribution for the reduction of pore radius and plugging of pore space
k_{est}	-	Estimated permeability
K_{min}	m^2	Biofilm permeability
K_P	m^2	Permeability reduction that results in the plugging of pore space
K_R	m^2	Permeability reduction that results in the reduction of pore radius
L	m	Strength line distance
L_t	m	Real length that fluid molecules transport in capillary tube
N_e	-	Fraction of surface area of deposited particles contributing to the modification of surface area of grain

ΔP	Pa	Pressure loss
q	m^3s^{-1}	Flow rate in capillary tube
R^2	-	Sum of squares
r	m	Radius of capillary tube
S_P	m^{-1}	Specific surface area of particle
S_{sf}	m^{-1}	Specific surface area of grain
u	ms^{-1}	Velocity in capillary tube
U	$m.s^{-1}$	Superficial velocity
Greek letters		
β	-	Relative critical porosity
β_B	-	Bulk factor
γ	-	Defined as: $\gamma = \beta_B N_e \frac{d_{G,0}}{d_P}$
μ	$kgm^{-1}s^{-1}$	Dynamic viscosity
$\emptyset$	-	porosity at time t
$\emptyset_0$	-	Clean bed porosity
$\emptyset_B$	-	Volumetric fraction of biofilm
$\emptyset_{B,c}$	-	Value of volume fraction of biomass which indicates how fast microcolonies are formed and plug pore space.
τ	-	Tortuousity of capillary tube

3.1 Introduction

Bioclogging refers to the phenomena of biofilm development in porous media, occupying pore spaces and driving the permeability reduction of porous media. Biofilm takes place in almost all the biofilm application processes, such as situ bioremediation of soil and groundwater, biofiltration for air and water treatment, carbon sequestration, microbial enhanced oil recovery (Orr, 2004; Dumont et al., 2008; Ivanov and Chu, 2008; Suthar 2009; Folch et al., 2013). Indeed, the growth of biofilm finished by occupying all the pore spaces in media, the permeability drops very sharply and as a result, affects directly the processes efficiency. So the knowledge of bioclogging is essential to control biofilm process performance. Biocloging is usually evaluated through the parameter which determines ability of fluid to flow through a media, and is expressed following Darcy‘s law

$$U = -\frac{K}{\mu}\frac{\Delta P}{L} \qquad (3.1)$$

Where U is the approaching velocity (ms^{-1}), K is the permeability of porous media (m^2), ΔP is the pressure loss (Pa), μ is the dynamic viscosity ($kgm^{-1}s^{-1}$) and L is the length of porous media (m).

In the study concerning microbial process in porous media, before being able to solve advection-diffusion-reaction equations that represent mass balance of solutes, one must deal with the momentum conservation that characterizes fluid pattern in porous media (Taylor and Jaffé, 1990a; Murphy and Ginn, 2000; Kildsgaard and Engesgaard, 2001; Seifert and Engesgaard, 2007; Brovelli et al., 2009; Karrabi et al., 2011).

Many studies have been performed to provide a mathematical model to predict permeability reduction in porous media. Since the biomass accumulation leads to the decrease of pore space and results in permeability reduction, this connection between permeability and porosity is the main objectives of these studies (Carman-Kozeny, 1937; Clement et al., 1996).

Existing models are usually developed based on several mechanisms that cause permeability reduction : (i) mass accumulation and coverage of the grain surface which leads to the reduction of pore radius, (ii) mass deposition which forms aggregation and plugs a portion of the pore and (iii) permeability reduction resulting from the combination of the two previous mechanisms.

The most popular permeability model was proposed by Carman-Kozeny (1937). In this model they stated that the magnitude of permeability reduction depends on the third power of porosity:

$$K = \frac{\emptyset^3}{C_K \tau^2 (1-\emptyset)^2 {S_{sf}}^2} = \frac{d_G^2 \emptyset^3}{180(1-\emptyset)^2} \qquad (3.2)$$

Where C_K is Kozeny constant. K, $\emptyset$, d_G are permeability (m^2), porosity (-) and grain diameter (m), respectively at time t when the geometry of porous media is affected by mass accumulation. The clean bed properties, without the effect of the mass deposit, will

be referred with the index "0". For a porous media packed by uniform spheres, it was assumed that $C_K\tau^2 = 5$ and $d_G=6/S_{sf}$.

The Equation 3.2 can be then rewritten in the form of relative permeability reduction:

$$\frac{K}{K_0} = \left(\frac{\emptyset}{\emptyset_0}\right)^3 \frac{(1-\emptyset_0)^2}{(1-\emptyset)^2}\left(\frac{d_G}{d_{G,0}}\right)^2 \qquad (3.3)$$

Thus, the relative permeability was found to have the power relationship with relative porosity, and this feature received consensus of many studies about permeability reduction in porous media. Clement et al. (1996) found that power number of 19/6 obtained the good match to the biofilm-based model proposed by Taylor et al. (1990b) and Eq (3.4) was referenced in some macroscopic models to predict permeability change in porous media (Kildsgaard and Engesgaard, 2001; Islam and Singhal, 2002; Ham et al., 2007)

$$\frac{K}{K_0} = \left(\frac{\emptyset}{\emptyset_0}\right)^{\frac{19}{6}} \qquad (3.4)$$

A similar form of the power relationship between permeability and porosity was reported by Verma and Pruess (1988). In this model (Eq 3.5), a new definition of critical porosity was introduced, which was based on the experimental observation that when porosity is less than a critical porosity, porous media no longer conveys fluid flow and permeability is then approximated to zero.

$$K = K_0\left(\frac{\frac{\emptyset}{\emptyset_0}-\beta}{1-\beta}\right)^3 \qquad (3.5)$$

where β is the relative critical porosity ($\beta = \frac{\emptyset_{crit}}{\emptyset_0}$). It should be noted that this number is dependent on geometry of the porous media and bacterial kinetic.

By simulating an interconnected network of capillaries, Thullner et al. (2002) proposed another model, which is similar to Verma and Pruess (1988) in term of critical porosity.

This model stated that when porosity reaches a critical value, the permeability of porous media was unchangeable and remained at the constant value of minimum permeability.

$$\frac{K}{K_0} = \left(\left(\frac{\frac{\emptyset}{\emptyset_0} - \beta}{1 - \beta} \right)^b + K_T \right) \frac{1}{1 + K_T} \qquad (3.6)$$

Where K_T is a fitted parameter proposed by Thullner et al. (2002). Eq (3.6) shows that when $\emptyset/\emptyset_0$ reaches to β, the relative permeability $\frac{K}{K_0}$ tends to be $\frac{K_T}{1+K_T}$. Since K_T is far smaller than 1, so the relative permeability is equal to K_T. Thus, K_T can be considered as the relative minimum permeability of porous media.

Based on experiments conducted by Cunningham et al. (1991), Ebigbo et al. (2010) deduced that the critical porosity was 0.6 for a sand filter filled with Pseudomonas aeruginosa biofilm. As it is shown in **Figure 3.1,** the relative permeability (defined as the ratio K/K_0) was close to zero when the volumetric fraction of biofilm reached 0.4. However, this value was obtained only for two sand size relatively small (dg=0.7mm and 0.5mm), not applicable for other biofilm processes.

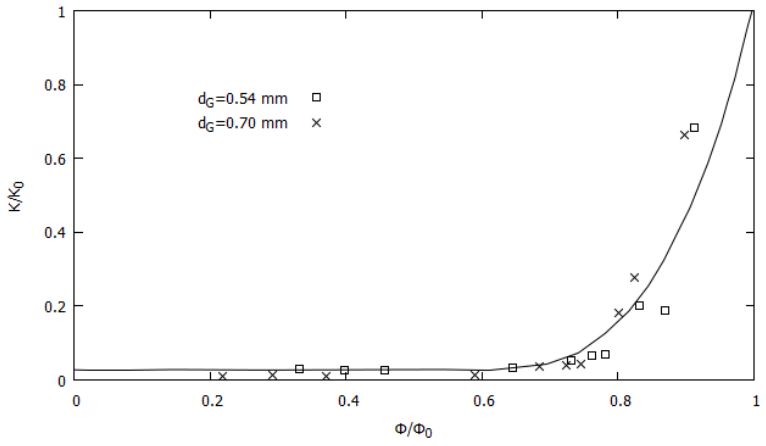

Figure 3.1: Profile of permeability reduction versus the volumetric fraction of biofilm in the column filled with sand of 0.7 mm and 0.54 mm (Ebigbo et al., 2010). The solid lines represent the relationship proposed by Ebigbo et al. (2002) with β=0.6

Other studies emphasizes on the possibility that a portion of pore may be plugged by mass deposition which induces permeability reduction. Thullner et al. (2002) applied this consideration in the simulation on an interconnected network of capillaries and introduced a new model:

$$\frac{K}{K_0} = a_{T1}\left(\frac{\frac{\emptyset}{\emptyset_0} - a_{T2}}{1 - a_{T2}}\right)^3 + (1 - a_{T1})\left(\frac{\frac{\emptyset}{\emptyset_0} - a_{T2}}{1 - a_{T2}}\right)^2 \qquad (3.7)$$

where a_{T1} and a_{T2} are fitting parameters.

In this point of view, the minimum permeability K_{min} can be considered as the permeability of plugged areas. That means biofilm can be implicitly treated as porous materials through which fluid moves at a very low rate. If the permeability reduction is assumed to be only the result of pore plugging, it can be represented by a harmonic relationship function of initial permeability K_0 and biofilm permeability K_{min} (Vandevivere, 1995)

$$\frac{K}{K_0} = \frac{K_{min}/K_0}{1 - \frac{\emptyset}{\emptyset_0} + \left(\frac{\emptyset}{\emptyset_0}\right)\left(\frac{K_{min}}{K_0}\right)} \qquad (3.8)$$

The value of K_{min} are usually estimated to be proportional to the initial permeability : $\frac{K_0}{K_{min}} = 2500 - 10000$ (Vandevivere, 1995)

Vandevivere (1995) later proposed a model to combine the effect of pore radius reduction and that of pore plugging. Following the concept, porous media is treated as bundles of capillary tubes which shelter for biofilm development. In the return, biofilm alter tube in both patterns: reduction of tube diameter and plugging of a portion of the tube

$$\frac{K}{K_0} = F(\emptyset_B)\left(\frac{\emptyset}{\emptyset_0}\right)^2 + \left(1 - F(\emptyset_B)\right)\frac{\frac{K_{min}}{K_0}}{1 - \frac{\emptyset}{\emptyset_0} + \left(\frac{\emptyset}{\emptyset_0}\right)\left(\frac{K_{min}}{K_0}\right)} \qquad (3.9)$$

The biofilm fraction that contributes to each pattern is characterized by $F(\emptyset_B)$ which is dependent on biomass concentration.

$$F(\emptyset_B) = \exp\left(-0.5\left(\frac{\emptyset_{B,rel}}{\emptyset_{B,c}}\right)^2\right) \qquad (3.10)$$

where $\emptyset_{B,rel}$ is the relative volumetric fraction of mass deposition, equal to the ratio of the volumetric fraction of mass deposition to the maximum porosity of porous media. $\emptyset_{B,c}$ is the constant value that affects the $F(\emptyset_B)$ curve shape and controls how fast mass aggregates are formed and plug pore space as seen in **Figure 3.2.** The small value of $\emptyset_{B,c}$ indicates that biofilm is likely to plug the pore spaces rather than to reduce the pore radius. $F(\Phi_B)$ drops down more quickly at small $\emptyset_{B,c}$. **Figure 3.2** shows that at the biofilm fraction $\emptyset_B/\emptyset_0$=0.2, $F(\emptyset_B)$ is equal to zero in case $\emptyset_{B,c} = 0.01$; approximate to 10% in case $\emptyset_{B,c} = 0.1$; and 95% in case $\emptyset_{B,c} = 0.5$

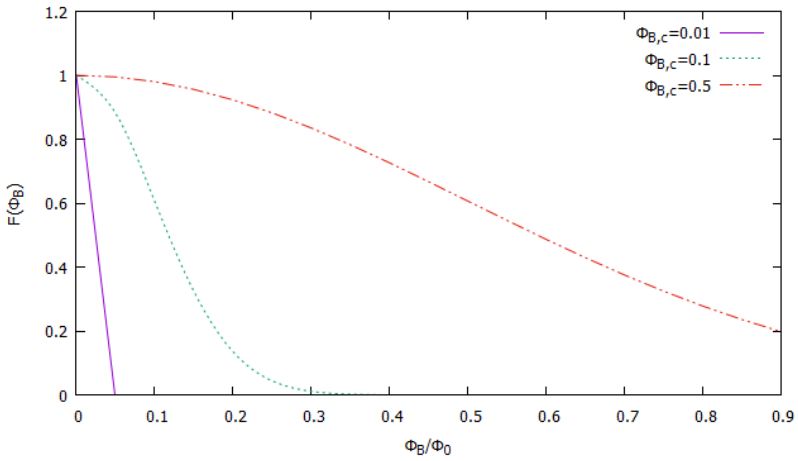

Figure 3. 2: The effect of $\emptyset_{B,c}$ on $F(\emptyset_B)$

As we have seen above, many permeability models have been developed and used to study the microbial processes in porous media (Carman-Kozeny, 1937; Verma and Pruess, 1988; Vandervivere, 1995; Clement et al., 1996; Thullner, 2002) . It should be noted that the existing models include empirical parameters that are specific for each experimental conditions or adjusted to theoretical assumptions. For example Carman-

Kozeny model (Eq 3.2) introduced the Kozeny constant C_K and the tortuosity τ. However, the tortuosity was not kept explicitly in his model, as the value of the product $C_K\tau^2$ was approximated to be constant 5. Vandervivere's model (Eq 3.9) assumed that the function $F(\emptyset_B)$ follows the normal distribution. Lets recall, that this function which controls the relative contribution of pore reduction or plug formation to the permeability is a way to represent the effect of the biofilm microstructure on the pressure loss. He reported that the critical parameter which determines the distribution is not available. In the case of Thullner (eq 3.7), the empirical parameters a_{T1} and a_{T2} were chosen so that they correlate to the numerical results of their pore-network model. In estimating permeability reduction, one may cope with the problem of the discrepancy in the predicted results from the existing models (Seifert and Engesgaard, 2007; Karrabi et al., 2011) (**Figure 3.3**)

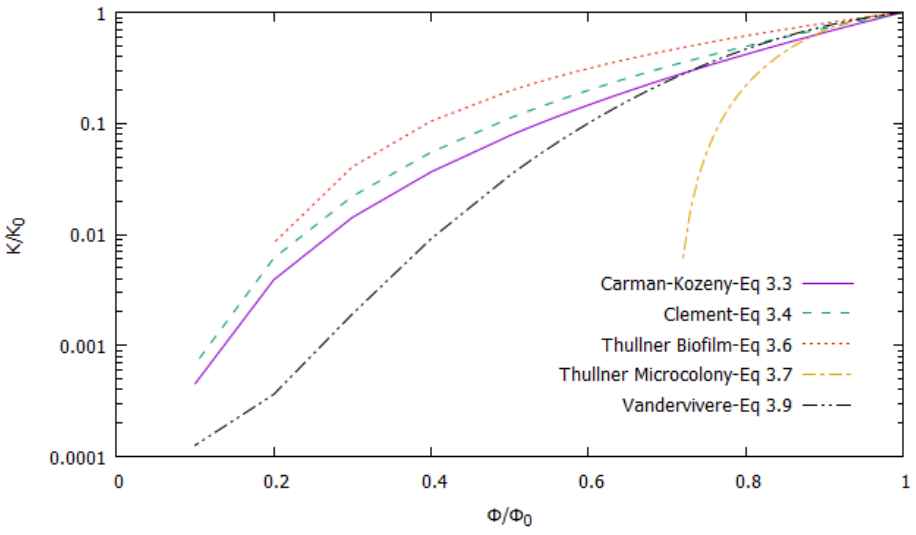

Figure 3. 3: Various profiles of permeability versus porosity of existing models. In the Thullner biofilm and Thullner microcolony models, the standard deviation of pore radii distribution was 0.33. The computation of Vandevivere model was based on the value of $\emptyset_{B,c}$=0.03, $K_{min}/K_{max}=10^{-4}$

In our study we aim to mathematically develop a permeability model for saturated porous media and in presence of biofilm. The important goal of the work is to provide a

macroscopic model that can be used to predict a wide range of experimental bioclogging data. Specifically, the model is mathematically derived from the laminar flow in the capillary tube and Darcy's law that defines fluid flow in porous media at macroscopic scale. The model also mathematically interprets two possibilities that result in permeability reduction: pore radius reduction and pore plugging : indeed, including these two processes allow a better representation of the physical process occurring during bioclogging of porous media.

3.2 Model development

Porous media can be represented by many conceptual models: sphere-in-shell (Happel 1958, Kuwabara 1959) capillary tube (Tien 1989), and constricted tube (Petersen 1958, Payatakes et al. 1973). In this study, for the simplicity porous media is treated as a bundle of capillary tubes and **Figure 3.4** presents the possible mechanisms that reduce pore space of porous media. On the one hand, biomass covers the inner wall, leading the decrease of pore radius from r_o to r. On the other hand, biomass also plugs some portion of capillary tubes, impeding fluid flow. Our work adopts the concept that permeability reduction by the reduction of pore radius (K_R) and permeability reduction by pore plugging (K_P) contribute to the overall permeability reduction of porous media (K).

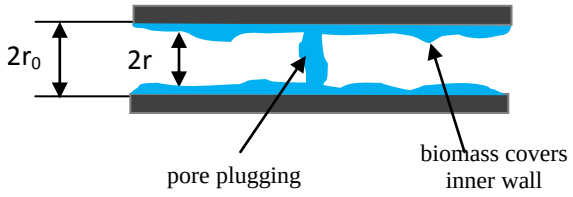

Figure 3. 4: Schematic representation of mechanisms that results in permeability reduction.

For the very low flow through pore section, the flow rate can be characterized by Hagen–Poiseuille equation (Du Plessis, 1994, Wu et al., 2008)

$$u = \frac{1}{8}\frac{\Delta P}{L_t}\frac{r^2}{\mu} \qquad (3.11)$$

where u is the flow velocity in the capillary tube (ms^{-1}). μ is the dynamic viscosity ($kgm^{-1}s^{-1}$). r is the radius of the capillary tube (m). L_t is the real length that fluid molecules transport in capillary tube (m) and it relates to straigth length of capillary tube through expression:

$$L_t = L \times \tau \qquad (3.12)$$

In the equation, τ is tortuosity of the capillary tube (-). The value of τ implies the level of tortuosity of the capillary tube ($\tau \geq 1$). There are many models to compute tortuosity (Du Plessis and Masliyah, 1991; Koponen et al., 1996; Yu and Li, 2004; Lanfrey et al., 2010, Ahmadi et al., 2011;). In this work, the model proposed by Yu and Li, (2004) is used to describe the flow path based on grain geometry:

$$\tau = \frac{1}{2}\left[1 + \frac{1}{2}\sqrt{1-\emptyset} + \sqrt{1-\emptyset} \times \frac{\sqrt{\left(\frac{1}{\sqrt{1-\emptyset}} - 1\right)^2 + \frac{1}{4}}}{1-\sqrt{1-\emptyset}}\right] \qquad (3.13)$$

On the one hand, fluid velocity in Eq (3.11) can be rewritten as a function of pressure gradient, tortuosity, dynamic viscosity and tube radius:

$$u = \frac{1}{8}\frac{\Delta P}{L\tau}\frac{r^2}{\mu} \qquad (3.14)$$

On the other hand, a laminar flow in porous media can be calculated by Darcy's law in which permeability is explicitly expressed:

$$u = \frac{U}{\emptyset} = \frac{K_R}{\emptyset\mu}\frac{\Delta P}{L} \qquad (3.15)$$

where U is superficial velocity (ms^{-1}). K_R is the permeability of capillary tube (m^2) or the permeability caused by the reduction of tube radius. Comparing Eq (3.14) and Eq (3.15), one can get easily the expression of permeability K_R:

$$K_R = \frac{\emptyset}{8}\frac{r^2}{\tau} \qquad (3.16)$$

where the pore radius can be related to hydraulic radius:

$$r = 2R_H \qquad (3.17)$$

and the hydraulic radius can be expressed through a function of porosity and specific surface area of capillary tube S_{sf} (as m^{-1}):

$$R_H = \frac{\text{cross} - \text{section of capillary tube}}{\text{perimeter of capillary tube}} = \frac{\text{volume of capillary tube}}{\text{wall surface of capillary tube}}$$

$$R_H = \frac{\text{total volume of capillary tube /volume of porous media}(V_T)}{\text{total wall surface of capillary tube /volume of porous media}(V_T)}$$

$$R_H = \frac{\emptyset}{S_{sf}} \quad (3.18)$$

Combining Eq. (3.16), Eq. (3.17) and Eq. (3.18) , K_R is expressed:

$$K_R = \frac{1}{2}\frac{\emptyset^3}{\tau S_{sf}^2} \qquad (3.19)$$

The total wall surface of capillary tube can be considered as the total surface of particles packed in porous media. Therefore S_{sf} can be expressed:

$$S_{sf} = \frac{N\pi D_P^2}{V_T} \quad (3.20)$$

with N is the number of particles packed in porous media and N can be calculated:

$$N = \frac{(1-\emptyset)V_T}{\frac{1}{6}\pi d_G^3} \quad (3.21)$$

Therefore S_{sf} can be expressed by a function of porosity and particle diameter

$$S_{sf} = \frac{(1-\emptyset)6}{d_G} \quad (3.22)$$

In the case of high biomass accumulation in porous media, thick biofilm covers grain surface and modifies the grain with the tendency of increasing the radius. With the assumption that biofilm is homogeneous and uniformly distributed on spherical grain, the grain diameter is determined through the relation with porosity

$$\frac{d_G}{d_{G,0}} = \sqrt[3]{\frac{1-\emptyset}{1-\emptyset_0}} \qquad (3.23)$$

where d_G is the diameter of grain at time t. The minimum value of d_G is the diameter of clean grain ($d_{G,0}$), without the effect of mass deposition. Substituting Eq (3.18), Eq (3.22) into Eq (3.23), the permeability K_R can be estimated as follows:

$$K_R = \frac{\emptyset^3}{72\tau}\frac{{d_{G,0}}^2}{(1-\emptyset)^{4/3}}\frac{1}{(1-\emptyset_0)^{2/3}} \qquad (3.24)$$

Eq (3.21) indicates that porosity, tortuosity, grain size determine the magnitude of permeability. Eq (3.24) can be used to estimate the permeability of clean bed packed with spherical grains by returning all the variables into initial ones ($\emptyset \rightarrow \emptyset_0$ and $\tau \rightarrow \tau_0$):

$$K_0 = \frac{\emptyset_0^3}{72\tau_0}\frac{{d_{G,0}}^2}{(1-\emptyset_0)^2} \qquad (3.25)$$

where the initial tortuosity can be calculated from Eq 3.13 by setting $\emptyset = \emptyset_0$

For a convenient monitoring, the evolution of permeability is usually presented in term of relative permeability, which is defined as the ratio of permeability $K_R(t)$ to clean bed permeability K_0.

$$\frac{K_R}{K_0} = \left(\frac{\emptyset}{\emptyset_0}\right)^3\left(\frac{\tau_0}{\tau}\right)\left(\frac{1-\emptyset_0}{1-\emptyset}\right)^{4/3} \qquad (3.26)$$

In order to compare with experimental data, the model needs to account the effect of biofilm components and morphology on the fluid movement in porous media (Veerapaneni and Wiesner, 1997). However, there is no universal model to characterize these effects. A bulk factor β_B was usually used to correct theoretical models (Tan et al.,2003), which defines the effective porosity:

$$\emptyset = \emptyset_0 - \beta_B\emptyset_B \qquad (3.27)$$

Thus, Eq (3.23) is transformed to new formula:

$$\frac{K_R}{K_0} = \left(\frac{\emptyset_0 - \beta_B \emptyset_B}{\emptyset_0}\right)^3 \left(\frac{\tau_0}{\tau}\right)\left(\frac{1-\emptyset_0}{1-\emptyset_0+\beta_B\emptyset_B}\right)^{4/3} \qquad (3.28)$$

However, Veerapaneni and Wiesner, (1997) reported that specific surface area that is modeled by Eq (3.19) might underestimate the surface modification by deposition of fine particles with a very high specific surface area. They conducted the experiment of the deposition of nanoparticles in packed column at very small volumetric fraction $\emptyset_B = 0.001$. Their result showed that relative permeability decreased severely at the order of magnitude of 10^{-3}. In such conditions, the specific surface area of particle was the main parameter driving clogging in the packed column and specific surface area can be calculated by the following equation:

$$S_{sf} = S_{sf,0} + N_e S_P \emptyset_B \qquad (3.29)$$

Where $S_{sf,0}$ and S_P are the specific surface area of clean bed (m^{-1}) and fine particle (m^{-1}). N_e is the fraction of surface area of deposited particles contributing to the modification of surface area of grain and always less than 1. The relative permeability is computed by

$$\frac{K_R}{K_0} = \frac{\tau_0}{\tau}\left(\frac{\emptyset}{\emptyset_0}\right)^3 \left(\frac{S_{sf,0}}{S_{sf}}\right)^2 \qquad (3.30)$$

In the case that mass deposition is very small compared to clean bed porosity, $\emptyset \approx \emptyset_0$, and $\tau \approx \tau_0$, combining Eq (3.29) and Eq (3.30), the relative permeability could be expressed as follows

$$\frac{K_R}{K_0} = \left(\frac{1}{1 + N_e \frac{S_P}{S_{sf,0}} \emptyset_B}\right)^2 \qquad (3.31)$$

For the simple, the grain and fine particle are assumed spherical, so the specific surface area can be calculated: $S_{sf,0} = \frac{(1-\emptyset_0)6}{d_{G,0}}$ and $S_P = \frac{6}{d_P}$, with d_P is the diameter of fine particle. So Eq (3.30) becomes:

$$\frac{K_R}{K_0} = \left(\frac{1}{1 + N_e \frac{d_{G,0}}{(1-\emptyset_0)d_P} \emptyset_B} \right)^2 \qquad (3.32)$$

By setting $\gamma = N_e \frac{d_{G,0}}{(1-\emptyset_0)d_P}$ this modified model is similar to published results of Mays and Hunt (2005), which was derived from a total different approach:

$$\frac{K_R}{K_0} = \left(\frac{1}{1 + \gamma \emptyset_B} \right)^2 \qquad (3.33)$$

However, the predicted permeability is not representative of overall permeability. The total permeability reduction should include the contribution of pore radius reduction (K_R) and of pore plugging (K_P). By following Vandervivere 's approach (Vandevivere and Baveye, 1992), one can obtain that

$$K = F(\emptyset_B)K_R + \left(1 - F(\emptyset_B)\right)K_P \qquad (3.34)$$

where K_R and K_P are computed from the Eq (3.28) and Eq (3.8), respectively and $F(\emptyset_B)$ is defined from Eq. (3.10). To recall these equations, the components of (Eq. 3.34) are given in the followings:

$$\frac{K_R}{K_0} = \left(\frac{\emptyset_0 - \beta_B \emptyset_B}{\emptyset_0} \right)^3 \frac{\tau_0}{\tau} \frac{(1-\emptyset_0)^{4/3}}{\left(1 - \emptyset_0 + \beta_B \emptyset_B\right)^{4/3}}$$

$$\tau = \frac{1}{2} \left[1 + \frac{1}{2}\sqrt{1-\emptyset} + \sqrt{1-\emptyset} \times \frac{\sqrt{\left(\frac{1}{\sqrt{1-\emptyset}} - 1 \right)^2 + \frac{1}{4}}}{1 - \sqrt{1-\emptyset}} \right]$$

$$\frac{K_P}{K_0} = \frac{K_{min}/K_0}{1 - \frac{\emptyset}{\emptyset_0} + \left(\frac{\emptyset}{\emptyset_0}\right)\left(\frac{K_{min}}{K_0}\right)}$$

$$F(\emptyset_B) = \exp\left(-0.5 \left(\frac{\emptyset_{B,rel}}{\emptyset_{B,c}} \right)^2 \right)$$

3.3 Result and discussion

3.3.1 Model discussion and sensibility

The modified model contains three empirical parameters: bulk factor β_B, biomass distribution $\emptyset_{B,c}$ and biofilm permeability K_{min}. The influence of these parameters on the modified model was studied through the sensibility analysis which the results are shown in **Figure 3.5.**

Sensibility to bulk factor

Bulk factor β_B characterizes the effective pore available for fluid flow, which is present in the equation to estimate K_R (Eq 3.28). So the influence of bulk factor β_B is considered in the cases that K_R is predominant in total permeability reduction. In the section below, a wide range of experimental data was fitted by the modified model. K_R governed the total permeability in the case of 1 mm glass beads (Cuningham et al., 1991). For this reason, this experimental data is used in this sensibility analysis. The results were shown in **Figure 3.5a.** Bulk factor β_B affects the permeability reduction. High value of bulk factor will increase permeability reduction.

The value of bulk factor β_B is dependent on clogging materials. In column experiment packed by glass beads and clogged by sand mixtures, Tan et al. (2003) reported that the value of bulk factor β_B varied from 5/3 to 11, dependent on sand properties. The sand mixture with wide range of sizes corresponded to high value of bulk factor β_B. Small particles can bridge the larger ones, increasing the formation of dead-ends and stagnant water, reducing less pore space available for fluid flow.

In biofilm system, the highly heterogeneous micro-structure of biofilm can reduce the effective pore space for fluid flow. However, the effective porosity may increase resulting from biofilm. It is well known that biofilm contains lots of voids and spaces (Lewandowski, 2000; Zhang and Bishop, 1994). Those voids and spaces can play an additional channels for fluid flow (Ebigbo et al., 2010; Delay et al., 2013). In this case, the effective porosity is higher than the global porosity of porous media (corresponding to β_B less than 1).

The value of bulk factor β_B is highly dependent on micro-structure of biofilm. This parameter is probably a time-dependent parameter. However, the information of biofilm structure and its evolution is not easy to access in macroscopic system. In the application of the permeability model, the bulk factor is treated as a fitted parameter for the simplicity.

(a)

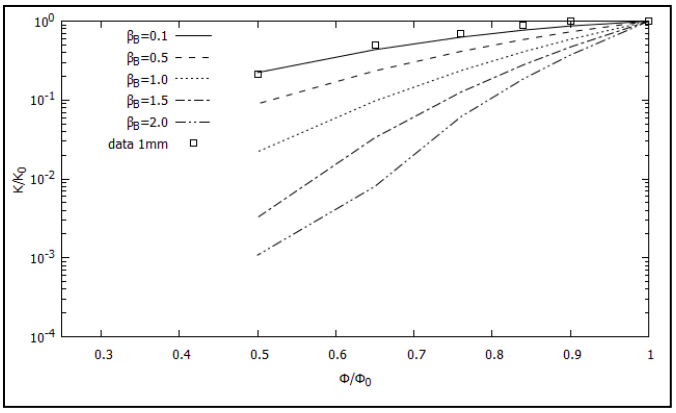

(b)

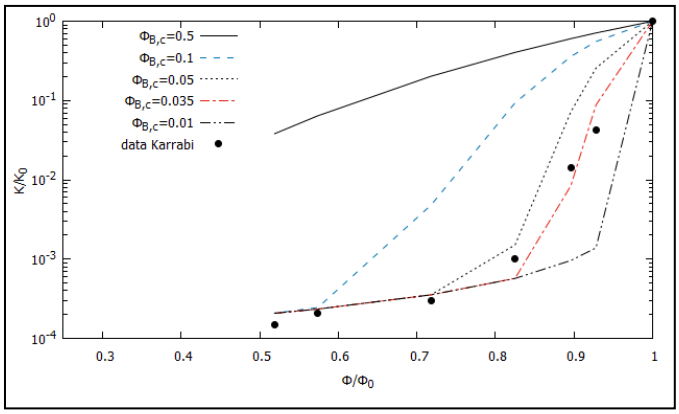

(c)

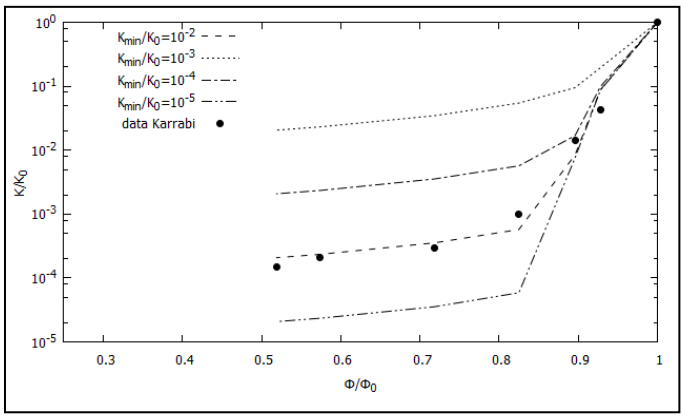

Figure 3.5: The sensibility of the modified model to (a) bulk factor, (b) biomass distribution and (c) biofilm permeability.

Sensibility to the distribution function F

The parameter $\emptyset_{B,c}$ used in function F determines the biomass fraction that results in plugging pore or reducing pore radius. The former results in drastic permeability drop as fluid should pass through biofilm, whose permeability is usually four orders less than clean bed permeability. Hence, the more biomass participates in plugging pore, the more severely the permeability is reduced. However, the distribution function $F(\emptyset_B)$ is assumed to follow a normal distribution. Vandervivere (1995) stated that the distribution is highly dependent on $\emptyset_{B,c}$, which define how fast (compared to the volume fraction of biofilm) mass aggregates are formed and plug pore space : small values of $\emptyset_{B,c}$ indicate that biomass tends to quicly form aggregates which plug the pore space compared to biofilm that covers surface grain.

The sensibility of biomass distribution function F is numerically investigated in the experiment by Karrabi et al. (2011). The $\emptyset_{B,c}$ is changed from small value to high value (0.01 to 0.5) to describe a wide variation of microstructure. **Figure 3.5b** shows that $\emptyset_{B,c}$ highly determines the shape and magnitude of permeability curves. Various forms of permeability curves are produced by changing the value of $\emptyset_{B,c}$. In case of high $\emptyset_{B,c}$ of 0.5, permeability is reduced gradually with the decrease of porosity. It is contrary to the case of smaller $\emptyset_{B,c}$ where permeability decline more drastically. In the case $\emptyset_{B,c}$ of 0.01 almost biomass is oriented to plug pore space and permeability reduction declines extremely ($K/K0 \approx 10^{-3}$ with $\emptyset/\emptyset_0 < 0.9$). In this case, steady state is reached quickly, and permeability is approximated to biofilm permeability.

Sensibility to biofilm permeability

Biofilm permeability is usually estimated by the ratio with clean-bed permeability (Vandervivere, 1995). In the case that biofilm tends to form aggregates to plug pore space, biofilter reaches steady-state quickly and permeability approaches biofilm permeability. Hence, biofilm permeability controls the magnitude of the permeability at steady-state. The influence of biofilm permeability is given in **Figure 3.5c**.

3.3.2 Model fitting to experimental data

A wide range of experimental bioclogging data has been used to validate the modified model. Firstly, the capacity of the modified model to estimate the permeability of clean-bed porous media has been tested. Experimental permeability of a clean bed can be measured indirectly through pressure gradient by Darcy's law (Eq 3.1). **Table 3.1** summarizes the parameters for calculation of clean bed permeability used in different experiments.

Table 3.1: Bioclogging experiments used to validate the modified model

Author	**Grain**	**Clean bed porosity**	**Experimental clean-bed permeability**
Cuningham et al., 1991	1 mm glass bead	0.48	$2.1x10^{-9}$ m^2
	0.7mm sand	0.35	$3.19x\ 10^{-10}$ m^2
	0.54 mm sand	0.35	$2.17x10^{-10}$ m^2
	0.12 mm sand	0.47	$9.7x10^{-11}$ m^2
Vandervivere and Baveye, 1992	0.09 mm sand	0.39	$8.17x10^{-12}m^2$
Kildsgaard and Engesgaard, 2001	0.32 mm sand	0.39	$9.8\ x\ 10^{-11}m^2$
Karrabi et al., 2011	4 mm glass bead	0.35	$1.28\ x\ 10^{-8}m^2$

The comparison of experimental data and clean-bed permeability predicted by Eq (3.25) are showed in **Figure 3.6**.The figure is presented in log-scale with the unit of 10^{-9} m^2. It is observed that the predicted values are very close to experimental ones, especially in cases of d_G=0.54 mm and d_G=4mm by the modified model. These values present linear relationship with the slope of 0.972, which indicates the good agreement between the compared values.

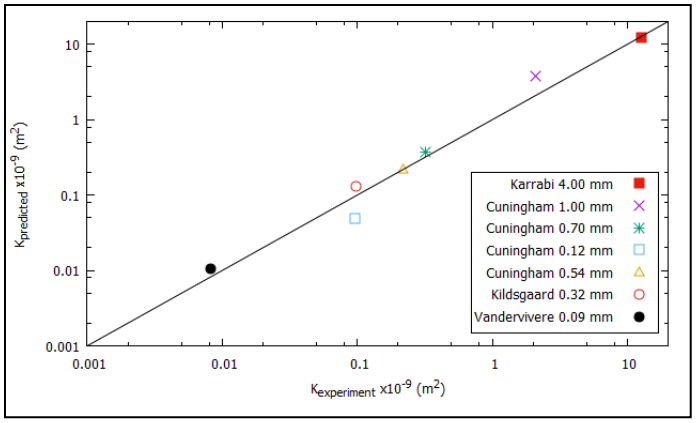

Figure 3.6: Comparison of experimental K_0 and that predicted from Eq 3.25

For the permeability evolution in porous media, the experiments of Cuningham et al. (1991), Vandervivere and Baveye (1992), Karrabi et al. (2011) have been used to test the capacity of the modified model for the prediction of permeability evolution. Before to simulate these experiments, one should note that there are three fitting parameters to be set β_B, $\emptyset_{B,c}$ and K_{min}

The fitting parameters needed for permeability estimation are given in **Table 3.2.** The bulk factor β_B may affect the permeability reduction of porous media when K_R is predominant. This can occur at the early stage of bioclogging or in the conditions that are not favorable to bioplugging. On the other hand, β_B can be neglected or mathematically set to 1 in the experiments that bioplugging plays an important role in permeability reduction.

K_{min} can be considered as biofilm permeability, which is controlled by bacterial strain, ages and exterior conditions applied to biofilm such as nutrient concentration, hydrodynamic forces. In the sensitivity analysis above, K_{min} is shown to determine the minimum permeability of porous media.

$\emptyset_{B,c}$ is the crucial parameter which influence the permeability pattern. $\emptyset_{B,c}$ is a global parameter which control the microstructure given the pore occupation (i.e, plugged part fraction and covered part fraction). One of the processes that influence $\emptyset_{B,c}$ is biofilm

detachment. Kim et al. (2010) reported that the increase of flow shear rate increased detached biomass, driving more biomass to plug the downstream of pore space. The grain sizes also affect $\emptyset_{B,c}$. Biomass is easier to plug the smaller pore space. Our fitted $\emptyset_{B,c}$ showed a consistency to this trend in Cuningham et al. (1991).

Table 3.2: Parameters needed for permeability estimation

Experiment	β_B	$\emptyset_{B,c}$	**Kmin/Kmax**
Cuningham-1mm	0.1	0.400	0.0010
Cuningham-0.7mm	0.1	0.100	0.0120
Cuningham-0.54mm	1	0.070	0.0120
Cuningham-0.12mm	1	0.030	0.0500
Vandervivere-0.09mm	1	0.050	0.0015
Karrabi-4mm	1	0.035	0.0001

In **Figure 3.7** the fitted $\emptyset_{B,c}$ was plotted as a function of grain sizes for the experiment of Cuningham et al. (1991).We chose that experiment because in their experiment, excluding the grain size, all the parameters (nutrient concentration, bacterial strain, flow rate...) are kept identical. The result, given in **Figure 3.7a**, shows the exponential correlation of $\emptyset_{B,c}$ with grain sizes in range from 0.12 mm to 1mm. $\emptyset_{B,c}$ decreases with the decrease of grain size or pore radius. It is noted that $\emptyset_{B,c}$ is less than 1. Hence, we hypothisize that the dependence of $\emptyset_{B,c}$ on grain size follows the sigmoidal curve **(Figure 3.7b)**

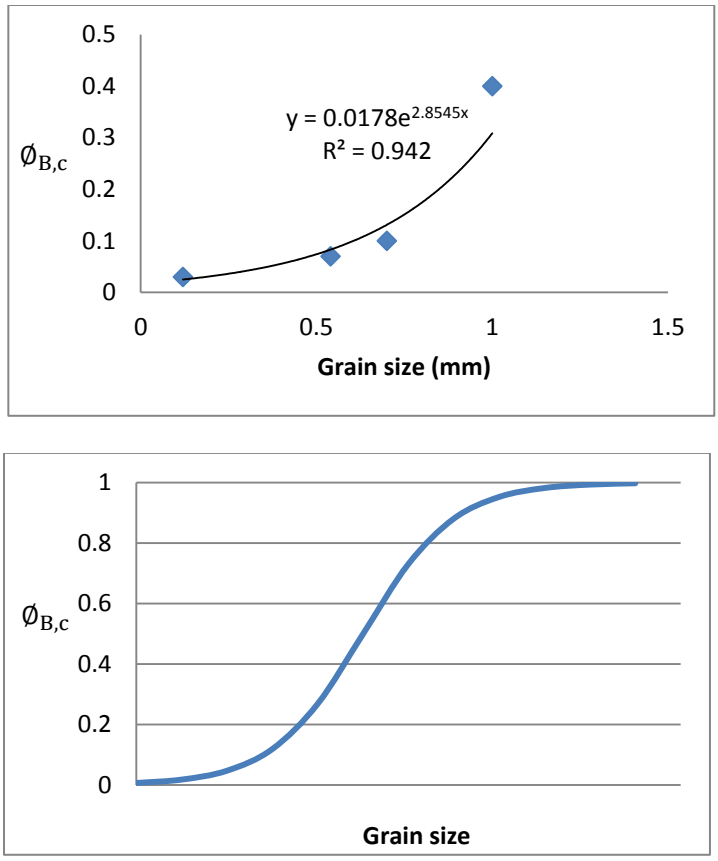

Figure 3.7: (a) The correlation of $\emptyset_{B,c}$ and grain size in experiment by Cuningham et al. (1991) and (b) the hypothesized dependence of $\emptyset_{B,c}$ on grain size

Profile of permeability evolution predicted by the modified model (Eq 3.34) have been compared to experimental data (Cuningham et al.,1991; Vandervivere and Baveye, 1992; Karrabi et al.,2011) in **Figure 3.8.** Experimental and predicted data show the good match in both decline tendency and magnitude of permeability reduction. However there are still differences in simulated and measured data. It may be explained by the drawback of the model assumption. Firstly, tortuosity calculated by Eq (3.13) is obtained with the simple assumptions of grain geometry and flow trajectory that are only appropriate for ideal porous media (Ghanbarian, 2013). It is not applicable for the heterogeneous and stratified biofilm whose average porosity is 0.8 (Zhang and Bishop, 1994; Lewandowski, 2000). The voids in the biofilm can convey fluid and contribute to global permeability (Pintelon et al., 2012; Deng et al., 2013). Although this contribution of biofilm is

implicitly included through the term of minimum permeability, biofilm permeability is not systematically incorporated in the modified model. Thirdly, the bulk factor that characterizes the biofilm component and morphology, is probably a time dependent variables depending on biofilm strain, nutrient concentration, hydrodynamic condition. By treating the bulk factor as a constant fitting parameter may explain some of the discrepancies that are observed.

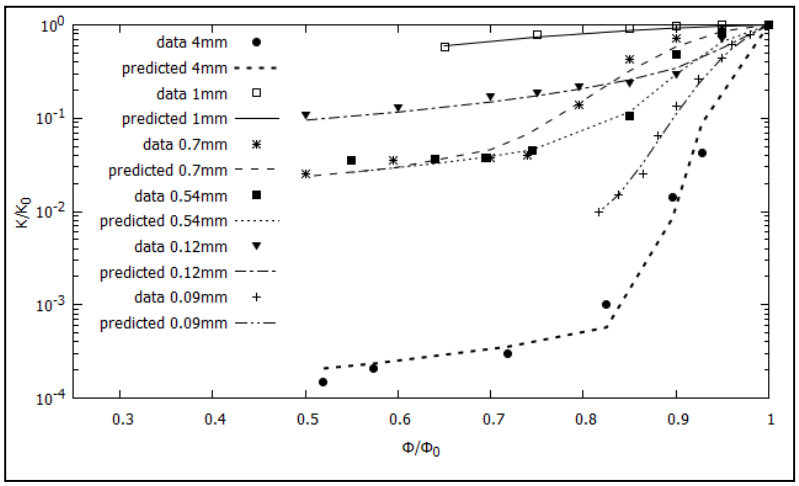

Figure 3.8: Profile of permeability evolution versus relative porosity ($\emptyset/\emptyset_0$) obtained from bioclogging experiments (points) and calculation from modified model (lines).

3.3.3 Modified model for the prediction of early-stage bioclogging (resulting from a small biofilm volumetric fraction)

In the case that bio-aggregates are prone to occur, the main mechanisms to reduce permeability is plugging pore spaces. For instance, K_P accounts for nearly 100% of total permeability reduction in biofilter (**Figure 3.9**) with a biofilm occupation $\emptyset_B/\emptyset_0 > 0.18$ (Karrabi et al., 2011). In such case, Eq 3.34 produces the similar prediction to that given by Vandervivere's model as the formulation of K_p is similar in both model. However, in the case that K_R is predominant, as the formulation of K_R differs between the two models, Vandervivere's model may underestimate permeability reduction because tortuosity is not explicitly accounted in Vandervivere's model.

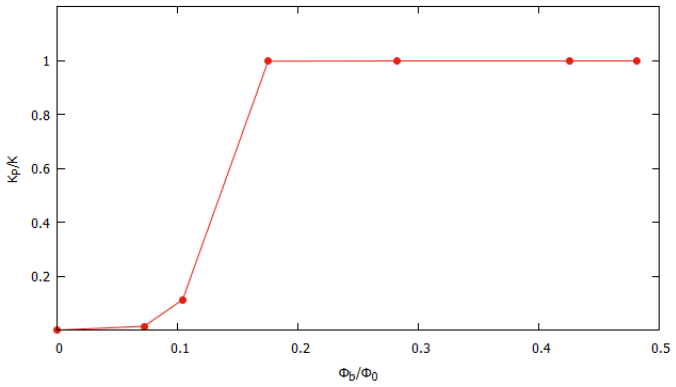

Figure 3. 9: The contribution of K_P to the total permeability reduction in biofilter experiment conducted by Karrabi et al. (2011)

In order to test the performance of our modified model for the early stage of bioclogging where both the two mechanisms contribute to permeability reduction, Eq 3.34 has been applied to the experiment conducted by Rolland du Roscoat et al. (2017). In their study, biofilms of *Pseudomonas putida* (DSM 6521) were grown in glass columns with 10mm inner diameter, and 200 mm long which were packed with 1mm-glass beads. The column was supplied by nutrient solution (casein peptone 1 g/l, yeast extract 0.5 g/l, NaCl 0.5g/l, Agar 2 g/l, pH 7± 0.2) with flow rate of 40ml/h in 12 days.

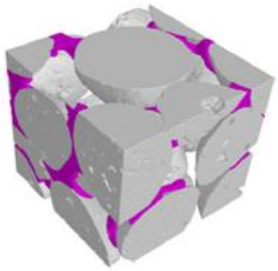

Figure 3. 10: 3D rescontructed structure of porous media using X-ray tomography (Rolland du Roscoat et al., 2017)

At the end of the experiment, through the image analysis (**Figure 3.10**) and numerical flow calculation on the real biofilm structure, the biofilm distribution and related properties were measured (**Table 3.3).** The samples are characterized by three numbers:

sample number, time for running the experiment (in days) and the position of measured section in the mini-biofilter that was applied X-ray tomography (in mm).

Table 3.3: Characteristics of biofilm structure and biofilter hydrodynamics (volumetric fraction of biofilm $\emptyset_B$, specific surface area $\mathbf{S_{sf}}$ and permeability $\mathbf{K_{tomo}}$), which were obtained from X-ray tomography (Rolland du Roscoat et al., 2017)

Sample	$\emptyset/\emptyset_0$	τ_B/τ_0	$S_{sf}/S_{sf,0}$	K_{tomo}/K_0
C22-12day-0mm	0,7026	0,2973	0,777	0,3036
C22-12day-40mm	0,7408	0,2591	0,720	0,4619
C24-7day-0mm	0,8492	0,1507	0,949	0,4991
C24-7day-40mm	0,8836	0,1163	0,970	0,6254
C28-3day-0mm	0,8843	0,1156	0,918	0,5806
C28-3day-40mm	0,9222	0,0777	0,942	0,7089
C13-7day-0mm	0,7596	0,1984	1,127	0,3288
C13-7day-40mm	0,9281	0,0552	1,112	0,6254
C18-4day-0mm	0,9865	0,0134	1,036	0,9215
C18-4day-40mm	0,9791	0,0209	1,036	0,8534
C19-1day-0mm	0,9518	0,0481	1,089	0,7546
C19-1day-0mm	0,9604	0,0395	1,050	0,7957

As mentioned above, when bioplugging occurs, permeability is highly sensitive to the empirical parameter $\emptyset_{B,c}$. This number is calibrated to secure the minimum value of *sum of squares(R^2)*

$$R^2 = \frac{\sum_{i=1}^{n}(K_{tomo,i} - K_{est,i})^2}{\sum_{i=1}^{n}(K_{tomo,i} - \overline{K_{tomo}})^2}$$

where n is the number of experimental data, $\overline{K_{tomo}}$ is the mean permeability computed by X-ray tomography, which is defined: $\overline{K_{tomo}} = \frac{1}{n}\sum_{i=1}^{n} K_{tomo,i}$. The subscript *tomo* indicates the values obtained by X-ray tomography and *est* indicates estimated values. The R^2 ranges from 0 to $+\infty$, with the value of 0 specifying the best fit of estimated permeability to experimental one, the higher the sum of squares indicating that the model is less accurate in predicting experimental data (K/K_0).

The estimated permeability (K/K_0) as well as the one obtained by the three models (Vandervivere, Carman-Kozeny, modified model-this study) are given in **Figure 3.11.**

The x-axis presents biomass volumetric fraction, and the y-axis presents permeability reduction at unit-scale.

For the permeability reduction calculation, the best fits were obtained for $\emptyset_{B,c} = 0.5$ in the case of the modified model, and $\Phi_{B,C}$=0.2 in the case of Vandervivere model. In the case of the modified model, given the value of Φ_{BC}, the value of $F(\Phi_B)$ is such that the contribution of pore plugging is very small (less than 20% for all the case). So the contribution to the permeability given by the modified model comes essentialy from pore radius reduction. The value of $F(\Phi_B)$ in the case of the Vandervivere model was always found lower than the modified model, indicating a more important contribution of the plugging mechanism to the calculation of the relative permeability.

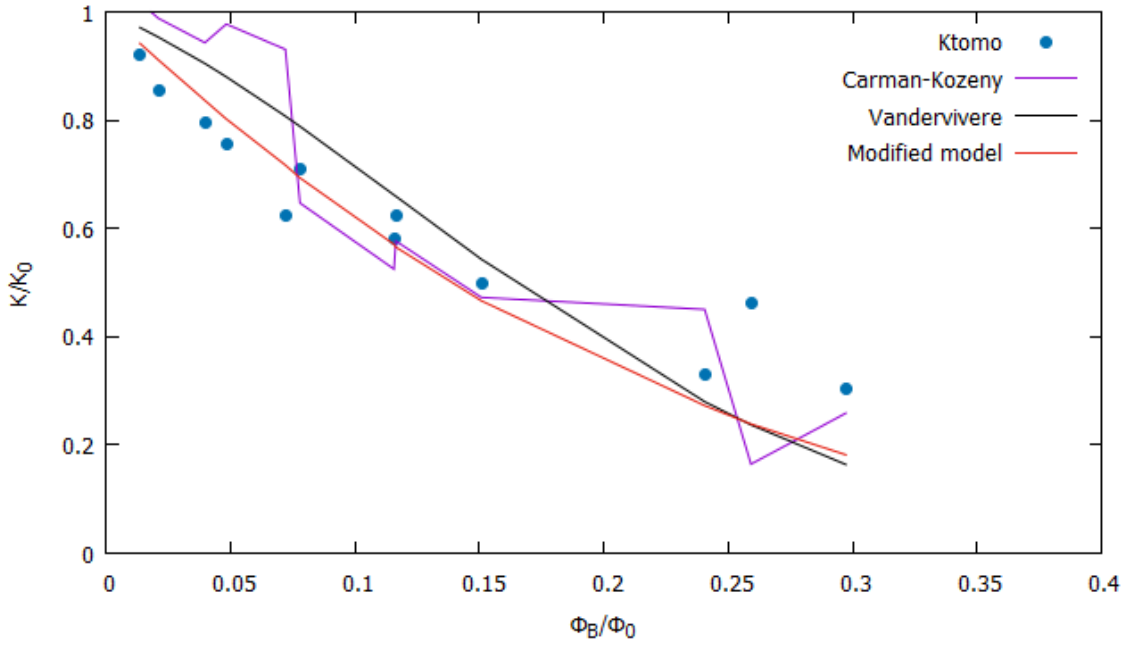

Figure 3.11: The application of modified model, Carman-Kozeny's model and Vandervivere's model to estimate permeability reduction in mini-biofilter

An unusual shape of Carman-Kozeny can be observed in **Figure 3.11**. It can be due to oscillation of specific surface area. In porous media, biofilm grows and modifies grain surface. The modification usually increases the specific surface area (Sample C13, C18,

C19) as the specific surface area of biofilm is higher than that of grains. However when micro-aggregates are formed, the space between grains are occupied by biomass or in other words, grains are stuck together and can decrease the specific surface area. The measurement of sample C12 showed that specific surface area declined after 12 days of running the mini-biofilter.

Comparing the three models, the modified model produced the best match to experimental data with R^2=0.21 for the new equation (R^2=0.38 for Vandervivere and R^2=0.72 for Carman-Kozeny). As in this case, the mechanism of pore reduction is predominant in the permeability calculation, it means that (i) biomass covering the grain surface is the main mechanism to reduce permeability in this mini-biofilter at the early-stage bioclogging, (ii) the modeling of K_R that we introduced in our model, is relevant in this situation (iii) the higher discrepancy given by the Vandevivere model compared to the experimental results may come for the different modelling of K_R compare to the modified model.

3.4 Conclusion of chapter 3

In this study, a permeability model is developed for modeling application at field-scale. Following Vandevivere, the model interprets two mechanisms resulting in bioclogging (i) pore radius reduction and (ii) micro-aggregates plugging pore space. In the modified model, permeability is a function of the geometry of porous media and biofilm characteristics. The geometry of porous media, which is represented by clean-bed porosity and grain diameter profoundly affect clean-bed permeability, while biofilm characteristics affect pattern and magnitude of bioclogging. In the case that micro-organisms tend to form aggregates that plug the pore space, bioplugging become the dominant process that governs permeability of porous media. The main difference between Vandevivere model and the new one consist in the modeling of the first mechanism (pore radius reduction) through the permeability K_R.

The new permeability model obtained a good agreement to a wide range of experimental data in the estimating: clean-bed permeability and bioclogging evolution of porous

media. Especially, through its confrontation with data gathered from an X-ray tomography experiment, it allowed a better prediction of the permeability reduction at low biofilm fraction.

However some simple assumptions in the model are limitative and should be revised. In the first mechanism that biofilm reduces pore radius, biofilm porosity was not accounted in the mathematical development the permeability model. It is well known that biofilm is stratified and contains lots of voids and channels. On the other hand, the biofilm microstructure can be such that dead zone for the fluid exist. Those two effect can be taken into account roughly in the model through the parameter β_B. This parameter is at the current state of our knowledge difficult to measure on real system. Furthermore, there is no reason that it is a constant knowing that the biofilm structure can vary with the biofilm age or through external constraints (shear force leading to detachment). With the simple assumption made in this study (β_B=1), the flow in biofilm, in the case of the mechanism of pore reduction, was ignored and biofilm permeability was considered to be zero.

In the second mechanism that biomass plugs the pore space, the mass distribution governs the pattern of permeability reduction in porous media. However, the function $F(\emptyset_B)$ which control the fraction of the plugged part of the system which contributes to the permeability was assumed to follow a normal distribution. This classical assumption may not be true depending on the considered systems. Recent advances in the frame of X-ray tomography could allow to investigate this issue. Indeed, this technique permits the reconstruction of the 3-D structure and biomass distribution of the porous media. A thorough analysis of the data could lead to a better understanding of the clogging mechanisms as well as the definition of the function $F(\emptyset_B)$ and $\emptyset_{B,C}$ parameter for different operating conditions and bacteria strains.

Chapter 4

The correlation equation for the estimation of initial attachment of bio-colloids on saturated porous media.

In this chapter, the initial biomass attachment has been studied. Following the concept that bacterial cell can be treated as soft colloids, a classical filtration approach (CFT) is applied to develop a new correlation equation to estimate the attachment efficiency. The new equation is based on the regression analysis of a wide range of experimental data of colloid deposition in various electrolyte conditions, flow rates, and geometries of porous media. New dimensionless parameters have been introduced to present the coupled effects of Derjaguin -Landau-Verwey-Overbeek (DLVO) forces and hydrodynamic forces. Specifically, the influence of grain size was also accounted in the description of hydrodynamic forces. The new correlation equation produced a good agreement between the attached efficiency prediction with the values given by experimental measurement.

List of symbol

Symbol	Unit	Definition
Basic notation		
a_0	m	Diameter of deformable area
A_H	kgm^2s^{-2}	Hamaker constant
As	-	Porosity-dependent parameter
dg	m	Collector diameter
dp	m	Particle diameter
D_∞	m^2s^{-1}	Bulk diffusion coefficient
E_{1max}	-	DLVO energy at primary maximum

E_{2min}	-	DLVO energy at secondary minimum
E_{EDL}	-	Repulsive energy
f_1	-	fraction of successful attachment at primary maximum
f_2	-	fraction of successful attachment at secondary minimum
f(v)		Maxwell distribution for velocity
F_A	$kgms^{-2}$	Adhesive force
F_D	$kgms^{-2}$	Drag force
F_L	$kgms^{-2}$	Lift force
g	(ms^{-2})	Gravitational acceleration
h	m	Separation distance
h_{1max}	m	Separation distance correspondent primary maximum
h_{2min}	m	Separation distance correspondent to secondary minimum
I	M	Ionic strength
k_{att}	s-1	Attachment rate
k_B	$kgm^2s^{-2}K^{-1}$	Boltzmann constant, $k_B = 1.38x10^{-23}$
K_1, K_2, K_4	-	arbitrary constants that depend on porosity
K_Y	$kg\ m^{-1}s^{-2}$	Young modulus
N_A	-	Attraction number
N_{Av}	-	Avogadro's number $6.022x\ 10^{23}$
N_{C-Lo}	-	Dimensionless parameter presenting van der Waals attractive fore in Chang and Chan, 2008
N_{C-E1}	-	Dimensionless parameter presenting repulsive fore in Chang and Chan, 2008
N_{C-DL}	-	Dimensionless parameter presenting repulsive fore in Chang and Chan, 2008
N_{col}	-	Dimensionless parameter in Elimelech, 1992
N_{DL}	-	Dimensionless parameter presenting repulsive force
N_{E1}	-	Dimensionless parameter presenting repulsive force
N_{E1*}	-	Dimensionless parameter used in the new correlation equation
N_{E2}	-	Dimensionless parameter presenting repulsive force
N_G	-	Gravity number
N_{Lo}	-	Dimensionless parameter presenting van der Waals attractive force
N_{LO*}	-	Dimensionless parameter used in the new correlation equation
N_{Pe}	-	Peclet number
N_R	-	Relative size number
N_{vdW}	-	Van der Waals number
T	K	Fluid absolute temperature

T_A	kgm^2s^{-2}	Adhesive torque
T_H	kgm^2s^{-2}	Hydrodynamic torque
U	ms^{-1}	Fluid approaching velocity
v	ms^{-1}	pore velocity
v_{2min}	ms^{-1}	velocity of particle at secondary minimum
w	-	arbitrary constants that depends on porosity
Greek letters		
α_{att}	-	Attachment efficiency
α_{BT}	-	Attachment efficiency provided by Bai and Tien, 1999
α_{CC1}	-	Attachment efficiency provided by Chang and Chan, 2008
α_{CC2}	-	Attachment efficiency provided by Chang and Chan, 2009
α_{exp}	-	Experimented attachment efficiency
α_E	-	Attachment efficiency provided by Elimelech, 1992
α_{max1}	-	Attachment efficiency at primary maximum
α_{min2}	-	Attachment efficiency at secondary minimum
$\alpha_{predicted}$	-	Attachment efficiency provided by new correlation equation
γ	-	Porosity-dependent parameter
ϵ_0	$CV^{-1}m^{-1}$	Permittivity of free space, $\epsilon_0 = 8.85 \times 10^{-12}$
ϵ_r	-	Relative dielectric constant of water (78.5)
η_0	-	Contacting efficiency
λ	m	Characteristic wave length of sphere-plate interaction
κ	m^{-1}	Debye-Huckel parameter
μ	$(kgm^{-1}s^{-1})$,	Absolute fluid viscosity
ρ_f	(kgm^{-3}),	Fluid density
ρ_p	(kgm^{-3}),	Particle density
$\emptyset$	-	Porosity of porous media
τ_R	s^{-1}	Shear rate
ζ_p	V	Zeta potential of particle
ζ_g	V	Zeta potential of collector

4.1 Introduction

One of the great difficulties of simulating the coupling between-biofilm growth and solute transport in porous media is to predict the unsteady behavior of the systems that depends strongly on the initial conditions. Indeed, in most experiments (and some industrial applications), bacteria are inoculated inside the column packed with porous media through a seeding process, before operating the system. This step aims to facilitate the biofilm formation by providing a bacteria distribution in the column. Depending on the initial biofilm distribution, the system behavior can be affected, especially during the transcient phase (Brovelli et al., 2009). However, initial biofilm distribution is not easily accessible so that this parameter is treated either as a calibration parameter (Brovelli et al., 2009), using *a priori* concentration profile (constant profile, exponential profile...) or calculated by modelling the colonization process with a simple attachment law, for instance linear with porosity (Obigbo et al., 2011)

On the physical point of view, during the inoculating process, seeding bacteria for biofilm formation on the grain surfaces is determined by the transfer of bacteria from the liquid phase to solid phase (grain surfaces)- or biomass attachment on that surface. Usually, it is assumed that the attached bacteria does not influence the upcoming deposition events at the initial attachment, so that the attachment rate can be quantified by using colloid filtration theory (CFT) (Clement et al., 1996; Kildsgaard and Engesgaard, 2001; Thullner et al., 2004; Tufenkji, 2007; Syngouna and Chrysikopoulos, 2011).

Attachment efficiency α_{att} is defined as the ratio of a number of successfully attached colloids to the total number of colloids contacting to collectors. The value of α_{att} is determined by the interaction of DLVO (Derjaguin -Landau-Verwey-Overbeek) energy and hydrodynamic condition. However, the interaction is complicated so that analytical solution may not be sufficient to estimate attachment efficiency. Correlation equation which consists of dimensionless parameters to account for the contribution of DLVO and hydrodynamic forces can be considered as an alternative in the estimation of the

attachment efficiency (Bai and Tien, 1999; Elimelech, 1992; Chang and Chan, 2008; Chang and Chan, 2009)

In this chapter, we aim to develop a new correlation equation to estimate the attachment probability of colloids to collector surfaces in the saturated condition. This equation is based on the regression analysis of a wide range of experimental data of colloid and bacterial deposition (118 data points) in various electrolyte conditions, flow rates, and geometries of porous media. The equation includes dimensionless parameters that interpret the contribution of hydrodynamic and DLVO forces to the attachment efficiency. Specifically, the influence of hydrodynamic force with the account of geometry of porous media is incorporated in the dimensionless parameters for the estimation of attachment efficiency.

4.2 Background

Following the CFT, the attachment rate k_{att} expressed in s^{-1} is linearly proportional to pore velocity, contact efficiency η_0 and attachment efficiency α_{att} (Harvey and Garabedian, 1991; Anders and Chrysikopoulos, 2005; Scheibe et al., 2007).

$$k_{att} = \frac{3(1-\emptyset)v}{2d_g\emptyset}\eta_0\alpha_{att} \qquad (4.1)$$

where $\emptyset$ is porosity, dg is collector diameter (m) and v is the pore velocity (ms^{-1}). Eq. (4.1) can be derived from a simple mass balance with the assumption that packing grain is an individual spherical particle (see detail in Appendix A 4.1)

4.2.1 Contact probability:

Generally, colloids contact to a collector in three main modes: interception, sedimentation and diffusion that linearly contribute to contact probability. In the interception mode, suspended colloids travel along the streamline. A critical streamline can be defined which divides the approaching section into 2 zones so that only particles approaching the grain in the interior zone can contact to the collector. In some conditions the streamline equations can be calculated and the interception probability calculated. Sedimentation and diffusion are the processes that colloids tend to separate from

streamline as the result of gravity force and Brownian motion, respectively, and strike to the collector. The contribution of diffusion process to contact probability is insignificant in case of colloids with size larger than 1 µm.

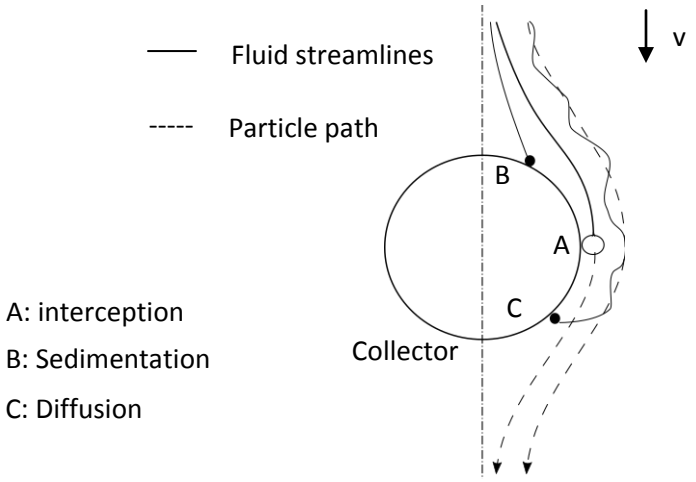

Figure 4.1: Schematic present of three different modes contributing to contacting efficiency.

Many studies have been carried out for the calculation of contact probability. For instance, assuming an idealized porous media geometry made of spheres and assuming a creeping flow, Zamani and Maini (2009) showed theoretically that the interception probability could be given by $\eta_{interception} = \frac{3}{2}\left(\frac{d_P}{d_G}\right)^2$ In the same way, including gravity, the same author calculated the contact probability through the sedimentation mode and found : $\eta_{gravité} = \frac{(\rho_s - \rho_f) g d_p^{\,2}}{18 \mu . v}$

Other approaches are rather semi-empirical. For instance, the equation proposed by Tufenkji and Elimelech (2007) for the contact probability is widely used. This equation resulted from the numerical simulation by solving convective−diffusive equation, the flow around the collector being treated by the application of Happel's model.

$$\eta_0 = \underbrace{0.55 A_s N_R^{1.675} N_A^{0.125}}_{\text{Interception}} + \underbrace{0.22 N_R^{-0.24} N_{vdW}^{0.053} N_G^{1.11}}_{\text{Sedimentation}} + \underbrace{2.4 A_S^{1/3} N_R^{-0.081} N_{Pe}^{-0.715} N_{vdW}^{0.052}}_{\text{Diffusion}} \quad (4.2)$$

The definition of dimensionless parameters are given the **Table 4.1**

Table 4.1: Definition of dimensionless parameters that are used in semi-empirical equation proposed by Tufenkji and Elimelech (2004)

Relative size number	$N_R = \frac{d_p}{d_g}$
Peclet number	$N_{Pe} = \frac{Ud_g}{D_\infty}$
Van der Waals number	$N_{vdW} = \frac{A_H}{kT}$
Attraction number	$N_A = \frac{A_H}{12\pi\mu r_p^2 U}$
Gravity number	$N_G = \frac{1}{18}\frac{d_p^2\left(\rho_p - \rho_f\right)g}{\mu U}$
Porosity-dependent parameter	$A_s = \frac{2(1-\gamma^5)}{2-3\gamma+3\gamma^5-2\gamma^6}$ With $\gamma = (1-\phi)^{1/3}$

Where:

dp is the particle diameter (m),

d_g is the collector diameter (m),

U is the fluid approaching velocity (ms^{-1}),

D_∞ is the bulk diffusion coefficient (m^2s^{-1}) that is defined as : $D_\infty = \frac{k_B T}{3\pi\mu d_p}$

A_H is the Hamaker constant (kgm^2s^{-2})

k_B is the Boltzmann constant $1.38x10^{-23}$ ($kgm^2s^{-2}K^{-1}$),

T is fluid absolute temperature (K),

ρ_p is the particle density (kgm^{-3}),

ρ_f is the fluid density(kgm^{-3}),

μ is the absolute fluid viscosity ($kgm^{-1}s^{-1}$),

and g is the gravitational acceleration (ms^{-2})

4.2.2 Attachment efficiency

In the classical DLVO theory of colloidal stability, the DLVO energy is governed by two forces: (1) van der Waals attraction and (2) electrical double layer forces **(Figure 4.2).**

Colloids are assumed to deposit on the surface at the secondary minimum and primary maximum of DLVO energy.

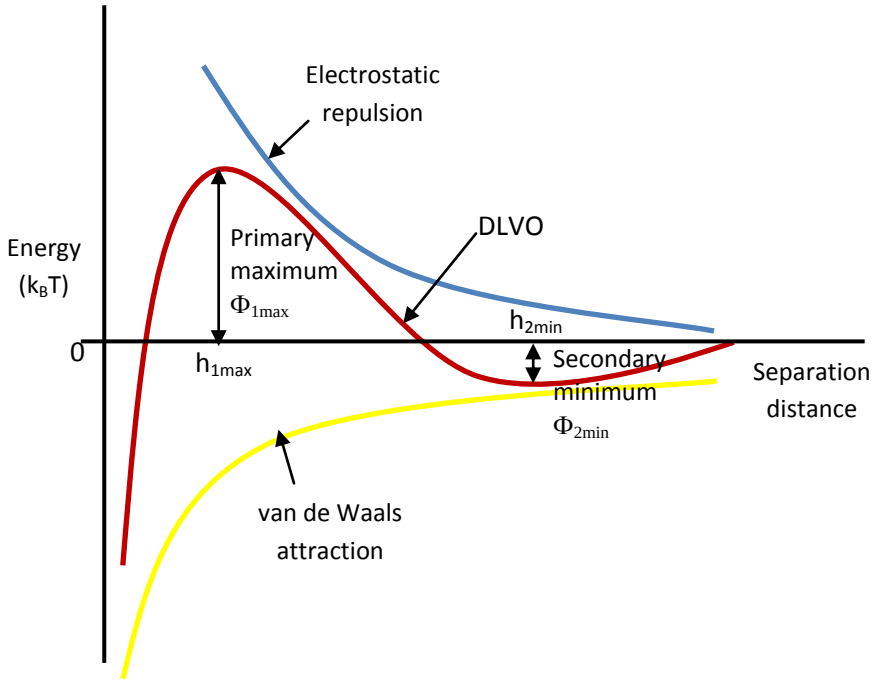

Figure 4.2: Schematic sketch of total energy (E_{tot}) with its components van der Waals attractive energy (E_{vdW}) and electrical double layer repulsive energy (E_{DL}) versus separation distance of particle and collector.

van der Waals attractive force

For a system of a particle with radius largely smaller than that of collector ($r_p << r_g$), the surface of collector is considered as a plate. The vdW attractive energy E_{vdW} for such sphere-plate geometry can be expressed by the following equation (Gregory, 1981)

$$E_{vdW} = -\frac{A_H r_p}{6h}\left[1 + \frac{14h}{\lambda}\right]^{-1} \qquad (4.3)$$

where: h is separation distance, A_H is the Hamaker constant for particle-water-collector. λ is the characteristic wave length of sphere-plate interaction, assumed to be 100nm in many studies (Syngouna and Chrysikopoulos, 2011)

Electrical repulsion forces

The Electrical repulsion forces E_{DL} can be computed as follows (Hogg et al., 1966):

$$E_{EDL} = \pi\epsilon_0\epsilon_r r_p \left[2\zeta_p\zeta_g \ln\left(\frac{1+e^{-\kappa h}}{1-e^{-\kappa h}}\right) + \left(\zeta_p^2 + \zeta_g^2\right)\ln\left(1 - e^{-2\kappa h}\right)\right] \quad (4.4)$$

where κ is Debye-Huckel parameter

$$\kappa = \left(\frac{2000e^2 N_{Av} I}{\epsilon_0\epsilon_r k_B T}\right)^{0.5} \quad (4.5)$$

ζ_p, ζ_g are the zeta potential of particle and the grain (V)

e is the electron charge 1.602 x 10^{-19} C

z is the valence of ion in bulk solution

N_{Av} is the Avogadro's number 6.022x 10^{23}

and I is the ionic strength (for DI water, I is assumed to be equal to $10^{-5.5}$ M)

ϵ_0 is permittivity of free space, $\epsilon_0 = 8.85$ x 10^{-12}

ϵ_r is relative dielectric constant of water (78.5)

DLVO energy is influenced by ionic strength, the increase of salt concentration drives the increase of van der Waals attraction and in consequence, alter the total interaction energy (**Figure 4.3**). Four types of total interaction energy curves can be found with the increase of salt concentration. Curve I: collector and colloids repel strongly, small colloid particles remain stable in the aqueous phase. Curve II: the colloid may approach the secondary minimum observed on the interaction energy curve, colloids coagulate slowly. Curve III: colloids may remain in secondary minimum, colloids coagulate rapidly. Curve IV: surfaces and colloids coalesce rapidly. In the scope of this chapter, we focus on the unfavorable attachment of curve II as it corresponds to the ionic strength close to the natural condition of ground water and nutrient solution for bacterial inoculation at seeding stage.

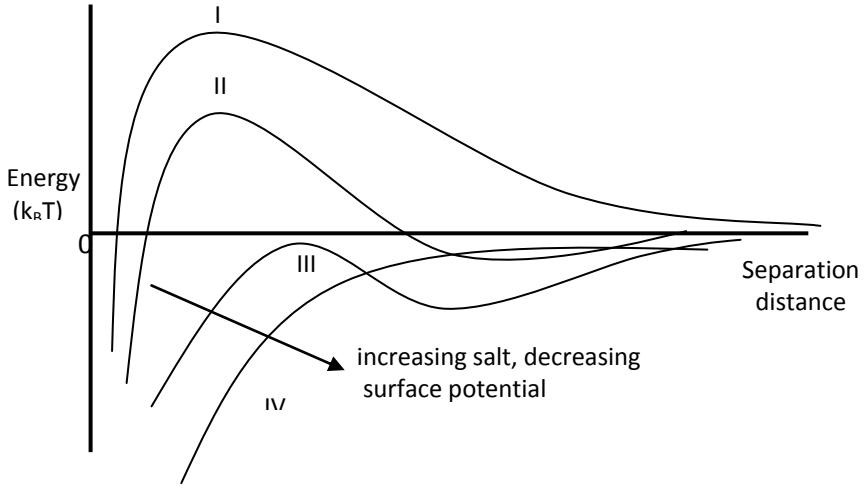

Figure 4. 3:The effect of ionic strength on total interaction energy.

4.2.3 Mechanistic approach for the calculation of attachment efficiency.

4.2.3.1 The application of Maxwell distribution

The mechanistic approach are based on the DLVO interaction energy to calculate attachment efficiency. In this approach we are interested the depositions of particles under unfavorable condition (type II, **Figure 4.3**) (Shen et al., 2007; Shen et al., 2010). In that case particles deposit on collector surface in both secondary minimum and primary maximum. The computation of attachment efficiency can be implemented with the following assumptions:

(i) When colloids reach a separation distance corresponding to secondary minimum, if the interaction energy of secondary minimum is higher than kinetic energy of colloids, they will be deposited there.

Following the first assumption, the deposition probability at the secondary minimum can be estimated:

$$\alpha_{2\min} = \int_0^{v_{2\min}} f(v)dv \qquad (4.6)$$

where $v_{2min}$is the velocity of particle at secondary minimum.

The Maxwell distribution f(v) was used to describe the velocity of colloid in secondary minimum and primary maximum (Shen et al., 2007, Shen et al., 2010, Syngouna and Chrysikopoulos 2012):

$$f(v) = 4\pi\left(\frac{m_p}{2\pi kT}\right)^{3/2} v^2 \exp\left(-\frac{m_p v^2}{2kT}\right) \qquad (4.7)$$

$$\int_0^\infty f(v)dv = 1 \qquad (4.8)$$

Where m_p is mass (kg) of a colloid and v is its velocity (ms^{-1}).

By setting the dimensionless kinetic energy $E_k = \frac{1}{2}\frac{m_p v^2}{kT}$, Eq. (4.8) is rewritten:

$$f(v)dv = 2\sqrt{\frac{E_k}{\pi}} \exp(-E_k) dE_k \qquad (4.9)$$

And the deposition probability at secondary minimum can be calculated in term of secondary minimum energy:

$$\alpha_{2min} = \int_0^{E_{2min}} 2\sqrt{\frac{E_k}{\pi}} \exp(-E_k) dE_k \qquad (4.10)$$

where: $E_{2min} = \frac{1}{2}\frac{m_p {v_{2min}}^2}{kT} = \frac{\Phi_{2min}}{kT}$

Knowing the surface properties of the collector and colloid as well as the electrolyte properties using eq (4.3) and (4.4), the total interaction energy curve can be calculated, the value of Φ_{2min} and E_{2min} determined, and so α_{2min} calculated with eq (4.10)

Similarly, the collision efficiency at primary maximum can be defined:

$$\alpha_{1max} = \int_{E_{1max}-E_{2min}}^\infty 2\sqrt{\frac{E_k}{\pi}} \exp(-E_k) dE_k \qquad (4.11)$$

(ii) the deposition of colloids at the primary minimum can occur when their kinetic energies are larger than total interaction energy of primary maximum and secondary minimum.

The total attachment efficiency is the summation of probability of deposition at secondary minimum (α_{min2}) and primary maximum (α_{max1})

$$\alpha_{att} = \alpha_{max1} + \alpha_{min2} \qquad (4.12)$$

4.2.3.2 Accounting of hydrodynamic forces on the calculation of attachment efficiency

The influence of hydrodynamic forces on particle attachment have been widely reported (Sharma et al., 1992; Bergendahl and Grasso, 2000). Burdick et al. (2005) stated that the particle attachment to the collector surface is the result of torque balance. The hydrodynamic torque (T_H) is the result of drag force (F_D) and lift force (F_L). The adhesive torque (T_A) is created from the adhesive force, which is controlled by DLVO energy. When torque of hydrodynamic forces (drag force, lift force) is less than the torque of adhesive force, the attachment of particle to collector surface is successful (Torkzaban et al., 2007; Shen et al., 2010**)**

$$T_A > T_H \qquad (4.13)$$

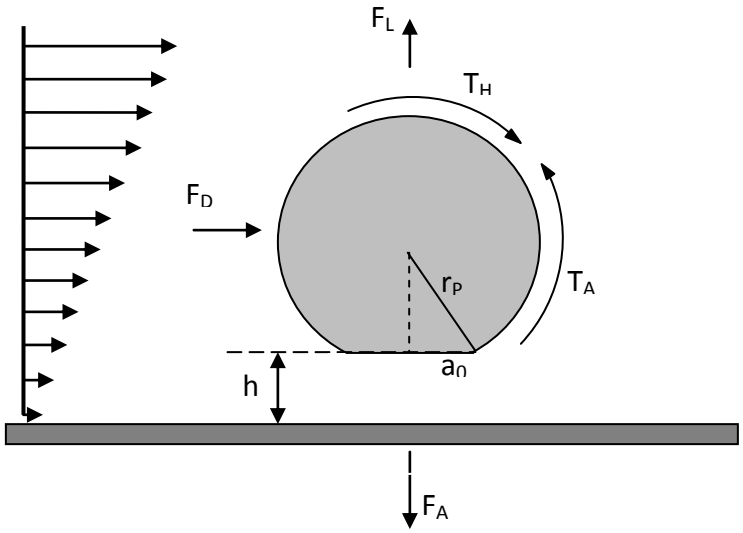

Figure 4. 4: Schematic present of forces and torques applied on particle in the vicinity of the collector surface

Adhesive torque:

Torque can be calculated by the following equations (Torkzaban et al., 2007):

$$T_A = F_A a_0 \qquad (4.14)$$

with $a_0 = \sqrt[3]{\frac{4F_A r_P}{K_Y}}$, and K_Y is the Young modulus (Nm^{-2}).

F_A is the adhesive force that depends on depth of DLVO energy.:

- Particle deposits in the secondary minimum, $F_{A2min} = \frac{E_{2min}}{h_{2min}}$ (4.15)

- Particle deposits in the maximum primary: $F_{A1max} = \frac{E_{1max}}{h_{1max}}$ (4.16)

with E_{2min}, E_{1max} are the depths of secondary minimum and primary maximum. h_{2min}, h_{1max} correspond to the separation distance of secondary minimum and primary maximum.

Hydrodynamic torque

Hydrodynamic torque is a summation of torques that results from lift force and drag force (Torkzaban et al., 2007):

$$T_H = F_L a_0 + F_D(\sqrt{r_P^2 - a_0^2} + h) \quad (4.17)$$

Under laminar flow, taking into account the collector surface, and assuming a linear shear flow, the lift force and drag force can be determined by the following equations (O'Neill, 1968):

$$F_D = 10.205\pi\mu\tau_R r_p^2 \quad (4.18)$$

$$F_L = \frac{81.2\mu{\tau_R}^2 r_p^3}{(\mu/\rho)^{0.5}} \quad (4.19)$$

where τ_R is the shear rate (s^{-1})

Shen et al. (2010) adopted Happel's model (Happel, 1958) and calculated flow field around collector **(Figure 4.5)** to define the shear rate:

$$\tau_R = \frac{1}{2} U r_G^2 \sin\theta \left[3K_1 \frac{r_G}{r^4} - K_2 \frac{1}{r_G r^2} + 8K_4 \frac{r}{{r_G}^4}\right] \quad (4.20)$$

with $r=r_G+h$, r_G being the collector radius and h the separation distance with the colloid.

Where K_1, K_2, K_4 are arbitrary constants that depend on porosity (Elimelech, 1994)

$$K_1 = \frac{1}{w};\ K_2 = -\frac{3+2\gamma^5}{w};\ K_4 = \frac{-\gamma^5}{w};\ w = 2 - 3\gamma + 3\gamma^5 - 2\gamma^6;\ \gamma = (1-\emptyset)^{1/3}$$

as r_G >>h, the maximum shear rate ($\tau_{R,max}$) and maximum drag force ($F_{D,max}$) can be approximated as:

$$\tau_{R,max} = \frac{1}{2}\frac{U}{r_G}[3K_1 - K_2 + 8K_4] \qquad (4.21)$$

$$F_{D,max} = 5.1025\pi\mu r_p^2 \frac{U}{r_G}[3K_1 - K_2 + 8K_4] \qquad (4.22)$$

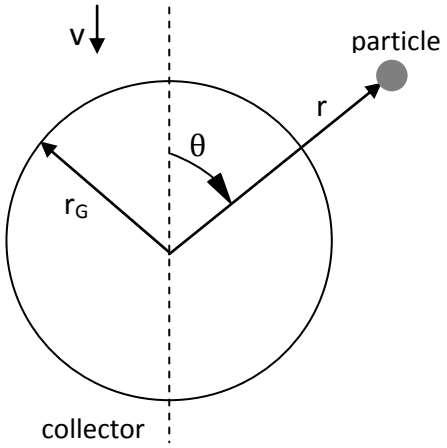

Figure 4.5: Schematic present of relative position of particle to collector in 2-D spherical coordinate system

Finally, a particle is considered to successfully attach to collector surface when the particle deposits under hydrodynamic forces (Shen et al., 2010). The attachment efficiency can be rewritten from Eq. (4.6) with the account of the influence of hydrodynamic condition.

$$\alpha_{att} = f_1\alpha_{max1} + f_2\alpha_{min2} \qquad (4.22)$$

where f_1, f_2 is the fraction of successful attachment, so that adhesive torque is higher than hydrodynamic torque.

Mechanistic models, although accounting for DLVO energy and influence of hydrodynamic conditions, may be not able to produce the satisfactory results in

predicting attachment efficiency. Syngouna and Chrysikopoulos (2011) adopted Maxwell distribution to describe the velocity of colloids in secondary minimum and primary maximum and calculated α_{att} of E.coli by the summation of the probability of deposition at the secondary minimum and primary maximum $\alpha_{att} = \alpha_{max1} + \alpha_{min2}$. The attachment efficiency was largely overestimated. At the grain sizes dg = 0.513 mm and dg= 1.4 mm, large discrepancy was observed as the predicted results were more than 100 times higher than experimental data at low Reynold number of 0.001 and 0.003.

Shen et al. (2010) accounted for torque balance to determine the coefficients f_1 and f_2 for the fraction of successful attachment of colloids with diameters of 30nm and 1156nm. The predicted attachment efficiency was underestimated, as the predicted results were more than 100 times less than experimental data at low ionic strength less than 0.01M.

It is also noted that the mechanistic approach calculated the attachment efficiency under the unfavorable conditions with the account of particle deposition at primary maximum and secondary minimum. Under the favorable conditions (type III and IV, **Figure 4.3**) the primary maximum and secondary minimum are undefined and this approach can not be used to calculate the attachment efficiency.

Moreover, in the account of hydrodynamic force, computing the diameter of deformable area (when particle contacts to collector surface) requires the information of Young modulus K_Y. For the polystyrene (foam) suspension used in the experiments by Elimelech and O'Melia (1990), Elimelech (1992), Bai and Tien(1999) (Table 4.4), K_Y can be taken at 4.014 x 10^9 Nm^{-2}(Bergendahl and Grasso 2000). However, for bacterial suspension, Young modulus depends on many factors (Tuson et al., 2012). For example, even with the same bacteria (E.coli), Young modulus can largely vary in a wide range depending on strain, live cells/dead cells ...as shown in **Table 4.2**. Hence, one must cope with the issue of Young modulus data, especially for the bacterial suspension to account the influence of hydrodynamic force to compute the attachment efficiency.

Table 4.2: Wide range of Young modulus of E.coli in documented experiments.

Microorganisms	Strain	K_Y (MPa)	Condition	Reference
E. coli	JM109	12.8	Whole cells	Abu-Lail and Camesano (2006)
E. coli	JM109	0.12	Whole cells	Chen et al. (2009)
E. coli	JM109	0.05	Whole cells + EDTA	Chen et al. (2009)
E. coli	DH5α	2-3	Whole cells (live)	Cerf et al. (2009)
E. coli	DH5α	6	Whole cells (dead)	Cerf et al. (2009)
E. coli	NCTC 9001	221	Whole cells	Eaton et al. (2008)
E. coli	NCTC 9001	182	Whole cells + COS	Eaton et al. (2008)
E. coli	BE100	32	Whole cells	Deng et al. (2011)
E. coli	ATCC 9637	2.6	Whole cells	Perry et al. (2009)

COS: chitooligosaccharide; EDTA, ethylenediaminetetraacetic acid.

Figure 4.6 presented the influence of Young modulus on calculated adhesive torque. The Young modulus was taken from the values given in **Table 4.2** for various E.coli strains**.** The other parameters were referenced from the experiment of E.coli deposition in sand columns by Syngouna and Chrysikopoulos (2011). This calculation showed that adhesive torque was sensitive to Young modulus whose values less than 6 MPa. Adhesive torque increased five times as Young modulus decreased from 6 MPa to 0.05 MPa. It should be mentioned that at a given hydrodynamic condition, adhesive torque defines the successful attachment of particle on grain surfaces. Hence, in certain conditions, Young modulus can highly influence the estimation of attachment efficiency.

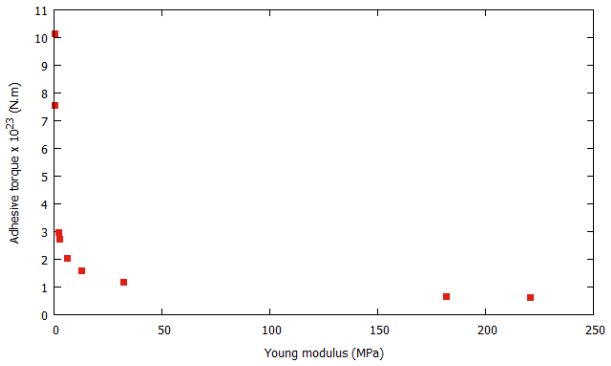

Figure 4.6: The calculated adhesive torque versus Young modulus of Ecoli strains. The calculation was implemented in Ecoli system with dp = 1.21 μm, dg=1.41 mm, I=0.002M, Z_p=-18.46 mV, Z_G=-53.03mV, T=25^{o}C

4.2.3.3 Attachment efficiency of Ecoli calculated by mechanistic model

The attachment efficiency of E.coli was calculated by the mechanistic model using Eq. (4.22). The experimental data was taken from Syngouna and Chrysikopoulos (2011) **(Table 4.3),** which E.coli CN-13(ATTC 700609) was used to study the bacterial attachment in sand column. Although the Young modulus of this E.coli strain is not available, the calculation referenced the Young modulus of bacteria that is close to this E.coli strain. Young modulus was taken at 2.6 MPa, which is the Young modulus of E.coli ATTC 9637 (Perry et al., 2009). It should be noted that in the experiment, the deposition of E.coli mainly occurred at the secondary minimum energy (Syngouna and Chrysikopoulos.,2011). Hence the calculation only accounted the torque balance at secondary minimum. The result of $\alpha_{caculated}$ can be seen in **Table 4.3**

Table 4. 3: Calculation of the attachment efficiency of Ecoli using mechanistic model

No	α_{exp}	Adhesive Torque	Maximum hydrodynamic torque (sinθ=1)	α_{min2}	f2	$\alpha_{caculated}$
1	0.0216	2.71E-23	1.33243E-19	0.0566	6.48764E-05	3.672E-06
2	0.0149	9.38E-23	3.66222E-19	0.053	8.1536E-05	4.321E-06
3	0.0001	9.23E-23	8.68334E-19	0.000064	3.38429E-05	2.166E-09
4	0.0015	1.01E-22	8.03524E-20	0.0566	0.000401543	2.273E-05
5	0.0004	9.38E-23	1.57889E-19	0.053	0.000189122	1.002E-05
6	0.0001	9.23E-23	4.16334E-19	0.000064	7.0585E-05	4.517E-09
7	0.0357	1.01E-22	4.17019E-20	0.0566	0.000773705	4.379E-05
8	0.0103	9.38E-23	1.14619E-19	0.053	0.000260517	1.381E-05
9	0.0013	9.23E-23	3.2486E-19	0.000064	9.04E-5	5.789E-09

Eq. (4.22) highly underestimated the attachment efficiency. The extreme differences between the predicted results and experimental data were also observed in the other calculations when Young modulus was taken from 0.05 MPa to 221MPa **(Table 4.2).** It should be noted that Eq. (4.22) neglected the possibility that the particles from the regions where hydrodynamic torque is higher than adhesive torque can be transferred to other regions. This possibility may become the main mechanism when particles deposit on the collectors having rough surface and in a solution at relatively low ionic strength (Shen et al.,2010).

The deposition of particles on the collector surfaces is a complicated process relating to many parameters (hydrodynamic conditions, solution chemistry, physiochemical properties of both collectors and particles). The mechanistic model uses Maxwell distribution to describe particle velocity at primary maximum and secondary minimum to calculate the fraction of particles attaching to collector surfaces. Torque balance is applied to account the influence hydrodynamic conditions, which defines the successful attachment. However, the application of the mechanistic model is still questionable because of its limits. For example, the transfer of particles from the regions where hydrodynamic torque is higher than adhesive torque to other regions is not included in the mechanistic model. Moreover, the requirement of Young modulus can be an issue for the bacterial system, which such property is hard to estimate.

The limits of mechanistic model have driven an alternative approach: correlation equation to estimate attachment efficiency, which is presented in section 4.2.4

4.2.4 Correlation equation for the estimation of attachment efficiency:

Correlation equations consist of dimensionless parameters that present the contribution of physicochemical processes in attachment efficiency. The coefficients and powers of dimensionless parameters are fitted from regression analysis of experimental data. The existing correlation equations can be found in **Table 4.4**

Table 4.4: Existing correlation equations in estimating attachment efficiency

Study	**Correlation**
Elimelech 1992	$\alpha_E = 0.0257(N_{col})^{1.19}$ (4.23) Dimensionless number: $N_{col} = \frac{\kappa A_H}{\epsilon_0 \epsilon_r \zeta_p, \zeta_g}$
Bai and Tien 1999	$\alpha_{BT} = 2.572 \times 10^{-3} {N_{Lo}}^{0,7031} {N_{E1}}^{-0.3121} {N_{E2}}^{3.5111} {N_{DL}}^{1.352}$ (4.24) Dimensionless numbers: $N_{Lo} = \frac{4A_H}{9\pi\mu {d_p}^2 U}$; $N_{E1} = \frac{\epsilon_0 \epsilon_r ({\zeta_p}^2 + {\zeta_g}^2)}{3\pi\mu d_p U}$; $N_{E2} = \frac{2\zeta_p \zeta_G}{{\zeta_p}^2 + {\zeta_g}^2}$; $N_{DL} = \kappa d_p$

Chang and Chan, 2008	$\alpha_{CC1} = 0.024{N_{Lo}}^{1.5}{N_{E1}}^{-0.423}{N_{E2}}^{2.88}{N_{DL}}^{0.969} + 3.176{A_S}^{1/3}{N_R}^{-0.081}{N_{Pe}}^{-0.715}{N_{Lo}}^{2.687} + 0.222A_S{N_R}^{3.041}{N_{Pe}}^{-0.514}{N_{Lo}}^{0.125} + {N_R}^{-0.24}{N_G}^{-1.11}N_{Lo}$ (4.25)
Chang and Chan, 2009	$\ln(\alpha_{CC2}) = \frac{1}{2}[ln(\alpha_{CC1}) + ln(\alpha_{BT})]$ (4.26)

Where:

A_H is the Hamaker constant (kgm^2s^{-2})

k_B is the Boltzmann constant $1.38x10^{-23}$ ($kgm^2s^{-2}K^{-1}$),

T is fluid absolute temperature (K),

K is the reciprocal of the Debye thickness (m^{-1})

$\epsilon_0\epsilon_r$: are permittivity in vacuum and relative permittivity of the liquid phase

ζ_p, ζ_g: the particle and collector zeta potentials, respectively, (V)

dp is the particle diameter (m),

d_g is the collector diameter (m),

U is the fluid approaching velocity (ms^{-1}),

μ is the absolute fluid viscosity ($kgm^{-1}s^{-1}$)

The accurate prediction of correlation equations strongly relies on how much the dimensionless parameters represent the involvement of physicochemical processes. The equation proposed by Elimelech (1992) is only related to the magnitude of repulsive forces to attachment efficiency (Eq 4.23). Later, Bai and Tien (1999), accounted repulsive-attractive forces and drag force to estimate attachment efficiency (Eq 4.24). Chang and Chan (2008) used Brownian dynamic simulation in triangular network model to develop a semi-empirical equation (Eq 4.25). The equation produced a good match to experimental data, especially for sub-microparticles for which the Brownian motion can not be neglected. Finally, Chang and Chan (2009) took the algebraic averaged value equations developed by Bai and Tien (1999) and Change and Chan (2008) for the better agreement to experimental data for both large and small size particles (Eq 4.26).

4.3 Development of correlation equation

Correlation equations have been developed to estimate attachment efficiency of colloid and bacterial deposition. Among the existing correlation equations (Elimelech, 1992; Bai and Tien, 1999; Chang and Chan, 2008; Chang and Chan, 2009), **Figure 4.6** shows that Bai and Tien 's equation gave the best agreement to the wide range of experimental data by Vaidyanathan and Tien (1989), Elimelech and O'Melia(1990), Elimelech (1992), Bai and Tien (1999), Walker et al. (2005), Syngouna and Chrysikopoulos (2011) (**Table 4.4)**

Figure 4.7 presented the prediction of (a) Elimelech (1992), (b) Bai and Tien (1999), (c) Chang and Chan (2008), (d) Chang and Chan (2009).The x-axis indicates the experimental values of attachment efficiency. The y-axis presents estimated values of attachment efficiency. To provide the more convenient viewing for readers, the figure is presented in log-scale for both x-axis and y-axis. The base line (blue line) contains points that both estimated and experimental values are the same. In other words, the more points in the base line the correlation equation produces, the higher predicting capacity it is. It can be seen from **Figure 4.7** that among the existing correlation equation (Elimelech, 1992, Bai and Tien, 1999, Chang and Chan, 2008, Chang and Chan, 2009), Bai and Tien 's equation showed that best agreement to experimental data with the slope of 0.76 and R^2=0.58.

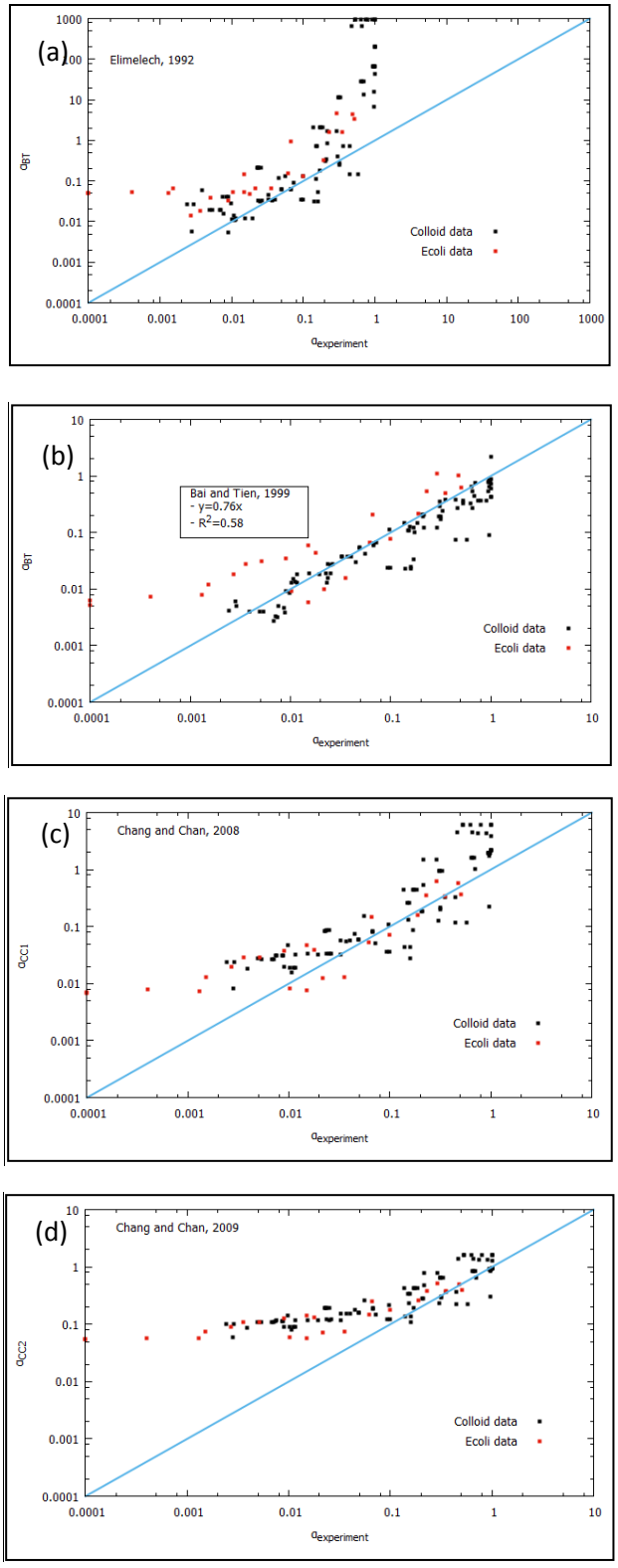

Figure 4.7: Predicted and experimented attachment efficiency from existing correlation equation (a) α_E from Elimelech (1992) , (b) α_{BT} from Bai and Tien (1999), (c) α_{CC1} from Chang and Chan (2008), (d) α_{CC2} from Chang and Chan (2009).

In Bai and Tien's equation, 4 dimensionless parameters: N_{LO}, N_{E1}, N_{E2}, N_{DL} **(Table 4.4)** are used to estimate the attachment efficiency. The influence of hydrodynamic force (in term of velocity), solution chemistry (ionic strength which in term of Debye-Huckel parameter- κ), the zeta potential of collector and particle, particle size (dp) are accounted in the dimensionless parameters. However, in these parameters, the influence of grain size is not considered.

Syngouna and Chrysikopoulos (2011) studied the attachment E.coli onto quartz sand and reported that the attachment efficiency was dependent on sand size. The experiments were conducted for the same solution chemistry and at the same hydrodynamic conditions. The zeta potential of quart sands are very similar, i.e. -62.25mV for medium sand (0.513 mm) and -64.72mV for fine sand (0.181 mm). The attachment efficiency of medium sand was 10-100 times higher than that of fine sand. The influence of grain size on attachment efficiency can be explained by the dependence of drag force on grain size. By using the Eq (4.18) and Eq (4.20) to calculate the drag force, one can find it is inversely proportional to grain size. The increase of grain size d_G decreases the drag force applied on particles, and as a result facilitate particle deposition.

Accounting porosity and grain diameter in the correlation equation

Recent studies (Torkzaban et al., 2007; Shen et al., 2010) have attributed torque balance to the successful attachment, which occurs when the torque of adhesive forces are higher than that of hydrodynamic forces. Using this approach requires the calculation of particle deformation and for bacterias, there are huge uncertainties in determining the Young Modulus (even for the same bacteria strains depending on there state. Although promising, this model is not easy to use in the frame of engineering purpose due to the difficulties to get this parameter.

Another approach based on force balances (Bai and Tien, 1999) has the advantage to not include the particle deformation (so the knowledge of this parameter). But currently, those correlation does not include the effect of the grain size, porosity on the drag force,

which was reported to influence the attachment efficiency (Syngouna and Chrysikopoulos 2011).

In this study, the correlation equation is developed which its formulation is based on force balances and the drag force is characterized by the account of grain size and porosity. Indeed, in Bai and Tien correlation (eq 4.24), the drag force involved in the dimensionless number N_{LO} and N_{E1} assume a Stokes flow around an isolated particle, leading to a drag force which writes : $F_D=3\pi\mu d_p U$

In our new dimensionless numbers, following O'Neil, (1968) and Shen et al, (2010) the influence of drag force is defined:

$$N_{Lo*} = \frac{A_H}{r_p F_{D,max*}};\ N_{E1*} = \frac{\epsilon_0 \epsilon_r \left(\zeta_p{}^2 + \zeta_g{}^2\right)}{F_{D,max*}}$$

with $\tau_{R,max*} = \frac{1}{2}\frac{U}{r_G}[3K_1 - K_2 + 8K_4]$

$$F_{D,max*} = 5.1025\pi\mu r_p^2 \frac{U}{r_G}[3K_1 - K_2 + 8K_4]$$

The term r_G and $(3K_1\text{-}K_2\text{+}8K_4)$ in $F_{D,max}$ present the influence of grain size and porosity on drag force through the calculation of the perturbated flow field around the collector with the Happel model. Furthermore, the drag force expression does not correspond anymore to an isolated particle but take into account the collector surface presence.

In the systems that flowrates and porosities are similar, grain size has a significant impact on drag force, which can influence on attachment efficiency.

It is noted that the porosity in column experiments was usually determined by the volumetric method, for which the porosity was approximated to the volume of the drained water from the packed column. However, this method may result in the uncertainties in the porosity calculation since a volume of water may be retained in the column. This study also examines the correlation with dimensionless numbers so that porosity is not accounted in as the followings:

$$N_{Lo**} = \frac{A_H}{r_p F_{D,max**}};\ N_{E1**} = \frac{\epsilon_0 \epsilon_r \left(\zeta_p{}^2 + \zeta_g{}^2\right)}{F_{D,max**}}$$

with $F_{D,max**} = 5.1025\pi\mu r_p^2 \frac{U}{r_G}$

The others dimensionless parameters that represent the influence of solution chemistry, zeta potential are taken from Bai and Tien (1999),

$$N_{E2} = \frac{2\zeta_p\zeta_G}{\zeta_p{}^2 + \zeta_g{}^2};\ N_{DL} = \kappa d_p$$

Finally, the attachment efficiency is estimated in our correlation equation through a set of dimensionless numbers

$$\alpha_{predicted-grain/porosity} = f(N_{Lo*}, N_{E1*}, N_{E2}, N_{DL}) \quad (4.27)$$

$$\text{and } \alpha_{predicted-grain} = f(N_{Lo**}, N_{E1**}, N_{E2}, N_{DL}) \quad (4.28)$$

The new correlation equation to estimate attachment efficiency is obtained from the regression analysis of experimental data set of deposition of colloids and bacteria provided by Vaidyanathan and Tien (1989), Elimelech and O'Melia(1990), Elimelech (1992), Bai and Tien (1999), Walker et al.(2005), Syngouna and Chrysikopoulos (2011), which is given in **Table 4.5**. For computing the dimensionless parameters of the new correlation equation, Ecoli diameter was set to 1.21 μm and Hamaker constant for Ecoli was set to $7.5\text{x}10^{-21}$ $\text{kgm}^2\text{s}^{-2}$ (Syngouna and Chrysikopoulos,2011) and for polystyrene was taken at $10\text{x}10^{-21}$ $\text{kgm}^2\text{s}^{-2}$ (Bai and Tien 1999, Chan and Chang 2008).The other parameters were referenced from measured data **(Table 4.5)**

Multiple nonlinear regression using the statistical software R version 3.3.2 (31-10-2016) was applied to define the exponent of dimensionless parameters. The p-values of all dimensionless parameters in the multiple regression analysis with α_{exp} were <0.05, indicating their significant contribution to the regression. The summary of regression analysis is given in Appendix A4.2.

Table 4.5: Documented experimental data applied for the development of new correlation equation. The experiments were implemented in the system Polystyrene/Glass bead (Elimelech and O'Melia, 1990; Elimelech, 1992; Bai and Tien, 1999) and styrene-divinylbenzene/Glass bead (Vaidyanathan and Tien, 1989), Ecoli/quart sand (Walker et al.,2005; Syngouna and Chrysikopoulos, 2011)

No	Reference	Dp(m)	Dg(m)	U(m/s)	porosity	I(M)	Zp(V)	Zg(V)	T(K)	alpha
1	Vaidyanathan and Tien, 1989	0.0000114	0.000345	0.02	0.38	0.181	-1.00E-03	-0.003	293	1
2		0.0000114	0.000345	0.03	0.38	0.181	-1.00E-03	-0.003	293	0.7937
3		0.0000114	0.000345	0.04	0.38	0.181	-1.00E-03	-0.003	293	0.6343
4		0.0000061	0.000345	0.02	0.38	0.181	-1.00E-03	-0.003	293	0.9086
5		0.0000114	0.000345	0.02	0.38	0.096	-1.00E-03	-0.003	293	0.6599
6		0.0000114	0.000345	0.02	0.38	0.01	-1.10E-02	-0.013	293	0.2892
7		0.0000114	0.000345	0.02	0.38	0.181	-1.00E-03	-0.003	293	1
8		0.0000114	0.000345	0.03	0.38	0.181	-1.00E-03	-0.003	293	0.5341
9		0.0000114	0.000345	0.04	0.38	0.181	-1.00E-03	-0.003	293	0.5341
10		0.0000061	0.000345	0.02	0.38	0.181	-1.00E-03	-0.003	293	0.7503
11		0.0000114	0.000345	0.02	0.38	0.096	-1.00E-03	-0.003	293	0.4685
12		0.0000114	0.000345	0.02	0.38	0.01	-1.10E-02	-0.013	293	0.213
13	Elimelech and O'Melia,1990	3.78E-07	0.0002	0.00136	0.4	0.00316	-9.50E-02	-0.056	298	0.0102
14		3.78E-07	0.0002	0.00136	0.4	0.00316	-9.50E-02	-0.056	298	0.0115
15		3.78E-07	0.0002	0.00136	0.4	0.01	-8.40E-02	-0.046	298	0.0234
16		3.78E-07	0.0002	0.00136	0.4	0.01	-8.40E-02	-0.046	298	0.0263
17		3.78E-07	0.0002	0.00136	0.4	0.0178	-7.00E-02	-0.042	298	0.049
18		3.78E-07	0.0002	0.00136	0.4	0.003162	-5.40E-02	-0.038	298	0.0933
19		3.78E-07	0.0002	0.00136	0.4	0.003162	-5.40E-02	-0.038	298	0.1
20		3.78E-07	0.0002	0.00136	0.4	0.05623	-4.20E-02	-0.03	298	0.2089
21		3.78E-07	0.0004	0.00136	0.4	0.1	-3.20E-02	-0.028	298	0.3548
22		3.78E-07	0.0002	0.00136	0.4	0.1	-3.20E-02	-0.028	298	0.4467
23		7.53E-07	0.0002	0.00136	0.4	0.00316	-8.80E-02	-0.056	298	0.0195
24		7.53E-07	0.0002	0.00136	0.4	0.00316	-8.80E-02	-0.056	298	0.0115
25		7.53E-07	0.0002	0.00136	0.4	0.01	-7.90E-02	-0.046	298	0.0407
26		7.53E-07	0.0002	0.00136	0.4	0.01	-7.90E-02	-0.046	298	0.0324

27		7.53E-07	0.0002	0.00136	0.4	0.01778	-7.20E-02	-0.042	298	0.0676
28		7.53E-07	0.0004	0.00136	0.4	0.00316	-6.00E-02	-0.038	298	0.1585
29		7.53E-07	0.0002	0.00136	0.4	0.00316	-6.00E-02	-0.038	298	0.1413
30		7.53E-07	0.0002	0.00136	0.4	0.05623	-5.00E-02	-0.03	298	0.3162
31		7.53E-07	0.0002	0.00136	0.4	0.01	-4.00E-02	-0.028	298	0.5754
32		7.53E-07	0.0004	0.00136	0.4	0.01	-4.00E-02	-0.028	298	0.4467
33	Elimelech,1992	1.21E-07	0.0002	0.00136	0.4	0.00316	-7.60E-02	-0.057	298	0.0107
34		1.21E-07	0.0002	0.00136	0.4	0.01	-6.10E-02	-0.047	298	0.0324
35		1.21E-07	0.0002	0.00136	0.4	0.01778	-5.10E-02	-0.043	298	0.0724
36		1.21E-07	0.0002	0.00136	0.4	0.003162	-3.70E-02	-0.039	298	0.1585
37		1.21E-07	0.0002	0.00136	0.4	0.05623	-3.30E-02	-0.033	298	0.302
38		1.21E-07	0.0002	0.00136	0.4	0.001	-8.60E-02	-0.061	298	0.0028
39		3.78E-07	0.0002	0.00136	0.4	0.00316	-9.60E-02	-0.057	298	0.011
40		3.78E-07	0.0002	0.00136	0.4	0.01	-8.60E-02	-0.047	298	0.0251
41		3.78E-07	0.0002	0.00136	0.4	0.01778	-7.00E-02	-0.043	298	0.049
42		3.78E-07	0.0002	0.00136	0.4	0.03162	-5.50E-02	-0.039	298	0.0977
43		3.78E-07	0.0002	0.00136	0.4	0.05623	-4.30E-02	-0.033	298	0.2042
44		7.53E-07	0.0002	0.00136	0.4	0.001	-8.90E-02	-0.061	298	0.0089
45		7.53E-07	0.0002	0.00136	0.4	0.00316	-8.70E-02	-0.057	298	0.0155
46		7.53E-07	0.0002	0.00136	0.4	0.01	-8.10E-02	-0.047	298	0.0372
47		7.53E-07	0.0002	0.00136	0.4	0.01778	-7.10E-02	-0.043	298	0.0676
48		7.53E-07	0.0002	0.00136	0.4	0.03162	-6.20E-02	-0.039	298	0.1514
49		7.53E-07	0.0002	0.00136	0.4	0.05623	-5.00E-02	-0.033	298	0.3162
50	Bai and Tien,1999	3.004E-06	0.00046	0.00103	0.41	0.00005	-2.05E-02	-0.025	298	0.0076
51		3.004E-06	0.00046	0.00103	0.41	0.0001	-1.96E-02	-0.0228	298	0.0098
52		3.004E-06	0.00046	0.00103	0.41	0.001	-1.81E-02	-0.0212	298	0.0552
53		3.004E-06	0.00046	0.00103	0.41	0.01	-1.39E-02	-0.0181	298	0.2126
54		3.004E-06	0.00046	0.00103	0.41	0.1	-6.00E-03	-0.0112	298	0.97
55		3.004E-06	0.00046	0.00103	0.41	0.2	-5.10E-03	-0.008	296	1
56		3.004E-06	0.00046	0.00103	0.41	0.1	-6.00E-03	-0.0228	295	0.9733
57		8.02E-07	0.00046	0.00103	0.41	0.0001	-2.07E-02	-0.0112	294	0.0039

58		8.02E-07	0.00046	0.00169	0.41	0.0001	-2.07E-02	-0.0228	294	0.0029
59		8.02E-07	0.00046	0.00272	0.41	0.0001	-2.07E-02	-0.0228	294	0.0024
60		8.02E-07	0.00046	0.00103	0.41	0.001	-1.93E-02	-0.0212	296	0.0453
61		8.02E-07	0.00046	0.00103	0.41	0.001	-1.57E-02	-0.0181	296	0.1704
62		8.02E-07	0.00046	0.00169	0.41	0.01	-1.57E-02	-0.0181	296	0.1562
63		8.02E-07	0.00046	0.00272	0.41	0.01	-1.57E-02	-0.0181	296	0.1506
64		8.02E-07	0.00046	0.00103	0.41	0.1	-7.00E-03	-0.0112	295	0.701
65		3.063E-06	0.00035	0.00103	0.41	0.00005	-2.55E-02	-0.0164	296	0.0049
66		3.063E-06	0.00035	0.00169	0.41	0.00005	-2.55E-02	-0.0164	296	0.0071
67		3.063E-06	0.00035	0.00272	0.41	0.00005	-2.55E-02	-0.0164	296	0.0068
68		3.063E-06	0.00035	0.00103	0.41	0.0001	-2.45E-02	-0.0129	297	0.0085
69		3.063E-06	0.00035	0.00169	0.41	0.0001	-2.45E-02	-0.0129	297	0.0088
70		3.063E-06	0.00035	0.00272	0.41	0.0001	-2.45E-02	-0.0129	297	0.0074
71		3.063E-06	0.00035	0.00103	0.41	0.001	-2.30E-02	-0.011	297	0.0226
72		3.063E-06	0.00035	0.00169	0.41	0.001	-2.30E-02	-0.011	296	0.0236
73		3.063E-06	0.00035	0.00272	0.41	0.001	-2.30E-02	-0.011	297	0.0233
74		3.063E-06	0.00035	0.00103	0.41	0.01	-1.50E-02	-0.008	297	0.136
75		3.063E-06	0.00035	0.00169	0.41	0.01	-1.50E-02	-0.008	294	0.17
76		3.063E-06	0.00035	0.00272	0.41	0.01	-1.50E-02	-0.008	297	0.1749
77		3.063E-06	0.00035	0.00103	0.41	0.03	-1.00E-02	-0.005	295	0.3119
78		3.063E-06	0.00035	0.00169	0.41	0.03	-1.00E-02	-0.005	295	0.3099
79		3.063E-06	0.00035	0.00272	0.41	0.03	-1.00E-02	-0.005	295	0.3304
80		3.063E-06	0.00035	0.00103	0.41	0.06	-8.00E-03	-0.004	295	0.643
81		3.063E-06	0.00035	0.00169	0.41	0.06	-8.00E-03	-0.004	295	0.6555
82		3.063E-06	0.00035	0.00272	0.41	0.06	-8.00E-03	-0.004	295	0.6888
83		3.063E-06	0.00035	0.00103	0.41	0.1	-6.80E-03	-0.003	297	0.9569
84		3.063E-06	0.00035	0.00169	0.41	0.1	-6.80E-03	-0.003	297	0.9584
85		3.063E-06	0.00035	0.00272	0.41	0.1	-6.80E-03	-0.003	297	0.9408
86		3.063E-06	0.00035	0.00103	0.41	0.2	-5.50E-03	-0.002	297	1
87		3.063E-06	0.00035	0.00169	0.41	0.2	-5.50E-03	-0.002	297	1
88		3.063E-06	0.00035	0.00272	0.41	0.2	-5.50E-03	-0.002	298	1

89		3.063E-06	0.00035	0.00103	0.41	0.00005	-2.55E-02	-0.0164	296	0.0054
90		3.063E-06	0.00035	0.00103	0.41	0.001	-2.30E-02	-0.011	296	0.0253
91		3.063E-06	0.00035	0.00103	0.41	0.01	-1.50E-02	-0.008	296	0.1859
92		3.063E-06	0.00035	0.00103	0.41	0.1	-6.80E-03	-0.003	296	0.9431
93		3.063E-06	0.00035	0.00103	0.41	0.1	-6.80E-03	-0.003	296	0.9589
94		3.063E-06	0.00035	0.00103	0.41	0.1	-6.80E-03	-0.003	295	0.99
95	Walker et al.(2005)	0.00000121	0.000205	0.00021	0.43	0.001	-0.0321	-0.0386	295	0.0089
96		0.00000121	0.000205	0.00021	0.43	0.003162	-0.0216	-0.0308	295	0.1
97		0.00000121	0.000205	0.00021	0.43	0.01	-0.0254	-0.0224	295	0.19
98		0.00000121	0.000205	0.00021	0.43	0.031623	-0.0186	-0.01387	295	0.23
99		0.00000121	0.000205	0.00021	0.43	0.1	-0.0169	-0.01131	295	0.29
100		0.00000121	0.000205	0.00021	0.43	0.001	-0.0507	-0.0386	295	0.0036
101		0.00000121	0.000205	0.00021	0.43	0.003162	-0.0522	-0.0308	295	0.018
102		0.00000121	0.000205	0.00021	0.43	0.01	-0.0481	-0.0224	295	0.062
103		0.00000121	0.000205	0.00021	0.43	0.031623	-0.0192	-0.01387	295	0.35
104		0.00000121	0.000205	0.00021	0.43	0.1	-0.0175	-0.01131	295	0.48
105		0.00000121	0.000205	0.00021	0.43	0.001	-0.0639	-0.0386	295	0.0027
106		0.00000121	0.000205	0.00021	0.43	0.003162	-0.0608	-0.0308	295	0.0051
107		0.00000121	0.000205	0.00021	0.43	0.01	-0.0499	-0.0224	295	0.015
108		0.00000121	0.000205	0.00021	0.43	0.031623	-0.0292	-0.01387	295	0.066
109		0.00000121	0.000205	0.00021	0.43	0.1	-0.022	-0.01131	295	0.51
110	Syngouna and Chrysikopoulos 2011	0.00000121	0.00141	0.000218	0.39	0.002	-1.85E-02	-0.05303	298	0.0216
111		0.00000121	0.000513	0.000218	0.39	0.002	-0.01846	-0.06225	298	0.0149
112		0.00000121	0.000181	0.000207	0.41	0.002	-0.01846	-0.06472	298	0.0001
113		0.00000121	0.00141	0.000132	0.39	0.002	-0.01846	-0.05303	298	0.0015
114		0.00000121	0.000513	0.00012	0.43	0.002	-0.01846	-0.06225	298	0.0004
115		0.00000121	0.000181	0.000118	0.44	0.002	-0.01846	-0.06472	298	0.0001
116		0.00000121	0.00141	6.83E-05	0.39	0.002	-0.01846	-0.05303	298	0.0357
117		0.00000121	0.000513	6.83E-05	0.39	0.002	-0.01846	-0.06225	298	0.0103
118		0.00000121	0.000181	6.83E-05	0.39	0.002	-0.01846	-0.06472	298	0.0013

Indeed the new correlation equation is based on Bai and Tien (1999), which the modification is the account of grain size and porosity in the description of drag force. Therefore, the prediction of new correlation equation is compared with Bai and Tien's equation. It is noted that the formation of the equation from the regression analysis highly depends on the given data. Therefore, for the better comparison, the Bai and Tien's equation was updated by the regression analysis with the data in **Table 4.5**.

Finally, three correlation equations for the estimation of attachment efficiency are given in the followings:

$$\alpha_{BT-updated} = 6.94 \times 10^{-3} {N_{Lo}}^{0.76} {N_{E1}}^{-0.53} {N_{E2}}^{4.88} {N_{DL}}^{1.20} \quad (4.29)$$

$$\alpha_{predicted-grain/porosity} = 1.93 \times 10^{-3} {N_{Lo*}}^{0,69} {N_{E1*}}^{-0.49} {N_{E2}}^{4.88} {N_{DL}}^{1.27} \quad (4.30)$$

$$\alpha_{predicted-grain} = 1.43 \times 10^{-3} {N_{Lo**}}^{0.74} {N_{E1**}}^{-0.54} {N_{E2}}^{4.74} {N_{DL}}^{1.15} \quad (4.31)$$

Eq. (29) is Bai and Tien's updated equation with all dimensionless parameters were similar to Bai and Tien (1999). The difference between Eq. (30) and Eq. (31) lies on the description of drag force in dimensionless parameters,which grain size and porosity (Eq 4.30), or only grain size (Eq 4.31) were included. **Figure 4.8** presented the prediction of (a) Eq. (4.29) (b) Eq. (4.30) and (c) Eq. (4.31). The results of all of the three correlation equations obtained a good agreement to experimental data. The modified correlation equations Eq. (4.30) and Eq. (4.31) obtained a slight improvement to Bai and Tien's equation updated by Eq. (4.29). Grain size and porosity should be included in the correlation equations to estimate attachment efficiency. Among of the equations, Eq. (4.31) gave the best agreement to experimental data. The predicted result of this equation is almost equal to experimental data (y=1.02x and R^2=0.71). Particle deposition is the result of the interaction of DLVO forces and hydrodynamic force (represented by drag force in this study). Grain size and porosity do play a role in drag force that can influence attachment efficiency. In the comparison of Eq. (30) and Eq. (31), there is no explanation for the slightly better prediction of Eq. (31). From the data of this study, the account of only grain size in dimensionless parameters can yield more resonable prediction.

Accepting this result, Eq . (31) does not require the information of porosity for the estimation attachment efficiency. It should also be reminded that compared to the approach that uses torque balance, Eq. (31) has the advantage to be more easy to use in an engineering purpose as this equation do not need the parameters linked to the bacteria mechanistic properties (Young modulus) that are hard to estimate.

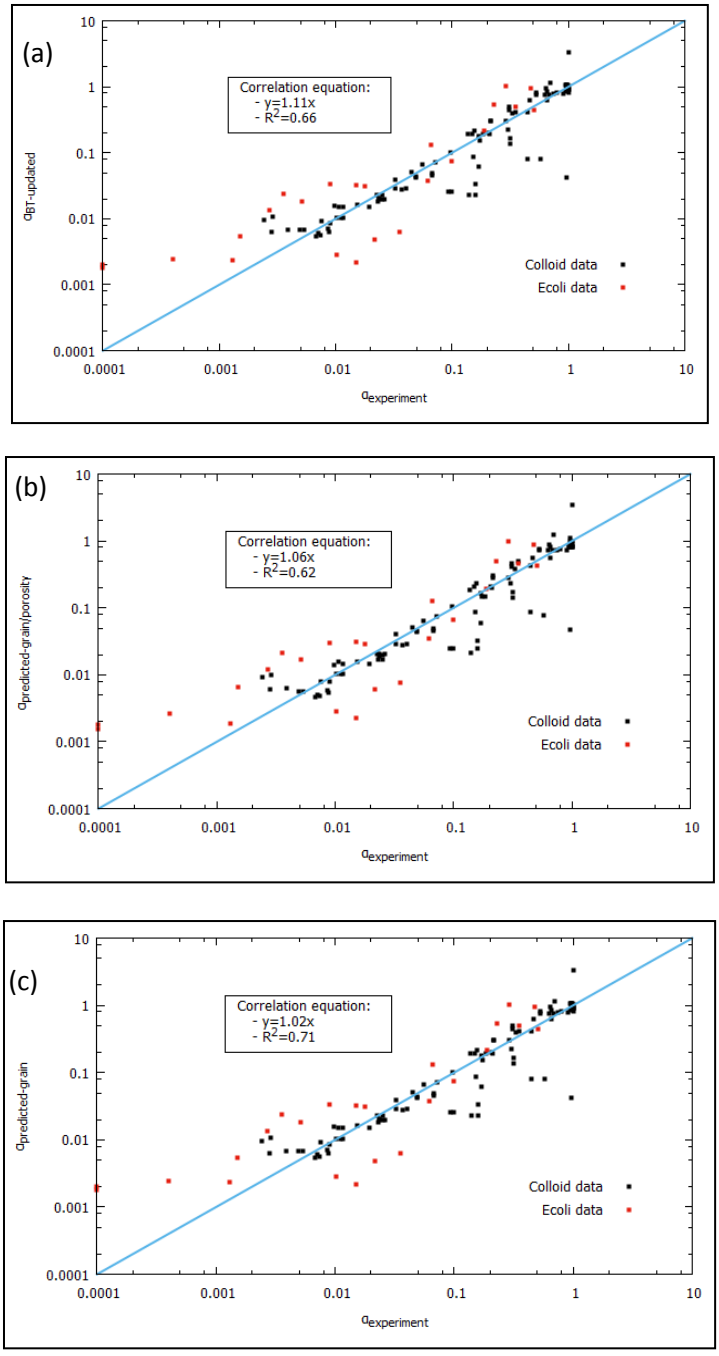

Figure 4. 8: Experimented attachment efficiency and $\alpha_{predicted}$ from (a) Eq. (4.29), (b) Eq (4.30) and (c) Eq. (4.31)

4.4 Conclusion of chapter 4

The particle depositions relate to multi-variable process: hydrodynamic conditions, solution chemistry, physiochemical properties of both collectors and particles. The mechanistic model has been developed to calculate attachment efficiency. However, the complexities related to particle deposition may not be accounted in the recent mechanistic models. An alternative approach: correlation equation can be used in the lack of the knowledge of particle depositions. From a wide range of experimental data of colloids and bacterial deposition, this study proposed a modified correlation equation to estimate attachment efficiency. The development of dimensionless parameter characterizing the interaction of DLVO forces and hydrodynamic forces was followed Bai and Tien (1999). The modified correlation equation also included the influence of grain size on drag force applied to particles. The equation produced a good agreement with a wide range of experimental data in various electrolyte conditions, flow rates, and geometries of porous media. On the other hand, the new correlation equation can be used to estimate initial biomass distribution resulting from seeding process and attachment efficiency of (bio)colloids deposition in porous media. It also should be noted that unlike mechanistic model, the modified correlation equation does not requires Young modulus to estimate attachment efficiency, which is the advantage to be more convenient to use in engineering purpose because such data is hard to estimate.

Chapter 5

Numerical modeling of biofilm development an transport in saturated porous media

In this chapter, a new macroscopic model with the update of recent advances in describing biofilm development and its transport in porous media is presented. In this model, mass accumulation due to biofilm growth and mass deposition caused by biofilm growth have been taken into consideration to define the permeability of the media. Attachment and detachment process have been incorporated in advection-diffusion-reaction equations for the description of biofilm transport in the media.The model is then validated on data gathered from two published column experiments. Permeability reduction, solute concentration, biofilm thickness are used to evaluate the capacity of the model in simulating the temporal and spatial variation of bioclogging in porous media.

List of symbols

Symbol	Unit	Definition
Basic notation		
C_b	kgm^{-3}	Biofilm concentration
$C_{b,max}$	kgm^{-3}	Maximum biomass that can be obtained in porous media.
c_{det1}	s^{-1}	Detachment coefficient in (Eq 5.11)
c_{det2}	-	Detachment coefficient in (Eq 5.11)
C_m	kgm^{-3}	Mobile biomass concentration

Co	kgm^{-3}	Oxygen concentration
C_s	kgm^{-3}	Solute concentration
D	m	Column diameter
dg	m	Grain diameter
Dm	m^2s^{-1}	Dispersion coefficient for mobile bacteria
Do	m^2s^{-1}	Dispersion coefficient for oxygen
Ds	m^2s^{-1}	Dispersion coefficient for solute
$F(\emptyset_M)$	-	Biomass distribution for the reduction of pore radius and plugging of pore space
g	ms^{-2}	Gravitational acceleration
H	m	Column height
K	m^2	Permeability of porous media
K_0	m^2	Clean-bed permeability
Kmin	m^2	Biofilm permeability
k_{decay}	s^{-1}	Biomass decay rate
K_P	-	Relative permeability reduction resulting from microbial aggregates plugging pore space
K_R	-	Relative permeability reduction resulting from biofilm covering grain surface
K_{rel}	-	Total relative permeability reduction
Ko	kgm^{-3}	Half-saturation constants of oxygen
Ks	kgm^{-3}	Half-saturation constants of substrate
L	m	Straight length of porous media
L_b	m	Biofilm thickness
M_b	m^{-1}	Specific area of biofilm
r_{att}	s^{-1}	Specific attachment rate
r_{det}	s^{-1}	Specific detachment rate
r_x	s^{-1}	Specific biomass growth rate
t	s	Time
U	ms^{-1}	Approaching velocity
v	ms^{-1}	Pore velocity
Yo	-	Yield coefficients for oxygen consumption
Ys	-	Yield coefficients for oxygen consumption
ΔP	Pa	Pressure drop
Greek letters		
$\emptyset$	-	Porosity
$\emptyset_b$	-	Volumetric fraction of biofilm
$\emptyset_{b,rel}$	-	Relative volumetric fraction of biofilm $\emptyset_{b,rel} = \frac{\emptyset_b}{\emptyset_0}$
$\emptyset_{B,c}$	-	$\emptyset_{B,c}$ is a the value that affects the $F(\emptyset_b)$ curve shape and controls how fast mass aggregates are formed and plug pore space
$\emptyset_0$	-	Clean-bed porosity

μ	$kgm^{-1}s^{-1}$	Fluid viscosity
μ_{max}	s^{-1}	Maximum biomass growth rate
α_{att}	-	Attachment probability
η_0	-	Contacting probability
η_{lmt}	-	Growth limiting factor
ρ_b	kgm^{-3}	Biofilm density
ρ_l	kgm^{-3}	Fluid density

5.1 Introduction

As mentioned in the previous section, macroscopic models play an important approach that can be applied independently or along with experimental data to study solute transport coupling with biofilm growth in porous media. Macroscopic models deliberately neglect processes at local scale but concentrate on prevailing processes that govern global change on the porous media transport properties media (Delay et al., 2013). Theoretically, the description of these processes close to nature principle should increase the predicting capacity of the models. However, actually not all these processes involved in biofilm growth are well understood so that simple assumptions are often considered to mathematically interpret experimental observations.

For example, classical filtration theory (CFT) usually used for colloids to describe biomass attachment is questioned due to the particular transport and deposition behaviors of living microorganisms (Tuefenkji, 2007), since in these processes, physiochemical mechanisms are typically coupled with the biological one.

The implementation of a continuous process to present biomass detachment is also controversial because it can not describe the oscillation of pressure drop due to discrete biomass sloughing (Stewart and Kim, 2004). One of the toughest challenges of biofilm modeling is to spatially and temporally capture bioclogging in porous media (Taylor et Jaffe, 1990a; Brovelli et al., 2009).

Bioclogging caused by local biomass accumulation reduces the permeability of porous media and alters global hydrodynamic conditions. Traditionally, permeability reduction is considered as a simple power function of porosity (Carman-Kozeny, 1937; Clement et

al., 1996), which was referred in many macroscopic modeling of bioclogging in porous media (Kildsgaard and Engesgaard, 2001; Ham et al., 2007).

However, microorganisms can develop biofilm to cover grain surface or to form microbial aggregates to plug the pore space (Vandervivere, 1995), the models that not account for pore plugging may be insufficient to model permeability reduction. Brovelli et al., 2009 considered bio-plugging as additional mechanisms contributing to bioclogging and applied Thullner's models (Thullner, 2002) to simulate permeability reduction. These models were derived from network simulation (Thullner, 2002) and it is questionable when applying in other experimental conditions. Brovelli et al. (2009) reported that the simulation only captured permeability reduction at the early stage of Taylor's experiment (Taylor et al., 1990). Many other models for permeability reduction have been developed and used in numerical study. The discrepancy in the predicted results from the existing models have been reported (Seifert and Engesgaard, 2007; Ebigbo et al., 2010; Karrabi et al., 2011). The origin of the discrepancy may come from the empirical parameters and simple assumption used for specific experimental conditions.

In this chapter, we aim to develop a one-dimension model to simulate biofilm growth and transport in porous media. The most important object of this model is to be simple for field-scale application but complex enough to capture prevailing processes in porous media, especially to be capable of spatially and temporally predicting of bioclogging and solute transport in porous media.

5.2 Model description

The continuum approach, widely applied in field-scale applications (Shafahi and Vafai, 2009) has been adopted for the development of 1D model. The model consists of a set of equations to solve momentum conservation relating to Darcy's equation, and mass conservation involved in advection-diffusion-reaction equations with the appropriate source and sinks term.

This model should be capable of representing the relevant processes involved in a system which consists of a porous medium with uniform initial porosity $\emptyset_0$, one fluid phase (water) denoted with *l* and biofilm denoted as *b*. This system can be characterized by several length scale: the cell scale with characteristic length about 1µm and the pore scale with characteristic length 100 µm and Darcy scale.

The biofilm is composed of the individual bacterial cells and EPS. The void spaces within a biofilm can serve as channels for fluid flow (Stoodley, 1994). However, it is very small compared to the pore scale. So in our model, the fluid flow inside the biofilm is neglected.

At the pore scale, the grains of the porous medium is considered as an impermeable solid phase. Biofilms attach and grow up on the surface of the grains. One part of the void space between the grains is occupied by the biofilm, the other is occupied by the fluid. The pore-scale parameter can be averaged on Darcy scale, where the effective macro-scale parameters and equation are given to describe the interaction between the solid, fluid and biofilm.

In term of biofilm thickness, with the assumption that biofilm is homogeneous, average biofilm thickness can be calculated by dividing biofilm volume by biofilm surface (**Figure 5.1**):

$$L_b = \frac{biofilm\ volume\ V_b}{biofilm\ surface\ S_b} \qquad (5.1)$$

This equation is rewritten :

$$L_b = \frac{biofilm\ volume\ V_b\ /unit\ volume\ V_T}{biofilm\ surface\ S_b\ /unit\ volume\ V_T}$$

so biofilm thickness can be simply defined by Eq. (5.2)

$$\mathrm{L_b} = \frac{\emptyset_\mathrm{b}}{\mathrm{M_b}} \qquad (5.2)$$

with $\emptyset_\mathrm{b}$ volumetric fraction of biofilm (-) and $\mathrm{M_b}$ specific surface area of biofilm ($\mathrm{m^{-1}}$)

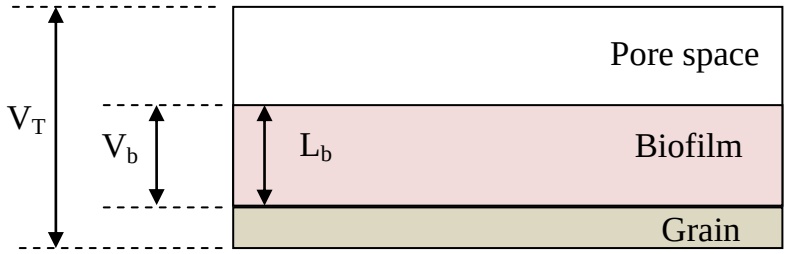

Figure 5.1: Schematic representation of biofilm in porous media in a unit volume.

5.2.1 Momentum conservation equation

In porous media, laminar flow is described by Darcy's equation:

$$U = -\frac{K}{\mu}(\nabla P - \rho_l g) \qquad (5.3)$$

where U is approaching velocity (ms^{-1}), K is permeability of porous media (m^2), μ is absolute viscosity ($kgm^{-1}s^{-1}$), ∇P is pressure drop ($kgm^{-2}s^{-2}$) ρ_l fluid density (kgm^{-3}) and g is gravitational acceleration (ms^{-2}).

In this model, we apply our modified model presented in chapter 3 to predict permeability reduction.

$$K_{rel} = F(\emptyset_B)K_R + \left(1 - F(\emptyset_B)\right)K_P \qquad (5.4)$$

K_{rel} is the total relative permeability reduction (-), $K_{rel}=K/K_0$ which K_0 is clean bed permeability (m_2), K_R, K_P are permeability reduction resulting from biofilm covering grain surface (-) and microbial aggregates plugging pore space (-), respectively. $F(\emptyset_B)$ determines biomass distribution for the reduction of pore radius and plugging of pore space

The permeability resulting from biofilm covering grain surface is expressed in the following equation:

$$\frac{K_R}{K_0} = \left(\frac{\emptyset_0 - \beta_b\emptyset_b}{\emptyset_0}\right)^3 \frac{\tau_0}{\tau} \frac{(1-\emptyset_0)^{4/3}}{(1-\emptyset_0+\beta_b\emptyset_b)^{4/3}} \qquad (5.5)$$

with β_b is the bulk factor used to define the effective pore space for fluid flow. As mentioned in chapter 3, the bulk factor can influence the hydraulic conductivity when K_R

dominates the permeability reduction. The value of bulk factor can be higher than 1 as the heterogeneous structure of biofilm reduces the available pore space for fluid flow, or less than 1 in some conditions which biofilm porosity is accounted and contribute to the global flow of porous media. τ is the tortuosity of porous media. There are many models to compute tortuosity (Du Plessis and Masliyah, 1991; Koponen et al., 1996; Yu and Li, 2004; Lanfrey et al., 2010; Ahmadi et al., 2011). In this work the model proposed by Yu and Li (2004) is used (Eq 5.6), in which the description of flow path is based on grain geometry and a cubic arrangement is used:

$$\tau = \frac{1}{2}\left[1 + \frac{1}{2}\sqrt{1-\emptyset} + \sqrt{1-\emptyset} \times \frac{\sqrt{\left(\frac{1}{\sqrt{1-\emptyset}} - 1\right)^2 + \frac{1}{4}}}{1-\sqrt{1-\emptyset}}\right] \qquad (5.6)$$

Permeability reduction caused by microbial aggregates plugging pore space is calculated in equation:

$$\frac{K_P}{K_0} = \frac{K_{min}/K_0}{1 - \frac{\emptyset}{\emptyset_0} + \left(\frac{\emptyset}{\emptyset_0}\right)\left(\frac{K_{min}}{K_0}\right)} \qquad (5.7)$$

with K_{min} and K_0 are biofilm permeability and initial permeability of clean-bed porous media, respectively.

The biomass that contributes to each pattern is characterized by $F(\emptyset_b)$ which is dependent on biomass concentration.

$$F(\emptyset_b) = \exp\left(-0.5\left(\frac{\emptyset_{b,rel}}{\emptyset_{B,c}}\right)^2\right) \qquad (5.8)$$

where $\emptyset_{b,rel}$ is the relative biofilm volumetric fraction equal to the ratio of the biofilm volumetric fraction to the maximum porosity of porous media. $\emptyset_{B,c}$ is a value that affects the $F(\emptyset_b)$ curve shape and controls how fast mass aggregates are formed and plug pore space.

5.2.2 Mass conservation equation

a) Biofilm

It is well known that biofilm is composed of live cells, dead cell, EPS (Flemming and Wingender, 2010). Although there are attempts to present biofilm close to its nature, modeling biofilm components separately requires many coefficients that unavailable in experimental data (see in Chapter 2). For the simplicity of field-scale application, biofilm in our model is represented by only one active biomass with a constant density. So the active biomass concentration is expressed through the term $\rho_b \emptyset_b$. The mass balance of biofilm concentration is given by the following equation

$$\frac{d(\emptyset_b \rho_b)}{dt} = \eta_{lmt} r_x \emptyset_b \rho_b - k_{decay} \emptyset_b \rho_b + r_{att} C_m - r_{det} \emptyset_b \rho_b \qquad (5.9)$$

where η_{lmt} is growth limit factor (-), r_x is biomass growth rate (s^{-1}), k_{decay} is biomass decay rate (s^{-1}), Cm is mobile biomass in liquid phase (kgm^{-3}), r_{att} and r_{det} are attachment rate and detachment rate (s^{-1}), respectively.

b) Mobile (suspended) biomass:

The mass balance of mobile biomass is governed by advection-diffusion-reaction equation with sink term accounting for biomass growth and decay and source terms accounting for biomass exchange from solid (biofilm) phase and liquid phase:

$$\frac{\partial(\emptyset C_m)}{\partial t} + \nabla(C_m U) = \nabla.(D_m \emptyset \nabla C_m) + r_x \emptyset C_m - k_{decay} \emptyset C_m - r_{att} \emptyset C_m + r_{det} \emptyset_b \rho_b \qquad (5.10)$$

with C_m mobile biomass concentration (kgm^{-3}), U approaching velocity (ms^{-1}), D_m effective dispersion coefficient for mobile biomass (m^2s^{-1}).

c) Substrate (electron donor) and Oxygen (electron acceptor)

The mass balance of substrate (electron donor) and oxygen (electron acceptor in aerobic conditions) are controlled by advection-diffusion-reaction equations with sink terms accounting for different mass consumption in both biofilm (solid) phase and liquid phase:

$$\frac{\partial(\emptyset C_s)}{\partial t} + \nabla(C_s U) = \nabla.(D_S \emptyset \nabla C_s) - \frac{r_x}{Y_s} \emptyset C_m - \frac{\eta r_x}{Y_s} \emptyset_b \rho_b \qquad (5.11)$$

$$\frac{\partial(\emptyset C_o)}{\partial t} + \nabla(C_o U) = \nabla.(D_o \emptyset \nabla C_o) - \frac{r_x}{Y_o}\emptyset C_m - \frac{\eta r_x}{Y_o}\emptyset_b \rho_b \qquad (5.12)$$

with C_S substrate concentration (kgm^{-3}), C_O oxygen concentration (kgm^{-3}), Y_S and Y_O yield coefficients for substrate consumption and oxygen consumption, respectively. D_s and D_o are effective dispersion coefficient for solute (m^2s^{-1}) and oygen (m^2s^{-1}).

5.2.3 Sink and source terms

a) Biomass growth rate:

In our model, biomass growth rate r_x follows Monod's law for two limiting substances:

$$r_x = \mu_{max} \frac{C_s}{K_s + C_s} \frac{C_o}{K_o + C_o} \qquad (5.13)$$

with μ_{max} maximum specific substrate utilization rate (s^{-1}), Cs substrate concentration (electron donor) (kgm^{-3}), C_o oxygen concentration (electron acceptor) (kgm^{-3}). K_S and K_O half-saturation constants of substrate and oxygen, respectively.

Growth limit factor η_{lmt}

Biomass growth rate inside biofilm is not uniform respecting with biofilm thickness. It can be explained by the stratified structure of biofilm, for which porosity in the upper layers is higher than that in the lower layers (Zhang and Bishop, 1994; Lewandowski, 2000). As biofilm increases its thickness, the channels, voids at the bottom available for nutrient fluxes are reduced, leading a limitation of the biological growth rate. A growth limit factor η_{lmt} is then proposed to adjust the growth rate kinetic. For its simplicity, the macroscopic equation suggested by Zysset et al. (1994) and Kildsgaard and Engesgaard (2001) was used in the model

$$\eta_{lmt} = 1 - \frac{C_b}{C_{b,max}}$$

With C_b is the biofilm concentration (kgm^{-3}) and $C_{b,max}$ (kgm^{-3}) is the maximum biomass that can be obtained in porous media. In the macroscopic equation, growth limit factor $\boldsymbol{\eta_{lmt}}$ is a function of immobile biomass concentration and its value is in range of [0-1].

Relating biofilm concentration in term of density and volumetric fraction, the growth limit factor can be rewritten as follows:

$$\eta_{\mathrm{lmt}} = 1 - \frac{C_b}{C_{b,max}} = 1 - \frac{\rho_b \emptyset_b}{\rho_b \emptyset_0} = 1 - \frac{\emptyset_b}{\emptyset_0} = \frac{\emptyset}{\emptyset_0} \qquad (5.14)$$

b) Biomass transfer

Biomass attachment

Biomass attachment relates to the transfer of suspended biomass from liquid phase to solid phase (grain surface, biofilm). In biofilm system, biomass attachment involves in two processes: the control of initial biofilm distribution in seeding process and the participation of mass build-up of the developed biofilm system. Due to their complexities, modeling biomass attachment for these two processes can be different.

Modeling biomass attachment in seeding process

In seeding process, it is assumed that attached bacteria does not influence the upcoming deposition events, so that the attachment rate can be quantified by using colloid filtration theory (CFT) (Clement et al., 1996; Kildsgaard and Engesgaard, 2001; Thullner et al., 2004; Tufenkji, 2007; Syngouna and Chrysikopoulos, 2011). The bacterial attachment can be estimated by the value of contacting efficiency (η_0) and attachment efficiency (α_{att})

$$r_{\mathrm{att}} = \frac{3(1-\emptyset)v}{2d_g\emptyset}\eta_0\alpha_{\mathrm{att}} \qquad (5.15)$$

with dg grain diameter (m), v pore velocity (ms^{-1})

The contacting efficiency (η_0) is often calculated by equation proposed by Tufenkji and Elimelech (2007). The attachment efficiency (α_{att}), however, is more complicated due to the interaction of aqueous chemistry and hydrodynamic forces (Bai and Tien, 1999; Shen et al., 2007; Torkzaban et al., 2007;Syngouna and Chrysikopoulos 2011). In chapter 4, we developed a correlation equation to estimate attachment efficiency

$$\alpha_{predicted} = 1.43 \times 10^{-3} {N_{Lo**}}^{0.74} {N_{E1**}}^{-0.54} {N_{E2}}^{4.74} {N_{DL}}^{1.15} \qquad (5.16)$$

with the dimensionless numbers were defined

$$N_{Lo**} = \frac{A_H}{\mathrm{F_{D,max**}} \mathrm{r_p}};\ N_{E1**} = \frac{\epsilon_0 \epsilon_\mathrm{r} \left(\zeta_\mathrm{p}{}^2 + \zeta_\mathrm{g}{}^2\right)}{\mathrm{F_{D,max**}}}$$

$$N_{E2} = \frac{2\zeta_\mathrm{p}\zeta_\mathrm{G}}{\zeta_\mathrm{p}{}^2 + \zeta_\mathrm{g}{}^2};\ N_{DL} = \kappa d_p \ \text{ with } \mathrm{F_{D,max**}} = 5.1025\pi\mu \mathrm{r_p^2} \frac{\mathrm{U}}{\mathrm{r_G}}$$

The definition of dimensionless numbers and parameters involved are given in detail in chapter 4. This correlation equation showed its predicting capacity by producing a good agreement to a wide range of experiment data in estimating the attachment efficiency of both colloid and Ecoli deposition. Using this correlation equation requires physicochemical properties of grain, bacterial cell and liquid solution.

Modeling biomass attachment to developed biofilm

For the system of developed biofilm, the biomass attachment is more complicated. The attachment is influced by biofilm compostion .i.e., extracellular polymetric substances. The use of equation proposed by Tufenkji (2007) to calculate contacting efficiency and coupling DLVO forces and hydrodynamic force to estimate attachment efficiency may be questionable. Several studies represented contacting efficiency and attachment efficiency by one parameters: attachment coefficient η_{att} (Clement et al., 1996; Kildsgaard and Engesgaard, 2001; Brovelli et al.,2009). This attachment coefficient follows the approximation by Bai and Tien, (1979)

$$\eta_{att} = 4\mathrm{A_s^{1/3}}.\mathrm{N_{pe}^{-2/3}} \qquad (5.17)$$

with

$$As = \frac{2(1-\beta^5)}{2-3\beta+3\beta^5-2\beta^6},\ Npe = \frac{3\pi\mu dpdgU}{k_B T}$$

where $\beta = (1-\emptyset)^{1/3}$, $\mathrm{d_p}$ (m) and $\mathrm{d_g}$(m) are diameters of bacterial cell and grain, respectively. U ($\mathrm{m.s^{-1}}$) is Darcy velocity. μ is water viscosity. $\mathrm{k_B}$ is Bolzmann constant and T (K) is temperature.

However, Eq (5.17) was approximated from a limited data of colloids deposition and the influence of aqueous chemistry was not accounted. In this chapter, due to the

complexities of biomass attachment and for the simplicity of macroscopic model, a colloid filtration theory was applied to describe biomass attachment. However, the attachment coefficient η_{att}, herein, is treated as a fitted parameter.

Biomass detachment

Biomass detachment is a crucial process that controls the mass balance of biofilm. If the force exerted on the biofim by the fluid exceeds the strength of the bioflm, biomass particles are removed from the biofilm. Many models have been proposed to determine detachment rate. They usually relate the detachment to biofilm thickness, amount of biomass, shear stress and sometimes biofilm growth rate. In our model, detachment rate is related to both fluid shear and biofilm growth rate (Speitel and DiGiano, 1987)

$$\mathrm{r_{det}} = c_{det1}(\emptyset|\nabla P - \rho g|)^{0.58} + c_{det2} r_x(\emptyset_b) \qquad (5.18)$$

In this equation, the two detachment coefficients c_{det1}, c_{det2} are fitted parameters. The first term on the right hand side accounts for the effect of local fluid shear and has the similar form to that of Rittmann (1982). The second one in the right hand side accounts for the effect of growth rate of biofilm so that high rapid growth rate or high volumetric fraction of biofilm induces high detachment rate.

It should be noted that Eq (5.18) represents biomass detachment as a continuous process. However, it is not always true. The adding of a discrete process for a better representation of biomass detachment may be necessary. In the next chapter, this discrete process will be discussed in detail.

5.3 Simulation work

The open source software OpenFoam (Open Source Field Operation and Manipulation) was used in simulation work.OpenFoam is written in C++ programming language, which is a modern and objected oriented language that makes the programming simple and visual. One of the advantages of OpenFoam is that it allows programming to use similar syntax as the mathematical expression to solve the problem. In addition, in OpenFoam modules addressing different physical problems have basically the same structure and users can create the new programs based on resources integrated into OpenFoam.

A new solver BiofilterFoam based on 'transportScalarFoam' has been created to solve the system of equations above. The global algorithm for each time step consists in:

a) Calculate (update flow properties): permeability, pressure

b) Calculate the sink/source terms

c) Solve the pressure equation (Eq.(5.3))

d) Solve suspended biomass (Eq .(5.10))

e) Solve biofilm growth (Eq .(5.9))

f) Solve substrate transportation (Eq .(5.11))

g) Solve oxygen transportation (Eq .(5.12))

The solver BiofilterFoam has been applied to 1-D modeling of biofiltration process. The numerical domain and numerical scheme used in the application are given in **Figure 5.2** and **Table 5.1,** respectively**.**

Concerning the boundary condition, the atmospherical pressure condition was applied at outlet. At inlet, a time dependent pressure gradient condition was used, since the inlet pressure gradient depends on the instantaneous permeability and the approaching velocity as indicated by Eq (5.4)

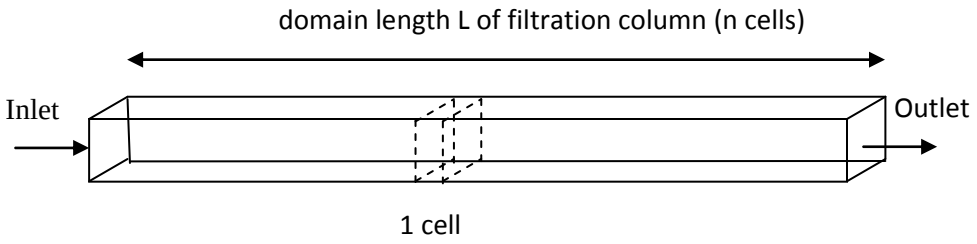

Figure 5. 2: Schematic presentation of the domain of the numerical simulation

At each time step, the pressure drop was computed at the center of each cell and a harmonic interpolation scheme was used to determine the fluid pressure at inlet face.

Table 5. 1: Numerical scheme used in the modeling

	Numerical Scheme	**Specified in OpenFoam**
Time term	Second order implicit	Backward
Gradient term	Center difference	Gauss linear
Convection term	Second order upwind	Gauss linear upwind
Diffusion term	Second order	Gauss linear corrected
Interpolation term	Center difference	Harmonic

5.4 Model validation

To set up a model, experimental observations are performed to obtain the mathematical descriptions of prevailing processes and in return, the macroscopic models should be validated by experimental data. In this work, two experiments were selected to test the predicting capacity of the model presented in the previous section. These experiments were conducted by Wanner et al. (1995) and that by Taylor and Jaffe (1990a) to investigate the influence of bioclogging in saturated porous media. The result of the validation will address the issues that whether a macroscopic model is capable of capturing the behavior of porous media

5.4.1 Column experiment performed by Wanner et al. (1995)

5.4.1.1 Experiment description

A column packed with glass beads of 1 mm in diameters was conditioned for the development of *Pseudomonas aeruginosa* biofilm in an aerobic environment (oxygen as an electron acceptor). The column was feed with glucose at a constant flowrate. The behavior of the column was characterized by daily profiles of inlet and outlet substrate concentration, biofilm thickness and pressure drop. The operation parameters of the experiment are given in **Table 5.2.**

Table 5. 2: Operational conditions in column experiment conducted by Wanner et al. (1995)

Parameter	**Unit**	**Value**
Column height H	M	0.05
Column diameter D	M	0.031
Inlet substrate concentration C_s	gCm^{-3}	7-16
Inlet oxygen concentration C_o	gO_2m^{-3}	9
Operation time t	Day	13
Clean-bed porosity $\emptyset_0$	-	0.38
Grain diameter d_{G0}	M	0.001
Flow rate Q	m^3d^{-1}	0.055

5.4.1.2 Numerical work

All the geometry parameters and operational conditions are the same as the experiment of Wanner et al. (1995) (**Table 5.2)**. Clean-bed permeability is calculated by using Eq. (5.18) developed in chapter 3 for a clean-bed porosity of 0.38 and grain size of 1mm.

$$K_0 = \frac{\emptyset_0^3}{72\tau_0}\frac{{d_{G,0}}^2}{(1-\emptyset_0)^2} \qquad (5.18)$$

with $\emptyset_0$, τ_0 are clean-bed porosity and tortuosity. $d_{G,0}$ is grain diameter of biofilter.

The column was fed with a constant flow rate of 0.055 m^3day^{-1} during the whole operation time t=13 days, which is equivalent to Darcy velocity of 8.4x $10^{-4}m.s^{-1}$. The physical properties of fluid: fluid viscosity and fluid density, are considered constant since the variationss of temperature is small. The dispersion coefficients and the growth kinetic of *Pseudomonas aeruginosa* was referenced from documented data **(Table 5.3)**

The parameters $\phi_{B,c}$, c_{det1}, c_{det2}, η_{att} are obtained by curve fitting to obtain a good agreement with experimental data. To estimate biomass attachment following classical filtration theory, physiochemical characteristic of the aqueous phase is required. However, such data can not be obtained in the porous media system for which biofilm temporally and spatially alters grain surface. For the sake of the simple in macroscopic

model, the parameter η_{att} is fitted to estimate biomass attachment (Brovelli et al.,2009). The specific surface area of grain is needed to determine biofilm thickness in our model. In this case, M_b=1000 m^{-1} an order magnitude similar to the value of 2500 m^{-1}, used by Taylor and Jaffe (1990b)

Table 5. 3: Parameters used for the simulation of experiment conducted by Wanner et al. (1995)

Parameter	**Unit**	**Value**	**Reference**
Clean-bed permeability K_O	m^2	2.1 x 10^{-9}	*calculated*
Darcy velocity U	ms^{-1}	8.4x10^{-4}	*Wanner et al., 1995*
Fluid viscosity μ	$kgm^{-1}s^{-1}$	0.001	-
Fluid density ρ_l	kgm^{-3}	1000	-
Dispersion coefficient for substrate D_s	m^2s^{-1}	6 x 10^{-10}	*Wanner et al., 1995*
Dispersion coefficient for oxygen D_o	m^2s^{-1}	2 x 10^{-9}	*Wanner et al., 1995*
Dispersion coefficient for bacterial cell D_m	m^2s^{-1}	1 x 10^{-9}	*Wanner et al., 1995*
Biofilm density ρ_b	kgm^{-3}	25	*Wanner et al., 1995*
Maximum specific growth rate μ_{max}	s^{-1}	2x10^{-5}	Beyenal et al., 2003
Saturation constant for substrate K_s	kgm^{-3}	0.002	*Wanner et al., 1995*
Saturation constant for oxygen K_o	kgm^{-3}	0.0002	*Wanner et al., 1995*
Yield coefficient for substrate Y_s	-	0.34	*Wanner et al., 1995*
Yield coefficient for oxygen Y_o	-	0.9	*Wanner et al., 1995*
Bacterial decay rate k_{dec}	s^{-1}	4x 10^{-6}	Martin et al. 2008
Biofilm permeability K_{min}	m^2	2.1x 10^{-12}	K_0/K_{min}=2500-10000 Vandervivere, 1995
Fitted parameters			
$\phi_{B,c}$	-	0.08	
Detachment coefficient c_{det1}	s^{-1}	0.8 x 10^{-8}	
Detachment coefficient c_{det2}	-	0.2	
Attachment coefficient η_{att}	-	1 x 10^{-4}	
Specific surface area of grain M_b	m^{-1}	1000	

The modeling domain is discretized with 50 uniform cells for a total column length of 5cm. The time step was set to 1s for the simulation and with this value, the Courant number was 0.84. For the initial conditions t=0, biofilm distribution is supposed to be uniform inside porous media with $\phi_b = 0.0001$. The constant and small value of the

volumetric fraction of biofilm in the assumption may be reasonable with the very short seed process of 4h in this experiment. Mobile biomass is assumed to be zero. It is noted that the assumption does not present exactly the real case as after seeding process. There exist an amount of mobile biomass in porous media. However, due to the lack of information about the seeding process and assuming that the initial mobile biomass has an insignificant effect on the porous media colonization, the assumption is accepted in our simulation .The boundary conditions required for numerical simulation are sumerized in **Table 5.4**

Table 5. 4: Boundary conditions required for numerical simulation

Parameters	**Inlet**	**Outlet**
C_s	Dirichlet condition with a constant: Cs(0,t)=0.01 kgm^{-3}	Neumann condition: $n.(D_s \nabla C_s) = 0$
C_o	Dirichlet condition with a constant: Co(0,t)=0.009 kgm^{-3}	Neumann condition: $n.(D_o \nabla C_o) = 0$
C_m	Dirichlet condition with a constant: Cm(0,t)=0	Neumann condition: $n.(D_m \nabla C_m) = 0$
ϕ_b	Neumann condition: $n.(\nabla \phi_b) = 0$	Neumann condition: $n.(\nabla \phi_b) = 0$

In this experiment, inlet substrate concentration fluctuated from 7 to 16 gCm^{-3}. Because of the lack of information of inlet substrate distribution and for the simplicity of numerical modeling, we assumed that inlet substrate concentration follows the distribution shown in **Figure 5.3.** Substrate remains constant in a period and suddenly drops down or jump up to a new value.

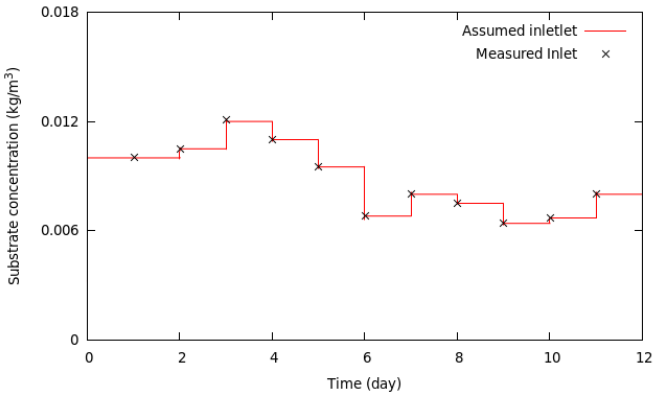

Figure 5. 3: Assumption of inlet substrate distribution in experiment by Wanner et al. (1995)

5.4.1.3 Results

In **Figure 5.4** the variation of pressure drop in the column, the substrate concentration at the outlet and the average biofilm thickness are plotted over the operation time. The model seemed to capture the column behavior. **Figure 5.4a** shows that biomass accumulation had no discernible effect on the pressure drop of sand packed during the first 6 days. It was quite reasonable since given the short seeding process time (5h), only a small quantity of biofilm was formed: the biofilm volumetric fraction after the seeding stage was indeed fitted to be 0.0001 as the initial condition. After 6 days, biofilm started to develop and reached the log-phase after 8 days, which led to the exponential increase of biofilm thickness **(Figure 5.4 c)** and pressure drop **(Figure 5.4a).** In **Figure 5.4a**, one can see that pressure drop increased to 14000Pa from 8^{th} day to 12^{nd} day. As a result, substrate consumption due to bacterial growth in this period was very high, indicated by low effluent substrate concentration **(Figure 5.4 b).**

Although the model appeared to quantitatively and qualitatively capture the behavior of packed column, there were differences between experimental results and modeled data. This discrepancy may result from the limit of 1D model, i.e., the simple assumption of an biofilm uniform to calculate biofilm thickness. Biofilm is well known to be heterogeneous and specific surface area of biofilm may vary biofilm age, nutrient concentrations and hydrodynamic conditions. Fitting M_b at constant of $1000m^2/m^3$ for the simplicity of the model can contribute to the dissimilarity between experimental results

and modeled data. Moreover, as the ratio of column's diameter to diameter is 0.6, the effect of radial dispersion can be not neglected. 1D modelization is in fact not suitable to describe real biofilm and substrate variation in 3D.

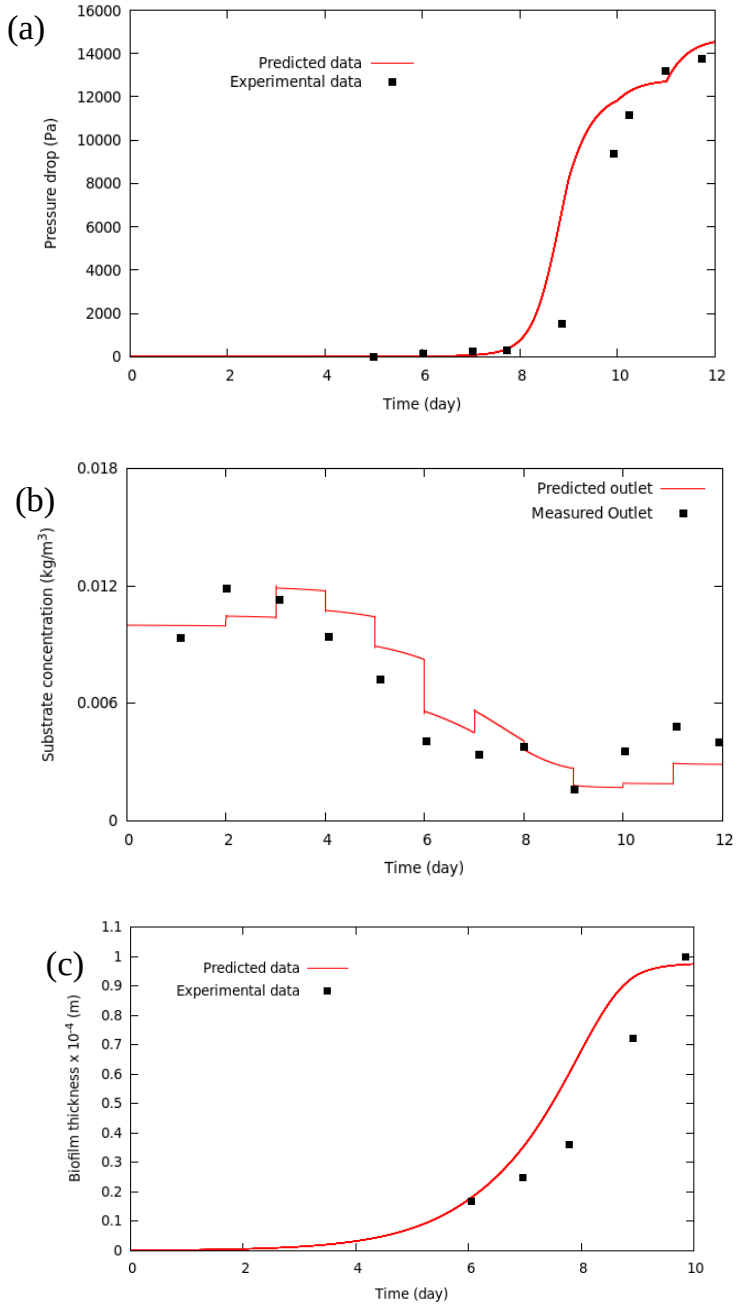

Figure 5.4: Comparison of predicted data to experiment ones of Wanner et al, 1995 in term of (a) pressure drop, (b) outlet substrate and (c) biofilm thickness

5.4.2 Column experiment by Taylor and Jaffe (1990a)

5.4.2.1 Experiment description

The bacterial-induced clogging in porous media was examined in two sand columns fed by nutrient solution with methanol as an electron donor for bacterial growth. Column dimension and operational parameters were given in **Table 5.5.** To study the extent of bioclogging in sand column, substrate concentration, biofilm thickness and permeability reduction were temporally and spatially monitored.

Table 5.5: Column dimension and operational conditions in experiment conducted by Taylor and Jaffe (1990a)

Parameter	**Unit**	**Value**		**Reference**
		Column 1	**Column 2**	Taylor and Jaffe (1990a)
Column height H	m	0.52		
Column diameter D	m	0.0508		
Inlet oxygen concentration	gO_2m^{-3}	10.2		
Clean-bed porosity	-	0.347		
Grain diameter	m	0.0007		
Seeding process				
Bacterial suspension	$kg.m^{-3}$	$5x\ 10^{-3}$		Ebigbo et al.(2010)
Substrate concentration	$kg.m^{-3}$	$6.67\ x\ 10^{-3}$		Taylor and Jaffe (1990a)
Seeding time	h	5		
Flow rate	$m^3.d^{-1}$	3.456		
Operation process				
Operation time	day	284	356	Taylor and Jaffe (1990a)
Inlet substrate concentration	gm^{-3}	7.2 (for $t \leq 149$ day) 5.2 (for $t > 149$day)	5.6 (for $t \leq 149$ day) 4.7 (for $t > 149$day)	
Flow rate	m^3d^{-1}	$20x10^{-3}$(for $t \leq 149$ day) $12x10^{-3}$(for $t > 149$day)	$6.4x10^{-3}$	

5.4.2.2 Numerical work

All the geometry parameters and operational conditions are the same as the experiments of Taylor and Jaffe (1990a), (**Table 5.5)**. The modeling biofilm experiments by Taylor and Jaffe (1990a) consisted of two steps. Step 1 was to model the seeding process to define the initial biofilm distribution. The numerical simulation of biofilm system was implemented in step 2 with the input data of biofilm concentration supplied from step 1.

It should be mentioned that different descriptions of biomass attachment were used in these two steps. In seeding process, biomass attachment was estimated by the correlation

equation that requires aqueous chemistry. However, such data was not available for the column experiments by Taylor and Jaffe (1990a). For the attempt to model biomass attachment in seeding process, such data was collected from others experiments of E.coli depositions. It is clear that this data reference can influence column behavior. Therefore, the sensibility of seeding process was also presented. **Table 5.6** presented the data of the aqueous chemistry from the experiments of E.coli deposition, which seemed close to Taylor and Jaffe (1990a) in term of ionic strength and pH. Case I was referenced from Syngouna and Chrysikopoulos, (2011), Case II and III were reference from Walker et al.,(2005).

Table 5.6: Aqueous chemistry of Ecoli-quartz sand system used for the seeding simulation

Case I	Case II	Case III
I =0.002 (M) Zp=-0.0185 (V) Zg= -0.0625 (V) pH=7	I =0.003162 (M) Zp=-0.0216 (V) Zg= -0.0308 (V) pH=5.7	I =0.03162 (M) Zp=-0.0186 (V) Zg= -0.01387 (V) pH=5.7
$\alpha_{estimated}$ =3.76 x 10^{-3}	$\alpha_{estimated}$=7.89 x 10^{-2}	$\alpha_{estimated}$=5.48 x 10^{-1}

$\alpha_{estimated}$ was calculated by Eq (5.16)

For the simulation of biofilm system in operation process, the numerical parameters were given in **Table 5.7.** The physical properties of fluid: fluid viscosity and fluid density, are considered to be constant. The dispersion coefficients and the growth kinetic of bacteria utilizing methanol was referenced from documented data (**Table 5.7**)

The parameters $\phi_{B,c}$, c_{det1}, c_{det2}, η_{att} are obtained by curve fitting as those used for Wanner's experiment validation. However, in this case c_{det2} was set to be 0.5, which is in the range 0.319 to 0.665 proposed by Speitel and DiGiano (1987). The specific surface is set to be 2500 m^{-1} (Taylor and Jaffe, 1990b). All the parameters are similar for the two experiments at column 1 and 2, except $\phi_{B,c}$. This difference is discussed in the section below.

Table 5.7: Parameters used for the simulation of experiment conducted by Taylor and Jaffe (1990a)

Parameter	**Unit**	**Value**	**Reference**
Clean-bed permeability K_O	m^2	2.93×10^{-10}	*Taylor et Jaffe, 1990*
Fluid viscosity μ	$kgm^{-1}s^{-1}$	0.001	-
Fluid density ρ_l	kgm^{-3}	1000	-
Dispersion coefficient for substrate D_s	m^2s^{-1}	6×10^{-10}	*Wanner et al., 1995*
Dispersion coefficient for oxygen D_o	m^2s^{-1}	2×10^{-9}	*Wanner et al., 1995*
Dispersion coefficient for bacterial cell D_m	m^2s^{-1}	1×10^{-9}	*Wanner et al., 1995*
Biofilm density ρ_b	kgm^{-3}	3	*Ebigbo et al., 2010*
Maximum specific growth rate μ_{max}	s^{-1}	8.91×10^{-5}	*Taylor et Jaffe, 1990b*
Saturation constant for substrate K_s	kgm^{-3}	0.000799	*Taylor et Jaffe, 1990b*
Saturation constant for oxygen K_o	kgm^{-3}	0.0002	*Wanner et al., 1995*
Yield coefficient for substrate Y_s	-	0.0975	*Taylor et Jaffe, 1990b*
Yield coefficient for oxygen Y_o	-	0.9	*Wanner et al., 1995*
Bacterial decay rate k_{dec}	s^{-1}	3.18×10^{-7}	*Taylor et Jaffe, 1990*
Biofilm permeability K_{min}	m^2	2.93×10^{-14}	K_0/K_{min}=2500-10000 Vandervivere,1995
Specific surface area of grain M_b	m^{-1}	2500	*Taylor et Jaffe, 1990*
Fitted parameters		**Colum 1**	**Column 2**
$\phi_{M,c}$	-	0.08	0.025
Detachment coefficient c_{det1}	s^{-1}	0.5×10^{-9}	
Detachment coefficient c_{det2}	-	0.5	
Attachment coefficient η_{att}	-	5×10^{-3}	
w_b	-	1	

The modeling domain is discretized with 260 uniform cells for a total length of 52cm. Time step for the simulation was set to 10s and with this value, the Courant number was 0.55. The boundary conditions required for numerical simulation are summarized in **Table 5.7.** Biofilm thickness is assumed uniform and can be estimated by Eq (5.2).

Table 5.8: Boundary conditions required for numerical simulation

Parameters	**Inlet**		**Outlet for both two columns**
	Colum 1	**Column 2**	
C_s	Dirichlet condition with a constant: Cs(0,t)=0.0072 kg.m^{-3}	Dirichlet condition with a constant: Cs(0,t)=0.0056 kg.m^{-3}	Neumann condition: $n.(D_s \nabla C_s) = 0$
C_o	Dirichlet condition with a constant: Co(0,t)=0.009 kg.m^{-3}		Neumann condition: $n.(D_o \nabla C_o) = 0$
C_m	Dirichlet condition with a constant: Cm(0,t)=0		Neumann condition: $n.(D_m \nabla C_m) = 0$
ϕ_b	Neumann condition: $n.(\nabla \phi_b) = 0$		Neumann condition: $n.(\nabla \phi_b) = 0$

5.4.2.3 Results and discussion

a) Seeding process

The influence of aqueous chemistry on the initial biofilm distribution along the column height was shown in **Figure 5.5.** Different profiles of biofilm volumetric fraction were observed in the 3 cases. Biofilm was well inoculated in case III whose attachment efficiency was very high at 0.548. In this case, biofilm showed an exponential decrease from the bottom to the top of column. Less biofilm was correspondent to case I and case II whose attachment efficiencies were small, 3.76x 10^{-3} for case I and 7.89x10^{-2} for case II. In the early state of the column, it is clear that seeding process influence column behavior **(Figure 5.6**). Log-phase of biofilm growth (presented by pressure drop) in transient-state was faster with the higher attachment efficiency and also the magnitude of pressure drop.

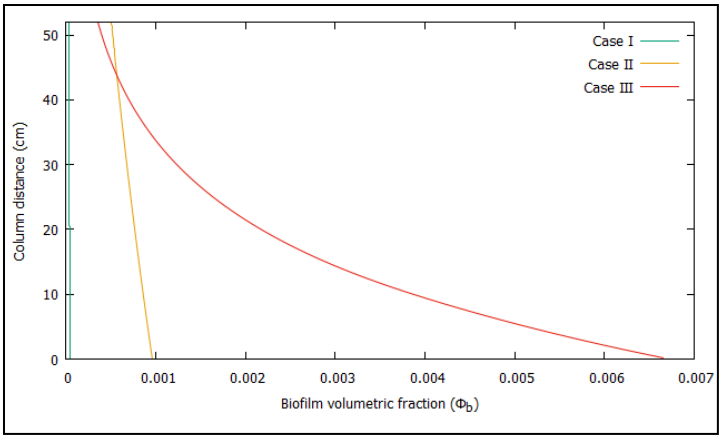

Figure 5. 5: Biofilm distribution along the column height after seeding process

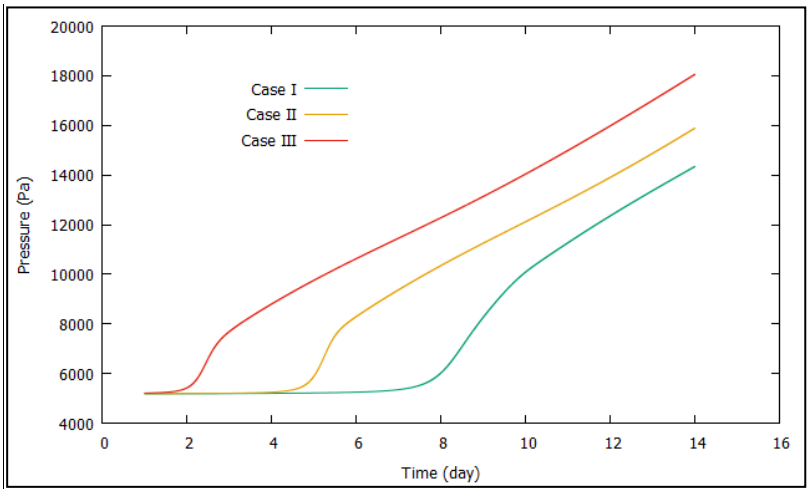

Figure 5. 6: The influence of seeding process on the column behavior in 14 days

The simulation of the seeding process showed that biomass attachment was important for the initial distribution of biofilm. The attachment can be estimated by the correlation equation developed in chapter 4 (Eq 5.16). However, the prediction capacity of the correlation equation was highly dependent on the aqueous chemistry, which can influence the transient-state of porous media.

b)Operation process

In the lack of knowledge of aqueous chemistry required for the correlation equation (Eq 5.16), this study used the parameters of case I for the estimation of biomass attachment in seeding process. Case I was close to the column experiments Taylor and Jaffe (1990a) in term of ionic strength and pH. Besides that, these experiments were run in a long time,

the influence of seeding process were expected not rigorously change the global behavior of porous media at steady-state.

Figure 5.7 shows the evolution of permeability reduction as a function of the column length at 14, 28, 42, 57 and 127 operating days. The continuous lines represent the modeling results and the points represent the experimentally measured value by Taylor and Jaffe (1990a).

(a)

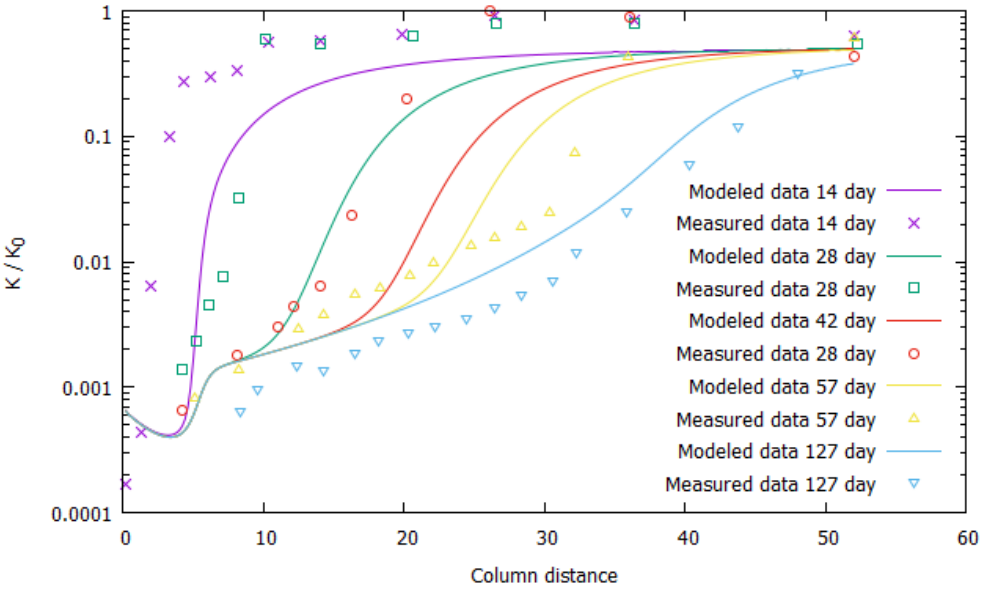

(b)

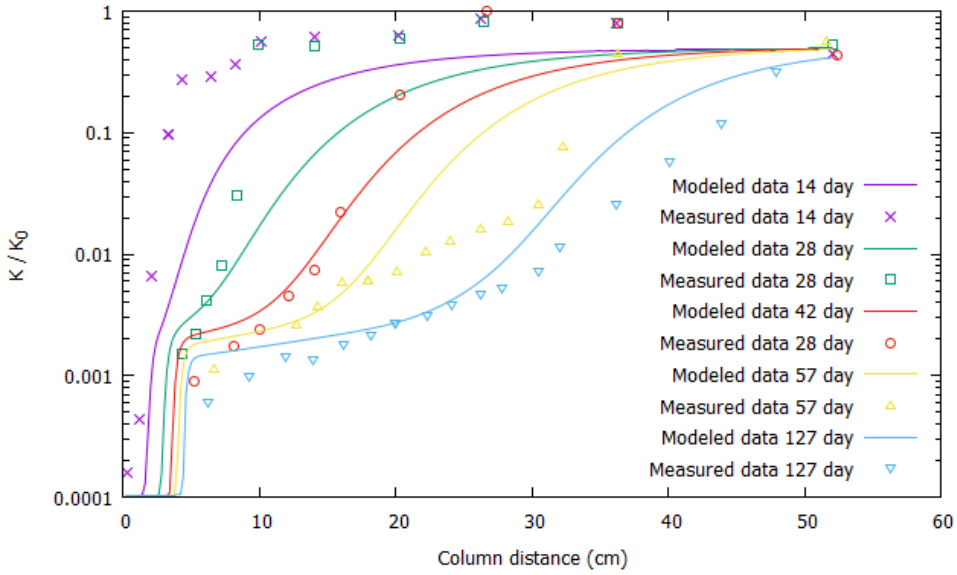

Figure 5. 7: Comparison of modeled data and experimental result of permeability reduction of (a): column 1 and (b): column 2 (Taylor and Jaffe, 1990a) at 14 , 28, 42, 57 and 127 days

The results showed that the model is capable of capturing the evolution of permeability reductions in both column 1 and column 2. Permeability reduction appeared severe at the bottom and less intensive at the top of the two columns. The profiles of biofilm thickness during the first 28 days are plotted in **Figure 5.8a** and **5.8b** for the column 1 and column 2, respectively. One can see that the biofilm thickness is very high at the first 5cm distance from the bottom. It corresponds to the most extreme permeability reduction of biofilter at the first 5cm distance from the bottom (**Figure 5.7a** and **5.7b**)

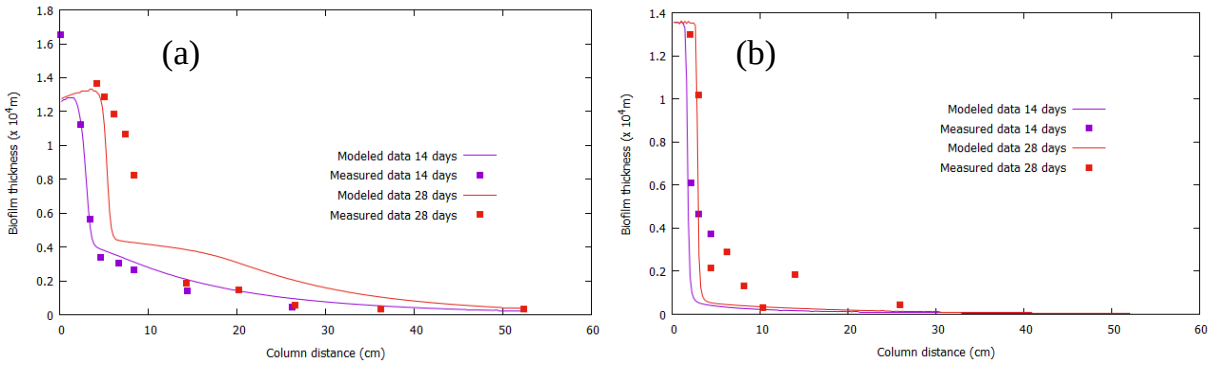

Figure 5. 8: Comparison of modeled data and experimental result of biofilm thickness of (a): column 1 and (b): column 2 (Taylor and Jaffe, 1990a) at 14 days and 28 days.

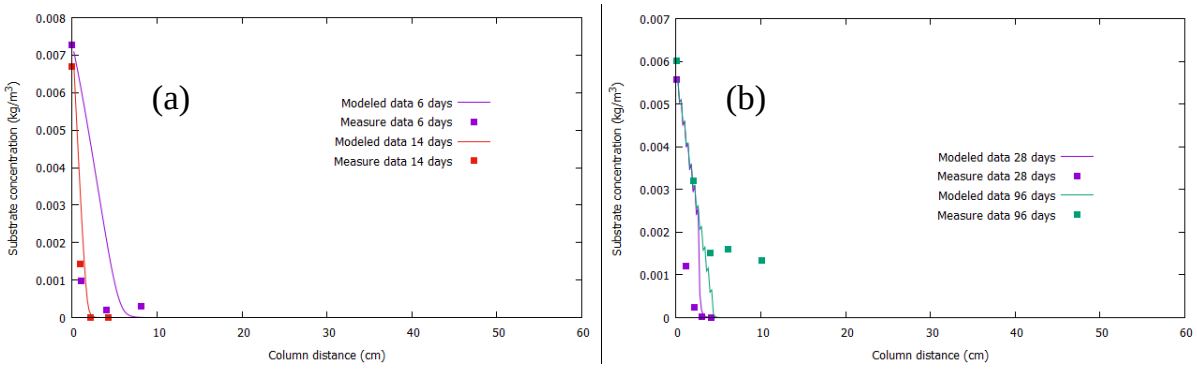

Figure 5. 9: Comparison of modeled data and experimental result of substrate profile of (a): column 1 (Taylor and Jaffe, 1990a) at 6 days and 14 days; and (b): substrate profile of column 2 (Taylor and Jaffe, 1990a) at 28 days and 196 days

The high development of biofilm at the bottom of the column can be explained by the nutrient assessment. The profiles of the substrate at 6 days and 14 days in column 1, as well as 28 days in column 2, are plotted in **Figure 5.9a** and **5.9b**. The profiles showed that substrate depleted very quickly from the first 5cm distance from the inlet. From these

periods (14 days for column1 and 28 days for column 2), permeability reduction may not relate to biofilm growth because all the substrate was consumed to maintained existing biomass (Broveli et al., 2009). Bio-plugging maybe the main mechanisms driving permeability reduction of sand columns. Several possibilities, i.e. the formation of micro-aggregates (Vandervivere, 1995) or dead ends (Kim et al., 2010) were suggested to explain the severe decline of column permeability. Some bacterial strains tend to form micro-aggregates in the sand column than biofilm or under the effect of biofilm sloughing, multicellular particles are detached from biofilm, plugging the pore space (Vandervivere 1995). Kim et al. (2010) observed the confocal laser scanning microscopy (CLSM) images of biofilms and found that dead ends occurred in the downstream which were influenced by velocity and substrate concentration.

In the numerical works, $\phi_{B,c}$ is the only parameter to determine the extent of bioclogging and it may be dependent on flow rate and substrate concentration (Vandervivere, 1995). However, knowledge of this relationship is not well addressed and $\phi_{B,c}$ was a fitted parameter. This consideration can not be appropriate for the case of varying operational conditions. In experiment conducted by Taylor and Jaffe (1990a), after 149 days, the operational condition was implemented to decrease flow rate and substrate concentration in column 1; and the same process was applied for substrate concentration in column 2. This alternation highly influences the clogging patterns of the two columns. In our numerical works, as $\phi_{B,c}$ was kept with the value used for the regime before switching to new operational conditions. Hence, the model aim to only simulate the behavior of biofilters during 149 days (before switching to the new operational condition). The influence of substrate of hydrodynamic condition of permeability is also the reason that all the parameters for numerical works are identical for column 1 and column 2, except $\phi_{B,c}$. In our model, $\phi_{B,c}$was 0.08 for column 1 and 0.025 for column 2.

The experiments of Taylor and Jaffe (1990a) were conducted over a long time, 149 days before switching to other operational conditions. The two sand columns were operated with two different hydrodynamic conditions. Temporally and spatially fitting the data of

experiments by Taylor and Jaffe (1990a) is a tough challenge for macroscopic models. The permeability reduction was the main objectives of some studies. Ebigbo et al. (2010) developed a dual-porosity model that accounted for biofilm porosity to solute transport. This model was successful to capture the permeability reduction of both two columns at the end of experiments, 283 days for column 1 and 356 days for column 2. Other studies targeted column behaviors at early times. Brovelli et al. (2009) proposed a conventional model that could capture the permeability reduction of column 1 in 14 days, 28 days and 42 days. Ham et al. (2007) suggested a more sophisticated model that included EPS in biomass growth. However, the results were similar to Brovelli's model that only predicted permeability reduction in early time of column 1, other parameters such as substrate concentration, biofilm thickness were not mentioned in these studies.

The modeled data of permeability reduction of this study, Ham et al. (2007) and Brovelli et al. (2009) versus the experimental data by Taylor and Jaffe (1990a) at 14 days, 28 days and 42 days are plotted in **Figure 5.10**. The results show that our model can capture the temporal and spatial variation of permeability reduction. Ham et al. (2007) used permeability model by Clement et al. (1999) and might underestimate the plugging effect resulting from micro-aggregates. It may explain for the discrepancy of the permeability curve and experimental data at 28 days and 42 days and the lack of the predicting capacity after 42 days. Brovelli et al. (2009) applied Thullner's permeability (Thullner 2002) which accounts for biomass plugging in porous media. However, this permeability model was derived from network simulation and may result in issues in other experimental conditions.

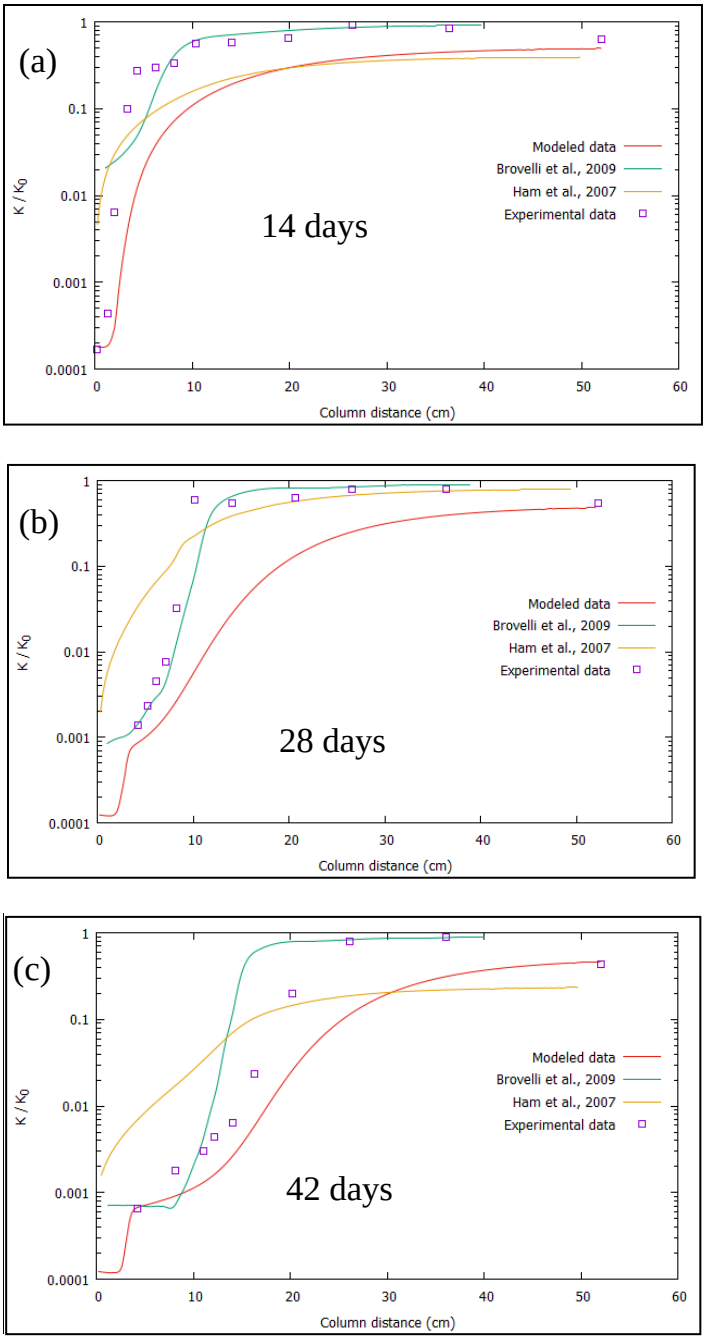

Figure 5.10: The modeled data of this study, Ham et al.(2007) and Brovelli et al. (2009) versus the experimental data by Taylor and Jaffe (1990a) at (a): 14 days, (b): 28 days and (c): 42 days.

c) Heterogeneous structure of biofilm

The account of the heterogeneous structure of biofilm is not in the scope of this study. However, biofilm structure was implicitly expressed by the value of bulk factor. In this study, biofilm was assumed impermeable and homogeneous; and β_b was also taken at 1

for this assumption and for the simplicity of macroscopic model. By a simple adjustation of the value of bulk factor higher than 1, the heterogeneous structure of biofilm is accounted, which reduces the available pore space for fluid flow. Or the value of bulk factor less than 1 indicates the contribution of biofilm porosity to the global flow of porous media. A range of bulk factor from 0.5 to 5 was tried in the simulation to analyze the effect of bulk factor (or biofilm structure) on the global behavior of porous media. **Figure 5.11** showed that higher value of bulk factor induced more severe permeability reduction. High value of bulk factor indicates the small effective pore space for fluid flow, which may be correspondent to a high heterogeneous structure of biofilm. However, it should be noted that biofilm heterogeneousness is a time-dependent variable that is influence by many factors: bacterial strain, nutrient concentration, hydrodynamic conditions, biofilm age...Therefore, bulk factor, even in a simple representation of biofilm structure, should not be a constant.

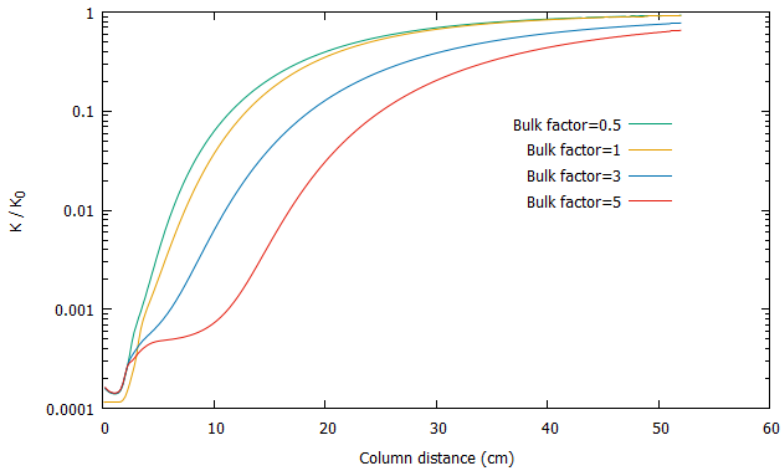

Figure 5. 11: The influence of bulk factor on the permeability reduction of column 1 at 14th day

d) Limits of the model on Taylor & Jaffe experiments

The numerical results showed that the model could capture the temporal and spatial permeability reduction of both two column experiments by Taylor and Jaffe (1990a) until 127 days. However, the predicted permeability showed a different trend with experimental data after the shift of operational conditions. At the 149th day, flow rate and

substrate concentration were reduced in column 1, and substrate concentration was reduced in column 2 (**Table 5.5**). Permeability of column 1 at the 155th day, 196th day and 283rd day showed a declining tendency. In column 2, the same tendency was observed in the 155th day, 196th day but permeability increased at 356thday (Taylor and Jaffe, 1990a). However, **Figure 5.12** showed that predicted permeability increased with time when the loadings were reduced.

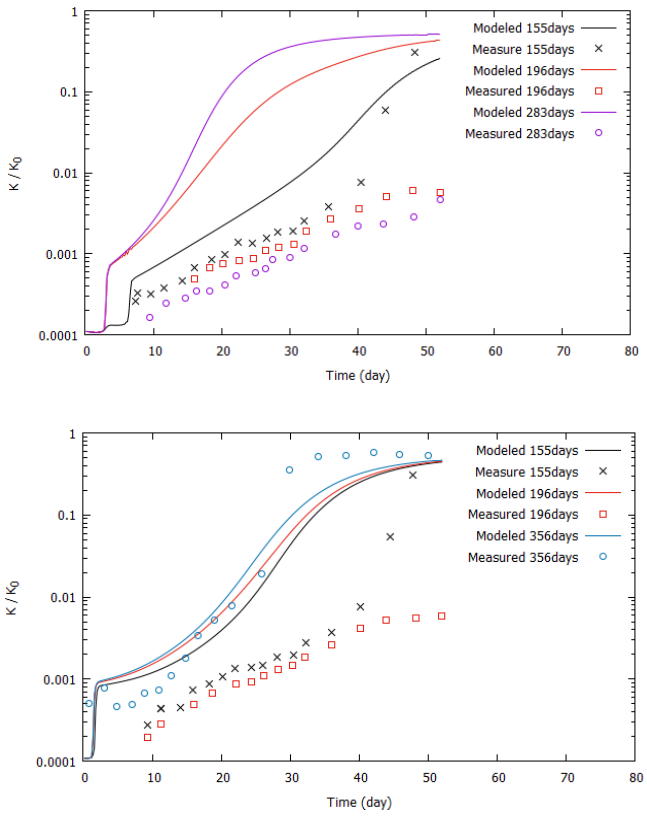

Figure 5.12: Modeled data and measured results of permeability reduction after the shift of operational conditions of (a): column 1 and (b): column 2 (Taylor and Jaffe, 1990a)

The difference between the predicted permeability and experimental data can be explained by the limits of the model. The mechanisms of bioclogging are very complicated so that the biomass content is not the only factor required to explain the permeability reduction as argued by Brovelli et al. (2009). Bielefeldt et al. (2002) performed sand column with propylene glycol as an electron donor and bacteria were enriched from soil. Although biomass content under low flow rate (8ml/min) was higher than that under high flow rate (12ml/min) in all column heights, permeability reductions

at these two flow rate were similar. It may be explained by involvement of biofilm component, such as EPS. Proto et al. (2016) reported that permeability could remain unchanged after two months of starvation condition. It was suggested that EPS was the primary mechanisms for permeability reduction and may induce permeability reduction even though substrate was not supplied for existing biofilm.

Meanwhile only biomass accumulation was assumed to result in permeability reduction in this study. With this assumption, the decrease of loadings, which drives to less biomass accumulation, will increase the permeability of column, as predicted by the model **(Figure 5.12).** However, this assumption may not be enough to capture the involvement of other factors, such as EPS to cause permeability reduction. As a consequence, the increasing tendency of permeability predicted by this model was different to experimental data after the loading reduction in two columns.

5.5 Conclusion of chapter 5

A macroscopic model was developed for the numerical simulation solute transport coupling with biofilm growth in porous media. The model was based on the solution of a set of advection-diffusion-reaction equations and involved in recent advances in describing dominant processes in porous media. Our new permeability model was used in Darcy's equation to define momentum conservation. Biomass attachment in seeding process was estimated by the correlation equation developed in chapter 4. Although the model was capable of capturing the behavior of porous media represented by permeability reduction, solute concentration, biofilm thickness, there were lots of aspects should be considered. Seeding process was important to the transient-state of porous media. The correlation equation can be used to estimate biomass attachment in seeding process. However, its application was sensitive to aqueous chemistry. The heterogeneous structure of biofilm may be accounted by bulk factor in macroscopic model, which was shown to influence to the behavior of porous media. However, the bulk factor, even in a simple representation of biofilm structure should be a time-dependent variable. The assumption that permeability only results from biomass content may not be enough to capture the involvement of other factor, such as EPS, which can drive the difference of predicted results and experimental data.

Chapter 6

Biofilm sloughing modeling

The influence of biofilm on the biofiltration performance depends on the processes involved in biofilm evolution, among which detachment is one of the primary elements that govern the mass balance of biofilm in its cycle. In biofilm detachment, biomass is continuously detached at small size aggregates or concretely removed at large size aggregates from the biofilm. The later process is defined as biofilm sloughing, which is very complicated and usually neglected or modeled in the combination with biomass erosion as a continuous process.

In this study, biofilm sloughing has been separately accounted in the numerical modeling porous media bioclogging. Biofilm sloughing was considered as a stochastic process and quantified by random generator. So this discrete events could be incorporated into other continuous processes to determine the biomass transfer from biofilm to the liquid phase. Numerical simulations have been performed using OpenFoam to study the capacity of the stochastic process to model biofilm sloughing.

List of symbols

Symbol	Unit	Definition
Basic notation		
C_b	kgm^{-3}	Biofilm concentration
$C_{b,max}$	kgm^{-3}	Maximum biomass that can be obtained in porous media.
c_{e1}	s^{-1}	Erosion coefficient in (Eq 6.2)
c_{e2}	-	Erosion coefficient in (Eq 6.2)
C_m	kgm^{-3}	Mobile biomass concentration
Co	kgm^{-3}	Oxygen concentration
C_s	kgm^{-3}	Solute concentration
D	M	Column diameter

dg	M	Grain diameter
Dm	m^2s^{-1}	Dispersion coefficient for mobile bacteria
Do	m^2s^{-1}	Dispersion coefficient for oxygen
Ds	m^2s^{-1}	Dispersion coefficient for solute
$F(\emptyset_M)$	-	Biomass distribution for the reduction of pore radius and plugging of pore space
g	ms^{-2}	Gravitational acceleration
H	M	Column height
K	m^2	Permeability of porous media
K_0	m^2	Clean-bed permeability
Kmin	m^2	Biofilm permeability
K_P	-	Relative permeability reduction resulting from microbial aggregates plugging pore space
K_R	-	Relative permeability reduction resulting from biofilm covering grain surface
K_{rel}	-	Total relative permeability reduction
Ko	kgm^{-3}	Half-saturation constants of oxygen
Ks	kgm^{-3}	Half-saturation constants of substrate
k_{decay}	s^{-1}	Biomass decay rate
k_{r1}	-	Fitted parameter in (Eq 6.3)
k_{r2}	s^{-1}	Fitted parameter in (Eq 6.3)
L	M	Straight length of porous media
L_b	M	Biofilm thickness
M_b	m^{-1}	Specific area of biofilm
n_r	-	Random number in (Eq 6.3)
R_D	$kgm^{-3}s^{-1}$	Detachment rate
r_{att}	s^{-1}	Specific attachment rate
$r_{erosion}$	s^{-1}	Specific erosion rate
$r_{sloughing}$	s^{-1}	Specific slounghing rate
r_x	s^{-1}	Specific biomass growth rate
t	S	Time
U	ms^{-1}	Approaching velocity
v	ms^{-1}	Pore velocity
Yo	-	Yield coefficients for oxygen consumption
Ys	-	Yield coefficients for oxygen consumption
ΔP	Pa	Pressure drop

Δt	S	Time step for continuous processes in numerical simulation
δt	S	Time step for discrete process in numerical simulation
Greek letters		
$\emptyset$	-	Porosity
$\emptyset_0$	-	Clean-bed porosity
$\emptyset_b$	-	Volumetric fraction of biofilm
$\emptyset_{b,rel}$	-	Relative volumetric fraction of biofilm $\emptyset_{b,rel} = \frac{\emptyset_b}{\emptyset_0}$
$\emptyset_{B,c}$	-	$\emptyset_{B,c}$ is a the value that affects the F($\emptyset_b$) curve shape and controls how fast mass aggregates are formed and plug pore space
μ	$kgm^{-1}s^{-1}$	Fluid viscosity
μ_{max}	s^{-1}	Maximum biomass growth rate
α_{att}	-	Attachment probability
η_0	-	Contacting probability
η_{lmt}	-	Growth limiting factor
ρ_b	kgm^{-3}	Biofilm density
ρ_l	kgm^{-3}	Fluid density

6.1 Introduction

In biofiltration process, biofilm grown under favorable conditions modify porous media structure and consequently alters its hydraulic conductivity. The influence of biofilm on the biofiltration performance depends on the processes involved in biofilm evolution, among which detachment is one of the primary elements that govern the mass balance of biofilm in its cycle.

In the general concept, detachment can be defined as the release of mass from attached biofilm to fluid phase, which is the results of different forces acting on biofilm. In other words, when the total external forces are higher than local biofilm strength, local particles are detached from the biofilm. Aggregates with the size smaller than 10 μm continuously detach from biofilm while those large up to several mm are discretely removed from the biofilm. These two processes are defined as erosion or sloughing, respectively (Horn and Lacker, 2014). However, the distinction between the two types of detachment, dependent on the aggregates size, may be arbitrary (Stewart, 1993). In conjunction with the

complex nature of both biomass erosion and sloughing, these two processes are conventionally modeled as one continuous process which is a function of shear stress, biofilm density, thickness, growth rate...etc. (Horn and Lacker, 2014). Apparently, this modeling approach underestimates or neglects the biomass sloughing and can not explain the oscillation of pressure drop profile or biomass distribution reported in many biofiltration experiments (Howell and Atkinson, 1966; Stewart and Fogler, 2001; Zippel et al., 2007; Karrabi et al., 2011). Biofilm sloughing was demonstrated to cause the oscillation tendency observed for the biomass hold up in a biofilter (**Figure 6.1a**-Howell and Atkinson, 1976). Zippel et al. (2007) used light absorbance to monitor the biofilm development in phototrophic biofilm experiment. The oscillation tendency in biomass concentration was reported in this study (**Figure 6.1b**).

Biofilm sloughing also induced the hydraulic change in biofilm experiment. In the experimental study of Karrabi et al. (2011), the interaction of hydrodynamic and *P. putida* biofilm produced oscillation in pressure curves in pilot biofilter at all experimental conditions (**Figure 6.1c**). The maximum amplitudes of oscillation were $\pm$ 20 mbar around the mean pressure, in comparison with the maximum value of measured pressure drop of 250 mbar at steady state. The similar behavior of pressure oscillations was reported by other authors. In the micromodel experiment for biomass plug of facultative anaerobic bacteria, Stewart and Fogler (2001) reported that sloughing is the main factor that can closely sweep out biofilm from substratum **(Figure 6.1d**). The recorded pressure presented a profile with extreme oscillation where the pressure drop suddenly dropped down from hundreds of kPa to nearly zero at each pressure cycle. Those experimental results pointed out the contribution of biofilm sloughing to mass balance in biofilm evolution. To some extent, sloughing can be the determinant factor that governs the detachment process.

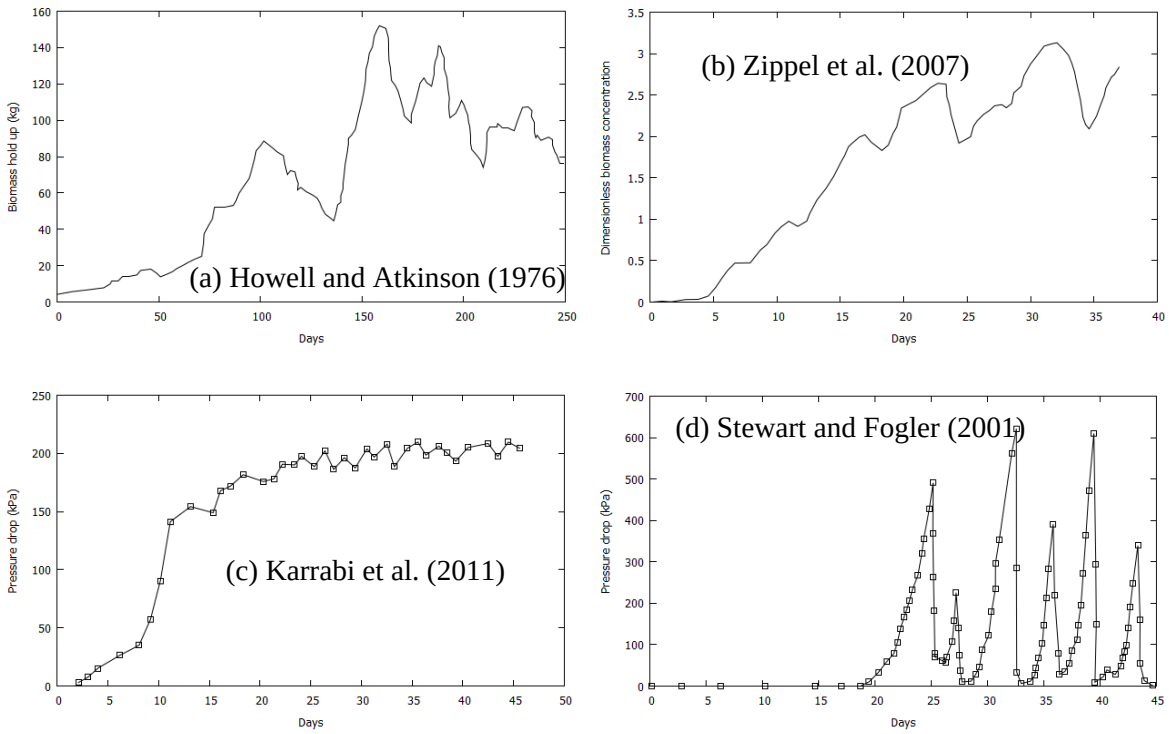

Figure 6.1: Observed oscillations in documented experiment investigating solute transport coupling with biofilm growth in porous media.

Concerning the important role of sloughing, recent efforts have been made to incorporate sloughing, along with erosion in biomass model (Stewart and Kim, 2004; Xavier et al., 2005; Bohn et al., 2007). In simulation studies, the complex nature of sloughing drives the modeling approach into two main groups with total different orientations. The first group concentrated on the balance between the external stress and local biofilm strength. The clusters of biofilm are removed when the cohesion strength of the clusters are less than external shear forces. Numerical investigation of sloughing influence on biofilm structure using this approach have been performed both in two dimensions (Picioreanu et al., 2001; Xavier et al., 2005; Duddu et al., 2009) and three dimensions (Xavier et al., 2005; Alpkvist and Klapper, 2007). In the attempt to systematically model for sloughing event, Stewart and Kim (2004) included sloughing term in advection-diffusion-reaction equations and the simulation was validated by the experiment conducted by Stewart and Fogler (2001) in the term of the oscillation of pressure profile or the fluctuation of permeability reduction.

The difficulty of this approach is to quantify biofilm strength since this information is not always available (Picioreanu et al., 2001) and not consistent with experimental results. Biofilm elastic modulus was usually used in the simulation works to represent biofilm strength. Its value varied from one study to another as shown in **Table 6.1**

Table 6.1: Various values of biofilm elastic modulus

References	Biofilm elastic modulus(N/m^2)
Ohashi et al. (1999)	0-1800
Stoodley et al. (1999)	20-240
Klapper et al. (2002)	0.8-640
Paramonova et al. (2009)	17-310

Biofilm strength was also observed to be a function of biofilm thickness. At the bottom, biofilm was very resistant to shear forces while moving to the interface of biofilm/fluid phase, biofilm cohesion decreased and was more likely detachable (Coufort et al., 2007).

Two major factors may result in the large variation in biofilm strength. The first one is the difficulty to implement experiments allowing to accurately evaluate this parameter. Recently new experimental techniques have been developed to make the measurement more precise, for example: microcantilever method for intact biofilms (Aggarwal et al., 2010) , atomic force microscopy methodology (Ahimou et al., 2007; Aggarwal et al., 2010 and Bol et al., 2012). The second factor is the complexity of biofilm structure. It is well known that biofilm is heterogeneous, stratified and contains channels, voids (Lewandowski, 2000). And its structure evolves with surrounding hydrodynamic conditions. As a consequence, biofilm strength is expected to be temporally and spatially variable. At the current stage, the experimental measurement only represents the biofilm strength at a given depth of biofilm, for a given time and under controlled operational conditions. Taking a constant value for the biofilm strength to model sloughing certainly leads to the discrepancy between numerical results and experimental data.

The second group introduces stochastic process as an important feature in biofilm development. Biofilm structure was reported to be influenced by uncertain factors. The same structures were not probably repeated in even identical experimental conditions

(Heydorn et al., 2000). It is probably due to the occurrence of stochastic processes during the formation of biofilm. For example, seeding process is determined by stochastic transport of singe cells in fluid phase to substratum due to convection or Brownian motion (Bohn et al., 2007). The cell diversity in biofilm was attributed as the stochastic consequence that different types of cells in respect of gene expression were found randomly adjacent under nearly identical environment conditions in the study of young biofilm *Pseudoalteromona* (Baty et al., 2000). The stochastic process also induces the different growth mode of single cell in noxious conditions so that the division rate of single *Escherichia coli* cells was found variable (Kussell et al., 2005; Balaban et al., 2004). In the study of EPS components, stochastic process was experimentally proved to play an important role in the matrix production of *Bacillus subtilis (*Chai et al., 2007)

As the presence of stochastic process is found throughout biofilm formation and sloughing is a discrete event at random time, it was natural to assume that sloughing can be considered as a stochastic process (Lewandowski et al., 2004). Following this concept, Bohn et al. (2007) proposed a new approach to model sloughing in which sloughing rate was quantified randomly. Biofilm detachment was modeled as the combination of deterministic process (erosion) and stochastic process (sloughing) that occur at different time scales. This modeling approach avoids the estimation of the biofilm strength. However, it still needs adjustable parameters to fit experiment result (Bohn et al., 2007), which reduce the freedom of numerical simulation.

In macroscopic modeling, the first approach based on forces balance seems to be inappropriate because it requires extensive computer cost to calculate total force applied on biofilm along its thickness to determine the possibility of biofilm clusters sloughing. One exception is the numerical study of Stewart and Kim (2004). They used this approach to characterize biomass sloughing in their two dimensional pore network model. Sloughing was incorporated under the specific condition that it always swept out biofilm. In other words, every time sloughing occurred, it took place at the bottom of biofilm and all the biomass attached was removed from the support. Such consideration may be reasonable under a very specific conditions (Stewart and Fogler, 2001) and can

not always be used to represent biomass sloughing. The second approach is more suitable for macroscopic modeling because it treats sloughing as a stochastic process so that sloughed biomass can be quantified by a random generator. Boln et al. (2007) showed the preliminary modeling results of the oscillation in biomass curve (represented by light absorbance) by using this approach. However, this simulation used a simple mathematical framework so that sloughing was not systematically incorporated with biofilm kinetics and hydrodynamic

In this study, a new model for bioclogging that includes sloughing in biomass detachment was developed. In order to provide a macroscopic description of the interaction of biofilm growth and hydrodynamic conditions in porous media, sloughing is considered as a stochastic process and can be quantified by random generator. These discrete sloughing events are incorporated with other continuous processes to determine the biomass transfer from biofilm to the liquid phase.

6.2 Model description

The continuum approach, widely applied in field-scale applications (Shafahi and Vafai, 2009) has been adopted for model development. The model consists of a set of equations to solve momentum conservation relating to Darcy's equation, and mass conservation involved in advection-diffusion-reaction equations with the appropriate source and sinks term.

6.2.1 Mass conservation

The macroscale model is based on the advection-diffusion-reaction equation for the evolution of the components in porous media such as electron donor, electron acceptor, biofilm, suspended biomass. The mass conservation for the evolution of these components are given in **Table 6.2**

Table 6.2: Mass conservation of the components in porous media

Biofilm

$$\frac{d(\emptyset_b \rho_b)}{dt} = \eta_{lmt} r_x \emptyset_b \rho_b - k_{decay} \emptyset_b \rho_b + r_{att} C_m - r_{det} \emptyset_b \rho_b \quad (6.1)$$

Mobile (suspended) biomass:

$$\frac{\partial(\emptyset C_m)}{\partial t} + \nabla(C_m U) = \nabla.(D_m \emptyset \nabla C_m) + r_x \emptyset C_m - k_{decay} \emptyset C_m - r_{att} \emptyset C_m + r_{det} \emptyset_b \rho_b \quad (6.2)$$

Substrate (electron donor)

$$\frac{\partial(\emptyset C_s)}{\partial t} + \nabla(C_s U) = \nabla.(D_S \emptyset \nabla C_s) - \frac{r_x}{Y_s} \emptyset C_m - \frac{\eta r_x}{Y_s} \emptyset_b \rho_b \quad (6.3)$$

Oxygen (electron acceptor)

$$\frac{\partial(\emptyset C_o)}{\partial t} + \nabla(C_o U) = \nabla.(D_o \emptyset \nabla C_o) - \frac{r_x}{Y_o} \emptyset C_m - \frac{\eta r_x}{Y_o} \emptyset_b \rho_b \quad (6.4)$$

where η_{lmt} growth limit factor (-),

r_x biomass growth rate (s^{-1}),

r_{att} attachment rate (s^{-1}),

r_{det} detachment rate (s^{-1}),

k_{decay} biomass decay rate (s^{-1}),

C_m mobile biomass in liquid phase (kgm^{-3}),

C_S substrate concentration (kgm^{-3}),

C_O oxygen concentration (kgm^{-3}),

U approaching velocity (ms^{-1}),

D_m, D_s, D_o effective dispersion coefficient for mobile biomass (m^2s^{-1}), for solute (m^2s^{-1}) and oxygen (m^2s^{-1}), respectively.

Y_S, Y_O yield coefficients for substrate consumption and oxygen consumption, respectively.

6.2.2 Momentum conservation:

In this study, we applied our modified model to predict permeability reduction.

$$K_{rel} = F(\emptyset_B)K_R + \left(1 - F(\emptyset_B)\right)K_P \qquad (6.5)$$

K_{rel} is total relative permeability reduction (-), $K_{rel}=K/K_0$ which K_0 is the clean bed permeability (m_2), K_R, K_P are permeability reduction resulting from biofilm covering grain surface (-) and microbial aggregates plugging pore space (-), respectively. $F(\emptyset_b)$ determines biomass distribution for the reduction of pore radius and plugging of pore space.

The permeability resulting from biofilm covering grain surface is expressed in the following equation:

$$\frac{K_R}{K_0} = \left(\frac{\emptyset_0 - \beta_b\emptyset_b}{\emptyset_0}\right)^3 \frac{\tau_0}{\tau} \frac{(1-\emptyset_0)^{4/3}}{\left(1-\emptyset_0+\beta_b\emptyset_b\right)^{4/3}} \qquad (6.6)$$

where β_b is the bulk factor used to define the effective pore space for fluid flow. As mentioned in chapter 3, the bulk factor can influence the hydraulic conductivity when K_R dominates the permeability reduction. The value of bulk factor can be higher than 1 as the heterogeneous structure of biofilm reduces the available pore space for fluid flow, or less than 1 in some conditions which biofilm porosity is accounted and contribute to the global flow of porous media. τ is the tortuosity of porous media. There are many models to compute tortuosity (Du Plessis and Masliyah, 1991; Koponen et al., 1996; Yu and Li, 2004; Lanfrey et al., 2010; Ahmadi et al., 2011). In this work the model proposed by Yu and Li (2004) is used (Eq 5.6), in which the description of flow path is based on grain geometry and a cubic arrangement is used:

$$\tau = \frac{1}{2}\left[1 + \frac{1}{2}\sqrt{1-\emptyset} + \sqrt{1-\emptyset} \times \frac{\sqrt{\left(\frac{1}{\sqrt{1-\emptyset}}-1\right)^2 + \frac{1}{4}}}{1-\sqrt{1-\emptyset}}\right] \qquad (6.7)$$

Permeability reduction caused by microbial aggregates plugging pore space is calculated in equation:

$$\frac{K_P}{K_0} = \frac{K_{min}/K_0}{1 - \frac{\emptyset}{\emptyset_0} + \left(\frac{\emptyset}{\emptyset_0}\right)\left(\frac{K_{min}}{K_0}\right)} \qquad (6.8)$$

with K_{min} and K_0 are biofilm permeability and initial permeability of clean-bed porous media, respectively.

The biomass that contributes to each pattern is characterized by $F(\emptyset_b)$ which is dependent on biomass concentration.

$$F(\emptyset_b) = \exp\left(-0.5\left(\frac{\emptyset_{b,rel}}{\emptyset_{B,c}}\right)^2\right) \qquad (6.9)$$

where $\emptyset_{b,rel}$ is the relative volumetric fraction of mass deposition, equal to the ratio of the volumetric fraction of mass deposition to the maximum porosity of porous media. $\emptyset_{B,c}$ is a value that affects the $F(\emptyset_b)$ curve shape and controls how fast mass aggregates are formed and plug pore space.

6.2.3 Sink and source terms

a) Biomass growth rate:

In our model, biomass growth rate r_x follows Monod's law for two limiting substances:

$$r_x = \mu_{max}\frac{C_s}{K_s+C_s}\frac{C_o}{K_o+C_o} \qquad (6.10)$$

with μ_{max} maximum specific substrate utilization rate (s^{-1}), Cs substrate concentration (electron donor) (kgm^{-3}), C_o oxygen concentration (electron acceptor) (kgm^{-3}). K_S and K_O half-saturation constants of substrate and oxygen, respectively.

Growth limit factor η_{lmt}

The macroscopic equation suggested by Zysset et al. (1994) and Kildsgaard and Engesgaard (2001) was used in the model

$$\eta_{lmt} = 1 - \frac{C_b}{C_{b,max}} \qquad (6.11)$$

where C_b is the biofilm concentration (kgm^{-3}) and $C_{b,max}$ (kgm^{-3}) is the maximum biomass that can be obtained in porous media. In the macroscopic equation, growth limit factor η_{lmt} is the function of immobile biomass and its value is in range of [0-1].

Relating biofilm concentration in term of density and volumetric fraction, the growth limit factor can be rewritten:

$$\eta_{\mathrm{lmt}} = 1 - \frac{C_b}{C_{b,max}} = 1 - \frac{\rho_b \emptyset_b}{\rho_b \emptyset_0} = 1 - \frac{\emptyset_b}{\emptyset_0} = \frac{\emptyset}{\emptyset_0} \qquad (6.12)$$

b)Biomass transfer

b1)Biomass attachment

In this study, the attachment rate is mathematically quantified following the CFT:

$$r_{att} = \frac{3(1-\emptyset)v}{2d_g\emptyset}\eta_{att} \qquad (6.13)$$

with r_{att} attachment rate (s^{-1}), dg grain diameter (m), v pore velocity (ms^{-1}), η_{att} attachment coefficient (-), which is a fitted parameter.

b2)Biofilm detachment

Biomass in bulk phase is additionally supplied by the mass loss of biofilm caused by detachment. In our model, detachment is specified in two different processes: erosion and sloughing, that detachment rate is dependent on first order of biofilm mass concentration:

$$R_D = r_{erosion} C_b + \text{stochastic term} \quad (6.14)$$

Where R_D is biomass detachment rate ($kgm^{-3}s^{-1}$), $r_{erosion}$ is specific erosion rate (s^{-1}) and specific sloughing rate (s^{-1}), respectively. C_b indicates biofilm mass concentration (kgm^{-3})

Erosion model

Many empirical models have been developed to mathematically describe erosion processes. A good review of these models is given by Kommedal and Bakke (2003). In our model, the combination of models proposed by Rittmann (1982) and Speitel and DiGiano (1987) was applied that erosion is dependent on shear stress and microbial growth rate:

$$r_{erosion} = c_{e1}\tau^{0.58} + c_{e2}r_X \qquad (6.15)$$

where $r_{erosion}$ is the specific erosion rate (s^{-1}), c_{e1}, c_{e2} are fitted parameters. τ is fluid shear stress and r_X is growth rate (s^{-1}).

Sloughing model

Sloughing is defined as a stochastic process to remove biofilm clusters. The size of clusters or the mass of biofilm detached at each sloughing event is arbitrary that in the extreme case, all biofilm is swept out. Bohn et al. (2007) proposed the stochastic term to describe biofilm sloughing. Eq (6.1) can be rewritten:

$$\frac{d\emptyset_b}{dt} = \Psi(\emptyset_b) \qquad (6.16)$$

with $\Psi(\emptyset_b) = \eta_{lmt} r_x \emptyset_b - k_{decay}\emptyset_b + r_{att}\frac{C_m}{\rho_b} - r_{det}\emptyset_b$

The stochastic term $\Omega(t)$ was added to Eq (6.16) to include sloughing process:

$$\frac{d\emptyset_b}{dt} = \Psi(\emptyset_b) - \Omega(t)\emptyset_b \qquad (6.17)$$

Discrete form of the Eq (6.17) with the simulation time step δt was used to solve the partial-stochastic differential equation:

$$\emptyset_b(t + \delta t) = \emptyset_b(t) + \delta t\Psi\big(\emptyset_b(t)\big) - \delta t\Omega(t)\emptyset_b(t) \qquad (6.18)$$

or

$$\emptyset_b(t + \delta t) = \emptyset_b(t) + \delta t\Psi\big(\emptyset_b(t)\big) - s\emptyset_b(t) \qquad (6.19)$$

with $s = \delta t\Omega(t)$

s is a random number in range from 0 to 1. The term $s\emptyset_b(t)$ represents the biofilm loss due to sloughing process between t and t+δt, when sloughing occur. s =0 indicates that no biofilm loss occurs and in case s=1, up to $\emptyset_b(t)$ is removed from the grain surface.

It is noted that biofilm sloughing is very complicated. The mass fractions detached in sloughing events are arbitrary so that using one random distribution may not be enough to describe these events. In addition, the occurrence of sloughing event at location z may influence the probability of upcoming sloughing event at next location z + Δz. However,

as a preliminary work, this study did not include those complicated features of sloughing process. For the 1-D simulation performed in this study, biofilm sloughing is modeled with the following assumptions:

- All the sloughing events follow the same random distribution.

- The sloughing events are independent on the location in biofilter.

To quantity the stochastic term, Bohn et al. (2007) proposed s as a function of uniformly distributed random number n_r in range [0:1].

$$s = (n_r)^{k_r} \qquad (6.20)$$

where k_r is a coefficient which allows to control the probability of occurrence of a given value of s, and thus the amount of biofilm removed when a sloughing event occurs. **Figure 6.2** presents an example of the influence of k_r on the sloughing pattern. The probability to remove a fraction s of biofim fraction which is ranging from 0 to 1, is tested through the generation of 10000 values of n_r , which follow the uniform distribution. The probabilities of occurrence of s are approximately equal as expected in case k_r=1 **(Figure 6.2 a).** Values of k_r greater than one shift the distribution toward low values of s : in that case, when sloughing occurs, it is more likely to remove small portion of biofilm than large patches **(Figure 6.2 b** with kr=10**).** The opposite trend is observed in the case of small value of kr =0.1 : in that case, the probability density function is shifted toward high values of s and it is more likely to remove large portion of biofilm when sloughing occurs (**Figure 6.2 c**)

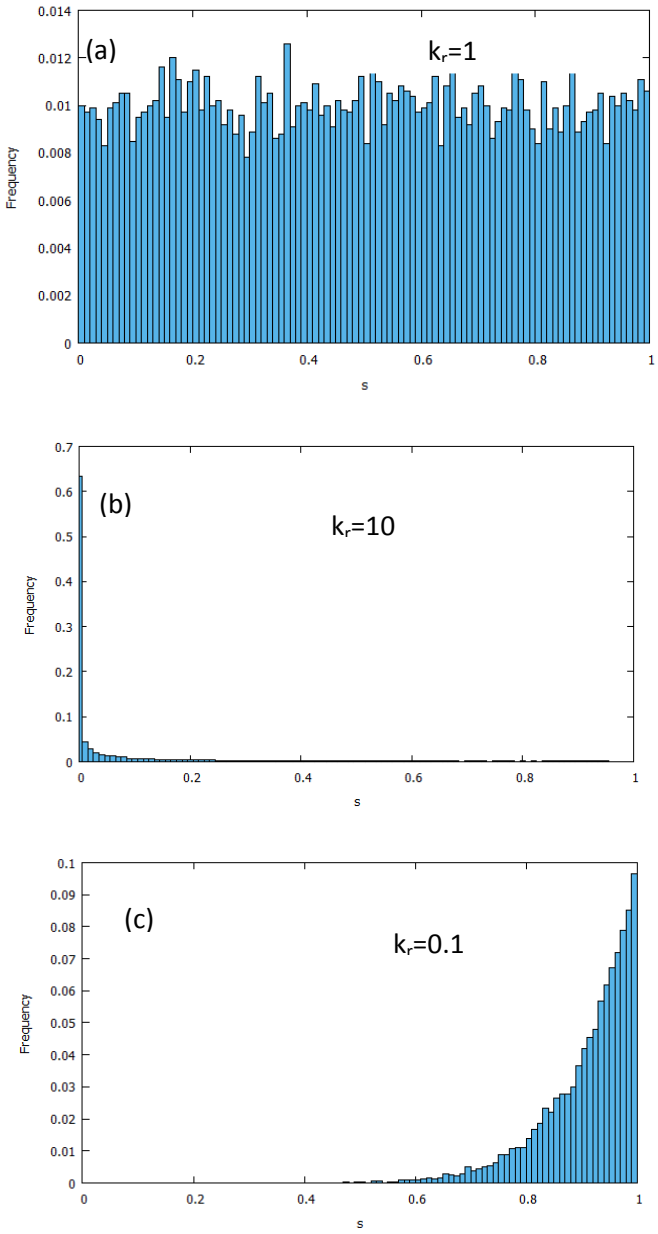

Figure 6.2: Example of the influence of k_r on the frequency of biofilm portion removed in sloughing process. The simulation was performed in the generation of 10000 uniformly distributed random numbers.

In Bohn's approach, the value of k_r permits to characterize various sloughing processes for which small portions of biofilm **(Figure 6.2 b)** or large portion of biofilm **(Figure 6.2 c)** is more likely to detach. To study other sloughing patterns, other distribution shape could be accounted. In the scope of this thesis, we attempt to apply normal distribution to quantity biofilm sloughing.

$$s = N(\mu_N, \sigma^2) \qquad (6.21)$$

The example of other forms of sloughing pattern generated by normal distribution is shown **Figure 6.3.** A removal of a certain portion of biofilm is more likely in sloughing process, which corresponds to the mean values μ_N of normal distribution. It is noted that sloughing pattern of $\mu_N = 0$ and very small value of σ^2 is quite correspondent to that of Bohn's approach with high value of k_r **(Figure 6.3b).** Sloughing pattern $\mu_N = 1$ and very small value of σ^2 is quite correspondent to that of Bohn's approach with small value of k_r **(Figure 6.3c).** In case of very high value of σ^2, the normal distribution can approximate to uniform distribution.

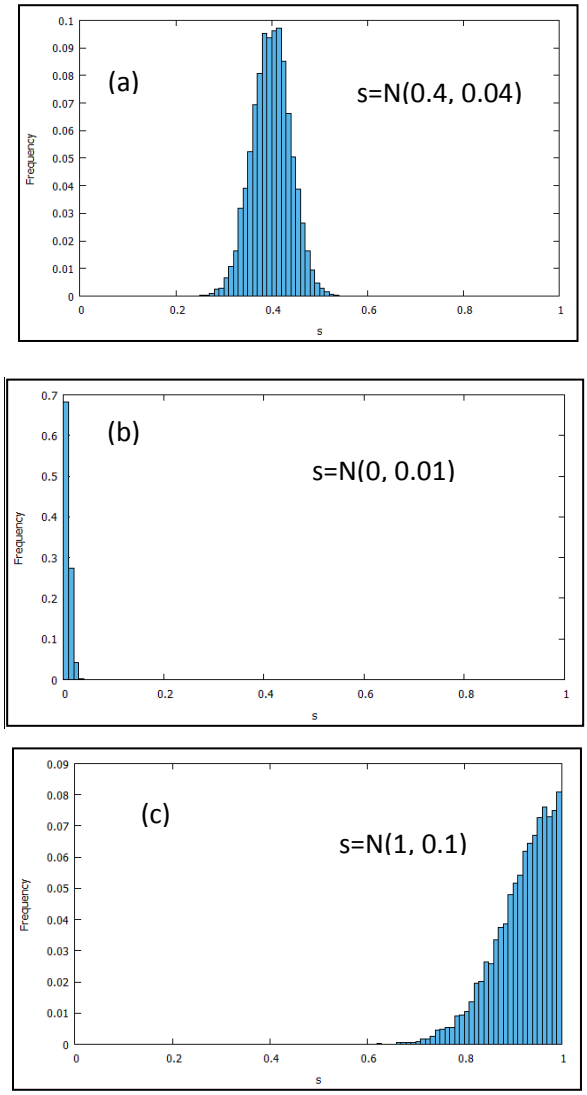

Figure 6. 3 Example of other forms of sloughing pattern generated by normal distribution. The simulation was performed in the generation of 10000 normal distributed random numbers.

6.3 Model implementation

The one dimension numerical simulation is implemented in the open source software OpenFoam by developing a new solver based on *"transportScalarFoam"* (see more detail in chapter 5). The domain of the simulation was presented in **Figure 6.4** and the numerical schemes was given in **Table 6.3**

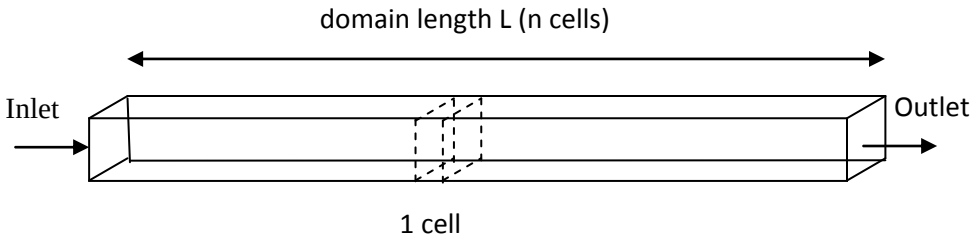

Figure 6.4: Schematic present of the domain of the numerical simulation

At each time step, the pressure drop was computed at the center of each cell and a harmonic interpolation scheme was used to determine the fluid pressure at inlet face. Concerning the boundary condition, the atmospherical pressure condition was applied at the outlet. At inlet, a time dependent pressure gradient condition was used, since the inlet pressure gradient depends on the instantaneous permeability and the approaching velocity as indicated by Eq (6.5)

Table 6.3: Numerical scheme used in the modeling

	Numerical Scheme	**Specified in OpenFoam**
Time term	Second order implicit	Backward
Gradient term	Center difference	Gauss linear
Convection term	Second order upwind	Gauss linear upwind
Diffusion term	Second order	Gauss linear corrected
Interpolation term	Center difference	Harmonic

One of the difficulties of the modeling implementation is to couple the different processes involved in bioclogging at different time scale. Sloughing modeled as a discrete process usually occurs at time scale largely higher than that of continuous

processes (Bohn et al., 2007). A small time step implies high frequency of the event and that results in more drastic loss of biofilm.

The algorithm of the new solver can be seen in **Figure 6.5**. Two time steps are used in the numerical simulation. In Eq (6.19), $s\emptyset_b(t)$is a "discrete" stochastic term that is added to the classical continuous mass balance equation. As sloughing event are random events , this term should be activated randomly over time. The continuous processes occur at every time step δt, while the discrete process, namely biofilm sloughing in this case, is taken into account only at large time step $\Delta t \gg \delta t$. Δt could be taken as a random variable, but following Bohn et al. (2007), it was taken constant in the model. Indeed, the shape of the s distribution account also partly for the time randomness of the sloughing events through the probability of very weak events (values of s=0: no sloughing; or value of s near 0:very small fraction of biofilm is removed). Proceeding that way, the numerical work can reduce the number of parameters

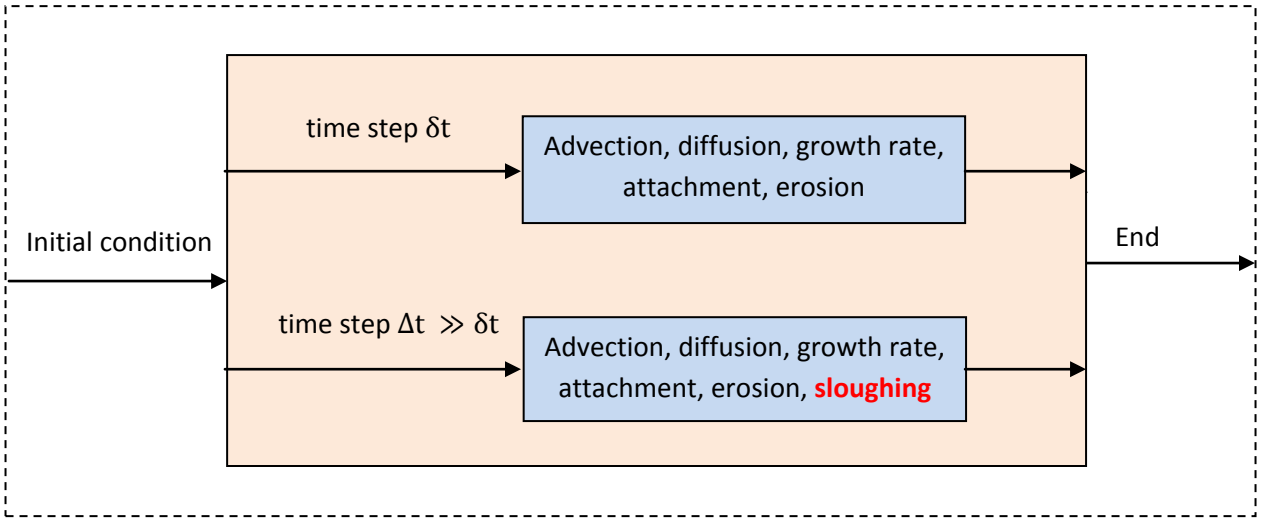

Figure 6. 5: Algorithm of the solver the coupling non-linear differential equation at different time scales.

6.4 Numerical work:

Numerical simulations have been performed to study the capacity of the stochastic process to model biofilm sloughing. The numerical parameters were referenced from experimental study of Karrabi et al.(2011). The interaction of hydrodynamic and biofilm was experimentally investigated at pilot scale bioreactor (0.6m in height and 0.15m in

diameter). The standard protocols for the granular media, substrate, culture medium and bacteria strain preparations as well as the column feeding can be found in Karrabi et al. (2011). In brief, biofilm was grown in a packed column filled with Biolite grain of 4mm in diameter in 14 days until the steady-state reached, and then during 45 days to monitor the long-term fluctuation of pressure loss. The experiments used phenol as the carbon source for *P.putida*. The operating conditions for the experiment were given in **Table 6.4**. Pressure and oxygen concentration along the column height were automatically recorded. The pressure drop between sampling ports was monitored online with an automat system Field Point^{TM} associated with Labview^{TM} software..

Table 6.4: Column characteristics and the operating conditions for experiment by Karrabi et al. (2011)

Parameter	**Value**	**Unit**
Column height H	0.6	M
Column diameter D	0.15	M
Clean bed porosity $\emptyset_0$	0.35	-
Biolite size dg	0.004	M
Temperature T	25	^oC
Operation time	45	Day
Flow rate Q	20	L/h
Influent phenol concentration $C_{s,0}$	0.2	kg/m^3
Influent oxygen concentration, $C_{o,0}$	0.006	kg/m^3

All the geometry parameters and operational conditions are taken from Karrabi et al. (2011), which is given in **Table 6.4**. The physical properties of fluid: fluid viscosity and fluid density, are considered constant since the variations of temperature is small. The dispersion coefficients and the growth kinetic of *Pseudomonas aeruginosa* was referenced from documented data **(Table 6.5).**

For the fitted parameters, Yo was set to 6, which is close to the magnitude of Borden and Bedient (1986) at the value of 3. β_b defining the interaction of fluid flow and biofilm

material were simply given at 1 The parameters $\phi_{B,c}$, c_{det1}, c_{det2}, η_{att} are obtained by curve fitting to obtain a good agreement with experimental data

Table 6.5: Parameters used for simulation

Parameter	Value	Unit	Reference
Water viscosity μ	1.139×10^{-3}	Pa.s	-
Water density ρ	1000	$kg.m^{-3}$	-
Maximum specific growth rate μ_{max}	5×10^{-5}	s^{-1}	*Kumar et al. (2005)*
Monod half-velocity coefficient for phenol K_s	0.011	$kg.m^{-3}$	*Kumar et al. (2005)*
Monod half-velocity coefficient for oxygen K_o	0.008	$kg.m^{-3}$	*Borden and Bedient (1986)*
Phenol Yield coefficient Y_s	0.84	$kg.kg^{-1}$	*Kotturi et al. (1991)*
Oxygen Yield coefficient Y_o	6	$kg.kg^{-1}$	Fitted
Endogenous decay rate μ_d	4×10^{-6}	s^{-1}	*Martin et al. (2008)*
Biofilm density ρ_b	25	$kg.m^{-3}$	Experimented *Karrabi et al. (2011)*
Effective diffusion coefficient D_{eff}^{s}	6×10^{-10}	$m^2.s^{-1}$	*Wanner et al. (1995)*
Effective diffusion coefficient D_{eff}^{o}	2×10^{-9}	$m^2.s^{-1}$	
Effective diffusion coefficient D_{eff}^{m}	1×10^{-9}	$m^2.s^{-1}$	
Attachment probability η_{att}	10^{-4}	-	Fitted
Erosion coefficient $c_{e,1}$	3×10^{-8}	s^{-1}	Fitted
Erosion coefficient $c_{e,2}$	0.31	-	Fitted
Sloughing coefficient kr	165	-	Fitted
Initial permeability K_0	1.2×10^{-8}	m^2	calculated
Minimum permeability K_{min}	1.2×10^{-12}	m^2	K_0/K_{min}=2500-10000 *Vandervivere (1995)*
Biomass distribution coefficient $\emptyset_{B,c}$	0.035	-	Fitted
Bulk factor β_B	1	-	Fitted
k_{r1}	85	-	Fitted

Time step for the simulation

Two time steps, δt for continuous processes and Δt for discrete slougging events were required for the simulation. δt was set to 5s. For the biofilm sloughing, it is noted that the frequency for this event varies with definition of the size of biofilm particles sloughed from biofilm (**Table 6.6).** Higher frequency were observed at the smaller size of sloughed particles.

Table 6.6: Various frequency of sloughing events correspondent with the definition of biofilm sloughing

Reference	Study	Sloughing definition	Frequency of Sloughing events
Hun et al.,2004	Modeling	Loss of 50% of biofilm biomass	$1h^{-1}$
Telgmann et al.,2004	Experiment	Large settled particles	At least 1 event/day
Xavier et al.,2005	Modeling	Detached particles larger than 50µm	day scale
Garny et al., 2009	Experiment	Detached particles larger than 25µm	79 events/day
Walter et al.,2013	Experiment	Detached particles larger than 2.5 µm	3-800 h^{-1}
Horn and Lackner, 2014	Review	mm scale	day scale

In this simulation, the sloughed particle from biofilm was defined from random process. The size of sloughed particles can be small and likely to occur at high frequency. Therefore, the time step for sloughing event was taken at 1h, the influence of time step of sloughing events was also presented in this simulation.

The modeling domain is discretized with 30 uniform cells for a total length of 0.6m. For the initial conditions At t=0, biofilm distribution is uniform inside porous media with $\phi_b = 0.001$.Mobile biomass is assumed zero at starting time. The boundary conditions required for numerical simulation are summarized in **Table 6.7**

Table 6.7: Boundary conditions required for numerical simulation

Parameters	**Inlet**	**Outlet**
C_s	Dirichlet condition with a constant: Cs(0,t)=0.2 kgm^{-3}	Neumann condition: $n.(D_s \nabla C_s) = 0$
C_o	Dirichlet condition with a constant: Co(0,t)=0.006 kgm^{-3}	Neumann condition: $n.(D_o \nabla C_o) = 0$
C_m	Dirichlet condition with a constant: Cm(0,t)=0	Neumann condition: $n.(D_m \nabla C_m) = 0$
ϕ_b	Neumann condition: $n.(\nabla \phi_b) = 0$	Neumann condition: $n.(\nabla \phi_b) = 0$

6.5 Result and discussion

6.5.1 The sensitive analysis of sloughing interval Δt

In the simulation, biofilm sloughing was presented in term of pressure drop oscillation and biofilm volume fraction in biofilter. The results of the numerical simulation of pressure drop and biofilm fraction, substrate concentration were given in **Figure 6.6** and **Figure 6.7**. Time step for sloughing Δt was set to 3600s and k_r was set to 500. The high value of k_r indicates that small biofilm fraction is often detached in sloughing process. Small oscillation was observed in pressure drop profile. It is noted that the numerical results should be averaged over several simulations (each simulation corresponding to one realization). In this study, for each numerical analysis, three simulation was implemented to obtain the average values, which is just an indication. However, the number of simulation should be higher for the performance of a real study on the average value.

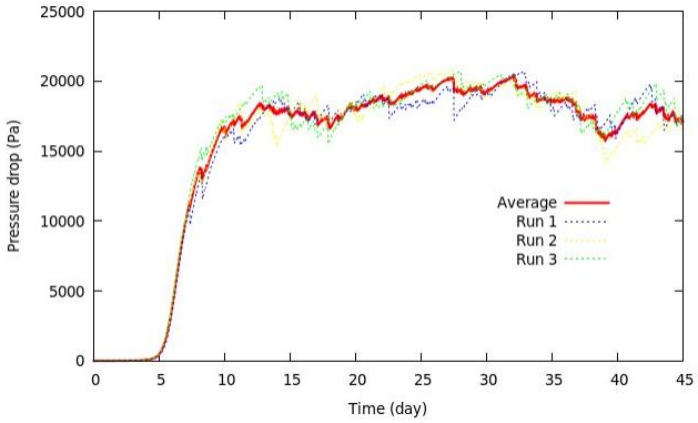

Figure 6.6: The numerical result of pressure drop oscillation . The dash lines present the simulation of N=5 runs in random generation. The red line presents the average of N=3 runs. $\Delta t = 3600s$, k_r=500 μ_{max}=5 10^{-5} s^{-1} ($1/\mu_{max}$=20000s)

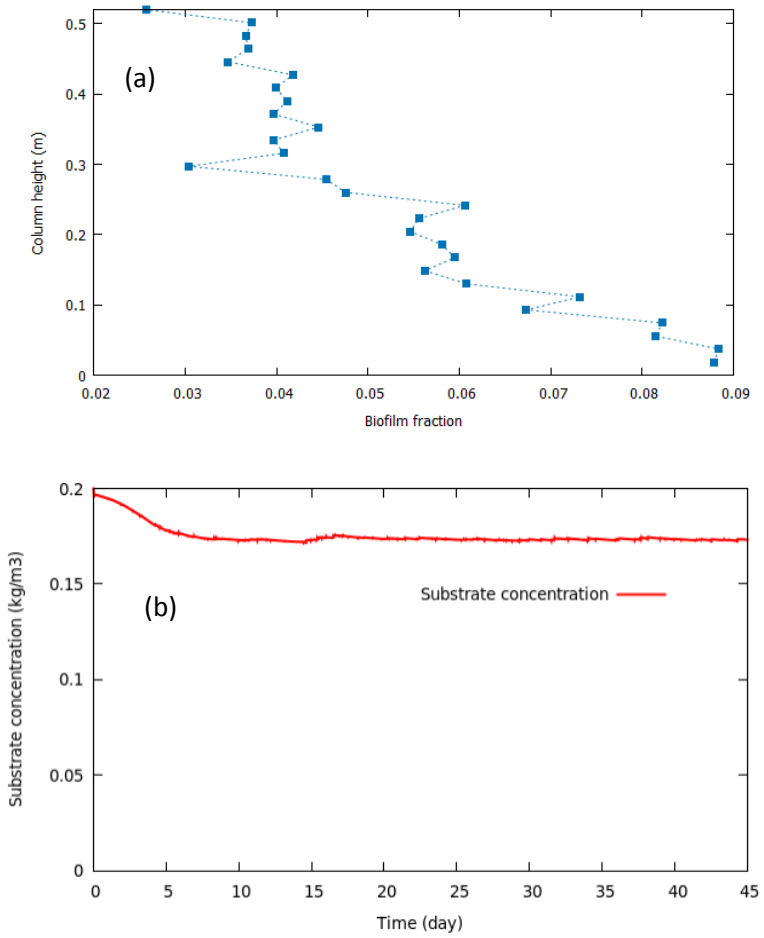

Figure 6. 7 The numerical result of (a) biofilm fraction and (b) outlet substrate concentration in the biofilter at 45 days. The values present the average of N=5 runs. $\Delta t = 3600s$, k_r=500 μ_{max}=5 10^{-5} s^{-1} ($1/\mu_{max}$=20000s)

The model produced the oscillation in pressure drop and biofilm volume fraction in the biofilter. This is an example of "small sloughing" where sloughing process is more likely to detach small biofilm fraction. It is distinguished from "high sloughing" for which large biofilm fraction is more likely to be removed. The extreme case of high sloughing is such that all of biofilm is swept out of grain surface. The outlet substrate concentration **(Figure 6.7b)** appreared not to be impacted by slouhing process in this simulation. This observation was reported by previous studies (Stewart, 1993; Horn and Lacker, 2014) that the substrate removal was not influenced by small sloughing.

In the simulation of biofilm sloughing, two parameters were involved: sloughing interval Δt and and the sloughing magnitude distribution shape (controlled by k_r) . The sloughing interval is considered many time higher than simulation time step (Bohn et al., 2007).

Figure 6.8 and **Figure 6.9** showed the influence of the sloughing interval. Less oscillation was observed when sloughing interval is increased to 18000s and more oscillation occurred with the decrease of sloughing interval to 600s (the sloughing magnitude was small keeping k_r=500 for both two cases)

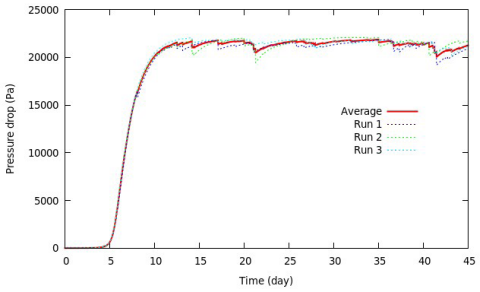

Figure 6.8:The numerical result of pressure drop oscillation. The dash lines present the simulation of N=3 runs in random generation. The red line presents the average of N=3 runs. **$\Delta t = 18000s$** , k_r=500. μ_{max}=5 10^{-5} s^{-1} ($1/\mu_{max}$=20000s)

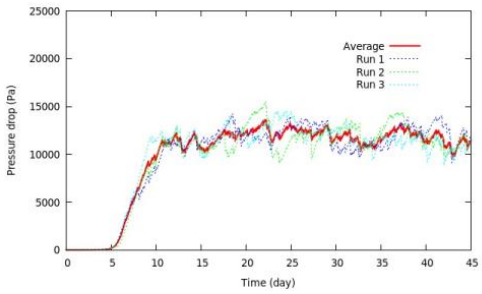

Figure 6.9: The numerical result of pressure drop oscillation. The dash lines present the simulation of N=3 runs in random generation. The red line presents the average of N=3 runs. **$\Delta t = 600s$** , k_r=500 μ_{max}=5 10^{-5} s^{-1} ($1/\mu_{max}$=20000s)

6.5.2 The sensitive analysis of k_r

An example of results is given in figure 6.10a and 6.10b. **Figure 6.10b** correspond to the case already presented in **Figure 6.6** (Δt =3600, kr=500, μmax=5x10^{-5} s^{-1}). **Figure 6.10a** correspond to a simulation run with a larger distribution for s (k_r=80). Higher oscillation are observed on (Figure **6.10a**) as expected as the probability to slough higher biofilm fraction as increased (even if this probability remains low). The oscillation accounted more than 50% of maximum pressure drop (day 38- 40) However, the maximum pressure drop declined due the high loss of biofilm.

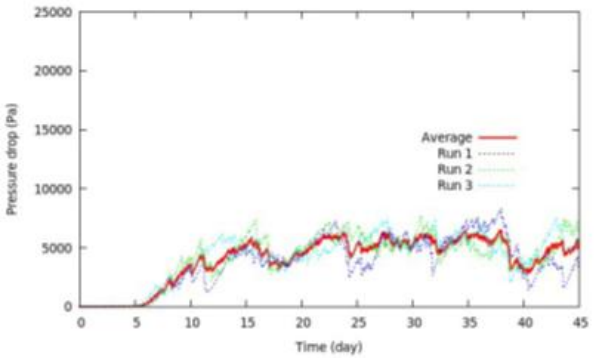

Figure 6.10a: The numerical result of pressure drop oscillation. The dash lines present the simulation of N=3 runs in random generation. The red line presents the average of N=3 runs. $\mathbf{\Delta t = 3600s}$, k_r=80. $\mu max=5.10^{-5}$ s^{-1} ($1/\mu max$=20000 s)

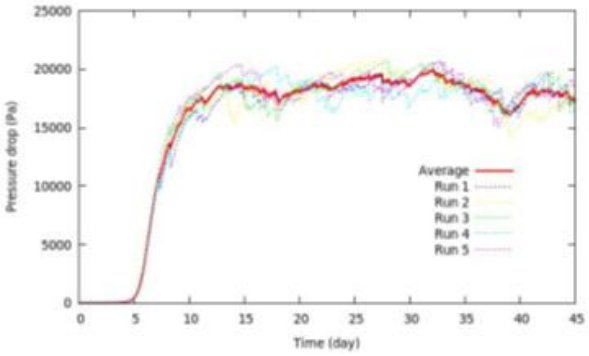

Figure 6.10b: The numerical result of pressure drop oscillation. The dash lines present the simulation of N=3 runs in random generation. The red line presents the average of N=3 runs. $\mathbf{\Delta t = 3600s}$, k_r=500 (same parameters as Figure 6.6)

It is noted that there are other parameters involved in oscillation patterns. The oscillation is the result of mass balance applied to biofilm: biomass attachment, biofilm growth, decay, erosion, sloughing.... In particular as sloughing counterbalance the continuous growing of the biofilm, the relative magnitude of the characteristic time scales accounting for these to processes (Δt and $1/\mu_{max}$) should have an important effect on the system global behavior (as it can be already seen on **Figure 6.6, 6.8 and 6.9** whent Δt is changed keeping μ_{max} constant) **Figure 6.11** presented another example of the influence of μ_{max} on the oscillation pattern keeping a small value of k_r (whose effect is to enhance the probability to removes biofilm portion of various size)

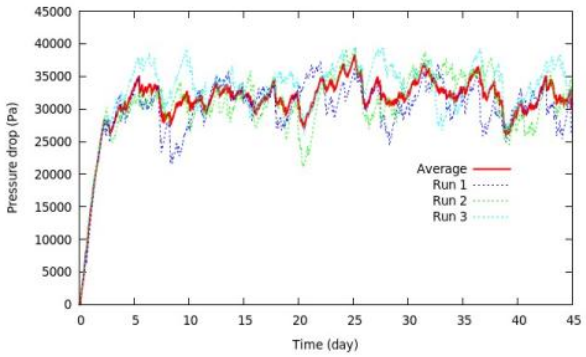

Figure 6. 11a: The numerical result of pressure drop oscillation. The dash lines present the simulation of N=3 runs in random generation. The red line presents the average of N=3 runs,$\Delta t = 3600s$, k_r=80, μmax=$10^{-3}s^{-1}$

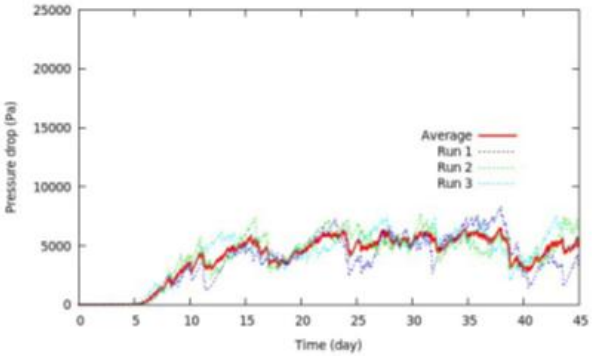

Figure 6.11b:The numerical result of pressure drop oscillation. The dash lines present the simulation of N=3 runs in random generation. The red line presents the average of N=3 runs. $\Delta t = 3600s$, k_r=80. μmax=5x10^{-5} s

In the case of **figure 6.11a**, the maximum characteristic time of growth $1/\mu_{max}$ =1000 (s), which is shorter than the sloughing interval (3600s). The sloughing process occurs more slowly than biofilm growth, which can result in more biomass build-up or high pressure drop of biofilter. In the case that sloughing process takes place faster than biomass growth, more biomass was removed and lead to the decline of maximum pressure drop (**Figure 6.11b**)

It is noted that all the simulations above are implemented with k_r >1.A specific case could occur when the value of k_r is below 1. In that case the probability distribution is shifted toward the high values of s: this case can correspond for instance to situation where sloughing event are less frequent (Δt greater) but with a higher probability to get an almost complete removal of the biofilm. An example of results is given in **Figure 6.12.,** which corresponds to the case Δt = 864000s (10days), k_r=0.1, μmax=510^{-5} s^{-1}. In this case, the effect of sloughing process nearly sweeps out all biofilm in biofilter. The pressure drop of the biofilter suddenly drops down to nearly zero within the occurence of sloughing process. This example is similar to slouhing experiment by Stewart and Fogler, (2001) in this pattern of pressure oscillation. The time interval for sloughing process should be large enough for biofilter to recover its global behavior. The time interval of

sloughing events in Stewart and Fogler, (2001) was about 5 days and in this simulation, the time interval was set at 10 days.

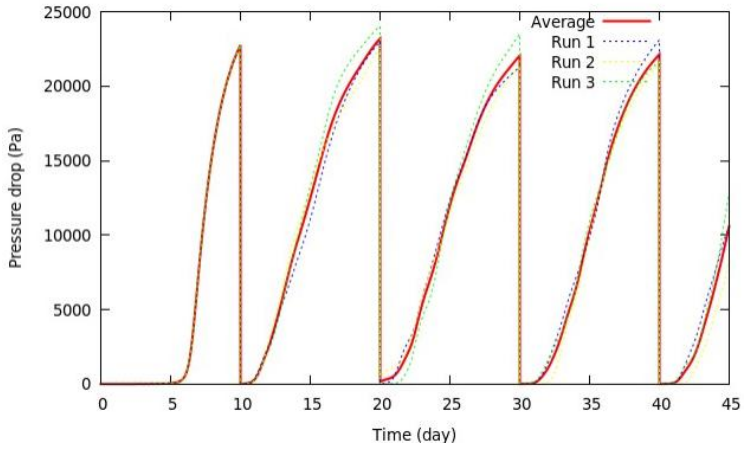

Figure 6. 12: The numerical result of pressure drop oscillation. The dash lines present the simulation of N=3 runs in random generation. The red line presents the average of N=3 runs. $\mathbf{\Delta t = 864000s}$ **(10 days)** , k_r=0.1. μ_{max}= 5.10^{-5} s^{-1} ($1/\mu_{max}$=20000s)

6.5.3 The influence of random distribution

The basis of the model consists in the determination of the biofilm fraction s detached in sloughing process. All the simulation above were implemented with the application of the uniform distribution and the coefficient k_r to characterize s. The shape of the s distribution may also affect the global behavior of the system. In the scope of the thesis, as no experimental data on this subject was available, we have tested the results sensibility to the distribution of s through the application of a normal distribution to model biofilm sloughing. A normal distribution was selected to favor the detachment of small biofilm fraction, s= N(0, 0.01) (**Figure 6.3b**), which roughly has the same probability for the smallest sloughing event as for the distribution builded with kr=10 (**Figure 6.2b**). However, for the normal distribution the probabilities to get larger values of s are lower. Therefore, the application of normal distribution only produce a very small oscillation and a higher total pressure drop **(Figure 6.13a),** while the simulation with kr=10 results in a larger oscillation and a lower total pressure drop (**Figure 6.13b**).

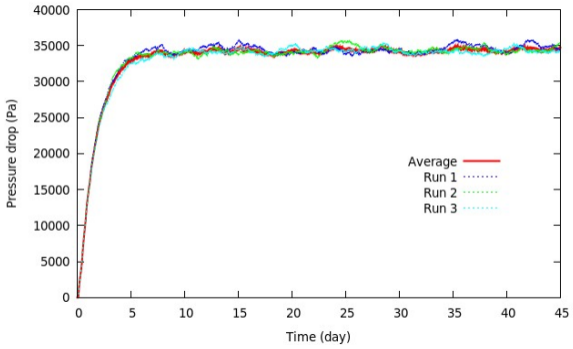

Figure 6.13a: The numerical result of pressure drop oscillation. The dash lines present the simulation of N=3 runs in random generation. The red line presents the average of N=3 runs, $\Delta t = 3600s$, s=N(0,0.01), μ_{max}= 10^{-3} s^{-1} ($1/\mu_{max}$=1000s)

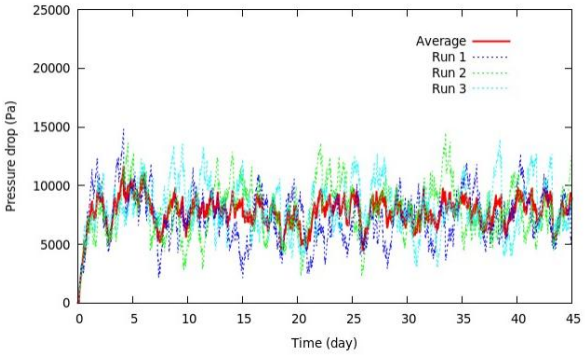

Figure 6.13b: The numerical result of pressure drop oscillation. The dash lines present the simulation of N=3 runs in random generation. The red line presents the average of N=3 runs,$\Delta t = 3600s$, kr=10, μ_{max}= 10^{-3} s^{-1} ($1/\mu_{max}$=1000s)

6.5.4 A proposed function of k_r

In this study, the application of an uniform distribution and shape coefficient k_r seemed to be able, at least qualitatively, to reproduce some features related to biofilm sloughing. The biofilm fraction removed in sloughing process in this approach depends on one parameter: k_r, which is set to be constant for the simulation. In the attempt to interpret the physical meaning of k_r, this study aims to relate k_r to the biofilm growth rate ($\mu_b = \eta_{lmt} r_x$). Indeed, depending on the biofilm "age" within the column, its structure and so its internal cohesion will make it more or less sensitive to sloughing events. In this work, as a first attempt, we have assumed that in the case where the nutrient availability was reduced, the biofilm was less cohesive and that it would led to a greater sloughing probability. This feature occurs for the deeper layer of thick biofilm (at the bottom of the column for instance) or when the nutrients are almost all consumed (especially at the top of the column). Making then k_r dependant on the local growth rate may be a simple way to take into account the biofilm resistance to the sloughing event without relying on a detailed description of the biofilm.

We have tested a simple arbitrary function to represent this feature:

$$\mu_b = \mu_{b,max} \qquad : k_r = k_{r,max}$$

$$\mu_b = \mu_{b,min} = 0 \qquad : k_r = k_{r,min} \qquad (k_{r,max} >> k_{r,min})$$

so that less biofilm fraction is detached from sloughing event in the case of high biofilm growth rate (higher biofilm resistance) compared to small biofilm growth rate (lower biofilm resistance). The extreme case occurs when there is no electron acceptor or electron donor ($\mu_b = 0$) which induces a large removal of biofilm fraction (that corresponds to $k_r = k_{r,min}$); When $k_{r,min}$=0, all the biofilm is detached by sloughing process.

Assuming a linear relationship of k_r and biofilm growth rate, one can obtain for instance the simple expression:

$$k_r = \frac{k_{r,max} - k_{r,min}}{\mu_{max}} \mu_b + k_{r,min} \qquad (6.22)$$

Figure 6.14 presents example of numerical simulation with the application Eq (6.22) for different parameters ($k_{r,max}$, $k_{r,min}$, substrate concentration). The results showed that the transient behavior of the system is greatly affected by sloughing process and that model can capture the effect, for instance, of the function of kr and inlet organic loading. In the example above, k_r is simply proposed to be linearly to biofilm growth rate and in range of $k_{r,max}$ and $k_{r,min}$. The increase or decrease of $k_{r,max}$, $k_{r,min}$ influence the pressure profile. Compared to **Figure 6.14a** (which is the reference case), the increasing $k_{r,max}$ resulted in less oscillation (**Figure 6.14c**) and lowering $k_{r,min}$ resulted in more oscillation in pressure profile (**Figure 6.14b**). In the case of reducing inlet substrate concentration (**Figure 6.14d**), the pressure profile is altered as expected : the magnitude of the pressure loss is lower as for low substrate loading, the growth rate is decreased. Eq 6.22 lead to lower value of k_r. That means that the probability distribution for s is wider, leading to more frequent sloughing event. However, it does not seem, for this set of parameters, to affect the oscillation amplitude. It can be due to the fact that for this case, that at the steady state, compare to the case on figure **6.14c**, the average growth rate is the same at the

steady state in both case (figure **6.14c**, high loading rate but high biofilm fraction (corresponding to thick biofilm. Figure **6.14d**, biofilm volumic fraction lower but inlet concentration lower too). The observations can also be explained by the shape of the probality distribution for s which makes the results not very sensitive to moderate variation on the growth rate.

It is difficult to go further on that point without the support of experimental data given the number of freedom degree in the choice of the probability distribution for s, the associated parameters to describe this probability distribution and their relation with the external conditions (flow, substrate concentration, biofilm state…..).

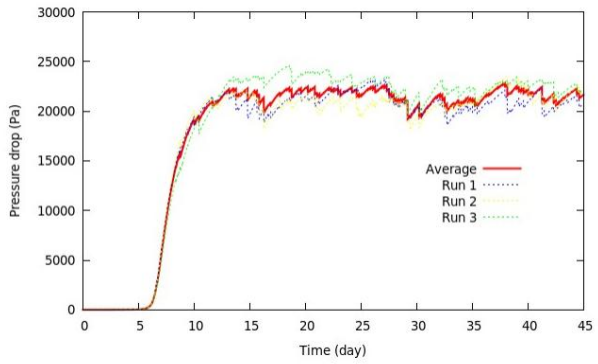

Figure 6.14a: $k_{r\,max}$=80, $k_{r\,min}$= 80, µmax=5.10^{-5} s^{-1}, Δt=18000s, Cs=0.2 kg/m^3

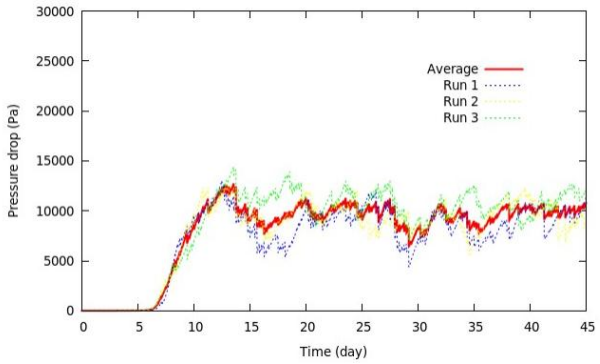

Figure 6.14 b: $k_{r\,max}$=80, $k_{r\,min}$= 1, µmax=5.10^{-5} s^{-1}, Δt=18000s, Cs=0.2 kg/m^3

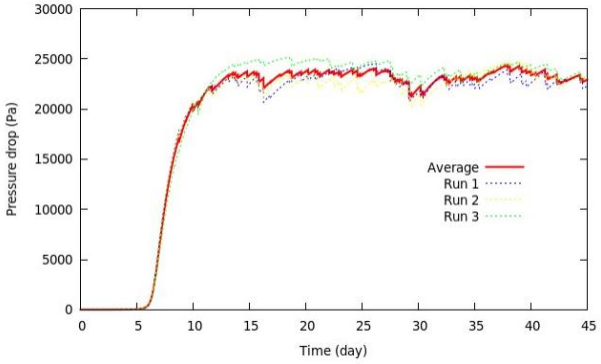

Figure 6.14c: $k_{r\,max}$=500, $k_{r\,min}$= 80,µmax=5.10^{-5} s^{-1}, Δt=18000s, Cs=0.2 kg/m^3

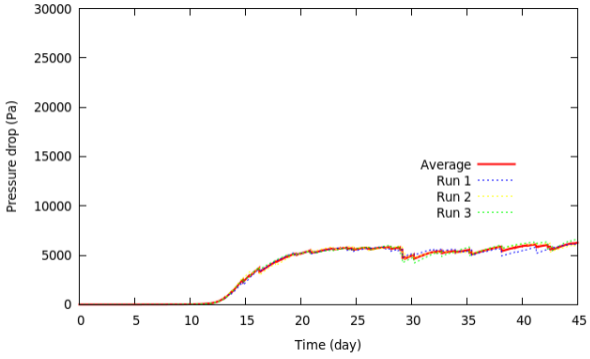

Figure 6.14d: $k_{r\,max}$=500, $k_{r\,min}$= 80,µmax=5.10^{-5} s^{-1}, Δt=18000s, Cs=0.02 kg/m^3

Finally, we present the average curves corresponding to one case (kr=80, references operating conditions table **6.5**). Results are presented in **Figure 6.15**. The aim is to compare the average behavior of the system including the sloughing term with the results obtained with the original model (chapter 5). Let us note, that in reality, it is not likely to get enough experimental realisation on a real process to be able to compare the average numerical and experimental behavior of the system during the transient phase. The purpose of these last simulation is rather to show the effect of the sloughing term on the different parameters accounting for the system behavior depending on if it is included or not in the model. In the example below, the simulation was performed 40 times which ensure convergence. The case with and without sloughing were simulated with the same parameters. For the case with sloughing, which a case of "small sloughing", the mean curves appeared more smooth than the curve corresponding to a single realisation (although a slight modulation on the pressure curve is still observed) s. As expected, without sloughing, less biomass was lost, driving higher pressure drop **(Figure 6.15 a**), as well as more substrate and oxygen consumption (**Figure 6.15 b and 6.15c**), which affects the system efficiency. However, in the condition simulated here (high inlet substrate concentration), the difference remains rather small and sloughing affects mainly the pressure drop. The effect of the sloughing incorporation on the system efficiency should however be tested on a wider range of inlet conditions provided data are available.

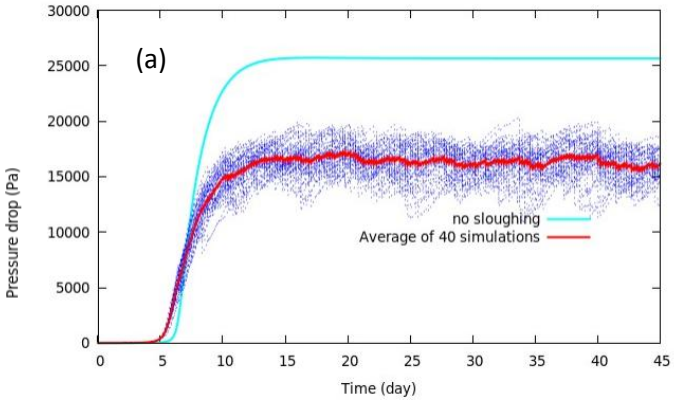

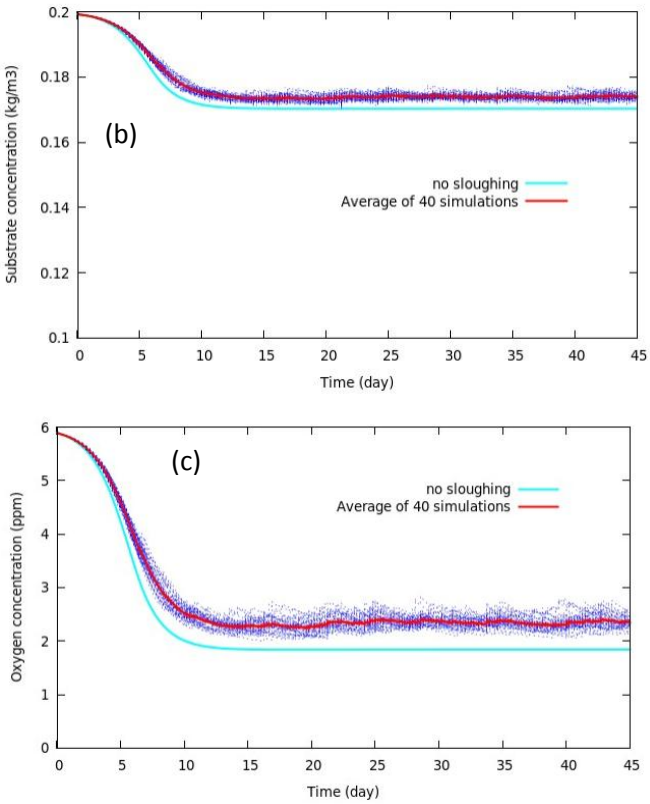

Figure 6. 15. The mean value of stochatic process (a) pressure loss, (b) substrate concentration and (c) oxygen concentration . The sloughing parameters in the simulation were ,$\Delta \mathbf{t} = \mathbf{18000s}$, k_r=80, μ_{max}= 5x10^{-5} s^{-1}

6.6 Conclusion of chapter 6

In this chapter, we made a first qualitative attempt to introduce the sloughing process in a 1D dimensional model. To our knowledge there exist no studies on that subject applied to macroscale systems (such as biofim in porous media or biofilters) Sloughing was treated as a stochastic process and can be quantified by random generator. The discrete sloughing events are incorporated with other continuous processes to determine the biomass transfer from biofilm to the liquid phase. In the numerical work, the time step of sloughing event was largely higher than the time step of other continuous processes.

The qualitative simulation results and the sensitivity analysis showed that, the stochastic process can be a promising method to model some feature of biofilm sloughing, Following the concept that the biofilm fraction s detached in sloughing process is calculated using a random variable taken in an uniform distribution and a coefficient k_r,

the model is capable to reproduce various oscillation patterns observed on the pressure drop. The sensitive analysis showed that the sloughing process is influenced by many parameters: Δt, k_r and other kinetic parameters, i.e: μ_{max}. Furthermore these parameter are not independent and are related to the biofilm structure evolution (in term of resistance)

Depending on the time scale chosen for the sloughing, that means that the probability distribution for s (and maybe Δt) must account for the local biofilm properties and history

A first attempt was made by proposing a simple model which links k_r to the actual biofilm growth rate, keeping Δt constant. Making k_r dependant on the growth rate is a simple way, although unperfect, to take into account the biofilm resistance. Indeed, the local growth rate decrease drastically when either the biofilm is thick and the porous media almost clogged (see Eq 6.12) or when the system is depleted with nutrient. This allow to "simulate" various situation such as a thick biofilm which becomes less resistant in the lower layer or a biofilm which is not resistance because of a low bacteria activity (nutrients completed consumed or low loading rate). In particular, the model seems to take into account the effect of the substrate loading. The comparison of averaged simulations with the results of the original model (chapter 5) seems to show that the sloughing processes affects the system efficiency.

However, the results were still at the preliminary stage and there are lots of works to implement.

- The sloughing interval Δt is set to be constant in the simulation. However Δt is maybe itself a random variable.

- In the simulation, the sloughing events have been treated as independent between two different locations.

- A simple function $kr=f(\mu_b)$ was proposed in this study. However, as the parameter kr, Δt μ_b... are not independent to each others, experimental investigations are required to find the exact formulation of the function $kr=f(\mu_b, \Delta t, \ldots)$.

Chapter 7

Conclusions and Perspectives

Summary of the work

The initial motivation for this work was the development of a macroscopic model able to describe the transport and degradation of a solute in a porous medium colonized by a biofilm. This problem is encountered in many industrial applications: the motivation of this work concern the effluents depollution using biofiltration, although the results can be partly applied to other applications involving porous media and biofilm (such as soil bioremediation or aquifer protection using bio-barrier).

The choice of a model written directly at the macroscopic scale comes from the fact that at the biofilm scale the different biological, chemical and mechanical couplings governing the evolution of the biofilm are far from being understood. Modeling this processes accurately at the fine scale can lead to models that are not necessarily more relevant in an operational point of view given the number of unknown parameters (kinetic parameters, descriptive parameters for biofilm properties…) as the model becomes complex. It is more complex in the biofilm application because the biofilm is a "living material" whose characteristic properties evolve temporally and spatially depending on the physical and chemical it undergoes.

A macroscopic model, although much less complex in its formulation, is not necessarily simplistic if the main phenomena governing the functioning of the system are sufficiently well taken into account. These phenomena are either mechanical processes directly involved in the coupling between macroscopic flow and biofilm development

(permeability, bacterial adhesion phenomena or biofilm detachment) or biochemical processes aiming to report at the macroscale the main kinetics of biofilm development.

As it has been seen in the bibliography, the kinetic aspect is particularly difficult given the very diverse interactions occurring at small scales (production of various compounds such as EPS but also chemical effectors allowing intracellular communication as well as inhibition or triggering of certain biological processes, leading to the modification of biofilm properties). The macroscopic translation of these processes is far from being resolved.

In this thesis we have been interested in the question of whether accurately taking into account the main mechanical processes governing the overall distribution of the biofilm and thus the flows and the transport of the different nutrients was sufficient, the "biological" part being governed by simple, simplified, kinetic equations. Given this issue, our work dealt mainly with the description of prevailing processes such as permeability reduction, initial biomass attachment as well as biofilm detachment (especially “sloughing”) in order to incorporate them in a numerical simulation at large-scale.

a) Permeability reduction:

The first part of this study focused on the effect of biomass accumulation in pore spaces that alters the porous media geometry and reduces its permeability.

As the microstructure at pore scale as a direct effect on the permeability, an issue was to develop a representative permeability model, based on simple macroscale variables and that emulates the effect of the microstructure on the permeability reduction.

In the model, the permeability is a function of the geometry of porous media and biofilm characteristics. The geometry of porous media, which is represented by clean-bed porosity and grain diameter profoundly affect clean-bed permeability, while biofilm characteristics affect pattern and magnitude of bioclogging. In the case that micro-organisms tend to form aggregates that plug the pore space, bioplugging becomes the dominant process that governs permeability of porous media.

Following VandeVivere (1995) approach, the model involves then two mechanisms which account for bioclogging (i) pore radius reduction and (ii) micro-aggregates which plug the pore space. Our model differs from VandeVivere model for the first mechanism which includes some additional effects such as tortuosity and porous media geometry. The overall permeability results from the averaged contribution of these two processes through a function $F(\Phi_B, \Phi_c)$ which account for the fraction of plugging pore for a given volume fraction Φ_B. The function F as well as parameter Φ_c account for the biofilm micro structuration. Compared with data gathered from X-Ray tomographic experiments, the model improves slightly the permeability reduction prediction compared to VandeVivere model for low to moderate biofilm fraction

b) Initial biomass attachment

Another objective of the thesis was to derive a relevant description of biomass attachment during the seeding stage, as this process determines initial biomass distribution inside the porous media. Bacterial cells are considered as soft colloids and CFT (Classical Filtration Theory) is applied to estimate the attachment efficiency. In the mechanistic approach, the calculation of attachment efficiency is based on the torque balance of hydrodynamic forces and DLVO forces. However, the attachment efficiency is sensitive to Young modulus, a parameter that can vary in a wide range which its value is highly dependent on bacterial strain, live cells/dead cells, experimental methods. The other approach-correlation equation to estimate attachment efficiency, is the objective of this study. We developed a new correlation equation, which attachment efficiency is dependent on physiochemical properties of bacterial cells, aqueous phase, geometry of porous media and hydrodynamic conditions. This study was performed in the frame of the DLVO theory : in the unfavorable condition, the depositions at both secondary minimum and primary maximum interaction energy play an important role in total attachment efficiency.

The equation introduces new dimensionless parameters presenting the influence of hydraulic forces with the account of grain size and porosity of porous media. The new correlation equation improved slightly predictions compared to existing correlations and

produced a relatively good agreement on a wide range of experimental data in various electrolyte conditions, flow velocities, and geometries of porous media.

c) Numerical simulation of the behavior of porous media at large-scale

An one-dimensional macroscopic model was developed for the numerical simulation of solute transport coupling with biofilm growth in porous media. In the model all the solute are considered to be dissolved (namely there is no dispersed phase as it is a case for the oxygen in an actual biofilter)

The model is based on the solution of a set of advection-diffusion-reaction equations. Our new permeability model is used in Darcy's equation to define momentum conservation. Biomass attachment follows CFT approach. Biofilm detachment is governed by both fluid shear and biofilm growth rate. The model is able to capture temporally and spatially the behavior of porous media represented by permeability reduction, solute concentration, biofilm thickness at steady-state. The results of this study proved that a simple macroscopic model, with the improvement of *ad-hoc* constitutive equation, is capable of reasonable prediction about solute transport coupling with biofilm growth in porous media at field-scale.

d) Accounting sloughing in biofilm detachment in numerical simulation the behavior of biofilter at pilot scale

Modeling as accurately as possible the detachment process was the last objective in this thesis : it participates strongly to the balance between the biomass growth and biomass loss and thus, to the overall pore occupation by the biomass. Biomass detachment combines processes including a continuous erosion of the biofilm surface, but also more or less frequent sudden release of biofilm “patches” of various sizes. In this thesis, we made a first qualitative attempt to introduce the sloughing process in a one-dimensional macroscopic model. To our knowledge, there is no study on that subject applied to macroscale systems and existing models treat biomass detachment as a continuous ‘erosion’ process.

The “sloughing” process results from the external stresses applied to the biofilm compared and their ability to overcome the biofilm internal cohesion. Although recent numerical research approach allowed to simulate various biofilm structures at the local scale by computing the shear stress due to the flow compared to the biofilm internal cohesion (the biofilm being treated as a material with known mechanical properties) these approaches are difficult to apply to the field scale : as seen in the literature survey, biofilm are living systems which adapt to the external conditions. Parameters which account for biofilm cohesion are then dependent with the biofilm age, biofilm physiological state and various biological processes not well understood. That is why we followed recent approaches which consider that it is more relevant to consider sloughing as random events. In our attempt to introduce sloughing in a simple macroscale model, this process was thus treated as a discrete stochastic process. The discrete sloughing events were incorporated with other continuous processes to determine the biomass transfer from biofilm to the liquid phase.

The detachment term is introduced in the model using the following concept: the biofilm fraction ‘s’ detached in sloughing process is calculated from a probability distribution generated using a random variable taken in a uniform distribution and a shape-factor coefficient k_r, the sloughing event occurring at a time step largely higher than the time step for other continuous processes. Because the sloughing process controls the amount of biomass in the system, the overall behavior of the system (at least in terms of total pressure loss) is dependent on the choice made for the shape coefficient k_r (which control the probability to loss a given fraction of biofilm), but also the characteristic time of the system represented by the sloughing time-step Δt and the growth kinetics μ_{max}.

The qualitative simulation results showed that, the stochastic process could be a promising method to model some feature of biofilm sloughing but we are far from of a realistic models, especially because of the lack of data on that subject at the field scale.

Results taken from experiments made by different authors at the biofilm scale in microflow cells report different time scale as well as amount of detached particles size distribution. Added to the evidence reported elsewhere from the literature survey on the

evolution of biofilm properties, the sloughing time scale is probably not unique and could be treated itself as a random variable, and the removed particles size distribution and sloughing time scale are probably not independent. Depending on the time scale chosen for the sloughing, that means that the probability distribution for ‘s' (and maybe Δt) must account for the local biofilm properties and history

We made a first attempt by proposing a simple model which links k_r to the actual biofilm growth rate, keeping Δt constant. Making k_r dependent on the growth rate is a simple way, although imperfect, to take into account the biofilm resistance. Indeed, the local growth rate decrease drastically when, either the biofilm is thick and the porous media almost clogged or when the system is depleted with nutrient. This allows to “simulate” various situation such as a thick biofilm which becomes less resistant in the lower layer or a biofilm which is not resistance because of a low bacteria activity (nutrients completed consumed or low loading rate).

Perspectives

This work paved the way of a simple 1D modeling of biofilm growth in porous media. Obviously given the assumption and simplification made, we are still far from getting an operational model able to predict industrial situation. The discrepancy observed between the model results and the available date that we used may come from the assumptions made in the development of the macroscopic model. We give hereafter some suggestion for improvement as well as some perspectives.

Biofilm representation

In the current model, the choice was made to represent the biofilm through a single parameter Φ_B which account for the total biofilm fraction . The corresponding kinetic parameters representing the biofilm growth and decay are then averaged parameters which does not distinguish between the actual bacterial cells division and lysis as well as some components production and decay such as EPS. This obviously is a source of discrepancy. Although some existing model introduce the EPS phase, the modeling of EPS production (often represented through a Monod like equation by analogy with the

bacteria growth) is still an open problem: EPS production is closely correlated with the bacteria strain, physiological state and its adaptation to external mechanical or biological stress Experimental evidences are still required on that specific point to have a better understanding on the EPS production kinetics compared to the bacteria adaptation to its environment

Permeability model :

Some simple assumptions made in the model may be still limitative and could be revised in the future. For instance, in the first mechanism which represents pore radius reduction, biofilm porosity was not accounted for in the mathematical development of the permeability model. On one hand, it is well known that biofilm is stratified and contains lots of voids and channels. On the other hand the biofilm geometrical structure can also lead to dead zone not available for the flow: so using only the volume fraction Φ_B may not be representative of the actual flow involved in the permeability reduction. In a macroscopic model, that process could be taken into account by a correction factor β applied to the biofilm volume fraction Φ_B , knowing that β is probably a function of the biofilm state (and so varies in space and time). With the simple assumption performed in the study (β=1), the flow in biofilm as well as those dead zone are ignored. The biofilm permeability is considered to be zero and does not contribute to the overall permeability reduction. Despite those simplifications, when pore radius reduction is the predominant mechanism, at the first order, the new permeability model gave a good agreement to a wide range of experimental data for the estimation of the clean-bed permeability and bioclogging evolution of porous media at low biomass fraction.

As far as the second mechanism is concerned (plugs formation in the pore space), the results in chapter 3 illustrate the important role of biomass plugging in the case of the development of thick biofilm in porous media. The function $F(\Phi_B,\Phi_c)$ account for the relative importance of the plugged part compared to the first mechanism for a given biomass fraction. This function represents also somewhat the microstructure at the mesoscale. In our work, function F was simply assumed *a priori* to follow a normal

distribution. Further study could be conducted to investigate the biofilm distribution within the porous media (especially plugs formation and distribution) and refine our knowledge on function F. This could be done using recent advanced image methods such as X-ray tomography (Rolland du Roscoat et al., 2014). This technique permits the reconstruction of the 3-D structure of porous media to get information of biomass distribution. Such data may elucidate biomass distribution in porous media and could be integrated into the development of permeability model by giving a better insight on the F function and parameter Φ_C

Attachment process

In the development of the correlation equation to estimate attachment efficiency, the conventional DLVO forces was used to determine energy interaction of bacterial cell (particle) and grain (collector) surface. Available data were taken from experiments performed on colloids and bacteria, for non contaminated synthetic water. However, with the existence of Natural Organic Matters (NOMs), i.e., in the case of real biofilter or groundwater contaminated by organic matters, the application of conventional DLVO forces needs to be revised. Bacterial cell can adsorb NOMs resulting in new forces (electro-sterical forces, Morale et al, 2011). So, besides vanderWaals attractive and electrostatic repulsive forces, these electro-sterical forces (namely osmotic and elastic repulsive forces) contribute to energy interaction and impede attachment efficiency. The effect of NOMs could be possibly accounted by including the new osmotic and elastic forces to determine the new energy interaction.

Detachment through sloughing

As stated previously, the stochastic process description for the sloughing event (frequency of sloughing event and removed particle size distribution) must certainly account for the local biofilm properties and history. The simple law $kr=f(\mu_b)$ that have been proposed was just an example on how a 1D macroscale model could include this feature by relying only on available macroscale parameters and without relying on a refined description of the biofilm evolution with age. Furthermore, the sloughing events

have been considered as spatially independent. However, it seems more relevant to consider that biofilm sloughing may influence its vicinity and so that there exists some spatial correlation in the biomass response to a sloughing event.

These two proposals (function accounting for k_r and correlation between sloughing events) will require specific experiments to advance on this point in the future.

As a suggestion, the analysis of the instantaneous pressure signal along the column could give some information in terms of sloughing event frequencies and the evolution of the relative magnitude of sloughing event with time. The correlation of the pressure signal between two positions would also help to study the spatial correlation between events along the column. In term of modeling, a solution could be also to mix a mechanistic approach with a stochastic approach, the stochastic model being applied only if the local shear stress is above a given threshold. This later approach would be especially interesting if the model is turned into a 2D-model. It would keep the advantage of the stochastic model (no refined description of the biofilm mechanical properties and their evolution with the biofilm age). In the other hand, the introduction of a condition on the shear stress would restricts those events for situation where the local shear stress is more likely to produce the removal of large patches. It would partially solve the problem of spatial dependence between random events. Below the shear stress threshold, the biofilm detachment would be treated as a classical continuous erosion process.

Reference

Abu-Lail N.I, and Camesano T.A. (2006) The effect of solvent polarity on the molecular surface properties and adhesion of *Escherichia coli*. *Colloids Surf B Biointerfaces* **51:** 62–70.

Aggarwal S, Poppele E. H, Hozalski R.M. 2010. Development and Testing of a Novel Microcantilever Technique for Measuring the Cohesive Strength of Intact Biofilms. *Biotechnology and Bioengineering*, Vol. 105, No. 5.

Ahimou F, Semmens M.J, Novak P.J, Haugstad G. 2007. Biofilm cohesiveness measurement using a novel atomic force microscopy methodology. *Appl Environ Microbiol* 73:2897–2904

Ahmadi M.M, Mohammadi S and Hayati A.N. 2011. Analytical derivation of tortuosity and permeability of monosized spheres: A volume averaging approach. *Phys. Rev*. E 83:026312.

Alpkvist E, and Klapper I. 2007a. Description of mechanical response including detachment using a novel particle model of biofilm/flow interaction. *Water Sci Technol* 55: 265–273.

Alpkvist E, and Klapper I. 2007b. A Multidimensional Multispecies Continuum Model for Heterogeneous Biofilm Development. *Bull Math Biol* 69: 765–789.

Alpkvist E, Picioreanu C, van Loosdrecht M.C.M, and Heyden A. 2006. Three-Dimensional Biofilm Model With Individual Cells and Continuum EPS Matrix. *Biotechnol Bioeng* 94: 961–979

Anders R, Chrysikopoulos C.V. 2005. Virus fate and transport during artificial recharge with recycled water, *Water Resour. Res.* 41.

Anderson G.G, and O'Toole G.A. 2008. Innate and induced resistance mechanisms of bacterial biofilms. *Curr Top Microbiol Immunol* 322: 85–105.

Bachu S. 2000. Sequestration of CO_2 in geological media: Criteria and approach for site selection in response to climate change, *Energy Convers. Manage.*, 41(9), 953–970.

Bai R, Tien C. 1999. Particle deposition under unfavorable surface interactions. *J Colloid Interface Sci*. 218:488–499.

Balaban N. Q, Merrin J, Chait R, Kowalik L, &Leibler S. 2004. Bacterial persistence as a phenotypic switch. *Science* 305, 1622–1625.

Baty A. M, Eastburn C. C, Techkarnjanaruk S, Goodman A. E. & Geesey G. G. 2000. Spatial and temporal variations in chitinolytic gene expression and bacterial biomass production during chitin degradation. *Appl. Environ. Microbiol.* 66, 3574–3585.

Baveye P, Valocchi A. 1989. An evaluation of mathematical models of the transport of biologically reacting solutes in saturated soils and aquifers. *Wat. Resour. Res*. 25(6): 1413-1421.

BEAR, J. 1972. Dynamics of fluids in porous media. Elsevier

Bergendahl J, Grasso D. 2000. Prediction of colloid detachment in a model porous media: Hydrodynamics. *Chem. Eng. Sci. 55*: 1523-1532.

Beyenal H, Chen S.N, Lewandowski Z. 2003. The double substrate growth kinetics of Pseudomonas aeruginosa Ha The double substrate growth kinetics of Pseudomonas aeruginosa. *Enzyme and Microbial Technology* 32 (2003) 92–98

Bielefeldt A.R, Illangasekare T, Uttecht M, LaPlante R. 2002. Biodegradation of propylene glycol and associated hydrodynamic effects in sand. *Water Research* 36: 1707–1714

Bohn A, Zippel B, Almeida J.S, Xavier J. B. 2007. Stochastic modeling for characterisation of biofilm development with discrete detachment events (sloughing). Water Science & Technology Vol 55 No 8–9 pp 257–264 *Q* IWA Publishing.

Böl M, Alexander E. E, Albero A. B, Hellriegel J, and Krull R. 2013. Recent advances in mechanical characterisation of biofilm and their significance for material modelling. *Critical Reviews in Biotechnology*, 2013; 33(2): 145–171

Borden R.C and Bedient P.B. 1986.Transport of dissolved hydrocarbons influenced by oxygen-limited biodegradation: 1. Theoretical development. *Water Resouces Research*. 1973 – 1982

Bradford S. A, Yates S. R, Bettahar M, Simunek J. 2002. Physical factors affecting the transport and fate of colloids in saturated porous media. *Water Resour. Res.*38: 1327.

Branda S. S, Chu F, Kearns D. B, Losick R, & Kolter R. 2006. A major protein component of the *Bacillus subtilis* biofilm matrix. *Mol. Microbiol.* 59, 1229–1238.

Branda S. S, Gonzalez-Pastor J. E, Ben-Yehuda S, Losick R, & Kolter R. 2001. Fruiting body formation by *Bacillus subtilis*. *Proc. Natl Acad. Sci. USA* 98, 11621–11626.

Brovelli A, Malaguerra F, and Barry D. 2009. Bioclogging in porous media: Model development and sensitivity to initial conditions. *Environmental Modelling & Software*, 24(5), 611-626.

Bryers J.D. 1988. Modeling biofilm accumulation. *Physiological models in Microbiology*. volume 2 pp. 109-144. Edited by M. J. Bazin and J. I. Prosser. CRC Press, Boca Raton, FLa.

Burdick G.M, Berman N.S, and Beaudoin S.P. 2005. Hydrodynamic particle removal from surfaces. *Thin Solid Films* 488:116–123

Canler J. P. and Perret J. M. 1994. Biological aerated filters: Assessment of the process based on the sewage treatment Plants. *Wat. Sci. Technol*. 29(1011), 13-22

Carman P.C., 1937. Fluid flow through granular beds. *Trans.-Inst. Chem. Eng*. 15, 150–166.

Cerf A, Cau J.C, Vieu C, and Dague E. (2009) Nanomechanical properties of dead or alive single-patterned bacteria. *Langmuir* 25: 5731–5736.

Chai Y, Chu F, Kolter R, Losick R. 2007. Bistability and biofilm formation in *Bacillus subtilis*. *Mol. Microbiol.* 67, 254–263.

Chambless J.D, Stewart P.S. 2007. A three-dimensional computer model analysis of three hypothetical biofilm detachment mechanisms, *Biotechnol. Bioeng*. 97 (6):1573–1584

Chang Y. I, Chan H. C. 2008. Correlation equation for predicting filter coefficient under unfavorable deposition conditions. *AIChE J*. 54 (5), 1235−1253

Chang Y.I, Cheng W.Y, Chan H.C. 2009. A proposed correlation equation for predicting filter coefficient under unfavorable deposition conditions. *Sep Purif Technol* 65(3):248–50

Chen X, Stewart P.S. 2002. Role of electrostatic interactions in cohesion of bacterial biofilms. *Appl. Microbiol. Biotechnol.* 59 (6), 718

Chen Y.Y, Wu C.C, Hsu J.L, Peng H.L, Chang H.Y,and Yew T.R. (2009) Surface rigidity change of *Escherichia coli* after filamentous bacteriophage infection. *Langmuir* **25:** 4607–4614.

Chmielewski R. A. N, & Frank J. F. 2003. Biofilm formation and control in food processing facilities. *Comprehensive Reviews in Food Science and Food Safety*, 2, 22–32

Claxton L.D, Houk V.S, Williams R & Kremer F. 1991. Effect of bioremediation on the mutagenicity of oil spilled in Prince William Sound, Alaska. *Chemosphere*, 23, 643-50.

Clement T.P, Hooker B.S, Skeen R.S. 1996. Macroscopic models for predicting changes in saturated porous media properties caused by microbial growth. *Ground Water* 34, 934–942.

Coufort C, Derlon. N, Ochoa-Chaves J, Line A and Paul E. 2007. Cohesion and detachment in biofilm systems for different electron acceptor and donors *Water Science & Technology* Vol 55 No 8–9 pp 421–428 Q IWA Publishing.

Cunningham A. B, Characklis W. G, Abedeen F, and Crawford D. 1991. Influence of biofilm accumulation on porous media hydrodynamics. *Environmental science & technology*, 25(7), 1305-1311.

Cunningham A. B, Sharp R. R, Hiebert R, and James G. 2003. Subsurface biofilm barriers for the containment and remediation of contaminated groundwater. *Bioremediation Journal*, 7:151–164.

Davit Y, Iltis G, Debenest G, Veran-Tissoires S, Wildenschild, D, Gerino M, & Quintard M. 2011. Imaging biofilm in porous media using X-ray computed microtomography.*Journal of Microscopy*, 242(1), 15–25.

Delay F, Porel G, Chatelier M. 2013. A dual flowing continuum approach to model denitrification experiments in porous media colonized by biofilms. *Journal of Contaminant Hydrology* 150 : 12–24

Deng W, Cardenas M.B, Kirk M.F, Altman S.J, Bennett P.C. 2013. Effect of Permeable Biofilm on Micro-And Macro-Scale Flow and Transport in Bioclogged Pores. *Env Sci Techol* 47:11092–11098

Deng Y, Sun M, and Shaevitz J.W. (2011) Direct measurement of cell wall stress stiffening and turgor pressure in live bacterial cells. *Phys Rev Lett* 107: 158101.

Drescher K, Shen Y, Bassler BL, Stone HA.. Biofilm streamers cause catastrophic disruption of flow with consequences for environmental and medical systems. 2013. PNAS 110:4345–4350.

Du Plessis J.P, and Masliyah J.H. 1991. Flow through isotropic granular porous media. *Transp. Porous Media* 6:207–221.

Duddu R, Chopp D.L, Moran B. 2008. A two-dimensional continuum model of biofilm growth incorporating fluid flow and shear stress based detachment. *Biotechnol Bioeng* 103:92–104

Dumont E, Andres Y, Le Cloirec P, Gaudin F. 2008. Evaluation of a new packing material for H_2S removed by biofiltration, *Biochem. Eng. J.* 42: 120–127

Ebigbo A, Helmig R, Cunningham A.B, Class H, Gerlach R. 2010. Modelling biofilm growth in the presence of carbon dioxide and water flow in the subsurface. *Advances in Water Resources* 33. 762–781

Elimelech M, O'Melia C.R. 1990. Effect of particle size on collision efficiency in the deposition of Brownian particles with electrostatic energy barriers. *Langmuir*. 6:1153–1163.

Elimelech M. 1992. Predicting collision efficiencies of colloidal particles in porous media. Water Res.26:1–8.

Elimelech M. 1994. Particle deposition on ideal collectors from dilute flowing suspensions: Mathematic formulation, numerical solution, and simulations, *Sep. Technol*., 4, 186–212.

Eaton P, Fernandes J.C, Pereira E, Pintado M.E, and Malcata F.X. (2008) Atomic force microscopy study of the antibacterial effects of chitosans on *Escherichia coli* and *Staphylococcus aureus*. *Ultramicroscopy* 108: 1128–1134

Features of openfoam. http://www.openfoam.com/features/ Accessed on 20th Oct 2012.

Fischetti V.A. 2005. Bacteriophage lytic enzymes: novel anti-infectives. *Trends Microbiol*, 13(10), 491-496

Fish. K, Osborn. A. M, Boxall. J. B, Biofilm structures (EPS and bacterial communities) in drinking water distribution systems are conditioned by hydraulics and influence discolouration. 2017. *Science of the Total Environment* 593–594: 571–580.

Flemming H.C and Wingender J. 2010. The biofilm matrix. *Nature Rev. Microbiol*. 8, 623–633.

Folch A, Vilaplana M, Amado L, Vicent T, and Caminal G. 2013. Fungal permeable reactive barrier to remediate groundwater in an artificial aquifer. *Journal of hazardous materials*, 262, 554- 560

Foppen J. W. A, Mporokoso A, Schijven J. F. 2005. Determining straining of Escherichia coli from breakthrough curves. *Journal of Contaminant Hydrology* 76: 191– 210.

Garny.K, Horn. H, Neu .T. R.2008. Interaction between biofilm development, structure and detachment in rotating annular reactors. Bioprocess Biosyst Eng: 31:619–629

Garny.K, Neu .T. R, Horn. H.2009. Sloughing and limited substrate conditions trigger filamentous growth in heterotrophic biofilms—Measurements in flow-through tube reactor. Chemical Engineering Science 64 : 2723 -- 2732

Ghanbarian B, Hunt A.G, Ewing R.P, Sahimi M. 2013. Tortuosity in porous media: a critical review, Soil *Sci. Soc. Am. J.* 77, 1461-1477.

Golfier F, Wood B.D, Orgogozo L, Quintard M, Buès M. 2009. Biofilms in porous media: development of macroscopic transport equations via volume averaging with closure for local mass equilibrium conditions. *Adv Water Resour* 32:463–85.

Gordon. V, Davis-Fields. M, Kovach. K, and Rodesney. D. Biofilms and mechanics: a review of experimental techniques and findings. 2017. *J.Phys D* : Appl. Phys.50.

Gregory J. 1981. Approximate expressions for retarded van der Waals interaction. *Journal of Colloid and Interface Science* 83, 138–145.

Habibi. S. An upscaled study of a membrane filtration process in presence of biofilms. 2014. Chemical and Process Engineering. PhD .Ecole Centrale Paris.

Hall-Stoodley L, Costerton J.W, Stoodley P. 2004. Bacterial biofilms: from the natural environment to infectious diseases. *Nat. Rev. Microbiol*. 2, 95–108

Ham Y.J, Kim S.B and Park S.J. 2007. Numerical experiments for bioclogging in porous media. *Environmental technology*, vol. 28. Pp 1079-1089

Hand V, Lloyd J.R, Vaughan D.J, Wilkins M.J , and Boult S. 2008. Experimental studies of the influence of grain size, oxygen availability and organic carbon availability on bioclogging in porous media. *Environ. Sci. Technol.*42*:* 1485–1491

Happel J. 1958. Viscous flow in multiparticle systems: slow motion of fluids relative to beds of spherical particles. *American Institute of Chemical Engineers Journal*, 4, 197-201.

Harleman D. R. F and R. R. Rumer .R.R. 1963.Longitudinal and lateral dispersion in an isotropic porous medium. *Fluid mechanics*, 16:385–394.

Harvey R.W, Garabedian S.P. 1991. Use of colloid filtration theory in modelling movement of bacteria through a contaminated sandy aquifer. *Environmental Science and Technology* 25, 178–185.

Hermanowicz SW. 2001. A simple 2D biofilm model yields a variety of morphological features. *Mathe Biosci* 169:1–14

Heydorn A, Ersboll B.K, Hentzer M, Parsek M.R, Givskov M and Molin S. 2000. Experimental reproducibility in flow-chamber biofilms. *Microbiol*., 146, 2409–2415.

Hogg R, Healy T.W, Fuerstenau D.W. 1966. Mutual coagulation of colloidal dispersions. *Transactions of the Faraday Society* 62, 1638–1651.

Horgue P, Soulaine C, Franc J, Guibert R, Debenest G. 2015 An open- source toolbox for multiphase flow in porous media. *Computer Physics Communications* vol. 187, pp. 217-226.

Horn H, Lackner S. 2014. Modeling of Biofilm Systems: A Review. *Adv Biochem Eng Biotechnol* 146, 53–76.

Houari A, Picard J, Habarou H, Galas L, Vaudry H, Heim V, Di Martino P. Rheology of biofilms formed at the surface of NF membranes in a drinking water production unit. 2008. *Biofouling*. 24(4): 235-240.

Howell J. A and Atkinson B. 1976. Sloughing of microbial film in trickling filters. *water research* vol. i0. pp. 307-315.

Hunt. S. M, Werner. E. N, Huang. B, Hamilton. M. A, and Stewart .P. S.2004. Hypothesis for the Role of nutrient Starvation in Biofilm Detachment. APPLIED AND ENVIRONMENTAL MICROBIOLOGY, Dec. 7418–7425

Inaba T, Hori T, Aizawa H, Ogata A and Habe H. 2017. Architecture, component, and microbiome of biofilm involved in the fouling of membrane bioreactors. *NPJ Biofilms and Microbiomes*; London 3 : 1-8.

Islam J, Singhal N . A one-dimensional reactive multi-component landfill leachate transport model. 2002. *Environmental Modelling & Software* 17: 531–543

Ivanov V, and Chu J. 2008. Applications of microorganisms to geotechnical engineering for bioclogging and biocementation of soil in situ. *Reviews in Environmental Science and Bio/Technology*, 7(2), 139-153.

Jayathilake. P.G, Gupta. P, Li. B, Madsen. C, Oyebamiji. O, GonzaÂlez-Cabaleiro. R. A mechanistic Individual-based Model of microbial communities.2017.PLoS ONE 12(8): e0181965.

Kao C, Chen S. and Liu J. 2001. Development of a biobarrier for the remediation of PCE contaminated aquifer. *Chemosphere*, 43(8), 1071-1078

Kapellos G.E , Alexiou T.S, Payatakes A.C. 2007. Hierarchical simulator of biofilm growth and dynamics in granular porous materials. *Advances in Water Resources* 30 : 1648–1667.

Karimi. A , Karig. D , Kumar. A and Ardekani. A. M . Interplay of physical mechanisms and biofilm processes: review of microfluidic methods. 2015. Lab Chip15: 23-42.

Karrabi M, Sechet P, Morra C, Cartellier A, Geindreau C, Martins J.M.F. 2011. Investigation of hydrodynamic/biomass growth coupling in a pilot scale granular bioreactor at low pore Reynolds number. *Chemical Engineering Science* 66 : 1765–1782

Karsten P. 1990. Biofilm development on stainless steel and pvc surfaces in drinking water. *Water Research.* Volume 24, Issue 2, Pages 239-243.

Kildsgaard J, Engesgaard P. 2001. Numerical analysis of biological clogging in two-dimensional sand box experiments. Journal of Contaminant Hydrology 50 : 261–285.

Kildsgaard J, Engesgaard P. 2002. Tracer tests and image analysis of biological clogging in a two-dimensional sandbox experiment. *Ground Water Monit.Remed*. 60, 60–67.

Kim J.W, Choi H, Pachepsky Y.A. 2010. Biofilm morphology as related to the porous media clogging. *water research* 44 : 1193 – 1201

Klapper I, Rupp C.J, Cargo R, Purvedorj B, Stoodley P. 2002. Viscoelastic fluid description of bacterial biofilm material properties. *Biotechnol Bioeng* 80: 289–296.

Komlos J, Cunningham A. B, Camper A. K, and Sharp R. R. 2004. Biofilm barriers to contain and degrade dissolved trichloroethylene. *Environmental Progress*, 23:69–77.

Kommedal R, Bakke R. 2003. Modeling pseudomonas aeruginosa biofi lm detachment HiT Working Paper no 3/2003, Telemark University College, Porsgrunn.

Kone T., Golfier F, Orgozogo L, Oltean C, Lefèvre E, Block J.C, Bues M.A, Impact of biofilm-induced heterogeneities on solute transport in porous media. 2014. *Water Resource Research,* Vol 50 (11), pp 9103-9119.

Kotturi G, Robinson C.W, and Inniss W.E. 1991. Phenol degradation by a psychrotrophic strain of Pseudomonas putida. *Appl Microbiol Biotechnol* 34:539-543.

Kovach. K, Davis-Fields. M, Irie. Y, Jain. K, Doorwar. S, Vuong. K, Dhamani. N, Mohanty. K, Touhami. A and Gordon. V. Evolutionary adaptations of biofilms infecting cystic fibrosis lungs promote mechanical toughness by adjusting polysaccharide production. 2017. *Biofilms and Microbiomes* 3:1.

Krauss E.D, Mays D.C .2014. Modification of the Kozeny-Carman equation to quantify formation damage by fines in clean, unconsolidated porous media. *SPE Reservoir Evaluation & Engineering* 17(4): 466–472.

Kussell E, Kishony R, Balaban N. Q, & Leibler S. 2005. Bacterial persistence: a model of survival in changing environments. *Genetics* 169, 1807–1814.

Kumar A, Kumar S, Kumar S. 2005. Biodegradation kinetics of phenol and catechol using *Pseudomonas putida* MTCC 1194. *Biochemical Engineering Journal* 22: 151–159

Kuwabara S. 1959. The Forces experienced by Randomly Distributed Parallel Circular Cylinders or Spheres in a Viscous Flow at Small Reynolds Numbers *J. Phys. Soc. Japan*, 14, 527.

Lanfrey P.Y, Kuzeljevic Z.V, and Dudukovic M.P. 2010. Tortuosity model for fixed beds randomly packed with identical particles. *Chem. Eng. Sci.* 65:1891–1896.

Langwaldt J.H, Puhakka J.A. 2000. On-site biological remediation of contaminated groundwater: a review. *Environ. Pollut*. 107, 187–197

Laspidou C.S and Aravas N. Variation in the mechanical properties of a porous multi-phase biofilm under compression due to void closure. *Water Science & Technology* Vol 55 No 8–9 pp 447–453 Q IWA Publishing 2007

Laspidou C.S, Rittmann B.E. 2002. A unified theory for extracellular polymeric substances, soluble microbial products, and active and inert biomass, *Water Res*. 36: 2711–2720.

Laspidou C.S, Rittmann B.E. 2004. Modeling the development of biofilm density including active bacteria, inert biomass, and extracellular polymeric substances. *Water Res* 38:3349–3361.

Lecuyer S, Rusconi R, Shen Y, Forsyth A, Vlamakis H, Kolter, R, & Stone H. 2011. Shear Stress Increases the Residence Time of Adhesion of Pseudomonas aeruginosa. *Biophysical Journal*, 100(2), 341–350.

Lembre. P, Lorentz. C and Martino. P.D. Chap 13 : Exopolysaccharides of the Biofilm Matrix: A Complex Biophysical World, in "The Complex World of Polysaccharides", book edited by Desiree Nedra Karunaratne, ISBN 978-953-51-0819-1, Published: October 31, 2012.

Lemos M, Mergulhao F, Melo L, & Simoes M. 2015. The effect of shear stress on the formation and removal of Bacillus cereus biofilms. *Food and Bioproducts Processing*, 93, 242–248.

Leriche V, Sibille P, & Carpentier B. 2000. Use of an Enzyme-Linked Lectinsorbent Assay To Monitor the Shift in Polysaccharide Composition in Bacterial Biofilms. *Applied and Environmental Microbiology*, 66(5), 1851–1856.

Lewandowski Z, Beyenal H, Myers J and Stookey D. 2007. The effect of detachment on biofilm structure and activity: the oscillating pattern of biofilm accumulation. Water Science & Technology Vol 55 No 8–9 pp 429–436 Q IWA Publishing.

Lewandowski Z, Beyenal H. and Stookey D. 2004. Reproducibility of biofilm processes and the meaning of steady state in biofilm reactors. *Wat. Sci. Tech* 49(11), 359–364.

Lewandowski Z. 2000. Notes on biofilm porosity. *Water Research*. Volume 34, Issue 9, 15, Pages 2620-2624

Lim C.P, Zhao D, Takase Y, Miyanaga K, Watanabe T, Tomoe Y, and Tanji Y. 2011. Increased bioclogging and corrosion risk by sulfate addition during iodine recovery at a natural gas production plant. *Applied microbiology and biotechnology*, 89(3), 825-834.

Liu Y. and Tay J.H. Detachment forces and their influence on the structure and metabolic behaviour of biofilms. 2001. *World J. of Microbiology and Biotechnology* 17, 111–117.

Lopez L.A.G, Veiga M.C, Nogueira R, Aparicio A, & Melo L. F. 2003. A technique using a membrane flow cell to determine average mass transfer coefficients and tortuosity factors in biofilms. *Water Science and Technology*, 47(5), 61–67.

Mack D, Rohde H, Harris LG. 2006. Biofilm formation in medical device-related infection. *Int J Artif Organs* 29(4):343–59

Majumdar U, Alexander T, Waskar M and Dagaonkar M.V. 2014. *Effect of biofilm on colloid attachment in saturated porous media*. Water Science & Technology 70.2. doi: 10.2166/wst.2014.197

Martin M.M.B, Perez J.A.S, Fernandez F.G.A, Sanchez J.L.G, Lopez J.L.C, and Rodriguez S. M. 2008. A kinetics study on the biodegradation of synthetic wastewater simulating effluent from an advanced oxidation process using pseudomonas putida CECT 324. *Journal of Hazardous Materials*, 151:780–788, 2008.

Mauclaire L, Schurmann A, and Mermillod-Blondin F. 2006. Influence of hydraulic conductivity on communities of microorganisms and invertebrates in porous media: a case study in drinking water slow sand filters. *Aquatic Sciences*, 68:100–108.

Mays D. C and Hunt J. R. 2005. Hydrodynamic Aspects of Particle Clogging in Porous Media. *Environ. Sci. Technol.* 39, 577-584

Mbaye S. 2011. Couplage hydrodynamique-biomasse dans les procedes de d'epollution: Approche locale des mecanismes de croissance et d'adhesion/d'etachement de micro-organismes sur substrats solides. These, Universite de Grenoble.

Mbaye S., Séchet P., Pignon F., and Martins J.M.F.2013.Influence of hydrodynamics on the growth kinetics of glass-adhering Pseudomonas putida cells through a parallel plate flow chamber, *Biomicrofluidics*, 7, 054105.

Medeiros A.C.A.P. 2016. Etude experimentale de la formation des biofilms sous conditions hydrodynamiques controlees. Mecanique des fluides. PhD. Universite Grenoble Alpes, 2016.

Melo. L. F. Biofilm physical structure, internal diffusivity and tortuosity. 2005. Water Science & Technology, Vol 52 (7), pp 77-84.

Mendoza J.A, Prado O.J, Veiga M.C, Kennes.C. 2004. Hydrodynamic behaviour and comparison of technologies for the removal of excess biomass in gas-phase biofilters. *Water Research*, Volume 38, Issue 2, January 2004, Pages 404–413

Menniti A, Kang S, Elimelech M, Morgenroth E. 2009. Influence of shear on the production of extracellular polymeric substances in membrane bioreactors. *Water Research* 43 (17), 4305e4315.

Mitchell A. C, Phillips A. J, Hiebert R, Gerlach R, Spangler L. H, and Cunningham A. B. 2009. Biofilm enhanced geologic sequestration of supercritical CO2. *International Journal of Greenhouse Gas Control*, 3:90–99.

Mitchell A. C, Phillips A. J, Kaszuba J. P, Hollis W. K, Cunningham A. L. B, and Gerlach R. 2008. Microbially enhanced carbonate mineralization and the geologic containment of CO2. *Geochimica et Cosmochimic Acta*, 72:A636.

Nadell, C.D., Ricaurte, D., Yan, J., Drescher, K. and Bassler, B.L. Flow environment and matrix structure interact to determine spatial competition in Pseudomonas aeruginosa biofilms. 2017. eLife 6, e21855.

Nielsen P.H, Jahn A, Palmgren R. 1997. Conceptual model for production and composition of exopolymers in biofilms. *Water Sci Technol* 36:11–9

O'Neill M. E. 1968. A sphere in contact with a plane wall in a slow linear shear flow. *Chem. Eng. Sci. 23:* 1293-1298

Ohashi A, Harada H. 1994. Adhesion strength of biofilm developed in an attached-growth reactor. *Water Sci Technol* 29:10–1.

Ohashi A, Koyama T, Syutsubo K, Harada H. 1999. A novel method for evaluation of biofilm tensile strength resisting erosion. *Water Sci Technol* 39: 261–268.

Orgaz B, Kives J, Pedregosa A.M, Monistrol I.F, Laborda F, San Jose C. 2006. Bacterial biofilm removal using fungal enzymes. *Enzyme Microb Technol* 40(1):51–6.

Orgogozo L, Golfier F, Bues M, & Quintard M. 2010. Upscaling of transport processes in porous media with biofilms in non-equilibrium conditions.*Advances in Water Resources*, 33(5), 585–600.

Orr Jr F. M. 2004. Storage of carbon dioxide in geologic formations, J. Pet. Technol., 56(9), 90–97.

Paramonova E, Krom B.P, van der Mei H.C, Busscher H.J, Sharma P.K. 2009. Hyphal content determines the compression strength of *Candida albicans* biofilms. *Microbiology* 155: 1997–2003.

Paul E, Ochoa J.C, Pechaud Y, Liu Y, Line A.2012. Effect of shear stress and growth conditions on detachment and physical properties of biofilms. *Water research* 46: 5499-5508

Payatakes A. C, Tien C, & Turian R. M. 1973. A new model for granular porous media: Part I. Model formulation. *American Institute of Chemical Engineers Journal*, 19, 58-66.

Pereira, M. A., M. Kuehn, S. Wuertz, T. Neu, and L. F. Melo. Effect of flow regime on the architecture of a Pseudomonas fluorescens biofilm. . 2002. *Biotechnol. Bioeng.* 78:164–171.

Perry C.C, Weatherly M, Beale T, and Randriamahefa A. (2009) Atomic force microscopy study of the antimicrobial activity of aqueous garlic versus ampicillin against *Escherichia coli* and *Staphylococcus aureus*. *J Sci Food Agric* 89:958–964.

Petersen E.E. 1958. Diffusion in a pore of varying cross section American Institute of Chemical Engineers Journal., 4, 343.

Picioreanu C, van Loosdrecht M.C.M, Heijnen J.J. 2001. Two-dimensional model of biofilm detachment caused by internal stress from liquid flow. *Biotechnol Bioeng* 72:205–218

Pintelon T. R. R, Picioreanu C, van Loosdrecht M. C. M, Johns M. L. 2012. The effect of biofilm permeability on bio-clogging of porous media. *Biotechnol. Bioeng*. 109 (4), 1031−1042.

Proto C. J, DeJong J. T, and Nelson D. C. 2016. Biomediated Permeability Reduction of Saturated Sands *Journal of Geotechnical and Geoenvironmental Engineering*. Volume 142 Issue 12.

Qi P.S, Wang W.B, & QI Z. 2008. Effect of Shear Stress on Biofilm Morphological Characteristics and the Secretion of Extracellular Polymeric Substances. Pages 3438–3441 of *: The 2nd International Conference on Bioinformatics and Biomedical Engineering, 2008. ICBBE 2008*.

Ramirez A. A, Benard S, Giroir-Fendler A, Jones J. P, and Heitz, M. 2008. Treatment of methanol vapours in biofilters packed with inert materials. *Journal of Chemical Technology and Biotechnology*, 83:1288–1297.

Redfield. R. J. Is quorum sensing a side effect of diffusion sensing. 2002. *Trends in Microbiology* Vol.10 No.8.

Rittman BE. 1982. The effect of shear stress on biofilm loss rate. Biotechnology Bioengineering.24:501-6

Rolland du Roscoat S, Martins M.F, Sechet. P, Vince E, Latil. P, Geindreau.C. 2014. Application of synchrotron X-ray microtomography for visualizing bacterial biofilms 3D microstructure in porous media. Biotechnol. Bioeng., 111 (6):1265-1271

Rubol S, Freixa A, Carles-Brangarí A, Fernàndez-Garcia D, Romaní A.M, Sanchez-Vila X. 2014. Connecting bacterial colonization to physical and biochemical changes in a sand box infiltration experiment. *Journal of Hydrology* 517:317–327.

Rusconi. R, Lecuyer. S, Guglielmini. L, Stone. HA. Laminar flow around corners triggers the formation of biofilm streamers.2010. *Journal of The Royal Society Interface* 7 (50), 1293-1299.

Scheibe T.D, Dong H.L, Xie Y.L. 2007. Correlation between bacterial attachment rate coefficients and hydraulic conductivity and its effect on field-scale bacterial transport. *Adv Water Resour* 30(6–7):1571–82

Seifert D, Engesgaard P.2007. Use of tracer tests to investigate changes in flow and transport properties due to bioclogging of porous media. *J. Contam. Hydrol*. 93 (14), 58–71

Shafahi M, Vafai K. 2008. Biofilm affected characteristics of porous structures.2008. *Int J Heat Mass Transfer*

Shareefdeen Z, Baltzis B.C, Oh Y. S, and Bartha R. 1993.Biofiltration of Methanol Vapor. *Biotechnol. Bioengineering*, 41, 512.

Sharma M. M, Chamoun H, Sita Rama Sarma D. S. H, Schechter R. S. 1992. Factors controlling the hydrodynamic detachment of particles from surfaces. *J. Colloid Interface Sci. 149* (1), 121-134.

Sharp R.R, Cunningham A.B, Komlos J, and Billmayer J.1999. Observation of thick biofilm accululation and structure in porous media and corresponding hydrodynamic and mass transfer effects. *Water Science and Technology*, 39:195–201.

Sharp R.R, Stoodley P, Gerlach R., Cunningham A.B. 2005. Visualization and characterization of dynamic patterns of flow, growth and activity of biofilms growing in porous media. *Water Science and Technology* 52 (7), 85–90.

Shaw J.C, Bramhill B, Wardlaw N.C, and Costerton J.W. 1985. Bacterial fouling in a model core system. *Applied and Environironmental Microbiology*, 49:693–701.

Shaw T, Winston M, Rupp C J, Klapper I & Stoodley P. Commonality of elastic relaxion times in biofilms. 2004. *Phys rev lett* 93: 1-4.

Shen C ,Huang Y, Li B and Jin Y. 2010. Predicting attachment efficiency of colloid deposition under unfavorable attachment conditions. *Water resources research*, vol. 46, W11526, doi:10.1029/2010WR009218

Shen C, Li B, Huang Y, and Jin Y. 2007. Kinetics of coupled primary and secondary minimum deposition of colloids under unfavorable chemical conditions, *Environ. Sci. Technol*., 41, 6976–6982.

Simoes, Manuel, Pereira, Maria O., Sillankorva, Sanna, Azeredo, Joana, &Vieira, Maria J. The effect of hydrodynamic conditions on the phenotype of Pseudomonas fluorescens biofilms. 2007. *Biofouling*, 23(4), 249–258.

Speitel GE, DiGiano FA. Biofilm shearing under dynamic conditions. *J Environ Eng- Asce* 1987;113(3):464–75.

Stephen P. Diggle, Klaus Winzer, Siri Ram Chhabra, Kathryn E. Worrall, Miguel Cámara, and Paul Williams. The Pseudomonas aeruginosa quinolone signal molecule overcomes the cell density-dependency of the quorum sensing hierarchy, regulates rhldependent genes at the onset of stationary phase and can be produced in the absence of LasR. 2003. *Molecular Microbiology* (50 (1), 29–43.

Stewart P. S. 1993. A model of biofilm detachment. *Biotechnol Bioeng* 41, 111–117.

Stewart T.L, Fogler H.S. 2001. Biomass plug development and propagation in porous media. *Biotechnol Bioeng* 72:353–63

Stewart T.L, Kim D.S. 2004. Modeling of biomass-plug development and propagation in porous media. *Biochemical Engineering Journal* 17: 107–119

Stoodley P, Lewandowski Z, Boyle J.D, Lappin-Scott H.M. 1999. Structural deformation of bacterial biofilms caused by short-term fluctuations in fluid shear: An in situ investigation of biofilm rheology. *Biotechnol Bioeng* 65:83–92.

Suthar H, Hingurao K, Desai A, and Nerurkar A. 2009. Selective plugging strategy-based microbial enhanced oil recovery using Bacillus licheniformis TT33. *Journal of microbiology and biotechnology*, 19(10), 1230-1237.

Sutherland I.W. 2001. The biofilm matrix — an immobilized but dynamic microbial environment. *Trends Microbiol* 9:222–7.

Syngouna V.I, Chrysikopoulos C.V. 2011. Transport of biocolloids in water saturated columns packed with sand: Effect of grain size and pore water velocity. *Journal of Contaminant Hydrology* 126: 301–314

Tabeling P. 2003. *Introduction a la microfluidique*. Belin.

Taylor S. W, Jaffé P. R. 1990a.Biofilm growth and the related changes in the physical properties of a porous medium: 1. Experimental investigation', Water resources research, 26(9), 2161-2169

Taylor S. W and Jaffé P. R. 1990b.Substrate and biomass transport in a porous medium. *WaterResour. Res*, 26(9), 2181-2194.

Telgmann. U, Horn. H, Morgenroth. E. 2004. Influence of growth history on sloughing and erosion from biofilms. Water Research 38: 3671–3684

Thullner M and Baveye P. 2008. Computational pore network modelling of the influence of biofilm permeability on bioclogging in porous media. *Biotechnol. Bioeng*. 99, 1337–1351

Thullner M, Schroth M.H, Zeyer J, Kinzelbach W. 2004. Modeling of a microbial growth experiment with bioclogging in a two-dimensional saturated porous media flow field. *J. Contam. Hydrol*. 70, 37–62.

Thullner M, Schroth M.H, Zeyer J, Kinzelbach W. 2004. Modeling of a microbial growth experiment with bioclogging in a two-dimensional saturated porous media flow field. *J. Contam. Hydrol*. 70, 37–62

Thullner M, Zeyer J, Kinzelbach W. 2002. Influence of microbial growth on hydraulic properties of pore networks. *Transp. Porous Media* 49, 99–122.

Tien C. 1989. In Granular filtration of aerosols and hydrosols (1st ed.). Boston: Butterworth.

Torkzaban S, Bradford S. A, and Walker S. L. 2007. Resolving the Coupled Effects of Hydrodynamics and DLVO Forces on Colloid Attachment in Porous Media. *Langmuir* 23: 9652-9660.

Towler B W, Rupp C J, Cunningham Al B & Stoodley P. Viscoelastic properties of a mixed culture biofilm from rheometer creep analysis. 2003. *Biofouling* 19: 279-285.

Tsai Y.P. 2005. Impact of flow velocity on the dynamic behaviour of biofilm bacteria. *Biofouling*, 21(5), 267–277.

Tufenkji N, Elimelech M. 2004. Correlation equation for predicting single-collector efficiency in physicochemical filtration in saturated porous media. *Environ. Sci. Technol*. 2004, 38 (2), 529–536

Tufenkji N. 2007. Modeling microbial transport in porous media: traditional approaches and recent developments. *Adv. Water Resour*. 30, 1455–1469.

Tufenkji N. 2007. Modeling microbial transport in porous media: traditional approaches and recent developments. *Adv. Water Resour*. 30, 1455–1469.

Vaidyanathan R, Tien C. 1989. HYDROSOL DEPOSITION IN GRANULAR BEDS—AN EXPERIMENTAL STUDY *Chem. Eng. Commun.* **81,** 123.

Vaidyanathan R, Tien C. 1991. Hydrosol deposition in granular media under unfavorable surface conditions. *Chemical Eng Sci* 46: 967–983.

Valiei A, Kumar A, Mukherjee PP, Liu Y, Thundat T. A web of streamers: biofilm formation in a porous microfluidic device. 2012. Lab Chip : 12(24):5133-7.

van Noorden, T. L., I. S. Pop, A. Ebigbo, and R. Helmig. An upscaled model for biofilm growth in a thin strip. 2010. *Water Resour. Res*., 46, W06505.

Vandevivere P, Baveye P. 1992. Saturated hydraulic conductivity reduction caused by aerobic bacteria in sand columns. *Soil Sci Soc Am J* 56:1–13

Vandevivere P. 1995. Bacterial clogging of porous media: a new modeling approach. Biofouling Vol. 8, pp. 281-291

VanGulck J. F, Rowe R. K, Rittmann B. E, and Cooke A. J. 2003. Predicting biogeochemical calcium precipitation in landfill leachate collection systems. *Biodegradation*, 14(5), 331–346.

Veerapaneni S and Wiesner M. R. 1997. Deposit Morphology and Head Loss Development in Porous Media. *Environ. Sci. Technol*. 31, 2738-2744

Verma A, Pruess K. 1988. Thermohydrological conditions and silica redistribution near high-level nuclear wastes emplaced in saturated geological formations. *J. Geophys. Res*. 93, 1159–1173

Vieira M. J, Melo L, & Pinheiro M. M. 1993. Biofilm formation: hydrodynamic effects on internal diffusion and structure. *Biofouling*, 7, 67–80.

Vinogradov A M, Winston M, Rupp C J & Stoodley P. Rheology of biofilms formed from dental plaque pathogen Streptococcus mutans.2004. *Biofilms* 1: 49-56.

Vrouwenvelder J.S, Picioreanu C, Kruithof J.C, van Loosdrecht M.C.M. 2010. Biofouling in spiral wound membrane systems: three-dimensional CFD model based evaluation of experimental data, J. *Membr. Sci*. 346: 71–85

Wanner O, Cunningham A. B, Lundman R. 1995. Modeling biofilm accumulation and mass transport in a porous medium under high substrate loading. *Biotechnol. Bioeng*. 47:703–712.

Walter M, Safari A, Ivankovic A, Casey E. 2013. Detachment characteristics of a mixed culture biofilm using particle size analysis. *Chemical Engineering Journal*. Volume 228, 15 Pages 1140-1147.

Whitchurch C B, Tolker-Nielsen T, Ragas P C, Mattick J S. Extracellular DNA required for bacterial biofilm formation. 2002. *Science* 295, 1487.

Wilson S. B, & Brown R. A. 1989. In situ bioreclamation: a cost-effective technology to remediate subsurface organic contamination. *Groundwater Monitoring Review*, 9, 173-9

Xavier J, Picioreanu C, van Loosdrecht M. 2005a. A framework for multidimensional modelling of activity and structure of multispecies biofilms. *Environ. Microbiol*. 7(8), 1085–1103.

Xavier J. B Picioreanu C, van Loosdrecht M.C.M. 2005b. A General Description of Detachment for Multidimensional Modelling of Biofilms. *Biotechnol Bioeng* 91, 651–669.

Xu S, Gao B, Saiers J. E. 2006. Straining of colloidal particles in saturated porous media. *Water Resour. Res* 42, W12S16,

Yao K.M, Habibian M.M, and OMelia C.R. 1971. Water and waste water filtration - concepts and applications. *Environmental science & technology* 5(11): p. 1105-&.

Yarwood J. M, Bartels D J, Volper E. M & Greenberg E. P. 2004. Quorum sensing in *Staphylococcus aureus* biofilms. *J. Bacteriol.* 186, 1838–1850.

Yazdi. S and Ardekani. A. M. Bacterial aggregation and biofilm formation in a vortical flow.2012. *Biomicrofluidics*.6(4): 044114.

Yu B.M, and Li J. H. 2004. A geometry model for tortuosity of flow path in porous media. *Chin. Phys. Lett*. 21:1569–1571.

Zamani A, Maini B. 2009Flow of dispersed particles through porous media — Deep bed filtration. Journal of Petroleum Science and Engineering 69: 71–88

Zhang T.C and Bishop P.L.1994 Density, porosity, and pore st ructure of biofilms. *Water Research*. Volume 28, Issue 11, Pages 2267-2277

Zippel B, Rijstenbil J, Neu T.R 2007. A flow-lane incubator for studying freshwater and marine phototrophic biofilms. *J. Microbiol. Methods* 70, 336–345.

Zysset A, Stauffer F, Dracos T. 1994. Modeling of reactive groundwater transport governed by biodegradation. *Water Resour Res* 1994;30:2423–34

Appendix

Appendix chapter 4

Appendix 4.1 Derivation of Eq (4.1) which is used to determine attachment rate of fine particles to collectors in CFT theory.

Considering grains as spherical particles, the simple diagram presenting the spherical collector and fluid stream is given in the **Figure F1**. Fine particles with concentration C approach with pore velocity v to a collector with diameter dg.

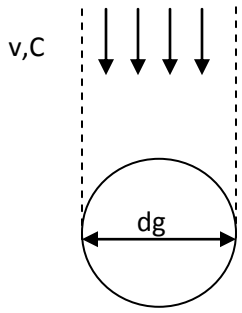

Figure F1: Simple diagram presenting the spherical collector and fluid stream

The volume of a single collector (V_g) is be defined in the following equation

$$V_g = \frac{\pi d_g^3}{6} \qquad \text{(A 4.1)}$$

Diving the total volume of collectors to the volume of a single collector, the number of collectors of a filter layer can be calculated:

$$N = \frac{(1-\emptyset)S\Delta z}{\frac{\pi d_g^3}{6}} \qquad (A4.2)$$

A mass balance on a collector

Mass flux approaching a collector: $vC\frac{\pi d_g}{4}$

Mass flux captured on a collector: $(\eta_0 \alpha_{att}) vC\frac{\pi d_g}{4}$

Mass balance on the filter layer: accumulatio rate = deposit mass = inlet flux - outlet flux

$$\mathrm{N}(\eta_0\alpha_{\mathrm{att}})vC\frac{\pi d_g}{4} = vC(z)S - vC(z+dz)S \qquad (A4.3)$$

Replacing $vC(z+dz)S = vC(z)S - v\frac{\partial C}{\partial z}S\Delta z$, Eq (A4.3) can be rewritten:

$$\mathrm{N}(\eta_0\alpha_{\mathrm{att}})vC\frac{\pi d_g}{4} = v\frac{\partial C}{\partial z}S\Delta z \qquad (A4.4)$$

Inserting Eq (A4.2) to Eq (A.4.4):

$$\frac{dC}{dz} = \frac{3}{2}\frac{(1-\emptyset)}{d_g}(\eta_0\alpha_{\mathrm{att}})C \qquad (A4.5)$$

The specific attachment rate over time unit (s^{-1}) can be defined through the relation with the the deposite rate over length unit of fitler layer (kg/m):

$$\mathrm{k_{att}} = \frac{dC}{Cdz}\frac{v}{\emptyset} \qquad (A4.6)$$

Finally, the specific attachment rate is obtained by combining Eq (A4.6) and Eq (A45)

$$\mathrm{k_{att}} = \frac{3(1-\emptyset)\mathrm{v}}{2\mathrm{d_g}\emptyset}\eta_0\alpha_{\mathrm{att}} \qquad (A4.7)$$

Apendix 4.2 Attachment efficiency from experiments (α_{exp}), our correlation ($\alpha_{\mathrm{predicted}}$), Elimelech, 1992 ($\alpha_{\mathrm{E}}$), Bai and Tien, 1999($\alpha_{\mathrm{BT}}$), Chang and Chan, 2008 (α_{CC1}), Chang and Chan, 2009 (α_{CC2})

Table T1: Attachment efficiency from experiments, existing correlation and our correlation (Will be updated)

References	Exp.No	α_{exp}	$\alpha_{predicted}$	α_{E}	α_{BT}	α_{CC1}	α_{CC2}
Vaidyanathan and Tien, 1989	1	0.2892	0,139775	1,66914	0,117738	1,50303	0,42067
	2	0.2130	0,10582	1,66914	0,117738	1,50303	0,42067
Elimelech and O'Melia,1990	3	0.0102	0,014324	0,011258	0,0157209	0,019021	0,015721
	4	0.0115	0,015976	0,011258	0,0157209	0,019021	0,015721
	5	0.0234	0,029332	0,032689	0,0301649	0,033598	0,030165
	6	0.0263	0,032622	0,032689	0,0301649	0,033598	0,030165
	7	0.0490	0,056341	0,063773	0,0549332	0,058081	0,054933
	8	0.0933	0,133224	0,034991	0,028962	0,036245	0,028962
	9	0.1000	0,141902	0,034991	0,028962	0,036245	0,028962
	10	0.2089	0,255842	0,346546	0,187343	0,182621	0,187343

	11	0.3548	0,483053	0,73236	0,350248	0,325301	0,350248
	12	0.4467	0,603979	0,73236	0,350248	0,325301	0,350248
	13	0.0195	0,016226	0,012331	0,0241435	0,032106	0,024144
	14	0.0115	0,010035	0,012331	0,0241435	0,032106	0,024144
	15	0.0407	0,030807	0,035165	0,0455655	0,055778	0,045566
	16	0.0324	0,025033	0,035165	0,0455655	0,055778	0,045566
	17	0.0676	0,048194	0,061629	0,0682922	0,079908	0,068292
	18	0.1585	0,135724	0,030856	0,0318193	0,044184	0,031819
	19	0.1413	0,123954	0,030856	0,0318193	0,044184	0,031819
	20	0.3162	0,22617	0,281614	0,180893	0,196386	0,180893
	21	0.5754	0,48665	0,142693	0,0925028	0,118465	0,092503
	22	0.4467	0,381207	0,142693	0,0925028	0,118465	0,092503
Elimelech,1992	23	0.0107	0,03014	0,014376	0,0149284	0,015135	0,014928
	24	0.0324	0,082158	0,046626	0,0347829	0,032251	0,034783
	25	0.0724	0,17509	0,090333	0,0573801	0,050852	0,05738
	26	0.1585	0,26936	0,053201	0,0257439	0,027455	0,025744
	27	0.3020	0,483079	0,412229	0,152427	0,1253	0,152427
	28	0.0028	0,009975	0,005773	0,0067165	0,007556	0,006717
	29	0.0110	0,015168	0,010887	0,0157531	0,019013	0,015753
	30	0.0251	0,030885	0,030983	0,0295545	0,032845	0,029555
	31	0.0490	0,055532	0,061971	0,056571	0,059573	0,056571
	32	0.0977	0,107194	0,130632	0,109382	0,10946	0,109382
	33	0.2042	0,235826	0,300845	0,193229	0,186105	0,193229
	34	0.0089	0,008761	0,005542	0,013258	0,019431	0,013258
	35	0.0155	0,01297	0,01224	0,0251389	0,033314	0,025139
	36	0.0372	0,025416	0,033272	0,044518	0,05438	0,044518
	37	0.0676	0,047499	0,060933	0,0725419	0,084441	0,072542
	38	0.1514	0,09983	0,113275	0,117269	0,130287	0,117269
	39	0.3162	0,213917	0,251418	0,202293	0,216132	0,202293
Bai and Tien,1999	40	0.0076	0,008416	0,015526	0,0123116	0,031357	0,012312
	41	0.0098	0,013185	0,007014	0,00523905	0,015652	0,005239
	42	0.0552	0,036995	0,130631	0,080337	0,156134	0,080337
	43	0.2126	0,15164	0,848713	0,329351	0,528223	0,329351
	44	0.0039	0,003203	0,060519	0,00830707	0,017878	0,008307
	45	0.0029	0,00175	0,025973	0,0107628	0,02345	0,010763
	46	0.0024	0,001487	0,025973	0,00980661	0,02345	0,009807
	47	0.0453	0,028603	0,007786	0,00325931	0,008072	0,003259
	48	0.1704	0,040755	0,186264	0,0529471	0,086284	0,052947
	49	0.1562	0,057261	0,73304	0,182831	0,263286	0,182831
	50	0.1506	0,055918	0,73304	0,166588	0,263286	0,166588
	51	0.0049	0,006422	0,019797	0,0102606	0,027045	0,010261
	52	0.0071	0,009089	0,019797	0,0093139	0,027045	0,009314
	53	0.0068	0,008822	0,019797	0,00848643	0,027045	0,008486
	54	0.0085	0,011353	0,041604	0,0118996	0,030516	0,0119
	55	0.0088	0,011833	0,041604	0,0108016	0,030516	0,010802
	56	0.0074	0,010203	0,041604	0,009842	0,030516	0,009842
	57	0.0226	0,023063	0,213367	0,0400328	0,084626	0,040033

	58	0.0236	0,024226	0,213795	0,0364764	0,085073	0,036476
	59	0.0233	0,024175	0,213367	0,0331106	0,084626	0,033111
	60	0.0054	0,007017	0,019777	0,0102412	0,026973	0,010241
	61	0.0253	0,025548	0,213795	0,0401841	0,085073	0,040184

Appendix 4.3 Summary of regression coefficients

Regression analyis of the new correlation equation

```
Coefficients:
            Estimate Std. Error t value Pr(>|t|)
(Intercept) -6.54829    0.75743  -8.645 4.09e-14 ***
ln_NLo2      0.74375    0.09471   7.853 2.55e-12 ***
ln_NE12     -0.54027    0.08210  -6.581 1.52e-09 ***
ln_E2        4.74258    0.53637   8.842 1.45e-14 ***
ln_DL        1.15249    0.08989  12.821  < 2e-16 ***
---
Signif. codes:  0 ‘***’ 0.001 ‘**’ 0.01 ‘*’ 0.05 ‘.’ 0.1 ‘ ’ 1

Residual standard error: 0.9071 on 113 degrees of freedom
Multiple R-squared:  0.8223,   Adjusted R-squared:  0.816
F-statistic: 130.7 on 4 and 113 DF,  p-value: < 2.2e-16
```